

**Development of novel small-molecule drug conjugates
for imaging and treatment of
prostate cancer**

Dissertation

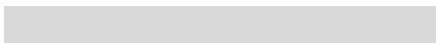
zur Erlangung des Grades eines
„Doktor rerum naturalium (Dr. rer. nat.)“
am Fachbereich Chemie, Pharmazie, Geographie und Geowissenschaften
der Johannes Gutenberg-Universität Mainz

vorgelegt von

Hanane Lahnif

Geboren in Nador, Marokko

Mainz, November 2021

Dekan: 

1. Berichterstatter: 

2. Berichterstatter: 

Tag der mündlichen Prüfung: 16.12.2021





Abstract

Prostate cancer (PCa) is the most frequent cancer in men worldwide, behind only lung cancer. Although the 5-year survival rate of localized PC is almost 100 %, it drops dramatically to just 30 % for the advanced and metastatic form. This high mortality rate highlights not only the importance of early diagnosis, but also the urgent need for the development of new therapeutic approaches.

The discovery of prostate-specific membrane antigen PSMA as a reliable tumor-associated biomarker for prostate cancer has revolutionized the management of this disease. Several efforts have been done in the last decade to develop selective and sensitive PSMA ligands for PET-imaging and endoradiotherapy. Among these radiopharmaceuticals [⁶⁸Ga]Ga-PSMA 11 was the first FDA-approved PSMA-PET radiotracer, followed with its therapeutic counterpart [¹⁷⁷Lu]Lu-PSMA 617. In the meantime, several groups have joined the run for the best PSMA ligand. However, the development of PSMA radiopharmaceuticals that have both favorable physicochemical properties and a beneficial pharmacokinetic profile remains a challenge which still need to be addressed.

In this dissertation, several PSMA ligands with different structural elements were designed and investigated for their *in vitro* and *in vivo* properties.

Based on preliminary studies, DATA^{5m}.SA.KuE and AAZTA⁵.SA.KuE were selected to be evaluated more thoroughly. Both PSMA tracers have a hybrid chelator that is easily labeled under mild conditions in addition to beneficial pharmacokinetic properties regarding selectivity and tumor accumulation. Furthermore, AAZTA⁵.SA.KuE has shown promising theranostic potential as it can be labeled with the PET nuclide scandium-44 as well as the therapeutic β⁻-emitter lutetium-177.

Moreover, a *dual-targeted* pamidronate-PSMA conjugate was developed to target both PSMA, which is highly expressed in tumor lesions, and the hydroxyapatite structures in bone metastases. This ¹⁷⁷Lu-labeled conjugate showed promising results in preclinical studies.

The unique and favorable properties of PSMA make it an optimal target not only in nuclear medicine and radiopharmacy but also in targeted chemotherapy. The advantages of the targeted therapy approach are obvious since the discovery of antibody-drug conjugates (ADCs). However, although ADCs have represented a breakthrough in the treatment of many cancers, efforts to develop PSMA-ADCs have failed due to lack of stability, premature drug release, and high toxicity.

In order to circumvent some of these challenges, small-molecule PSMA binding moieties were used instead of antibodies. The resulting small-molecule drug conjugates (SMDCs) showed some advantages over the ADCs, such as better tumor penetration due to lower molecular weight, fast clearance, and cost-effective synthesis.

The SMDCs developed in this dissertation can be divided into two groups. The first group includes dimeric SMDCs consisting of a PSMA binding unit and the antimitotic agent MMAE. Both units are conjugated to each other via the enzyme-cleavable linker valine-citrulline. The second group consist of trimeric conjugates (radiolabeled SMDCs) that, in addition to the PSMA-binding moiety and the cytostatic drug, contain a chelator which is able to complex both diagnostic and therapeutic nuclides. Hence, the low-dose ^{68}Ga -labeled SMDC is supposed to be used in the determination of the patient's suitability for therapy. In case of positive response, the patient is then treated with the ^{177}Lu -labeled conjugate. In addition to the thereby implemented personalized medicine approach, the combination of targeted chemotherapy and radiotherapy in a single molecule, may have several advantages, such as circumventing the development of resistance or enhancing a synergistic effect. Preclinical studies showed the promising potential of this approach in terms of good tolerability and efficacy *in vivo*. However, further optimization on the molecular structure of these compounds is necessary to enable a translational development.

Kurzzusammenfassung

Prostatakrebs (PCa) ist nach Lungenkrebs die häufigste Krebserkrankung bei Männern weltweit. Obwohl die 5-Jahres-Überlebensrate bei lokalisiertem PC nahezu 100 % beträgt, sinkt sie bei der fortgeschrittenen und metastasierten Form dramatisch auf nur noch 30 %. Diese hohe Sterblichkeit macht nicht nur deutlich, wie wichtig eine frühzeitige Diagnose ist, sondern auch, wie dringend die Entwicklung neuer Behandlungsansätze notwendig sind.

Die Entdeckung des prostataspezifischen Membranantigens PSMA, als zuverlässiger tumor-assoziiertes Biomarker hat die Behandlung des Prostatakarzinoms revolutioniert. In den letzten Jahren wurden mehrere Anstrengungen unternommen, um selektive und empfindliche PSMA-Liganden für die PET-Bildgebung und Radiopharmakotherapie zu entwickeln. Unter diesen Radiopharmazeutika war [⁶⁸Ga]Ga-PSMA 11 der erste, von der FDA, zugelassene PSMA-PET Radiotracer, gefolgt von seinem therapeutischen Pendant [¹⁷⁷Lu]Lu-PSMA 617. In der Zwischenzeit haben sich mehrere Gruppen dem Wettlauf um den besten PSMA-Liganden angeschlossen. Allerdings bleibt die Entwicklung von PSMA-Tracern, die sowohl günstige physikochemische Eigenschaften haben als auch einen vorteilhaften pharmakokinetischen Profil aufweisen, weiterhin eine Herausforderung, die es noch zu bewältigen gilt.

In Rahmen dieser Arbeit wurden mehrere PSMA-Liganden mit unterschiedlichen Strukturelementen entwickelt und nach ihren *in vitro* und *in vivo* Eigenschaften untersucht.

Auf der Grundlage vorheriger Studien wurden die beiden PSMA-Liganden DATA^{5m}.SA.KuE und AAZTA⁵.SA.KuE für eine präklinische Evaluierung ausgewählt. Beide PSMA-Tracer haben einen hybriden Chelator, der sich unter milden Bedingungen leicht markieren lässt sowie vorteilhafte pharmakokinetische Eigenschaften in Bezug auf Selektivität und Tumoranreicherung. Darüber hinaus hat sich AAZTA⁵.SA.KuE als vielversprechende theranostische Verbindung erwiesen, da sie sowohl mit dem PET-Nuklid Scandium-44 als auch mit dem therapeutischen β^- -Emitter Lutetium-177 markiert werden kann.

Des Weiteren wurde ein *dual-targeted* Pamidronat-PSMA-Konjugat entwickelt, das sowohl die, in den Tumorkläsionen hochexprimierte, PSMA als auch die Hydroxyapatit-Strukturen in den Knochenmetastasen adressiert. Dieses ¹⁷⁷Lu-markierte Konjugat zeigte in präklinischen Studien vielversprechende Ergebnisse.

Die einzigartigen und vorteilhaften Eigenschaften von PSMA machen es zu einem optimalen Target nicht nur in der Nuklearmedizin und Radiopharmazie, sondern auch in der zielgerichteten Chemotherapie. Spätestens seit der Entwicklung der Antikörper-Wirkstoff-Konjugate (ADCs) liegen die Vorteile des zielgerichteten Therapieansatzes auf der Hand. Doch obwohl ADCs einen Durchbruch bei der Behandlung von vielen Krebserkrankungen darstellt haben, sind die Bemühungen, ein PSMA-ADC zu entwickeln, aufgrund mangelnder Stabilität, vorzeitiger Wirkstofffreisetzung und hoher Toxizität, gescheitert.

Um einige dieser Herausforderungen zu umgehen, wurden niedermolekulare PSMA-Bindungseinheiten anstatt Antikörper verwendet. Die daraus resultierenden niedermolekularen Wirkstoffkonjugaten (SMDCs) zeigten einige Vorteile gegenüber ihren Vorgängern, den ADCs wie z. B. eine bessere Tumorpenetration aufgrund des geringeren Molekulargewichts, eine schnellere Clearance sowie eine kosteneffektive Synthese.

Die im Rahmen dieser Arbeit entwickelten SMDCs unterteilen sich in zwei Gruppen. Die erste Gruppe beinhaltet dimere SMDCs, die aus einer PSMA-Bindungseinheit und dem antimitotischen Wirkstoff MMAE besteht. Beide Einheiten sind über den enzymspaltbaren Linker Valin-Citrullin miteinander konjugiert. Die zweite Gruppe besteht aus trimeren Konjugaten (radiomarkierten SMDCs), die zusätzlich zu der PSMA-Bindungseinheit und dem Zytostatikum auch einen Chelator beinhalten, der in der Lage ist, sowohl diagnostische als auch therapeutische Nuklide zu komplexieren. Damit wird mit dem niedrigdosierten ⁶⁸Ga-markierten SMDC die Eignung des Patienten für die Therapie festgestellt. Im Falle eines Ansprechens wird der Patient mit der ¹⁷⁷Lu-markierten Verbindung behandelt. Zusätzlich zu dem damit implementierten Ansatz der personalisierten Medizin könnte die Kombination einer zielgerichteten Chemotherapie und Strahlentherapie in einem einzigen Molekül einige Vorteile mit sich bringen, wie z.B. die Umgehung einer Resistenzbildung oder die Verstärkung eines synergistischen Effekts. Präklinische Studien zeigten das vielversprechende Potential dieses Ansatzes im Sinne einer guten Verträglichkeit und Wirksamkeit *in vivo*. Allerdings sind weitere Optimierung an der molekularen Struktur dieser Verbindungen notwendig, um eine translationale Weiterentwicklung zu ermöglichen.

Table of content

1	Introduction	17
1.1	Prostate Cancer	19
1.1.1	Epidemiology	19
1.1.2	Diagnosis of PC	20
1.1.3	Therapy	22
1.2	Targeted therapy	25
1.2.1	Antibody drug conjugates ADCs	25
1.2.2	Small-molecule drug conjugates SMDCs	30
1.3	Prostate-specific membrane antigen	32
1.3.1	Biological function and physiological expression	32
1.3.2	PSMA molecular structure	34
1.3.3	PSMA inhibitors for imaging	38
1.3.4	PSMA inhibitors for therapy	41
1.3.5	PSMA drug conjugates	42
2	Objectives	49
3	Manuscripts	57
3.1	Squaric acid based-radiopharmaceuticals for tumor imaging and therapy	63
3.2	Hybrid chelator-based PSMA-radiopharmaceuticals: translational approach	91
3.3	Old drug, new delivery strategy: MMAE repackaged	125
3.4	DOTA conjugate of Bisphosphonate and PSMA-inhibitor: A promising combination for therapy of prostate cancer related bone metastases	151
4	Summary and outlook	181
5	Appendix	195
5.1	References	197
5.2	List of abbreviations	206
5.3	Danksagung	209
5.4	Curriculum Vitae	215

1 Introduction

1.1 Prostate Cancer

1.1.1 Epidemiology

Cancer is one of the leading causes of death worldwide with more than 10 million deaths in 2020¹. The incidence and mortality of cancer diseases has been drastically increasing in the last decades, particularly in the industrial world. This increase in cancer incidence and mortality depends on several factors e.g., socioeconomic development, life style, genetics and exposure to carcinogens.

Prostate cancer (PC) is the second most common cancer in men worldwide. Although the incidence of PC is about 60 % in men older as 65, the 5-year survival rate is compared to other cancer diseases very high 98%. However, this rate is strongly dependent on cancer stage and time point of diagnosis. Once the cancer has metastasized, the 5-year survival rate decreases dramatically to 30 %^{2,3}.

1.1.2 Diagnosis of PC

Prostate cancer is a very slow-growing cancer and progresses in most cases asymptotically. Nevertheless, an early detection of this disease has a significant impact on the clinical outcome. Besides the digital rectal exam (DRE), determination of the PSA-level is a common screening method which is based on the measurement of the prostate-specific antigen (PSA) concentration in the blood. In case of a positive result, the prostate gland has to be imaged via magnetic resonance imaging (MRI).

A subsequent prostate biopsy helps confirming the diagnosis and grading the tumor. According to the corresponding Gleason-Score, the cancer is classified in low-, intermediate- or high-risk disease. However, prior to therapy, the tumor stage, described as TNM system (T=Tumor; N= Nodes; M= Metastasis), has to be determined (Figure 1). In addition, imaging tests such as ^{99m}Tc bone scan, CT, MRI scan or PSMA PET-CT are used to localize the tumor. A general overview of the diagnostic scheme according to the guidelines of the European Society for Medical Oncology (ESMO) is shown in figure 2.

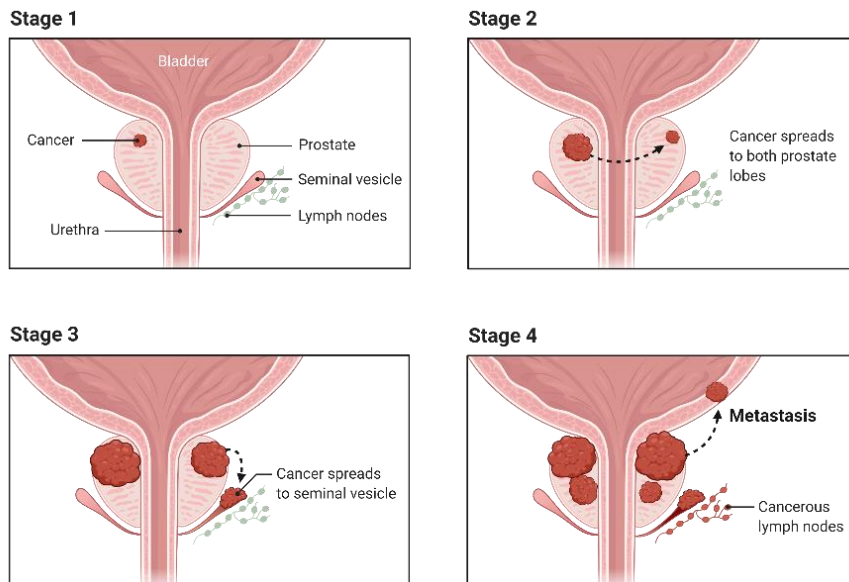


Figure 1 Staging of prostate cancer. Reprinted from "Prostate Cancer Stages", by BioRender.com (2021). Retrieved from <https://app.biorender.com/biorender-templates>

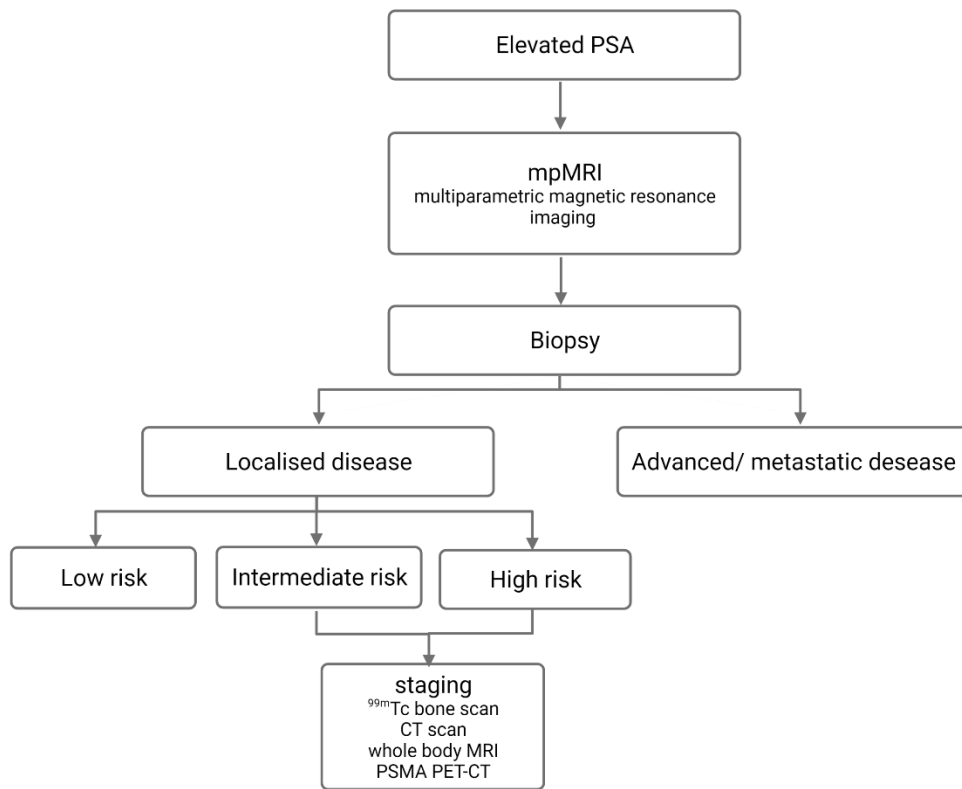


Figure 2 Diagnosis guidelines for PC according to ESMO Guidelines Committee 2020 ⁴

1.1.3 Therapy

Treatment of prostate cancer depends on several factors, e.g., the stage and grade of the tumor, the risk of the disease and mainly from the physical condition of the patient.

In case of localized disease, active surveillance is an option applied by asymptomatic slow-growing and low risk disease. Hereby the cancer is not actively treated but closely monitored using regular PSA tests and DREs as well as repeated biopsies or pmMRI scans.

However, there are also curative options in the management of local prostate cancer e.g., the radical prostatectomy where the entire prostate gland is removed, or the radiation therapy which can be divided into internal radiation (brachytherapy) and external beam radiation.

Hormone therapy is one of the most important pillars of the management of hormone-sensitive cancer diseases. Concerning PCa, androgen deprivation therapy ADT aims to lower the level of Testosterone and dihydrotestosterone, thus inhibit or even reduce tumor growth. There are two different approaches of ADT used in the treatment of locally advanced PCa. In the surgical castration or orchiectomy, androgen suppression is reached by removing the testes, the organ where most androgens are produced. In contrast, chemical or medical castration seems to be more advantageous since it does not require any surgery. In this therapy option, patients are treated with luteinizing hormone-releasing hormone (LHRH) agonists like leuprolide or goserelin. These drugs reduce the testosterone production by downregulation of LHRH receptors as a consequence of constant stimulation. Nevertheless, initial treatment with LHRH agonists leads to a temporary increase in testosterone level, hence promoting tumor growth. To avoid this so-called *flare phenomenon*, LHRH antagonist like abarelix can be used. However, since testosterone could be produced in lower amount in adrenal glands and in the prostate cancer itself, ADT is often combined with anti-androgen drugs like enzalutamide or apalutamide, which inhibit the signal transduction of testosterone.

Although hormone therapy is playing a crucial role in the management of PC, it can be only used as combination with other treatment strategies like radiation therapy, since ADT does not lead to tumor regression.

While local prostate cancer could be cured with the therapy options mentioned above, metastatic prostate cancer is considered to be incurable. Nevertheless, there are several treatment strategies applied in this stage depending on the androgen-sensitivity of the tumor as well as the site of metastasis. In metastatic hormone-sensitive PC (mHSPC), ADT represents the first-line therapy and the mainstay of management of this PC stage. ADT is combined with either anti-androgen drugs or chemotherapy.

Once mHSPC develops to the metastatic castration-resistant PCa (mCRPC) the severity of the disease increases dramatically. Standard treatment of mCRPC is the use of docetaxel-based chemotherapy or, in a post-docetaxel setting, cabazitaxel.

Additionally, an important concern in the therapy of metastatic PCa is the treatment of metastases. Since most common metastatic sites of PCa are bones (84%)⁵, patients are treated with the α -emitter ²²³Ra (Xofigo®) as first-line therapy of osseous metastases. The use of bisphosphonates or beta-emitting radio-nuclides like strontium-89 or samarium-153 as part of the palliative care can help alleviating some of the severe symptoms caused by bone metastases. Figure 3 gives an overview of the therapy options in dependence of several factors.

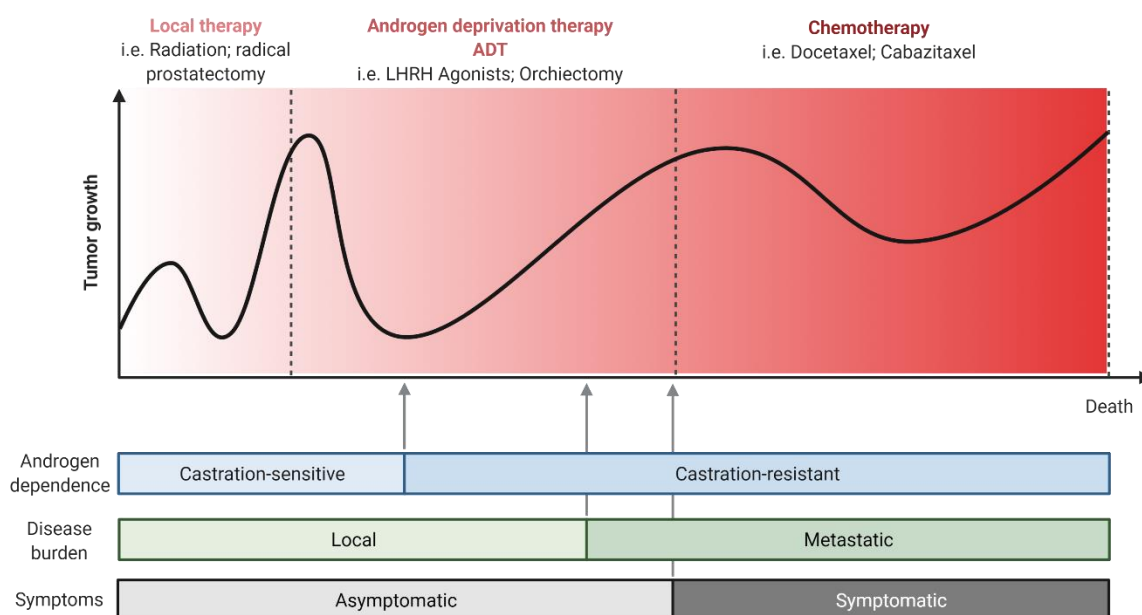


Fig-

ure 3 Different therapy regimen of PCa depending on androgen sensitivity, disease burden and symptoms. Based on The ESMO Guidelines Committee⁶. Adapted from "natural History of Prostate Cancer", by BioRender.com (2021). Retrieved from <https://app.biorender.com/biorender-templates>.

Beside the different treatment options mentioned above, there are several novel approaches studied so far, especially in the field of immunotherapy. Sipuleucel-T (PROVENGE) was the first FDA-approved cancer vaccine for treatment of mCRPC. This vaccine stimulates the immune system by inducing T-cells that are capable to recognize the prostate acid phosphatase which is exclusively expressed by PCa cells. Although this strategy seemed to be promising, Sipuleucel-T was not able to cure PCa but only prolonged the overall survival by few months ^{7,8}.

Finally, targeted therapy, which moved more and more into the focus of cancer research in general, has shown its promising potential in the management of prostate cancer. The discovery of prostate-specific membrane antigen PSMA was a game changer in both diagnosis and treatment of metastatic PC. [⁶⁸Ga]Ga-PSMA-11 was the first FDA-approved PSMA-targeted PET Imaging drug for patients with metastatic PCa ⁹ followed by [¹⁷⁷Lu]Lu-PSMA-617 that has been recently granted Breakthrough Therapy designation for radioligand therapy of metastatic PCa ¹⁰.

1.2 Targeted therapy

In the last decades, a paradigm shift in oncology has taken place. Researchers worldwide are focusing their work on the discovery and development of new diagnosis and therapy approaches which are specific to the target that should be addressed. A new era has begun: the era of targeted therapy. In contrast to traditional cancer treatment, targeted therapy is supposed to be highly specific to tumor cells and therefore avoid the severe side effects caused by chemotherapy, surgery or even radiation therapy, which are the three pillars of cancer management so far. The specificity of this approach is based on the use of target vectors with high affinity to certain molecular structures which are either exclusively expressed on tumor cells (tumor-specific) or upregulated in cancerous tissue (tumor-associated). Depending on the art of the target vector, a classification can be made into antibody drug conjugates ADCs and small-molecule drug conjugates SMDCs.

1.2.1 Antibody drug conjugates ADCs

ADCs represent an important tool in targeted therapy. In the last years, several ADCs have been investigated in clinical trials. With the turn of the millennium in 2000, The FDA approved the first ADC: Gemtuzumab ozogamicin, an anti-CD33 mAb conjugated to calicheamicin, for the treatment of patients with acute myeloid leukemia. However, in 2010 this ADC has been withdrawn from the market due to severe toxicity^{11,12}. This unexpected outcome highlighted the challenges in the implementation and clinical translation of ADCs.

The first step in the development of targeted therapeutics is to identify an appropriate target structure. The target should be located on the surface of cancer cells thus be accessible to the circulating antibody. Furthermore, the target antigen has to be exclusively expressed on tumor cells or at least at significant higher levels than on other healthy tissue. Since the cytotoxic payload should be released intracellularly, the target antigen has to be internalized upon ligand-binding. Non-internalized ADC could lead to a decrease in antitumor effect and even enhance toxicity via bystander effect.

Subsequent to the identification of targetable tumor-specific antigens, the synthesis of the mAb with high binding potency and stability, sufficient homogeneity and low immunogenicity, represents one of the most challenging steps in the development of ADCs.

Moreover, the selection of the suitable cytotoxic drug that can be used as warhead is also fundamental in the preliminary development of new ADCs. These chemotherapeutic drugs should fulfill several criteria such as high potency (IC_{50} in the nanomolar range) since the concentrations applied in drug conjugates are often much lower than in conventional therapy. Most ADCs that are in clinical trial have a drug-to-antibody ratio ADR of about 4, which means that the amount of drug molecules delivered into tumor cells is restricted. Consequently, the most applied drugs display high systemic toxicity due to a narrow therapeutic window, thus are not clinically used as single drugs ^{13,14}.

These warheads should have functional groups that make a conjugation to linker moieties feasible without compromising the antitumor efficacy of the drug. Indeed, there are only few cytotoxic drugs that can meet these criteria. The majority of them belong to the group of anti-microtubule agents such as auristatins or tubulysins.

Obviously, a premature release of these highly toxic drugs should be inhibited to avoid a systemic toxicity. Herein lies the importance of effective linker design. The selection of the linker plays a crucial role in the determination of the pharmacokinetic profile of the ADC, since the chemical properties of the linker impact the drug release, thus the therapeutic index of the drug formulation at whole.

In general, there are two main groups of linkers used in drug conjugates (Figure 4), cleavable and non-cleavable linkers. However, as mAb have a half-life of several days in blood circulation, the stability of the ADC should be ensured independently of the group the linker belongs to ¹⁵.

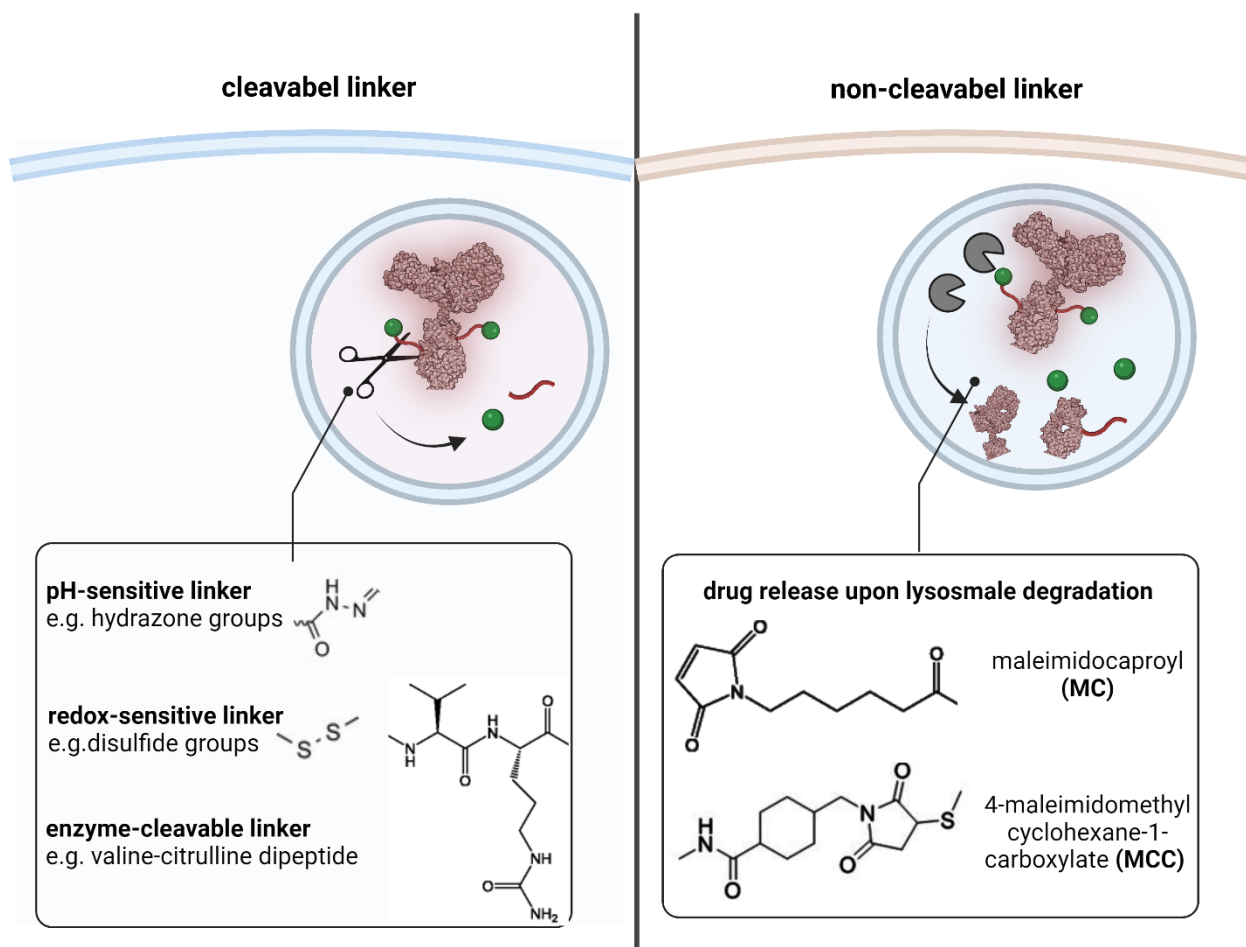


Figure 4 Schematic illustration of the most common used linker in drug conjugates. Created with Biorender.com

Cleavable linkers can be further divided into several subgroups depending on the drug-release conditions. pH-sensitive linkers e.g., hydrazone groups, remain stable in the neutral pH of the blood circulation but are hydrolyzed in the acidic intracellular environment.

Redox-sensitive linkers, based on disulfide groups, take advantage of the significantly higher concentration of glutathione in tumor cells to release the drug.

Nevertheless, this approach seems to have some limitations since some studies reported an association of chemically labile linkers with non-specific drug liberation due to insufficient stability¹⁶. Another emerging subgroup of cleavable linkers are enzyme-sensitive linkers, such as valine-citrulline dipeptide. These linkers are cleaved by lysosomal proteases such as cathepsin B, which is highly expressed in tumor cells. However, an essential requirement of this enzyme-specific drug release is the internalization of the antibody-antigen complex. An example of an ADC that includes a valine-citrulline linker is brentuximab vedotin (Adcetris) which is already on the market since 2011¹⁷.

Another strategy in linker design is the use of non-cleavable linkers to ensure higher stability in blood circulation. But even here an internalization of the ADC is required as the payload can only be released after lysosomal degradation of the mAb. The ADC Kadcycla (Trastuzumab emtansine) was the first ADC that includes a non-cleavable linker. It was approved in 2013 for the treatment of HER2-positive breast cancer¹⁸, which is a breast cancer with an elevated expression of the human epidermal growth factor receptor 2 (HER2). Figure 5 shows a schematic illustration of the ADC-based drug targeting. Some of the already approved ADCs are listed in table 1.

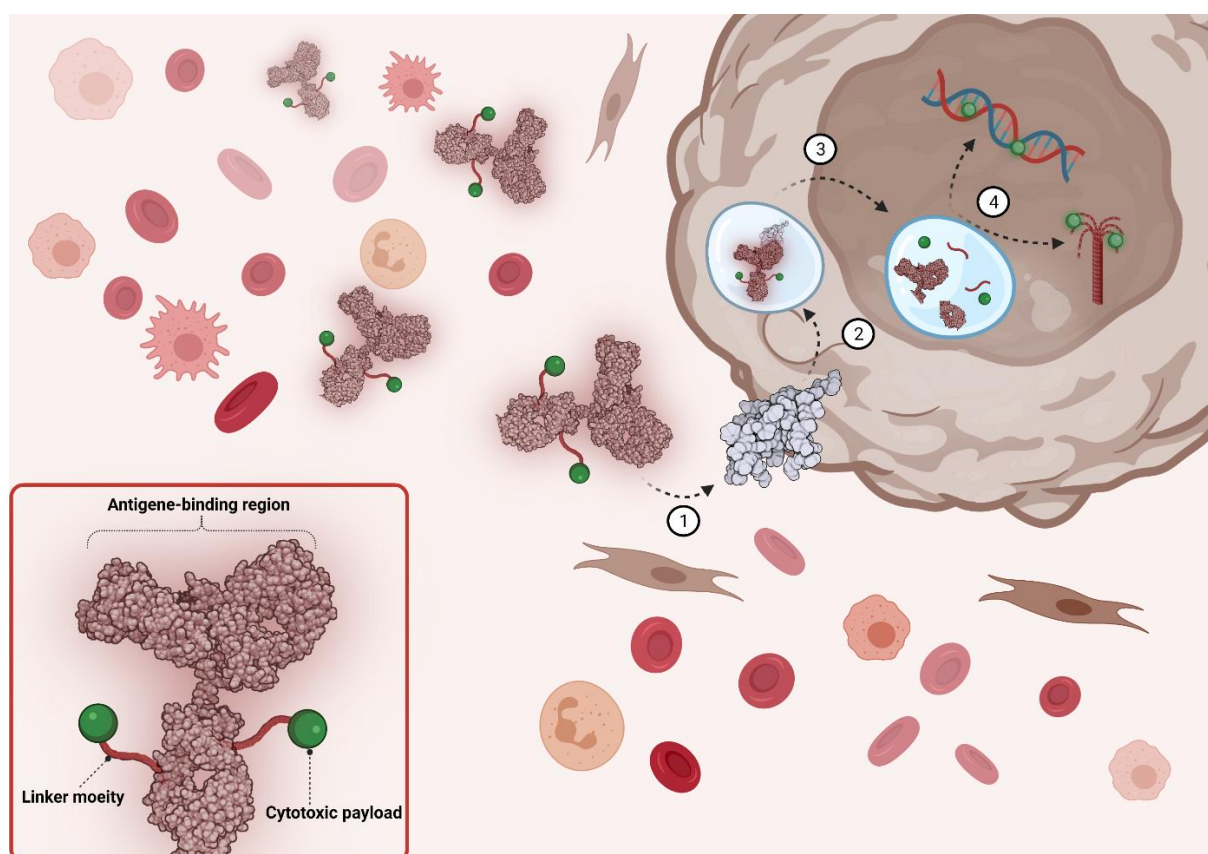


Figure 5 Schematic illustration of the uptake of ADCs. Upon binding to the antigen (1) the ADC-Antigen complex is internalized via endocytosis (2). The cytotoxic payload is released after either lysosomal degradation of the mAb or cleavage of linker unit (3). The free drug binds to the its intracellular target (4). Created with Biorender.com.

Table 1 FDA-approved ADCs

Drug name	Target	Payload	Indication	FDA approval
Gemtuzumab ozogamicin ^{11,12}	CD33	calicheamicin	acute myeloid leukemia	approval in 2000; withdrawn in 2010; reapproval in 2017
Brentuximab vedotin ¹⁷	CD30	MMAE	HER2-positive breast cancer	2011
Trastuzumab emtansine ¹⁹	CD22	calicheamicin	acute lymphoblastic leukemia	2017
Polatuzumab vedotin-piiq ²⁰	CD79b	MMAE	relapsed or refractory diffuse large B-cell lymphoma	2019
Belantamab mafodotin ²¹	B-cell maturation antigen BCMA	MMAF	relapsed or refractory multiple myeloma	2020
Loncastuximab tesirine-lpyl ²²	CD19	SG3199	diffuse large B-cell lymphoma	2021

Although ADCs have proved to be valuable tools in cancer treatment, ADC development reveal serious limitations and challenges such as aggregation, which can lead to structural modification, thus loss of antigen-binding potency, or degradation which presents a major drawback in terms of drug formulation and stability, during the production process, as well as during transport and long-term storage²³⁻²⁵. Moreover, the large molecular size of mAb as target vectors in ADCs leads to poor tumor penetration. The slow diffusion rate, poor vascularization and mostly lack of functional lymphatic system of solid tumors are major reasons for the severely restricted antibody-based drug delivery. One of the strategies developed to circumvent some of these hurdles is the use of small-molecules as target vectors instead of mAbs resulting in the so-called small-molecule drug conjugates SMDCs.

1.2.2 Small-molecule drug conjugates SMDCs

In the last years, small-molecule drug conjugates have shown their promising potential as alternative approach to ADCs. The most important advantage of small molecules over mAb is their low molecular weight that enables good cell penetration in solid tumors. Moreover, as most SMDCs are smaller than 40 kDa, they are rapidly excreted from the blood through glomerular filtration, thus display a lower off-target cytotoxicity than ADCs. Noteworthy is also their simplified and manageable synthesis compared to the sophisticated manufacture process of mAbs as well as more straightforward transportation and storage processes which are of immense value in regard to a translational use of the corresponding drug conjugates^{26,27}.

While the design strategies and selection criteria of linker moiety and cytotoxic payload of SMDCs are similar to these of ADCs, the targeting unit makes the decisive difference between the two drug-delivery systems. Small-molecule targeting units should fulfill the same requirements as mAbs, in terms of high binding affinity and selectivity to the target in order to ensure effective drug delivery along with a reduced off-target cytotoxicity. This unit is mostly based on inhibitors or ligands of transmembrane receptors or enzymes involved in carcinogenesis or tumor metabolism. Table 2 gives an overview of some preclinically and clinically investigated SMDCs.

Table 2 Examples of SMDCs investigated in preclinical and clinical trials. NCT= National Clinical Trial.

Drug name	target	Payload	Disease	NCT
PEN-866 ²⁸	Heat shock protein 90 HSP90	SN-38	solid tumors	NCT03221400 (Phase1/2)
EC1456 ²⁹	Folate receptor FR	tubulysin	advanced Solid tu- mors	NCT01999738 (Phase 1)
EC1169 ³⁰	Prostate-specific membrane antigen PSMA	tubulysin	prostate cancer	NCT02202447 (Phase 1)
ZnDPA-SN-38 ³¹	Phosphatidylserine PS	SN-38	solid tumors	--
PTX-SS-DUPA ³²	Prostate-specific membrane antigen PSMA	paclitaxel	prostate cancer	--
GRN1005 ³³	low-density lipoprotein receptor-related protein 1 LRP-1	paclitaxel	non-small cell lung cancer with brain metastases	NCT01497665 (Phase 2)

1.3 Prostate-specific membrane antigen

Prostate-specific membrane antigen PSMA is one of the most investigated tumor-associated targets in the last decade. There are currently more than 400 clinical trials of PSMA-targeting conjugates for imaging and therapy listed in the U.S. National Library of Medicine NIH ²².

PSMA was first described in 1987 by Horoszewicz et.al ³⁴ as an antigen with high expression in LNCaP cells (Lymph Node Carcinoma of the Prostate) thus suitable for use as tumor biomarker. In the following years PSMA research has achieved major milestones such as molecular cloning in 1993 ³⁵ and determination of the crystal structure in 2005 ³⁶. Furthermore, several studies have revealed the potential of PSMA as molecular target of prostate cancer PC resulted from the unique properties of this antigen.

1.3.1 Biological function and physiological expression

PSMA is a membrane-bound transmembrane glycoprotein belonging to the family of zinc-metalloproteases. In the proximal small intestine, PSMA is known as folate hydrolase 1 since it is responsible for the cleavage of glutamate residues from poly- γ -glutamated folate, which enables folate reabsorption. The same enzymatic activity is also found in the nervous system, where PSMA acts as N-acetyl- α -linked acidic dipeptidase (NAALADase), thereby hydrolyzing and inactivating the neurotransmitter N-acetyl-L-aspartyl-L-glutamate (NAAG) ^{37,38} (Figure 6).

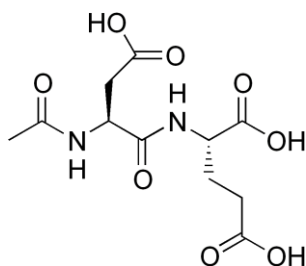


Figure 6 Chemical structure of the natural substrate N-acetylaspartylglutamic acid NAAG.

While the physiological role of PSMA in the small intestine and the nervous system is well understood, its function in healthy prostate cells, in the proximal tubules of the kidneys and in salivary glands is not fully elucidated. However, PSMA may be involved in the folate metabolism in these tissues ³⁵.

Furthermore, cloning and sequencing of PSMA revealed a certain homology to the transferrin receptor. Both structures are internalized via clathrin-coated pits. It has been shown that this internalization occurs after the interaction of a specific motif localized in the intracellular domain of PSMA with the clathrin adaptor protein 2-complex. It should be noticed, that the PSMA internalization rate is significantly increased upon ligand binding indicating a possible unknown transport function of PSMA ^{35,39}.

The expression of PSMA in prostate cancer was found to be up to 1000-fold higher than in other healthy tissues. Moreover, this overexpression correlates with the invasiveness and the severity of the disease ^{40,41}. The role of PSMA in promoting cancer growth is still unknown. However, there are some studies suggesting an association with the elevated folate level in tumor cells resulted from the overexpression of PMSA ^{42,43}. Interestingly, PSMA has been also detected in neovasculature of solid tumors such as breast cancer, renal cancer and lung cancer ^{44,45}. Although the role of PSMA in angiogenesis is not known so far, the restricted expression in tumor-associated neovasculature renders PSMA a promising molecular target for an antiangiogenic therapy ⁴⁶⁻⁴⁸. Figure 7 gives an overview of both pathological and physiological PSMA-expression.

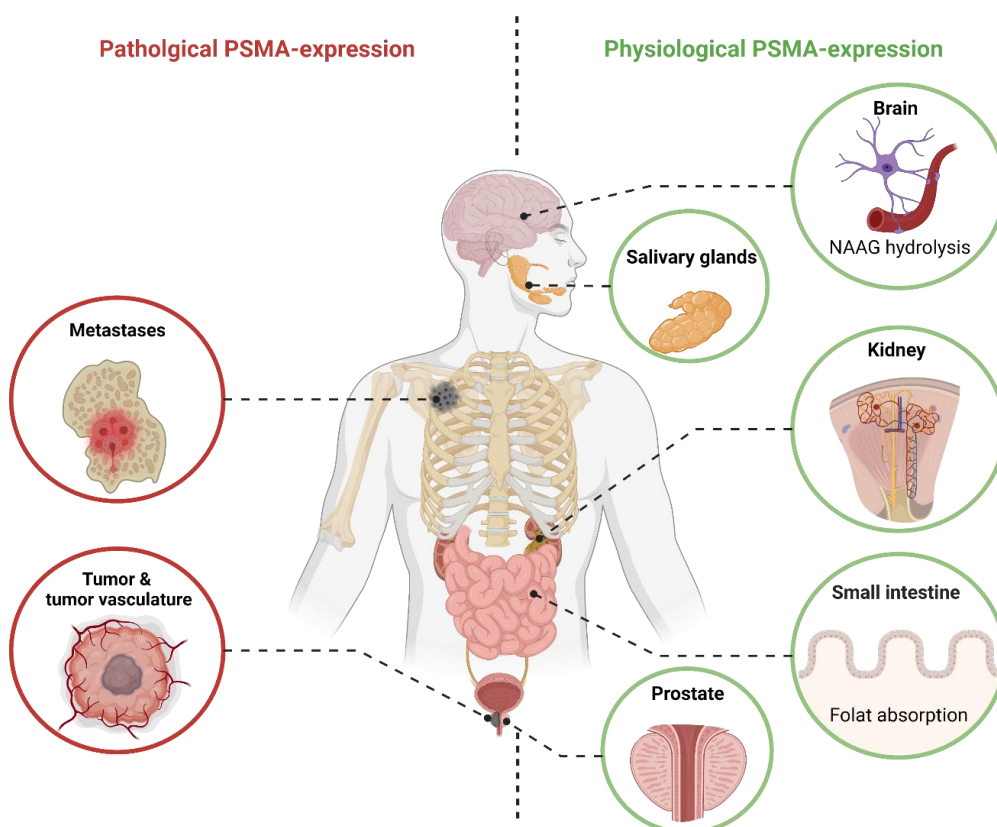


Figure 7 Schematic illustration of PSMA expression. Created with Biorender.com.

1.3.2 PSMA molecular structure

According to crystallographic structural studies^{36,49}, PSMA consists of three main domains: a) the extracellular C-terminal domain, b) the lipophilic transmembrane domain and c) the N-terminal intracellular domain. The extracellular domain contains the active site of the enzyme and can be divided in a binuclear Zn active site with catalytic residues and an arginine-rich patch responsible for the right orientation of PSMA ligands in the entrance funnel.

The active site of PSMA is formed by two pockets, S1' and S1 (Figure 7). Whereas the S1 pocket also called arginine patch, due to the three arginine residues located there, is rather flexible in terms of binding of different chemical groups, the S1' pocket is the pharmacophore unit of PSMA and thus responsible for the binding of glutamate, the natural substrate of PSMA. Consequently, an interaction with this binding site is crucial in the design of high-affinity ligands⁴⁹⁻⁵¹.

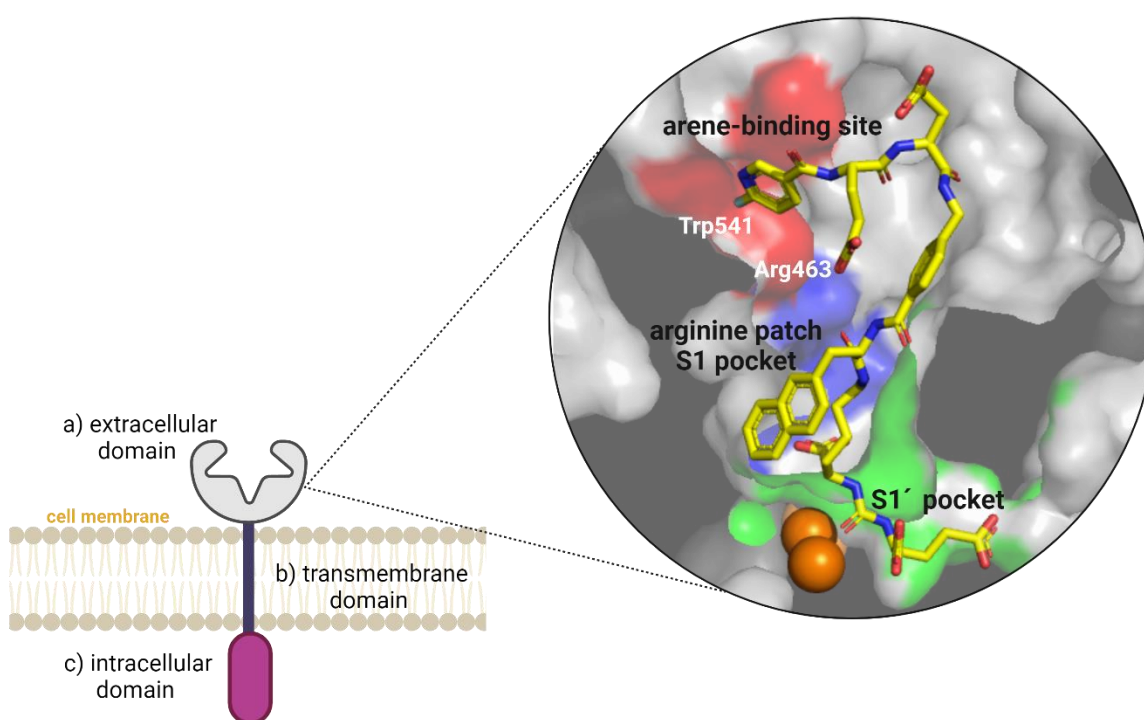


Figure 8 Schematic illustration of PSMA (left) with the three main domains of the enzyme. the molecular structure of the binding pocket, which is located in the extracellular domain, in complex with the PSMA ligand PSMA-1007 (PDB code 5O5T) is depicted on the right side. Main regions are highlighted in different colors: the S1' pharmacophore unit in green; the S1 arginine-patch in blue and the arene-binding region in red. The two zinc ions are depicted as orange spheres. Both amino acids tryptophan-541 and arginine-463 seem to play a crucial role in improving ligand binding affinity. The figure is constructed with the PyMOL Molecular Graphics System, Version 2.4.1 Schrödinger, LLC and created with Biorender.com.

The first designed PSMA ligands were as expected NAAG-analogues developed as PSMA inhibitors with neuroprotective properties, since high glutamate level and the resulting excitotoxicity are associated with several neurodegenerative diseases such as Alzheimer's or Parkinson's disease ⁵². To better understand the binding mode of the natural PSMA substrates, several studies on structure-activity relationships were performed to identify key amino acid interactions and possible modifications to the designed lead structures in order to improve the chemical and biological properties of target ligands ^{49,50}.

Since the pharmacophore pocket S1' displays high binding affinity only to glutamate and glutamate isosteres, almost all synthesized PSMA ligands were developed on the basis of glutamate or NAAG. However, efforts were made to identify suitable binding motif that coordinate the two zinc ions localized in the S1' pocket. Interestingly, Zhang et al discovered an additional binding region on PSMA, the arene-binding site ⁵³. They developed a series of PSMA ligands and investigated the role of linker length and substitutional groups on the binding affinity. Among these different ligands, DNP-ARM-P2 (dinitrophenol-antibody-recruiting molecule targeting prostate cancer) displayed the most interesting features not in terms of ultra-high affinity (IC_{50} in the picomolar range) but also regarding the interaction with the arene-binding region through π -stacking of the nitroarene group with Trp541. Electrostatic interactions between the two nitro groups in the dinitrophenol ring (DNP) and the guanidinium group of Arg463 seem also to be of major importance.

First SAR studies led already in 1996 to the discovery of 2-phosphonomethyl pentanedioic acid (PMPA), a highly potent phosphonate-based PSMA inhibitor with PSMA binding affinity in the picomolar range ⁵⁴. However, PMPA as well as several phosphonate-based PSMA inhibitors displayed poor pharmacokinetic properties resulting in a limitation of their potential therapeutic use.

The insertion of a phosphoramidate group for zinc coordination resulted in the development of a new class of PSMA pseudo-irreversible inhibitors ⁵⁵. These non-hydrolysable transition-state analogs of NAAG (Figure 11B) displayed increased PSMA affinity due to additional hydrogen bonds between the nitrogen of the phosphoramidate functionality and the oxygen of vicinal amino acids. The irreversible binding mode of phosphoramidate-based inhibitors and thus expected favorable *in vivo* properties regarding higher affinity and internalization rate as well as rapid tumor uptake have encouraged researchers to develop [¹⁸F]F-CTT1057 which is the most prominent phosphoramidate-based inhibitors so far. [¹⁸F]F-CTT1057 has even entered clinical trial as PET imaging agent in patients with prostate cancer prior to radical prostatectomy and in patients with metastatic castration resistant prostate cancer (mCRPC) ⁵⁶.

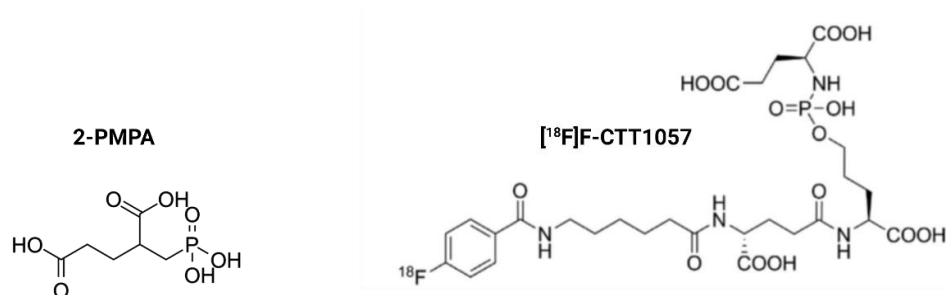


Figure 9 Phosphonate-based PSMA inhibitors

Another approach in the design of PSMA inhibitors was the replacement of the phosphonic functionality by an ureido group resulting in a compound that mimics the planar peptide bond of PSMA substrates such as NAAG without the ability to be hydrolyzed by the enzyme (Figure 11A). The resulted glutamate-ureido-based inhibitors have been the most investigated and applied group of PSMA inhibitors especially in nuclear medicine and radiopharmacy.

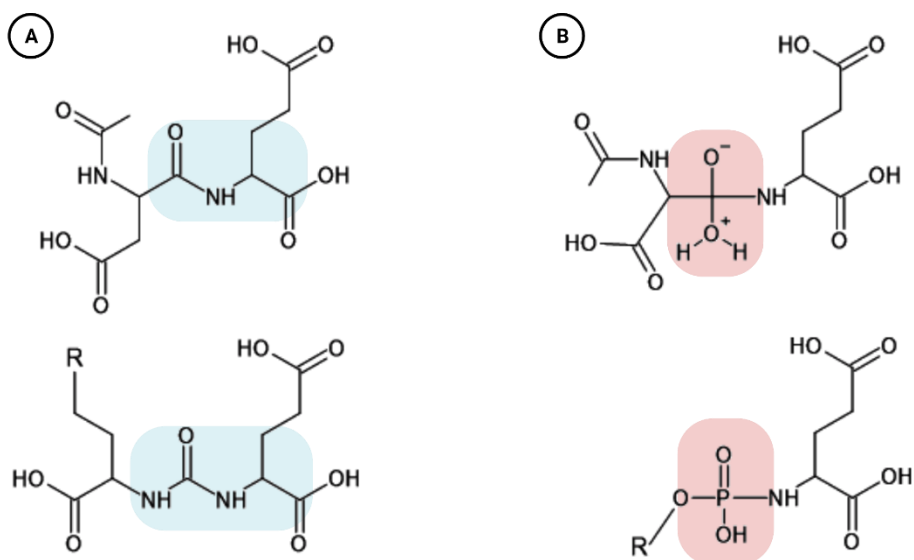


Figure 10 Design of PSMA inhibitors is based on two different approaches: urea-based PSMA inhibitors imitate the peptide bond of NAAG (A) whereas the phosphonate-based PSMA inhibitors mimic the transition state (B).

1.3.3 PSMA inhibitors for imaging

The first FDA-approved imaging agent targeting PSMA was the ^{111}In -labeled murine mAb 7E11-C5 (ProstaScint). However, one major limitation of 7E11-C5 is that it binds to the intracellular domain of PSMA, therefore can only detect apoptotic cells ^{57,58}. In order to overcome this drawback, the humanized mAb J591 which binds to an extracellular site of PSMA was developed ⁵⁹. Several clinical trials were conducted to investigate the pharmacokinetic profile of ^{89}Zr -labeled J591 for PET imaging as well as the therapeutic counterpart ^{177}Lu -labeled J591 which showed a hematological toxicity due to a long blood circulation half-life. In order to reduce this dose-limiting myelosuppression, ^{177}Lu -labeled J591 was applied in fractionated doses in several cycles ⁵⁹. This dose-fractionation strategy was also used in the study design of the ongoing clinical trial of ^{225}Ac -labeled J591 ⁵⁹.

Another radiolabeled PSMA antibody is ^{227}Th -labeled PSMA-TTC. The alpha-emitter thorium-227, with a half-life of more than 18 days, is complexed via the 3,2-HOPO chelator covalently bound to a fully human PSMA antibody. ^{227}Th -labeled PSMA-TTC is currently tested in a large multi-center, international, phase 1 study in pre-treated mCRPC patients ⁶⁰.

In addition to PSMA antibodies, efforts were made to exploit the advantages of small-molecule inhibitors for PSMA targeting (Figure 12). In the early 2000 Pomper et al. developed the first radiolabeled PSMA ligand [^{11}C]C-DCMC ⁶¹. Although this radiopharmaceutical displayed PSMA specificity and good tumor uptake in PSMA-positive xenografts, the short half-life of ^{11}C of about 20 min limited its clinical application and resulted in a shift towards the use of other radioisotopes with better characteristics.

[^{18}F]F-DCFBC was a fluorine-18 labeled derivative of DCMC, developed to take advantage of the favorable properties of the most predominate PET-nuclide fluorine-18 such as half-life of 109 min, low maximum positron energy resulting in higher spatial resolution and in particular lower radiation dose of patients due to high positron emission yield of 97%.

Although [^{18}F]F-DCFBC has been studied in several clinical trials, it displayed a major disadvantage, namely the long blood retention time due to high albumin-binding, thus a reduced tumor-to-blood ratio ^{62,63}. [^{18}F]F-DCFPyL was developed to overcome this drawback and has been so far one of the most PSMA imaging agents investigated in clinical trials ⁶⁴⁻⁶⁷.

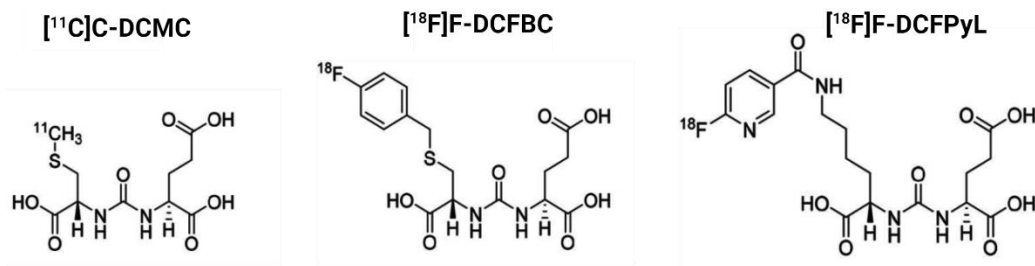


Figure 11 Radiolabeled PSMA-based PET imaging agents

The increasingly better understanding of the PSMA binding pocket led to a change of direction in the design of novel PSMA radiopharmaceuticals towards a modification of the linker moiety. Several PSMA inhibitors with different linkers were developed to enhance the binding affinity and improve the interaction of the PSMA ligands with the amino acids in the binding pocket. Herein, a group from Molecular Insight Pharmaceuticals (MIP) used an aminohexanoyl moiety to develop MIP-1072 and MIP-1095 (Figure 13), both labeled with the SPECT nuclide iodine-123. These PSMA ligands were the first halogenated urea-based PSMA agents with excellent inhibition potency and high tumor uptake^{68,69}. Their favorable properties paved the way for the development of ^{99m}Tc-labeled urea-based imaging agents. Among these ^{99m}Tc-labeled tracers, [^{99m}Tc]Tc-MIP-1404 showed the best pharmacokinetic properties and is the first PSMA SPECT diagnostic agent to complete a phase 3 clinical trials^{70,71}.

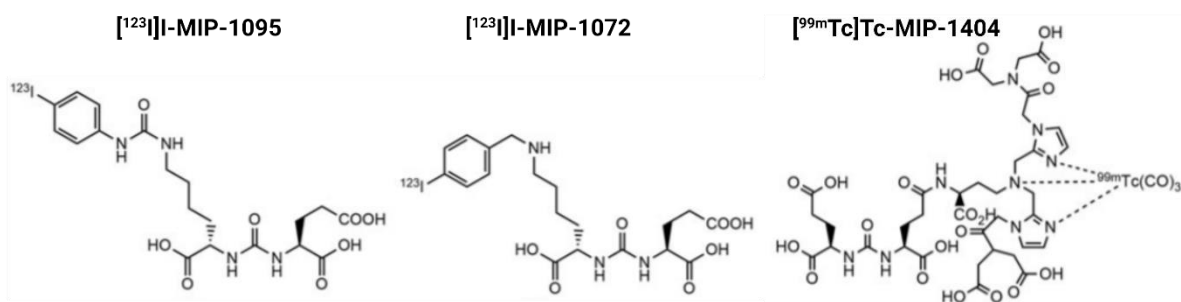


Figure 12 Radiolabeled PSMA-based SPECT imaging agents

In addition to the described radioisotopes, gallium-68 became more and more one of the most important radioisotopes in molecular imaging. Apart from its favorable properties, the availability of gallium-68 via a $^{68}\text{Ge}/^{68}\text{Ga}$ generator and therefore its cyclotron-independency was the major reason for its broad application in the design of novel PSMA imaging agents. In 2010 Banerjee et al. described the synthesis and preclinical evaluation of two $[^{68}\text{Ga}]\text{Ga}$ -DOTA-conjugated PSMA inhibitors and investigated the impact of the linker properties on binding affinity and *in vivo* pharmacokinetics ⁷². According to the obtained results, the use of an appropriate linker to guarantee a correct orientation of the radiotracer within the 20 Å tunnel as well as to provide a specific distance between the KuE binding motif and the gallium complex is of major importance. In addition, a hydrophobic linker seems to increase the binding potency probably through interaction with the lipophilic S1 pocket.

Further optimization of the linker moiety led to the development of the most prominent and the first FDA-approved PSMA PET imaging agent, $[^{68}\text{Ga}]\text{Ga}$ -PSMA-11 or $[^{68}\text{Ga}]\text{Ga}$ -PSMA-HBED-CC ^{73,74} (Figure 14). The KuE binding unit is coupled to the HBED-CC chelator via a 6-aminohexanoic acid linker resulting in an increase in lipophilicity thus improved binding affinity and internalization ratio. Furthermore, the HBED-CC chelator allows a straightforward radiolabeling with gallium-68 at room temperature in high yield and purity.

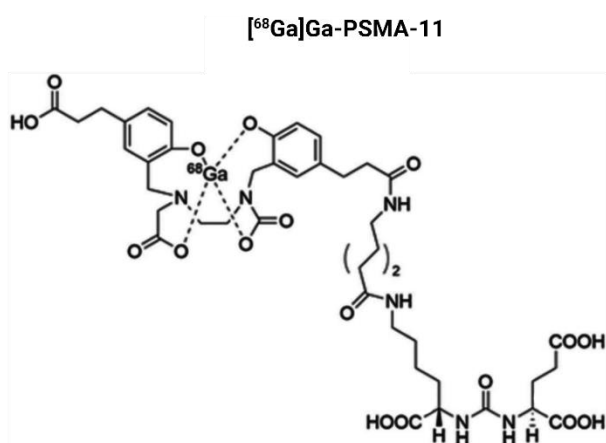


Figure 13 Chemical structure of $[^{68}\text{Ga}]\text{Ga}$ -PSMA-11

1.3.4 PSMA inhibitors for therapy

The positive results obtained from the several studies described above and in particular the successful translation of many of the PSMA radiopharmaceuticals to the clinic paved the way for the development of PSMA inhibitors for endoradiotherapy. Although the HBED-CC chelator displayed favorable properties, it is not suitable for complexing therapeutic nuclides such as lutetium-177. However, Benešová et al. could develop PSMA-617, a DOTA-based PSMA inhibitor that can be used for both diagnostic and therapeutic purposes. The DOTA chelator was conjugated to the KuE (lysine-urea-glutamate) unit by a hydrophilic 2-naphthyl-L-alanine linker which led to an improved pharmacokinetic profile of the tracer ⁷⁴. Subsequent to the outstanding results from clinical studies, [¹⁷⁷Lu]Lu-PSMA-617 was recently granted Breakthrough Therapy designation for treatment of patients with metastatic castration-resistant prostate cancer (mCRPC) ⁷⁵.

Parallel to the studies of Benešová et al., Weineisen et al. have developed PSMA I&T (imaging & therapy) using the bifunctional chelator DOTAGA and a D-amino acid linker to increase the metabolic stability *in vivo* ^{76,77}. Moreover, [⁶⁸Ga]Ga-PSMA-I&T displayed similar clinical efficacy as [⁶⁸Ga]Ga-PSMA-11 ⁷⁸. The therapeutic counterpart [¹⁷⁷Lu]Lu-PSMA-I&T is currently being tested in several clinical studies ⁷⁹. Noteworthy is that [²²⁵Ac]Ac-PSMA I&T has received the FDA Authorization of Investigational New Drug (IND) application for providing Targeted Alpha Therapy (TAT) for mCRPC in August 2021 ⁸⁰.

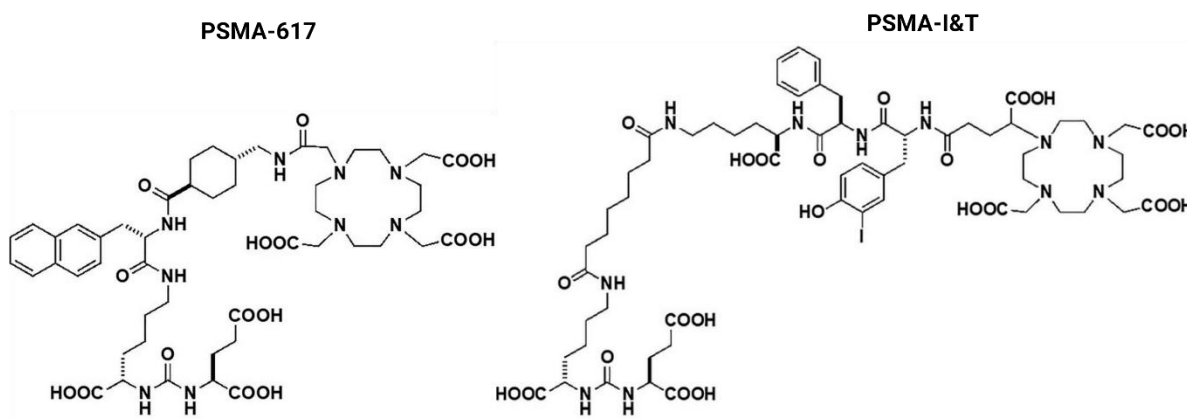


Figure 14 Chelator-based PSMA tracer for use in PC therapy

1.3.5 PSMA drug conjugates

Although the number of clinical trials with PSMA radioligands for either imaging or therapy has significantly increased in the last years, there are only few PSMA-targeted drug conjugates investigated so far. Targeting PSMA via mAb was the strategy adopted in the development of MLN2704 which was the first clinically tested PSMA-ADC. MLN2704 consists of the mAb J591 conjugated to the microtubule inhibitor maytansinoid 1 via a redox-sensitive disulfide linker⁸¹. Although MLN2704 displayed satisfying results in phase 1 clinical trial conducted with 23 patients, the further application was discontinued after phase 2 large cohort study due to severe adverse effects such as neurotoxicity. It was assumed that the instability of the ADC and the resulting premature release of the cytotoxic drug were the major reasons for this negative outcome⁸².

PSMA-MMAE is another PSMA-targeting ADC being recently investigated in several clinical trials. The main component of PSMA-MMAE is the fully human mAb IgG1 which is conjugated to the antimetabolic drug MMAE through a protease cleavable linker⁸³. Although the results of the phase 2 clinical trial, reported in 2020, showed a lower neurotoxicity than MLN2704, instability of the drug conjugates and subsequent deconjugation even though an enzyme cleavable linker is used, were still the major limitation of further clinical application^{83,84}. A similar fate was faced by MEDI3726, a PSMA-ADC with high specific cytotoxicity *in vitro* but insufficient tolerability in patients. Further development was discounted after the outcomes of the phase 1 study⁸⁵.

Generally, it can be concluded that the investigated PSMA-ADC have failed so far in delivering the cytotoxic payload specifically to the tumor due to their instability in blood circulation and the subsequent premature drug release. One possible approach to avoid these pitfalls is the development of small-molecule drug conjugates through replacement of the mAb in ADCs with small-molecule inhibitors. Inspired by the successful implementation of this approach in PSMA radiopharmaceuticals, several efforts were made to apply the lessons learned from the PSMA-research until now.

Roy et al. described a PSMA-SMDC consisting of the high affinity targeting moiety DUPA, a disulfide linker and an indenoisoquinoline topoisomerase I inhibitor (Figure 16). Additionally, a peptide linker is used to improve the hydrophilicity and improve the orientation of the SMDC within the PSMA binding pocket. The DUPA-drug conjugate displayed high binding affinity *in vitro* along with antitumor efficacy and good tolerability in xenograft models ⁸⁶.

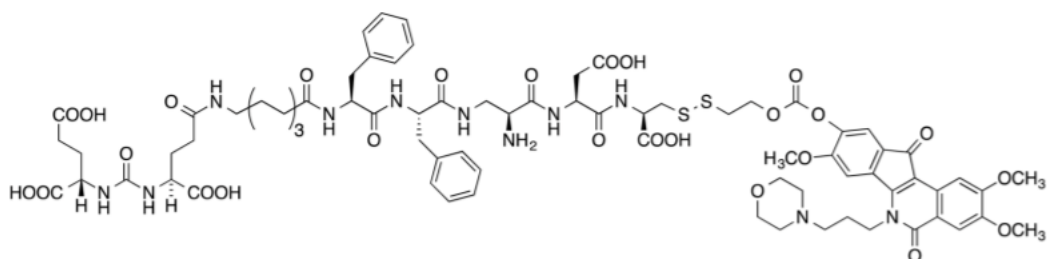


Figure 15 DUPA-based PSMA topoisomerase I inhibitor conjugate

Based on these promising results, another DUPA-SMDC (Figure 17) was developed using paclitaxel as cytotoxic drug in addition to a disulfide linker to ensure a tumor specific release. DUPA-PTX could also achieve encouraging results in cell assays and animal studies ⁸⁷.

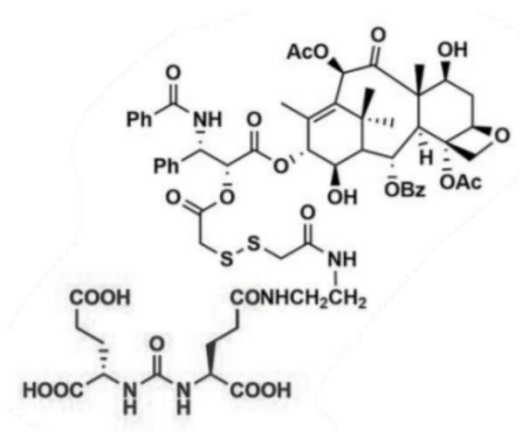


Figure 16 DUPA-based PSMA paclitaxel conjugate

In 2019, a research group from the Endocyte company published preclinical results of EC1169 which is the first PSMA-SMDC to enter clinical trials. EC1169 is composed of the KuE-PSMA binding unit, the antimitotic drug tubulysin B hydrazide and a disulfide-based linker (Figure 18). It showed outstanding features in terms of good binding affinity *in vitro*, high therapeutic efficacy and safety *in vivo* compared to docetaxel, which is the standard of care chemotherapeutic agent in the management of mCRPC ⁸⁸. This favorable profile encourages the further testing in a phase 1 clinical trial ⁸⁹.

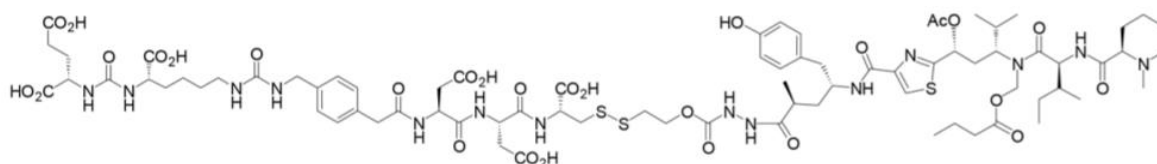


Figure 17 Chemical structure of EC1169

In January 2021, Wang et. al presented the results obtained from preclinical studies of a novel PSMA targeting SMDC. PSMA-1-VcMMAE was developed based on PSMA-ADC through replacement of the mAb through the small molecule PSMA-1. Both PSMA drug conjugates use MMAE as cytotoxic drug and the cathepsin cleavable linker valine-citrulline (Figure 19). However, PSMA-ADC displayed a higher cytotoxic potency in PSMA-positive cells probably due to the higher affinity of the mAb to PSMA. Nevertheless, animal studies proved the superiority of PSMA-1-VcMMAE over PSMA-ADC in terms of a larger therapeutic index ⁹⁰.

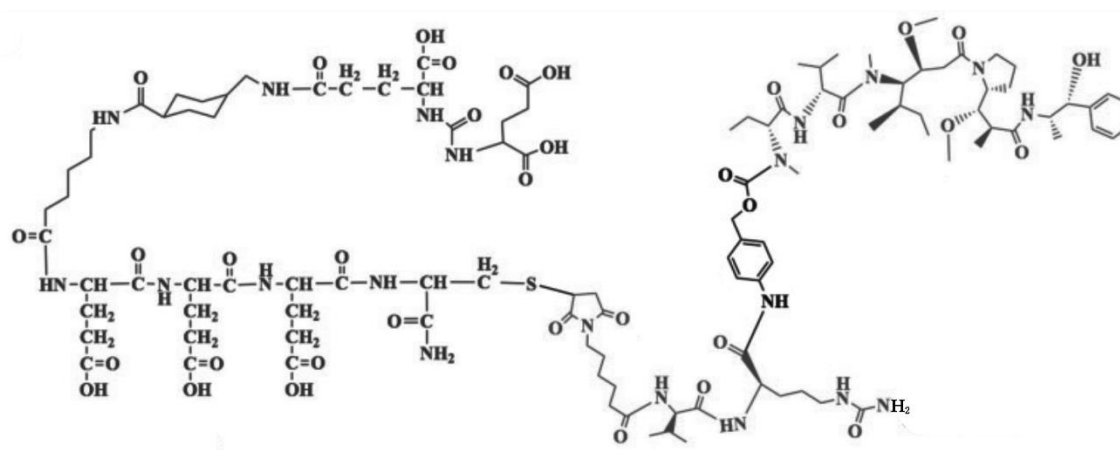


Figure 18 Chemical structure of PSMA-1-VcMMAE

Table 3 PSMA drug conjugates that are either preclinically or clinically investigated.

	PSMA drug conjugates	Targeting unit	payload	status
PSMA ADCs	MLN2704	J591	maytansinoid 1	discontinued at phase 2
	PSMA-MMAE	IgG1	MMAE	discontinued at phase 2
	MEDI3726	IgG1	pyrrolobenzodiazepine	discontinued at phase 1
PSMA SMDCs	DUPA-SMDC	DUPA	indenoisoquinoline topoisomerase I inhibitor	preclinical studies
	DUPA-PTX	DUAP	paclitaxel	preclinical studies
	EC1169	KuE	tubulysin B	phase 1 NCT02202447
	PSMA-1-VcMMAE	PSMA-1	MMAE	preclinical studies
	SBPD-1	KuE	MMAE	preclinical studies

2 Objectives

Cancer diseases are the second-leading cause of death worldwide. The demographic shift toward an aging society especially in the industrial world, the unhealthy life-style and the increased exposure to cancerogenic agents, mainly because of the rising pollution, are some of the reasons of this dramatic development.

Conventional imaging and in particular treatment approaches have shown significant limitations and restrictions thus demonstrating the urgent need for new efficient and particularly specific anti-cancer strategies. In the last decades a fundamental change has taken place from a systemic therapy targeting all proliferating cells, even healthy cells such as cells of the bone marrow and gastrointestinal tract, toward a targeted and personalized therapy. Major advances in the field of molecular analysis and biotechnology paved the way for the discovery of novel tumor biomarker and enabled a profound understanding of carcinogenesis and tumor metabolism.

The identification of tumor-associated biomarker such as HER² (human epidermal growth factor receptor 2) in breast cancer, EGFR (epidermal growth factor receptor) mutations in lung cancer or BCR-ABL (breakpoint cluster region gene-Abelson) in chronic myeloid leukemia are few examples of breakthrough innovations in cancer research.

Accordingly, the discovery of PSMA in the late 90's has also revolutionized the management of prostate cancer resulting in a development of a series of high affinity selective PSMA radiopharmaceuticals for imaging as well as for endoradiotherapy. this intensive research has recently led to the approval of two PSMA inhibitors, [⁶⁸Ga]Ga-PSMA-11 and [¹⁷⁷Lu]Lu-PSMA-617. However, the approval of further PSMA ligands would certainly follow soon.

In contrast, research in the field of drug delivery conjugates could not yet achieve such milestones. The developed PSMA-ADCs failed in demonstrating safety and tolerability in clinical trials although they displayed outstanding preclinical properties. Research groups are now focusing their efforts in optimizing alternative drug conjugates with small-molecules as targeting vector. Nevertheless, there is only one PSMA-SMDC in clinical trial until now. Thus, the next few years will reveal if the SMDCs will make the translational leap to a clinical application.

Although most PSMA ligands investigated so far displayed promising results in preclinical and even in clinical studies, they still have some major drawbacks especially regarding their pharmacokinetic properties. Clinical studies with [^{177}Lu]LuPSMA-617 showed high uptake in salivary glands which seems to be partly PSMA-specific since there are a lower level of PSMA expression in this organ. The irradiation of the salivary glands particularly with therapeutic nuclides such as lutetium-177 and actinium-225 and the resulting xerostomia are dose-limiting adverse effects of PSMA-617 radioligands impacting severely the safety and tolerability of the treatment⁹². The physiological expression of PSMA in the kidney should also be taken into account by the design of PSMA ligands for endoradiotherapy to avoid possible nephrotoxicity.

Additionally, the change of direction in the management of cancer diseases toward a personalized therapy requires a profound characterization of the molecular profile of the tumor prior to treatment. In the case of PSMA, PET/CT imaging should be conducted prior to therapy in order to localize the tumor and more importantly assess its PSMA expression and thus the suitability of a PSMA endoradiotherapy. In this concern, developing a theranostic compound, that is able to complex both diagnostic and therapy nuclides, is of great benefit. This theranostic approach is to some extent realized through the use of theranostic pairs such as [^{68}Ga]Ga-PSMA-11 for PET/CT imaging followed by [^{177}Lu]Lu-PSMA-617 or [^{225}Ac]Ac-PSMA-617 for Therapy. However, the varying molecular structure of these PSMA radiopharmaceuticals and the resulting differences, not only in physicochemical properties but more importantly in the pharmacokinetic behavior, should be taken into account.

Besides, it has been shown that the use of PSMA as molecular target for drug delivery is an equally promising approach as its application in nuclear medicine and radiopharmacy. However, PSMA-targeted drug delivery is still in its early stages. The currently reported drug conjugates have to be either optimized in terms of safety profile or clinically validated.

This dissertation aims to address some of these needs and challenges and can be divided into several parts as shown in figure 21.

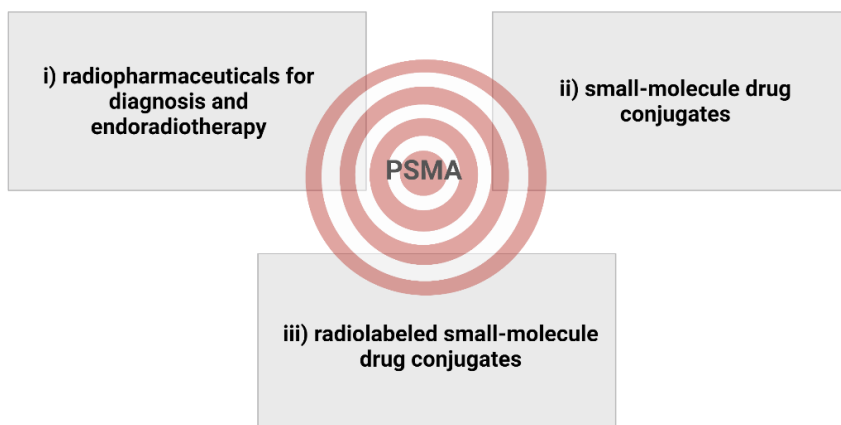


Figure 20 Overview of the projects of the PhD thesis

In the first part (i), several structure-activity relationship studies are conducted to investigate the impact of targeting unit, linker moiety and chelator on PSMA binding affinity. The goal of these studies was to identify appropriate candidates that were not only easily synthesized and effectively labeled but that especially displayed favorable pharmacokinetic properties, high PSMA binding affinity and selectivity. Additionally, one of the major objectives of this research was also the development of theranostic PSMA radioligands that can be labeled with diagnostic nuclides such as gallium-68 or scandium-44 as well as with the therapeutic isotope lutetium-177.

Furthermore, the focus of this PhD project was also the design and preclinical evaluation of PSMA-targeted SMDCs (ii). Beside the selection of appropriate drugs that can be used as active compounds, intensive considerations about the molecular design of such drug conjugate were made prior to synthesis. In addition, it was also of crucial importance to establish cell- and enzyme-based assays that were required to assess the cytotoxicity and selectivity of the synthesized compounds.

Finally, a novel strategy that incorporate an active drug in PSMA radiopharmaceuticals resulting in radiolabeled SMDCs should be investigated for its feasibility (iii). These “trimeric” conjugates consist of three main parts: a PSMA binding unit to ensure tumor targeting, an active pharmaceutical ingredient and a chelator able to complex diagnostic as well as therapeutic isotopes. The concept of this strategy was on the one hand, to assess the patient suitability with e.g., gallium-68-labeled low-dose SMDC using PET/CT prior to therapy with the same SMDC, this time, however, labeled with lutetium-177.

On the other hand, a bisphosphonate radiolabeled SMDC should be developed to treat bone metastases frequently occurring in mCRPC. In the context of dual targeting principle, both PSMA and hydroxyapatite bone structures are addressed. Figures 22-23 summarize the implied *in vitro* and *in vivo* characterization methods.

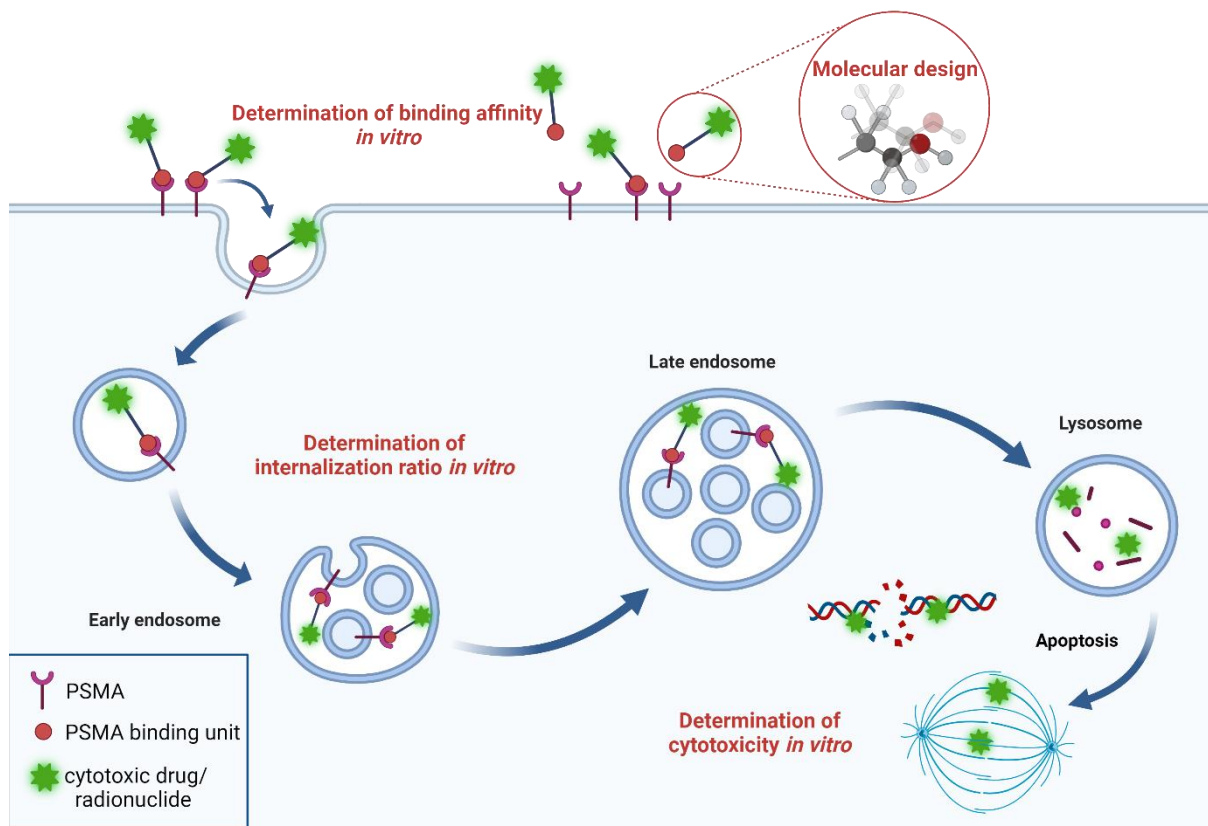


Figure 21 Schematic illustration of the applied *in vitro* experiments. Several considerations on the appropriate molecular design are conducted prior to synthesis. The binding affinity as well as the internalization ratio are determined using PSMA⁺-cells. In case of the SMDCs, cytotoxic studies are performed to assess the potency of the drug conjugates as well as the mechanism of action.

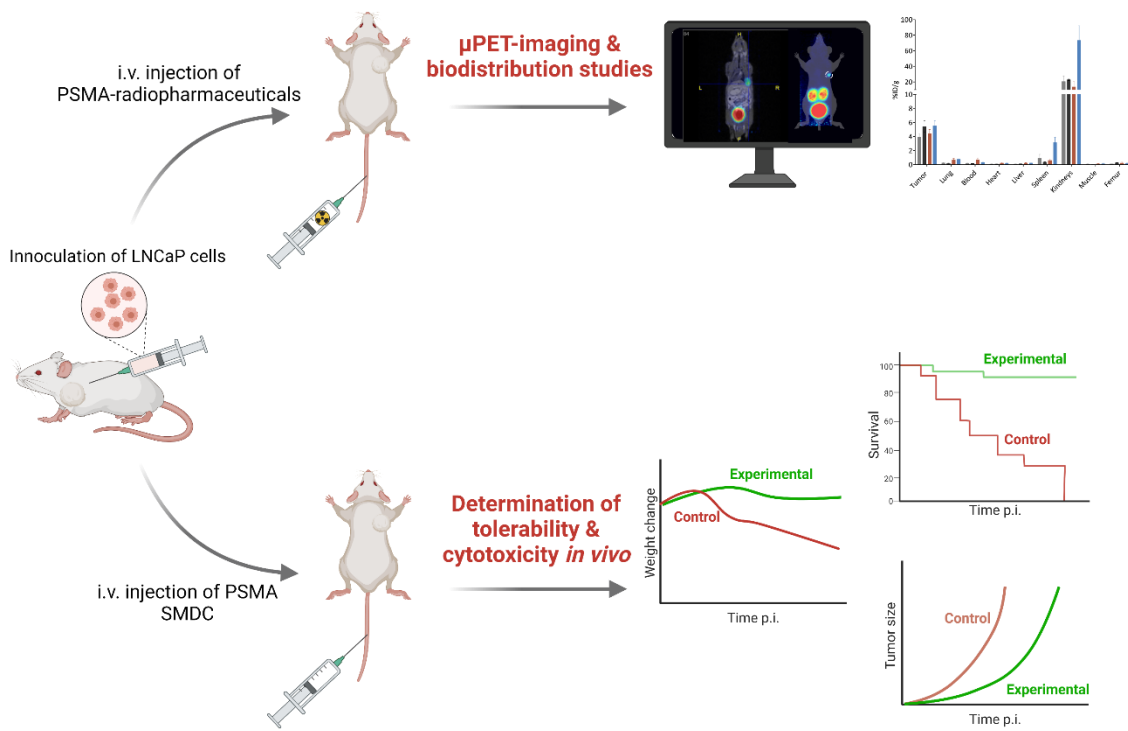


Figure 22 Schematic illustration of the applied in vivo experiments. The PSMA radiopharmaceuticals are tested in tumor-bearing mice via μ PET imaging and biodistribution studies. Efficacy and tolerability of the PSMA-SMDC are determined through monitoring of changes in weight and tumor volume. The survival rate is characterized as Kaplan-Meier curves. Studies are carried out with well-known reference substances to provide adequate comparability.

3 Manuscripts

This dissertation is based on several manuscripts, which are listed below along with their respective author involvement.

Squaric acid based-radiopharmaceuticals for tumor imaging and therapy

Published in *Bioconjugate Chemistry* 2021;32(7):1223-1231

Author contribution: [REDACTED] conducted literature research to the Methods for linking biomolecules and stated the synthetic features and benefits of squaric acid. **H. Lahnif** conducted literature research to the use of squaric acid as linker moiety for radiopharmaceuticals targeting prostate-specific membrane antigen. [REDACTED] summarized the role of squaric acid as linker moiety for radiopharmaceuticals targeting Fibroblast Activation Protein. [REDACTED] resumed the benefits of squaric acid as linker in antibody-based radiopharmaceuticals. [REDACTED] and **H. Lahnif** wrote the introduction and conclusion. [REDACTED] critically reviewed the manuscript. [REDACTED] supervised the project.

Hybrid chelator-based PSMA-radiopharmaceuticals: translational approach

Published in *Molecules* 2021; 26(21), 6332.

Author contribution: [REDACTED], **H. Lahnif**, [REDACTED], and [REDACTED] conceived and planned the experiments; [REDACTED] performed the synthesis and radiolabeling and carried out the *in vitro* stability studies. **H. Lahnif** maintained the LNCaP cells and carried out the *in vitro* binding studies and the internalization studies. [REDACTED], **H. Lahnif** and [REDACTED] conducted the *in vivo* studies. **H. Lahnif** evaluated the data from *in vitro* binding studies and internalization studies as well as from animal studies. [REDACTED] and **H. Lahnif** wrote and edited the manuscript. [REDACTED] and [REDACTED] supervised the project and reviewed the manuscript.

Old drug, new delivery strategy: MMAE repackaged

In preparation

Author contribution: [REDACTED], **H. Lahnif**, [REDACTED], and [REDACTED] conceived the experiments; [REDACTED] performed the synthesis. **H. Lahnif** maintained the LNCaP cells and carried out the *in vitro* binding studies, the immunofluorescence studies and the cytotoxicity studies. [REDACTED] and **H. Lahnif** planned the animal experiments. [REDACTED] conducted the *in vivo* studies. **H. Lahnif** evaluated the data from *in vitro* binding studies and cytotoxicity studies as well as from animal studies. [REDACTED], **H. Lahnif** and [REDACTED] wrote and edited the manuscript. [REDACTED] supervised the project and reviewed the manuscript.

DOTA conjugate of Bisphosphonate and PSMA-inhibitor: A promising combination for therapy of prostate cancer related bone metastases

In preparation

Author contribution: [REDACTED], **H. Lahnif** and [REDACTED] conceived the experiments; [REDACTED] performed the synthesis, the radiolabeling, the stability and lipophilicity studies and the binding studies on HAP. **H. Lahnif** maintained the LNCaP cells and carried out the *in vitro* binding studies. [REDACTED], **H. Lahnif** and [REDACTED] conducted the animal experiments. [REDACTED] evaluated the data from stability, lipophilicity and HAP-binding studies. **H. Lahnif** evaluated the data from *in vitro* binding studies and animal studies. [REDACTED], **H. Lahnif** wrote and edited the manuscript [REDACTED] and [REDACTED] supervised the project and reviewed the manuscript.

Squaric acid based-radiopharmaceuticals for tumor imaging and therapy

[REDACTED]#, Hanane Lahnif#, [REDACTED], [REDACTED],
[REDACTED], [REDACTED]

#Both authors contributed equally

Department of Chemistry – TRIGA site, Johannes Gutenberg University Mainz, 55128 Mainz, Germany

ABSTRACT

Targeting vectors bound to a chelator represent a significant fraction of radiopharmaceuticals used nowadays for diagnostic and therapeutic purposes in nuclear medicine. The use of squaramides as coupling units for chelator and targeting vector helps to circumvent the disadvantages of several common coupling methods. This review gives an overview of the use of squaric acid diesters (SADE) as linking agent. It focuses on the conjugation of cyclic chelators, e.g., DOTA (1,4,7,10-tetraazacyclododecane-1,4,7,10-tetraacetic acid), as well as hybrid chelators like AAZTA⁵ (6-pentanoic acid-6-amino-1,4-diazepine tetracetic acid) or DATA^{5m} (6-pentanoic acid-6-amino-1,4-diazapine-triacetate) to different targeting vectors, e.g., prostate-specific membrane antigen inhibitors (KuE; PSMAi), fibroblast activation protein inhibitors (FAPi) and monoclonal antibodies (mAbs). An overview of the synthesis, radiolabeling, *in vitro* and *in vivo* behavior of the described structures is given. The unique properties of SADE enable a fast and simple conjugation of chelators to biomolecules, peptides and small molecules under mild conditions. Furthermore, SA-containing conjugates could not only display similar *in vitro* characteristics in terms of binding affinity when compared to reference compounds, they may even induce beneficial effects on the pharmacokinetic properties of these radiopharmaceuticals.

Keywords: Squaric acid, Squaramide, PSMA, FAP, monoclonal antibodies

Introduction

The development of effective cancer diagnosis and treatment strategies is one of the most important concerns of cancer research and patient treatment. Over the last decades, the use of radiolabeled compounds has become increasingly important. With the use of radiopharmaceuticals for diagnostic imaging as well as for therapeutic approaches, nuclear medicine provides an important contribution to medical health care. This strategy is described as “Theranostics”, which supports “precision oncology”. Figure 1 gives a simplified sketch on the targeting vectors discussed in the following sections.

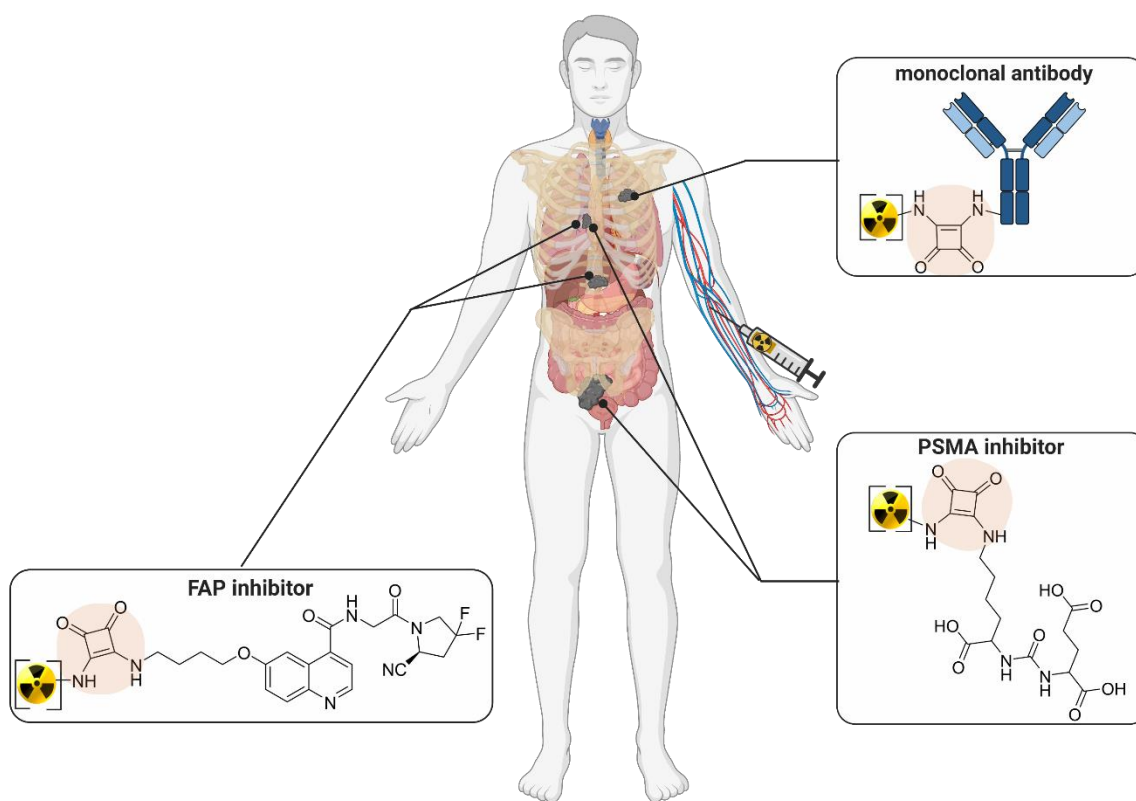


Figure 1 Benefits of tumor-targeting in nuclear medicine. Bifunctional chelators labeled with radioisotopes for diagnosis (e.g., ^{68}Ga , ^{44}Sc) or therapy (e.g., ^{177}Lu , ^{225}Ac) attached to a targeting moiety e.g., antibody, PSMA-inhibitor or FAP-inhibitor via appropriate linker. Radiotracers accumulate in target tissue and allow precise diagnosis and treatment with reduced side-effects. (Created with BioRender.com)

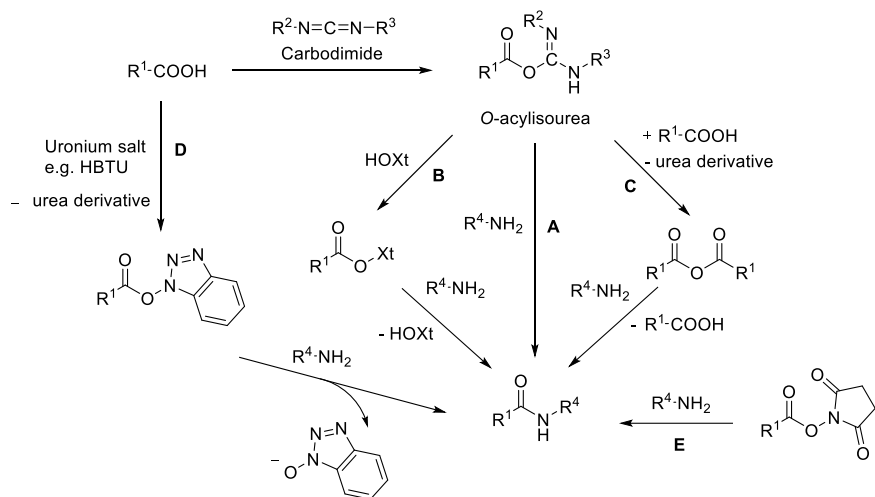
The use of radiometals in radiotracers is highly relevant in both imaging and systemic targeted radiotherapy. However, they necessitate a complexation through a chelator since they can't be covalently bound in contrast to other radioisotopes such as fluorine-18. The chelators are covalently bound to target vectors^{1,2} This linkage normally involves typical amide formation reactions or other linkage types like thioureas or triazoles. Alternatively, coupling via squaric acid diethyl ester (SADE) enables the synthesis of asymmetric squaric acid based bisamides. This review highlights the advantages of the use of SADE as coupling agent in radiopharmaceutical chemistry in terms of versatility and ease of synthesis. In addition, it summarizes recent results of radiolabeling, *in vitro* and *in vivo* studies of SADE conjugated radiopharmaceuticals.

Overview of methods for linking biomolecules

One of the most used synthetic reactions in medical chemistry nowadays is amide bond formation³. There are several coupling reagents for amide bond formation and methods for the conjugation of biomolecules. These methods include the use of carbodiimides (Figure 2; A)^{4,5} as well as carbodiimides in combination with additives such as N-hydroxyl derivatives of benzotriazoles (Figure 2; B)^{4,5}, anhydrides (Figure 2; C)⁴, uronium salts, such as HBTU (Figure 2; D)⁴⁻⁷ or NHS esters (Figure 2; E)^{8,9}. One major drawback of all of these approaches is the possibility of excessive formation of side products. This is due to the high reactivity of the formed amine intermediates. A common side-product of e.g., carbodiimides is the formation of unreactive *N*-acylurea of the acid used in the synthesis^{4,5}. In addition, many functional groups must be protected, otherwise they may also react and form side-products^{4,6,7}. Also, instability (anhydrides) or sensitivity to water (NHS esters) is a problem with some coupling reagents^{4,8,9}.

Apart from the coupling reagents mentioned here as examples, a large number of other methods and compounds for the formation of amide bonds have been developed in recent decades⁴

Amide bond formation strategies



Other coupling strategies

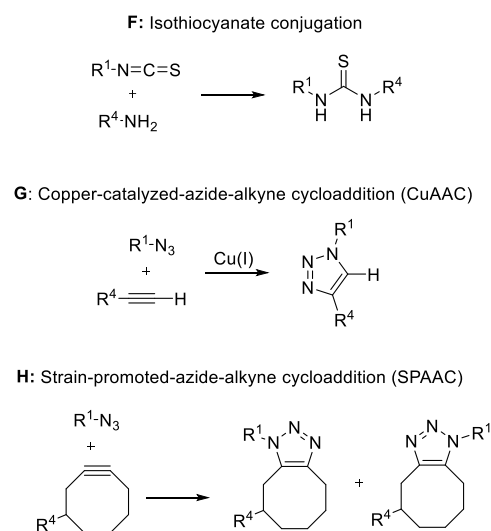


Figure 2: Some examples of widely used coupling techniques in medicinal chemistry

A variety of other methods for linking biomolecules are also available. For example, isothiocyanates (Figure 2; F) can be used. These isocyanates are more stable than e.g., NHS esters due to their lower reactivity. However, it is described that some thiourea conjugates tend to decompose over time¹⁰. Another important method is the copper(I)-catalyzed Huisgen 1,3-dipolar cycloaddition which is a typical “Click reaction”. This Cycloaddition is widely used not only in medicinal chemistry but also in fields like material sciences (Figure 2; G)^{11,12} and has received more and more attention in radiopharmacy¹³. The copper catalyzed cycloaddition (CuAAC) of an azide residue and a terminal alkyne leads to the formation of a 1,2,3-triazole. This method of coupling is highly selective, but both reactive groups usually have to be synthetically integrated into the corresponding compounds prior to the reaction. High-coupling yields at mild temperatures can be achieved in short reaction times. However, cytotoxic copper(I) used here as catalyst, needs to be removed prior to *in vivo* applications^{14,15}. The strain-promoted-azide-alkyne-cycloaddition (SPAAC) avoids the problem of using cytotoxic metal catalysts by using strained cyclooctyne rings (Figure 2; H). This forces the ring system into a geometric state similar to the transition state of CuAAC, thus reducing the activation energy without the need for a catalyst. However, this introduces another large unit into the molecule, which can have an influence on pharmacology. Another major drawback is the lack of regioselectivity in the transition state, leading to the formation of two regioisomers^{16-18, 93-95}.

Synthetic features of squaric acid and squaric acid diesters

Due to the strong mesomeric stabilization of the dianion, the cyclic diacid so called squaric acid (3,4-dihydroxycyclobut-3-en-1,2-dione, SA) is a strong acid comparable to sulfuric acid ($pK_{a1} = 0.5-1.2$; $pK_{a2} = 2.2-3.5$) and has an aromatic character. Squaric acid is planar and follows the Hückel's rule for aromatic systems ($[4n+2]$ π -electrons). This results in the delocalization of the cyclic electrons of the ring system and leads to an energetic stabilisation of the dianion ¹⁹⁻²¹.

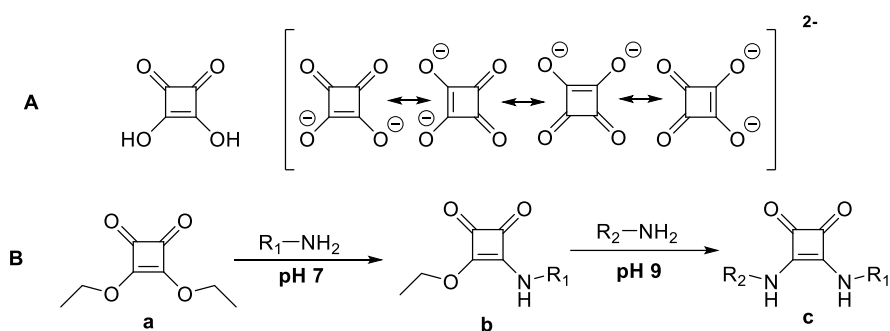


Figure 3: A) Structure and mesomeric stabilization of squaric acid. B) Scheme asymmetric amidation of SADE with different amines. First amidation is carried out at pH 7. Reaction at pH 9 leads to an amidation of the second amine. pH values apply to aqueous solutions. The reactions are driven by change in aromaticity ^{22,23}.

Cohen first described the synthesis of squaric acid in 1965 ²⁴. Over the years, interest in the use of squaric acid has grown. This ranges from the use as organocatalyst ^{25,26}, supramolecular self-assembly motifs ^{26,27}, chelating agent for metal ions ²⁸, bioisosteres in drug design ²⁹ and the use in bioconjugation ^{20,26}.

SADE as coupling reagent shows advantages over other coupling agents. The ester groups react selectively with amines. It is not necessary to protect other nucleophilic groups and therefore deprotection of potentially sensitive biomolecules is not required. Amines are often already components of biomolecules and do not need to be inserted preparatively. Additionally, no side reactions can be observed. Hydrolysis was not observed in the previous work and the work summarized here. This could be explained by the aromatic stability of the amide-like bonds, as described below ²⁰. The reaction takes place under mild conditions ^{20,30}. There is no limitation to specific solvents. Both organic and aqueous media are possible

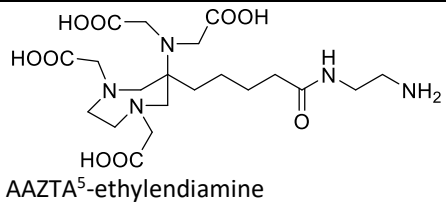
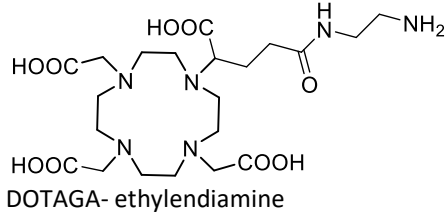
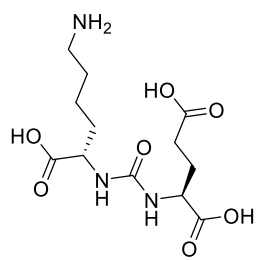
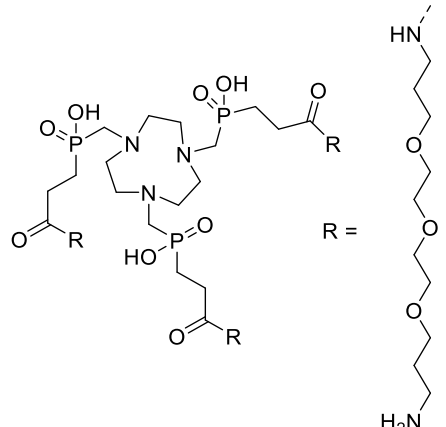
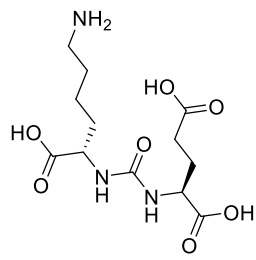
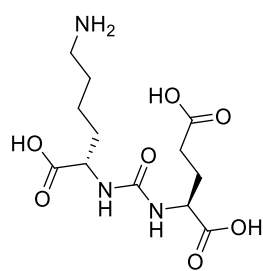
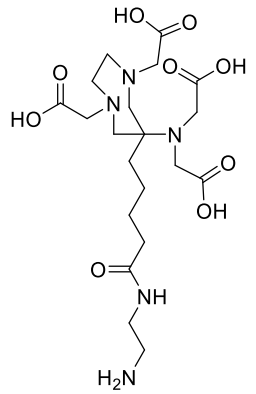
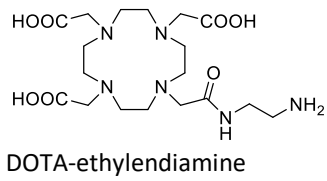
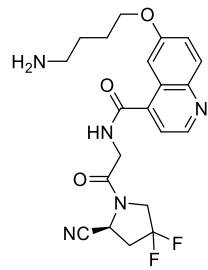
^{20,31,32} 96-98

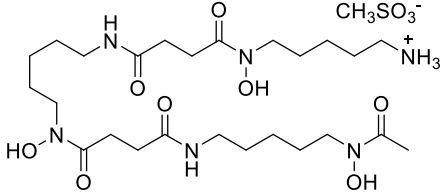
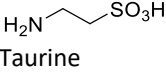
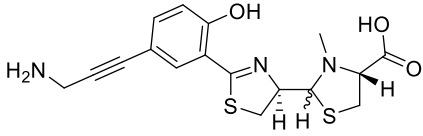
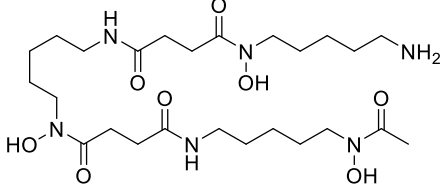
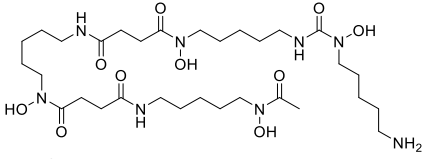
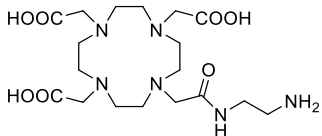
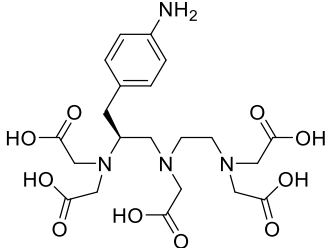
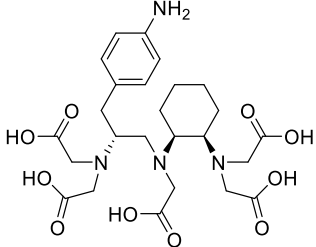
Amidation can be performed asymmetrically by controlling the pH-value in aqueous conditions or the basic conditions in organic solvents (Figure 3B) ³⁰. The asymmetrical reaction process is enabled by the change in aromaticity of the intermediate stages at different basic conditions ^{30,33}. The first amidation results in a monoamide (Figure 3B, b). Under more basic conditions, this monoamide is deprotonated, enabling a second amidation. The formed diamide (Figure 3B, c) is most stable since it has the highest aromatic stability of the series ^{22,31,33}.

SA (squaric acid) can provide donor atoms for complexations of metal ions, which may have both positive and negative effects on the complexation of the chelator and stability ²³. The negative effect of SA influence can be observed when TRAM.SA.KuE (**9**, Table 1) is labeled with ⁶⁸Ga. Actually, the TRAM ((1,4,7-triazonane-1,4,7-triyl) tris(methylene)) tris((1-amino-15-oxo-4,7,10-trioxa-14-azaheptadecan-17-yl) phosphinic acid) chelator is known for its perfect labelling properties with ⁶⁸Ga ³⁴. In this case, radiolabeling is not possible at moderate temperatures. The reason can be seen in a steric hindrance and a competition of the carbonyl groups of the SA units for complexation of Ga(III) ³⁴. On the other hand, It is postulated that the squaric acid motif coordinates to Zr(IV) in addition to the three hydroxamate groups of DFO, potentially providing an octadentate chelating unit and thus being responsible higher radiochemical yields and higher chelator/metal complex stabilities ³⁵. However, these findings are still under discussion ^{36,37}.

Table 1: Overview of squaric acid mediated conjugations in radiopharmaceutical sciences (* = unpublished data)

#	R ¹	R ² -NH ₂	Cond. A	R ³ -NH ₂	Cond. B	Ref.
1	Ethyl	 NODAGA-ethylendiamine	Phosphate buffer (0.5M, pH 7), r.t. 2h, 93 %	 KuE	Phosphate buffer (0.5M, pH 9), r.t. 36 h, 20 %	99
2	Ethyl	 DATA ^{5m} -ethylendiamine	Phosphate buffer (0.5M, pH 7), r.t. 16 h, 31 %	 NH ₂ -UAMC1110 (NH ₂ -FAPi)	Phosphate buffer (0.5M, pH 9), r.t. 16 h, 42 %	100
3		 H ₃ DFO mesylate	Ethanol, DI-PEA, 50 °C, 0.5h, 83 %	Trastuzumab	Borate buffer (0.5M, pH 9), r.t., overnight.	101
4	Methyl	 spermexatol	Methanol, NEt ₃ , 23 °C, 6h, 86 %	Polycyclic peptide antibiotic Gallidermin	Borate buffer (pH 9), 4 °C, 14h, 58 %	102
5	Ethyl	 H ₃ DFO mesylate	Ethanol, DI-PEA, 50 °C, 0.5h, 83 %	Monoclonal IgG antibody against herpes simplex viral protein glycoprotein D (gD)	Borate buffer (0.5M, pH 9), r.t., overnight	101,103

6	Ethyl	 <p>AAZTA⁵-ethylenediamine</p>	Phosphate buffer (0.5M, pH 7), r.t. 24 h, 29 %	Bevacizumab	Phosphate buffer (0.5M, pH 9), r.t. 24 h, Chelator-to-antibody-ratio (CAR): 0.29	104
7	Ethyl	 <p>DOTAGA-ethylenediamine</p>	Phosphate buffer (0.5M, pH 7), r.t. 2h, 75 %	 <p>KuE</p>	Phosphate buffer (0.5M, pH 9), r.t. 24 h, 39 %	99
8	Ethyl	 <p>NH₂-TRAM</p>	Phosphate buffer (0.5M, pH 7), r.t. 36h, 20 %	 <p>KuE</p>	Phosphate buffer (0.5M, pH 9), r.t. 36 h, 20 %	99
9	Ethyl	 <p>KuE</p>	Phosphate buffer (0.5M, pH 7), r.t. 12h, 23 %	 <p>AAZTA⁵-ethylenediamine</p>	Phosphate buffer (0.5M, pH 9), r.t. 12 h, 30 %	97
10	Ethyl	 <p>DOTA-ethylenediamine</p>	Phosphate buffer (0.5M, pH 7), r.t. 16 h, 63 %	 <p>NH₂-UAMC1110 (NH₂-FAPi)</p>	Phosphate buffer (0.5M, pH 9), r.t. 16 h, 73 %	100

11	Ethyl	 <p>H₃DFO mesylate</p>	Ethanol, DIPEA, 50 °C, 0.5h, 83 %	 <p>Taurine</p>	Ethanol/ water (1:1), 60 °C, 6h	101
12	Methyl		Methanol, NEt ₃ , 23 °C, 6h, 24 %	Polycyclic peptide antibiotic Gallidermin	Borate buffer (pH 9), 23 °C, 14h, 40 %	102
13	Methyl	 <p>H₃DFO</p>	Methanol, NEt ₃ , 23 °C, 6h, 88 %	Polycyclic peptide antibiotic Gallidermin	Borate buffer (pH 9), 23 °C, 14h, 45 %	102
14	Ethyl	 <p>DFO*</p>	Ethanol, DIPEA, 50 °C, 3h, 39 %	Monoclonal IgG antibody against herpes simplex viral protein glycoprotein D (gD)	Borate buffer (0.5M, pH 9), r.t., overnight	101,103
15	Ethyl	 <p>DOTA-ethylendiamine</p>	Phosphate buffer (0.5M, pH 7), r.t. 24 h, 41 %	Bevacizumab	Phosphate buffer (0.5M, pH 9), r.t. 24 h.	104
16	Ethyl	 <p>DTPA-<i>p</i>-Bn-NH₂</p>	Phosphate buffer (0.5M, pH 7), r.t. 24 h, 7 %	Bevacizumab	Phosphate buffer (0.5M, pH 9), r.t. 24 h, CAR: 5.4	104
17	Ethyl	 <p>CHX-A''-DTPA-<i>p</i>-Bn-NH₂</p>	Phosphate buffer (0.5M, pH 7), r.t. 24 h, 16 %	Bevacizumab	Phosphate buffer (0.5M, pH 9), r.t. 24 h, CAR: 6.1	104

Squaric acid mediated conjugation of bifunctional chelators to biomolecules or small molecules and radiolabeling of those conjugates

Despite the broad application of SADE in synthetic organic chemistry or chemistry in general as previously described, it received little attention in radiopharmaceutical chemistry. In literature few compounds are known where SADE serves as a linker of bifunctional chelators and a target structure. Most prominent is the conjugation of the chelator deferoxamine to complex ^{89}Zr for immuno-PET imaging ^{35,38,39}.

Yet, there is a number of radiometals other than ^{89}Zr and a variety of chelators other than DFO. Among several cyclic chelators, DOTA (1,4,7,10-tetraazacyclododecane-1,4,7,10-tetraacetic acid) and NOTA (1,4,7-triazacyclononane-1,4,7-triacetic acid) are prominent representatives. DOTA and its derivatives, like DOTAGA (1,4,7,10-tetraaza-cyclododecane-1-pentandiacid-4,7,10-triacetic acid), are suitable for several relevant radiometals (e.g. ^{68}Ga , ^{44}Sc , ^{111}In , ^{225}Ac , ^{177}Lu). Therefore, they are the most frequently used chelators in nuclear medicine ¹.

The use of NOTA for ^{68}Ga -labeling offers an interesting alternative. It can be labeled with ^{68}Ga at room temperature and shows high stabilities ⁴⁰. The NOTA derivative TRAP (1,4,7-triazacyclononane-1,4,7-tris(methyl(2-carboxyethyl))-phosphinic acid) shows even better labeling properties ⁴¹. However, the number of nuclides suitable for complexation by NOTA and its derivatives is lower compared to DOTA which limits the use of NOTA in theranostic approaches ⁴².

Hybrid chelators combine the stable complexation of cyclic chelators with the fast and mild radiolabeling properties of acyclic chelators. For example, AAZTA⁵ (6-pentanoic acid-6-amino-1,4-diazepine tetra-acetic acid) provides fast and complete complexation (e.g., with ^{68}Ga , ^{44}Sc , ^{64}Cu , ^{177}Lu) leading to complexes of high stability (e.g., with ^{68}Ga , ^{44}Sc , ^{177}Lu). Same results can be achieved for ^{68}Ga labelling of DATA^{5m} (6-pentanoic acid-6-amino-1,4-diazapine-triacetate) ^{32,43-45}.

Details for the synthetic procedure for coupling of bifunctional chelators to target structures such as biomolecules or small molecules of selected examples and references can be found in Table 1.

For a coupling of a target vector to a bifunctional chelator using squaric acid, two slightly different synthetic routes are possible. It is possible to first couple SADE to the chelator, then conjugate the chelator monoamide to the target structure (path A). On the other hand, the target structure monoamide can first be synthesized, followed by the conjugation of the chelator unit (Path B). With a view to the synthesis of various bioconjugates bearing squaric acid by coupling a bioactive structure to various labeling units Path B is so far advantageous as the squaric acid monoamide structure conjugated to the target vector unit can be produced and purified in a large batch. If a chelator is to be coupled to many different target vectors, path A is preferable. Importantly both synthetic strategies enable simple synthetic routes to conjugates. The synthesized compounds can be labeled with a metallic radioactive isotope before evaluation and later application *in vivo* (e.g., PET imaging). An overview of the labeling chemistry can be found in the supporting information.

Squaric acid as linker moiety for radiopharmaceuticals targeting prostate-specific membrane antigen

Prostate cancer is one of the most common types of cancer among men ⁴⁸. In the last decade, the membrane-bound glycoprotein prostate-specific membrane antigen (PSMA) became an important target for both diagnosis and therapy of prostate cancer ⁴⁹. PSMA expression is relatively low in healthy prostate tissue, whilst it is highly expressed in prostate cancer cells. This PSMA-overexpression correlates with severity and aggressiveness of this malignancy ⁵⁰.

In recent years, several urea-based PSMA radiopharmaceuticals such as PSMA-11, PSMA-617 or PSMA-I&T have been established ⁵¹⁻⁵⁴. Herein the lysine-urea-glutamate-target vector KuE has been used as PSMA-targeting moiety. The insertion of a hydrophobic linker in these PSMA-ligands has led to a higher binding affinity due to an improved interaction with the PSMA-binding pocket ⁵⁵. In terms of radionuclide complexation, several chelators have been functionalized using SA as coupling unit with KuE. Among those are cyclic chelators like DOTAGA, NODAGA (1,4,7-triazacyclononane,1-glutaric acid-4,7-acetic acid) and TRAP ((1,4,7-triazonane-1,4,7-triyl)tris(methylene))tris((1-amino-15-oxo-4,7,10-trioxa-14-azaheptadecan-17-yl)phosphinic acid) ³⁴, as well as hybrid chelators like AAZTA ⁵³². In the context of PSMA inhibitor-based radiopharmaceuticals, SA is part of the linker moiety and should interact as aromatic unit, increasing the binding affinity of the compound.

DOTAGA.SA.KuE (**7**, table 1) displays high PSMA-binding affinity ($K_i=14.8 \pm 4.3$ nM) similar to PSMA-617 ($K_i=13.3 \pm 3.3$ nM) and an even better value than PSMA-11 ($K_i=23.8 \pm 3.9$ nM) ³⁴. Thus, the exchange of the hydrophobic linker of PSMA-11 and PSMA-617 against SA seems to have no negative impact on PSMA-binding affinity.

Although [⁶⁸Ga]Ga-PSMA-11 shows a better accumulation in the tumor in contrast to the cyclic chelator based radiotracers [⁶⁸Ga]Ga-NODAGA.SA.KuE, [⁶⁸Ga]Ga-DOTAGA.SA.KuE, [⁶⁸Ga]Ga-TRAM.SA.KuE and [⁶⁸Ga]Ga-PSMA-617, the measured tracer fraction in the kidneys (420.37 ± 22.76 %ID/g) was significantly higher than those of the SA-containing radiotracers [⁶⁸Ga]Ga-NODAGA.SA.KuE, [⁶⁸Ga]Ga-DOTAGA.SA.KuE, [⁶⁸Ga]Ga-TRAM.SA.KuE and [⁶⁸Ga]Ga-PSMA-617 (3.18 ± 0.64 %ID/g; 2.51 ± 1.09 %ID/g; 8.45 ± 4.31 %ID/g and 6.97 ± 4.49 %ID/g respectively). With a tumor uptake of around 3 to 6 %ID/g the SA-containing compounds [⁶⁸Ga]Ga-NODAGA.SA.KuE, [⁶⁸Ga]Ga-DOTAGA.SA.KuE and [⁶⁸Ga]Ga-TRAM.SA.KuE showed a similar uptake than [⁶⁸Ga]Ga-PSMA-617 (6.51 ± 0.98 %ID/g) (Figure 4) ³⁴.

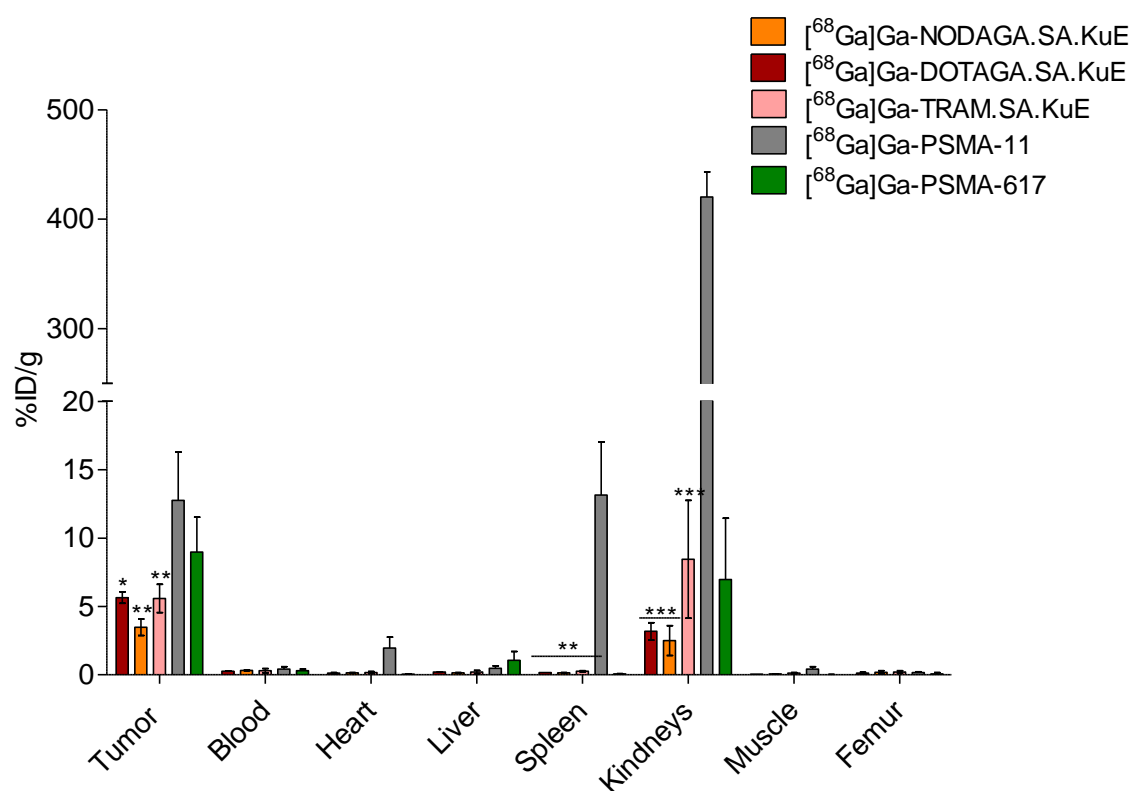


Figure 4 Data from ex vivo biodistribution studies. The activity in the selected organs is expressed as percent of injected dose per gram (%ID/g). Figure was created with GraphPad Prism version 9. Statistics are calculated with Student's t-test by GraphPad Prism version 9. Significances are defined as **: $P < 0.01$ and ***: $P < 0.001$ (compared to [⁶⁸Ga]Ga-PSMA-11). Adapted with permission from Greifenstein, L., Engelbogen, N., Lahnif, H., Sinnes, J.-P., Bergmann, R., Bachmann, M., and Rösch, F. (2020) Synthesis, labeling and preclinical evaluation of a squaric acid containing PSMA-inhibitor labeled with ⁶⁸Ga – a comparison with PSMA-11 and PSMA-617. *ChemMedChem* 1–11. Copyright 2020 Wiley-VCH.

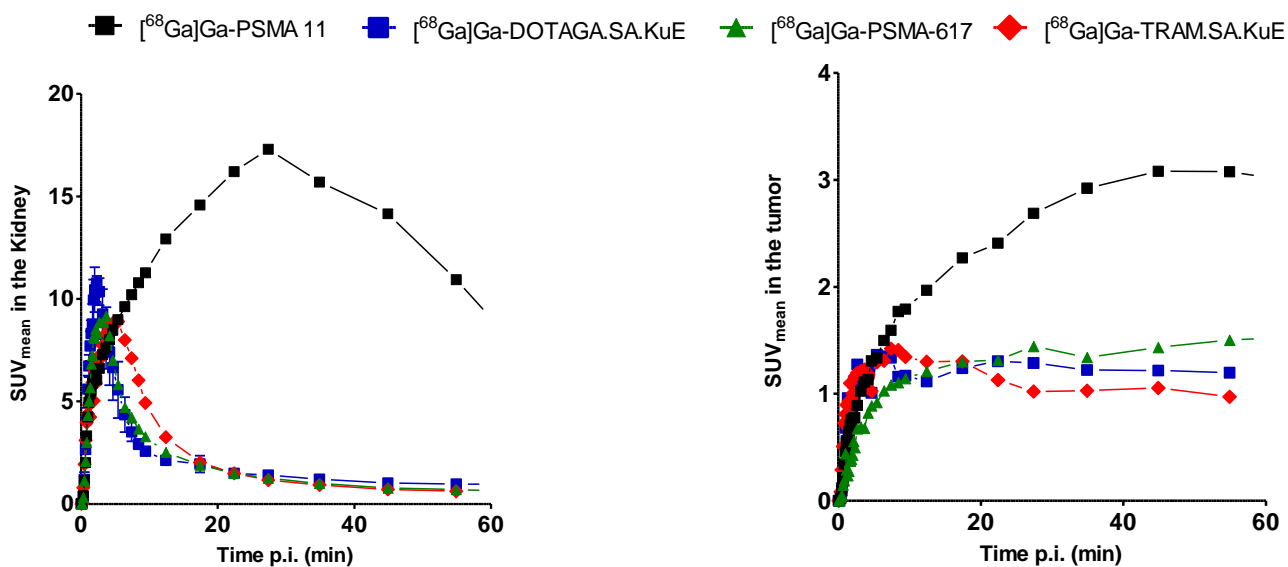


Figure 5: Time-activity curve of the SA-conjugates $[^{68}\text{Ga}]\text{Ga-DOTAGA.SA.KuE}$ and $[^{68}\text{Ga}]\text{Ga-TRAM.SA.KuE}$ compared to $[^{68}\text{Ga}]\text{Ga-PSMA-11}$ and $[^{68}\text{Ga}]\text{Ga-PSMA-617}$. SUV: standardized uptake value. Figure was created with GraphPad Prism version 9.

The renal uptake of the SA-containing conjugates was remarkably lower than for $[^{68}\text{Ga}]\text{Ga-PSMA-11}$. These compounds as well as $[^{68}\text{Ga}]\text{Ga-PSMA-617}$ were almost cleared from the kidney within the first 20 minutes (Figure 5). The rapid clearance enables not only a better visualization of the adjacent prostate but reduces nephrotoxicity especially with regard to the application of therapeutic isotopes like ^{177}Lu and ^{225}Ac ³⁴.

In conclusion, the investigated $[^{68}\text{Ga}]\text{Ga-SA.KuE}$ constructs showed comparable *in vivo* properties to $[^{68}\text{Ga}]\text{Ga-PSMA-617}$ and in some extent to $[^{68}\text{Ga}]\text{Ga-PSMA-11}$. Most presumably, this is because of the interaction of the SA motif with the aromatic pocket of PSMA, meaning that SA resembles the complex linker structure of PSMA-617. The SA-unit seems to have a positive impact on the pharmacokinetic behavior of the PSMA ligands regarding kidney accumulation. The reduction of radiation exposure of the kidney is a major concern in the elaboration of novel radiotracers, since the kidney is the dose-limiting organ in radionuclide therapy ^{56,57}.

Squaric acid as linker moiety for radiopharmaceuticals targeting Fibroblast Activation Protein

The fibroblast activation protein (FAP) is a type II transmembrane glycoprotein and is related to the dipeptidyl peptidases (DPP2, DPP4, DPP8 and DPP9) and the endopeptidase prolyl oligopeptidase (PREP)⁵⁸. It is expressed in pathophysiological lesions, characterized by tissue remodeling (e.g., cancer or fibrosis) but not in healthy tissues^{59,60}. In tumors, FAP is expressed on cancer associated fibroblasts (CAFs)⁶¹. CAFs seem to have a regulatory role in tumor biology and extracellular matrix composition⁶². The stromal tissue of over 90 % of epithelial carcinomas (e.g., colon or breast cancer) shows CAFs expressing FAP⁶³. Thus, targeting of FAP-CAFs can be used for diagnosis and therapy of several types of cancer.

Based on a high affinity and highly selective 4,4-difluoroproline-quinoline FAP inhibitor (so called UAMC1110) multiple radiopharmaceuticals were developed at the DKFZ in Heidelberg recently⁶⁴⁻⁶⁶.

First radiopharmaceuticals containing the FAP inhibitor UAMC1110 and a SA unit were developed using DOTA and DATA^{5m} as bifunctional chelators⁴⁶. The affinity towards FAP of DOTA.SA.FAPi (0.9 ± 0.1 nM), as well as of DATA^{5m}.SA.FAPi (0.8 ± 0.2 nM) are comparable to the affinity of UAMC1110 (0.43 ± 0.07 nM)⁶⁶. Both compounds showed high selectivity towards FAP (low nM of IC₅₀ values).

PET studies in HT-29 tumor-bearing mice were performed using [⁶⁸Ga]Ga-DOTA.SA.FAPi. There is a clear tumor uptake (SUV_{mean} of 0.75 ± 0.09 in tumor, figure 6) and overall good tumor-to-organ ratios at 60 min p.i., due to fast blood clearance and renal excretion⁴⁶.

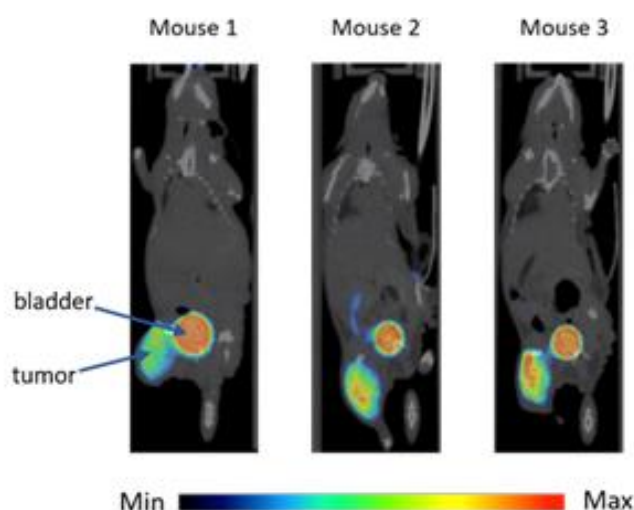


Figure 6 [⁶⁸Ga]Ga-DOTA.SA.FAPi uptake in vivo. Representative coronal small-animal PET/CT image (MIP) 1 h p.i. Reprinted from Moon, E. S., Elvas, F., Vliegen, G., De Lombaerde, S., Vangstel, C., De Bruycker, S., Bracke, A., Eppard, E., Greifenstein, L., Klasen, et al. (2020) Targeting fibroblast activation protein (FAP): Next generation PET radiotracers using squaramide coupled bifunctional DOTA and DATA^{5m} chelators. *EJNMMI Radiopharm Chem.* 5, 1–35. (Open Access, licensed under Creative Commons Attribution 4.0. International License (<http://creativecommons.org/licenses/by/4.0/>)).

Additionally, first clinical investigations were carried out with both radiotracers. Preliminary clinical studies of $[^{68}\text{Ga}]\text{Ga-DOTA}^{5\text{m}}\text{SA.FAPi}$ in focal nodular hyperplasia, a type of liver cancer, have evidenced FAP-specific uptake ⁶⁷. Clinical investigations on biodistribution and pharmacokinetics of $[^{68}\text{Ga}]\text{Ga-DOTA.SA.FAPi}$ in fifty-four patients with various cancer types were conducted ⁶⁸. Figure 7 gives examples of $[^{68}\text{Ga}]\text{Ga-DOTA.SA.FAPi}$ PET/CT scans of three female patients with breast cancer and lung cancer and demonstrates the intense and selective uptake of $[^{68}\text{Ga}]\text{Ga-DOTA.SA.FAPi}$ at several time points. Accumulation is seen in primary lesions (black arrow), pancreas (red arrow) and salivary glands ⁶⁸. Additionally, in the same study, clinical PET/CT comparisons between $[^{18}\text{F}]\text{FDG}$ and $[^{68}\text{Ga}]\text{Ga-DOTA.SA.FAPi}$ have shown coincident SUL values (standardized uptake value (SUV) normalized by lean body mass) in diseases, lesions and metastases (except in brain metastases, where SUL values of $^{68}\text{Ga-FAPi}$ were significantly higher) of various cancer types. Moreover, first successful 24-h post-therapeutic whole-body and SPECT/CT scans with $[^{177}\text{Lu}]\text{Lu-DOTA.SA.FAPi}$ were recently reported ⁶⁹.

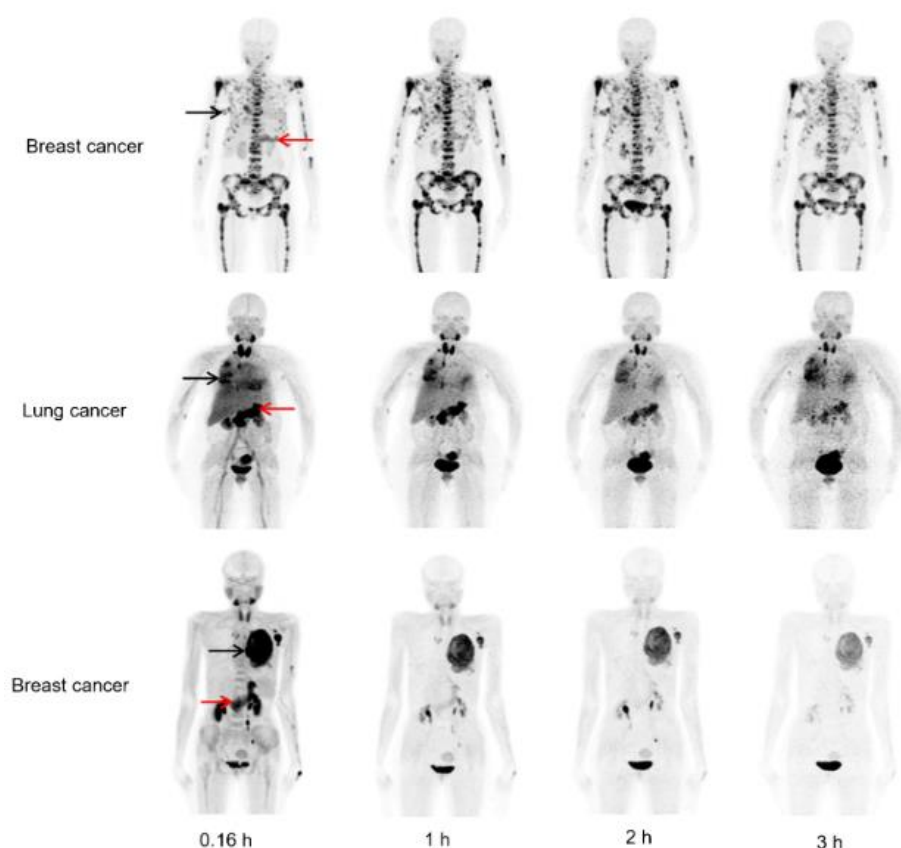


Figure 7 $[^{68}\text{Ga}]\text{Ga-DOTA.SA.FAPi}$ images of three female patients with breast cancer and lung cancer at different time points. An accumulation is seen in primary lesions (black arrow), pancreas (red arrow) and salivary glands. Reprinted by permission from Springer Nature: Springer Nature, *European Journal of Nuclear Medicine*, Ballal, S., Yadav, M. P., Moon, E. S., Kramer, V., Roesch, F., Kumari, S., Tripathi, M., AnrunRaj, S. T., Sarswat, S., and Bal, C. (2020) Biodistribution, pharmacokinetics, dosimetry of $[^{68}\text{Ga}]\text{Ga-DOTA.SA.FAPi}$, and the head-to-head comparison with $[^{18}\text{F}]\text{F-FDG}$ PET/CT in patients with various cancers. *Eur. J. Nucl. Med. Mol. Imaging*. Copyright 2020 Springer Nature.

Squaric acid as linker moiety for antibody-based radiopharmaceuticals

A further promising approach to benefit from the unique advantages of the squaric acid moiety in radiopharmaceutical chemistry is coupling of a suitable chelator to terminal amine groups of large biomolecules such as antibodies. Besides the native therapeutic anti-cancer effects of unmodified monoclonal antibodies (mAbs), their highly selective binding can also be used to transport either conventional chemotherapeutic drugs or both diagnostically and therapeutically relevant radionuclides to a specific target.⁶⁸

Rudd et al. compared the conjugation of the chelator deferoxamine B (DFO) to the antibody trastuzumab using SADE and *p*-phenyl-isothiocyanate, a popular variant for antibody conjugation. It could be shown that the conjugation of H₃DFOSAME (table 1, comp. 3) to the antibody provides simple and fast conjugation chemistry leading to sufficiently high antibody-to-chelator ratios and doesn't require more complicated procedures, such as slow addition to prevent antibody aggregation, as is the case with the *p*-PhNCS derivative (H₃DFO-*p*-PhNCS). Using the squaric acid containing derivative also led to both faster labelling kinetics and higher complex stability in combination with the PET nuclide ⁸⁹Zr. Additionally, [⁸⁹Zr]Zr-DFO.SA.trastuzumab showed a better imaging performance than the compared compound [⁸⁹Zr]Zr-DFO-*p*-Ph.trastuzumab in mouse models of HER2 positive tumors³⁵. Since tetravalent Zr⁴⁺ prefers a coordination number of eight, the six oxygen donors of DFO are supplemented by two additional water molecules in aqueous solution. Therefore, the resulting complex is characterized not only by an unsaturated chelation, but also by sensitivity to deprotonation⁷²⁻⁷⁴. As a result, ⁸⁹Zr-labeled DFO-conjugates frequently show a certain instability *in vivo* leading to a release of the osteophilic radiometal and undesired accumulation in the bones⁷⁵⁻⁷⁸. Even though this effect mainly occurs in small animal studies (and rather less in the human organism) presumably due to a faster metabolism, development of novel improved chelator derivatives is subject of current research^{75,79}. Rudd et al. assumed the enhanced complex stability of [⁸⁹Zr]Zr-DFO.SA to be due to a participation of the squaric acid dione backbone to the complexation of the radiometal leading to an octadentate coordination. However, this assumption has not yet been confirmed. Chomet et al. could not reproduce a significantly improved stability³⁶. Furthermore, Holland recently showed by DFT (density functional theory) calculation that only one of the two oxygen atoms is involved in the complexation indicating a heptadentate chelator³⁷.

Berg et al. also investigated the behaviour of squaric acid coupled chelator-antibody conjugates in comparison to *p*-phenyl isothiocyanate mediated analogues in rhesus monkeys. On the one hand, this study indicated an advantage of the SA-containing compound in terms of bioconjugation stability of the ^{89}Zr -DFO complex and the antibody. In contrast, the thiourea coupled compounds showed very high activity levels in the bladder in early measurements. This could be evidence of instability in terms of NCS-antibody conjugation, as the stand-alone [^{89}Zr]Zr-DFO complex is known to be rapidly excreted via the renal system³⁹. On the other hand, the squaric acid coupled compounds showed higher bone uptake in monkeys, which clearly contradicts the assumption of an increased complex stability based on the provision of additional donor atoms.

As SADE enables mild coupling conditions, it allows the conjugation of sensitive molecules such as antibodies without damaging their sensitive structure and can improve stability of the chelator-antibody conjugate. Compared to NCS coupling, it seems that the SA-strategy leads to a protein-binding of higher *in vivo* stability. Therefore, SA represents a promising and suitable linker moiety that provides easy and stable functionalization of an antibody with an appropriate chelator molecule under mild conditions.

Conclusion

In summary, the developed and in this review described SA-containing radiopharmaceuticals present promising conjugation, radiolabeling, *in vitro* as well as *in vivo* properties for application in nuclear medicine.

It could be demonstrated through several studies that SA is a valuable tool in the development of targeted radiopharmaceuticals. The unique properties of SADE enable fast and simple conjugation of chelators to biomolecules, proteins, peptides and small molecules under mild conditions without the need of excessive protecting group chemistry. Additionally, the use of SAME building blocks allows a simplified organic synthesis. The insertion of SA as linker demonstrated no negative effect on the labeling properties of the radiopharmaceuticals, since high radiochemical yields were achieved with all conjugates described herein.

Beside the several chemical advantages of SA regarding conjugation, labeling and stability of the corresponding complexes, the SA-containing ligands indicate a similar or even improved pharmacokinetic characteristics compared with established radiopharmaceuticals in terms of binding affinity to the addressed target and tumor accumulation *in vivo*.

Acknowledgment

References

- (1) Price, E. W., and Orvig, C. (2014) Matching chelators to radiometals for radiopharmaceuticals. *Chem. Soc. Rev.* 43, 260–290.
- (2) Sarko, D., Eisenhut, M., Haberkorn, U., and Mier, W. (2012) Bifunctional Chelators in the Design and Application of Radiopharmaceuticals for Oncological Diseases. *Curr. Med. Chem.* 19, 2667–2688.
- (3) Brown, D. G., and Boström, J. (2016) Analysis of Past and Present Synthetic Methodologies on Medicinal Chemistry: Where Have All the New Reactions Gone? *J. Med. Chem.* 59, 4443–4458.
- (4) El-Faham, A., and Albericio, F. (2011) Peptide coupling reagents, more than a letter soup. *Chem. Rev.* 111, 6557–6602.
- (5) Rehman, M.-U., Jabeen, A., and Mariya, M. (2018) Side reactions in peptide synthesis: An overview. *Int. J. Pharm. Res. Technol.* 10.
- (6) El-Faham, A., and Albericio, F. (2010) COMU: A third generation of uronium-type coupling reagents. *J. Pept. Sci.* 16, 6–9.
- (7) Yang, Y. (2015) Side reactions in peptide synthesis, in Chapter 5 - Side Reactions Upon Amino Acid/Peptide Carboxyl Activation, pp 95–118.
- (8) Mädler, S., Bich, C., Touboul, D., and Zenobi, R. (2009) Chemical cross-linking with NHS esters: A systematic study on amino acid reactivities. *J. Mass Spectrom.* 44, 694–706.
- (9) Klykov, O., and Weller, M. G. (2015) Quantification of N-hydroxysuccinimide and N-hydroxysulfosuccinimide by hydrophilic interaction chromatography (HILIC). *Anal. Methods* 7, 6443–6448.
- (10) Banks, P. R., and Paquette, D. M. (1995) Comparison of Three Common Amine Reactive Fluorescent Probes Used for Conjugation to Biomolecules by Capillary Zone Electrophoresis. *Bioconjug. Chem.* 6, 447–458.
- (11) Thirumurugan, P., Matosiuk, D., and Jozwiak, K. (2013) Click chemistry for drug development and diverse chemical-biology applications. *Chem. Rev.*
- (12) Hou, J., Liu, X., Shen, J., Zhao, G., and Wang, P. G. (2012) The impact of click chemistry in medicinal chemistry. *Expert Opin. Drug Discov.* 7, 489–501.
- (13) Kettenbach, K., Schieferstein, H., and Ross, T. L. (2014) ¹⁸F-labeling using click cycloadditions. *Biomed Res. Int.* 2014.
- (14) Marik, J., and Sutcliffe, J. L. (2006) Click for PET: rapid preparation of [¹⁸F]fluoropeptides using Cu(I) catalyzed 1,3-dipolar cycloaddition. *Tetrahedron Lett.* 47, 6681–6684.

- (15) Rostovtsev, V. V., Green, L. G., Fokin, V. V., and Sharpless, K. B. (2002) A stepwise Huisgen cycloaddition process: Copper(I)-catalyzed regioselective “ligation” of azides and terminal alkynes. *Angew. Chemie - Int. Ed.* 41, 2596–2599.
- (16) Jewett, J. C., Sletten, E. M., and Bertozzi, C. R. (2010) Rapid Cu-free click chemistry with readily synthesized biarylazacyclooctynones. *J. Am. Chem. Soc.* 132, 3688–3690.
- (17) Sletten, E. M., and Bertozzi, C. R. (2011) Bioorthogonal Reactions. *Acc. Chem. Res.* 44, 666–676.
- (18) Gröst, C., and Berg, T. (2015) PYRROC: The first functionalized cycloalkyne that facilitates isomer-free generation of organic molecules by SPAAC. *Org. Biomol. Chem.* 13, 3866–3870.
- (19) Semmingsen, D. (1973) The structure of squaric acid (3,4-dihydroxy-3-cyclobutene-1,2-dione). *Tetrahedron Lett.* 807–808.
- (20) Wurm, F. R., and Klok, H. A. (2013) Be squared: Expanding the horizon of squaric acid-mediated conjugations. *Chem. Soc. Rev.* 42, 8220–8236.
- (21) West, R., and Powell, D. L. (1963) New Aromatic Anions. III. Molecular Orbital Calculations on Oxygenated Anions. *J. Am. Chem. Soc.* 85, 2577–2579.
- (22) Prohens, R., Portell, A., Font-Bardia, M., Bauzá, A., and Frontera, A. (2014) Experimental and theoretical study of aromaticity effects in the solid state architecture on squaric acid derivatives. *Cryst. Growth Des.* 14, 2578–2587.
- (23) Lim, N. C., Morton, M. D., Jenkins, H. A., and Brückner, C. (2003) Squaric Acid N-Hydroxylamides: Synthesis, Structure, and Properties of Vinylogous Hydroxamic Acid Analogues. *J. Org. Chem.* 68, 9233–9241.
- (24) Cohen, S., and Cohen, S. G. (1966) Preparation and Reactions of Derivatives of Squaric Acid. Alkoxy-, Hydroxy-, and Aminocyclobutenediones. *J. Am. Chem. Soc.* 88, 1533–1536.
- (25) Bae, H. Y., and Song, C. E. (2015) Unprecedented hydrophobic amplification in noncovalent organocatalysis “on water”: Hydrophobic chiral squaramide catalyzed Michael addition of malonates to nitroalkenes. *ACS Catal.* 5, 3613–3619.
- (26) Marchetti, L. A., Kumawat, L. K., Mao, N., Stephens, J. C., and Elmes, R. B. P. (2019) The Versatility of Squaramides: From Supramolecular Chemistry to Chemical Biology. *Chem* 5, 1398–1485.
- (27) Prohens, R., Portell, A., and Alcobé, X. (2012) Effect of preorganization on the polymorphism and cocrystallization of a squaramide compound. *Cryst. Growth Des.* 12, 4548–4553.
- (28) Seleem, H. S., Ramadan, A. A. T., Taha, A., Eid, M. F., and Samy, F. (2011) The complexation of a novel squaric bis(thiosemicarbazone); 3,4-bis[[[aminothioxomethyl]amino]azamethylene]cyclobut-ene-1,2-diol. *Spectrochim. Acta - Part A Mol. Biomol. Spectrosc.* 78, 1097–1104.
- (29) Agnew-Francis, K. A., and Williams, C. M. (2020) Squaramides as Bioisosteres in Contemporary Drug Design. *Chem. Rev.*
- (30) Tietze, L. F., Arlt, M., Beller, M., Glüsenkamp, K., Jahdeb, E., and Rajewsky, M. F. (1991) Squaric Acid Diethyl Ester: A New Coupling Reagent for the Formation of Drug Biopolymer Conjugates. Synthesis of Squaric Acid Ester Amides and Diamides. *Anticancer Agents* 124, 1215–1221.
- (31) Dingels, C., Wurm, F., Wagner, M., Klok, H. A., and Frey, H. (2012) Squaric acid mediated chemoselective PEGylation of proteins: Reactivity of single-step-activated α -amino poly(ethylene glycol)s. *Chem. - A Eur. J.* 18, 16828–16835.

- (32) Greifenstein, L., Grus, T., Nagel, J., Sinnes, J. P., and Rösch, F. (2020) Synthesis and labeling of a squaric acid containing PSMA-inhibitor coupled to AAZTA5 for versatile labeling with ^{44}Sc , ^{64}Cu , ^{68}Ga and ^{177}Lu . *Appl. Radiat. Isot.* 156.
- (33) Quiñonero, D., Frontera, A., Ballester, P., and Deyà, P. M. (2000) A theoretical study of aromaticity in squaramide and oxocarbons. *Tetrahedron Lett.* 41, 2001–2005.
- (34) Greifenstein, L., Engelbogen, N., Lahnif, H., Sinnes, J.-P., Bergmann, R., Bachmann, M., and Rösch, F. (2020) Synthesis, labeling and preclinical evaluation of a squaric acid containing PSMA-inhibitor labeled with ^{68}Ga – a comparison with PSMA-11 and PSMA-617. *ChemMedChem* 1–11.
- (35) Rudd, S. E., Roselt, P., Cullinane, C., Hicks, R. J., and Donnelly, P. S. (2016) A desferrioxamine B squaramide ester for the incorporation of zirconium-89 into antibodies. *Chem. Commun.* 52, 11889–11892.
- (36) Chomet, M., Schreurs, M., Bolijn, M. J., Verlaan, M., Beaino, W., Brown, K., Poot, A. J., Windhorst, A. D., Gill, H., Marik, J., et al. (2020) Head-to-head comparison of DFO* and DFO chelators: selection of the best candidate for clinical ^{89}Zr -immuno-PET. *Eur. J. Nucl. Med. Mol. Imaging.*
- (37) Holland, J. P. (2020) Predicting the Thermodynamic Stability of Zirconium Radiotracers. *Inorg. Chem.* 59, 2070–2082.
- (38) Yoganathan, S., Sit, C. S., and Vederas, J. C. (2011) Chemical synthesis and biological evaluation of gallidermin-siderophore conjugates. *Org. Biomol. Chem.* 9, 2133–2141.
- (39) Berg, E., Gill, H., Marik, J., Ogasawara, A., Williams, S., van Dongen, G., Danielle, V., Cherry, S. R., and Tarantal, A. F. (2020) Total-Body PET and Highly Stable Chelators Together Enable Meaningful ^{89}Zr -Antibody PET Studies up to 30 Days After Injection. *J. Nucl. Med.* 61, 453–460.
- (40) Kilian, K. (2014) ^{68}Ga -DOTA and analogs: Current status and future perspectives. *Reports Pract. Oncol. Radiother.* 19, 13–21.
- (41) Notni, J., Pohle, K., and Wester, H. J. (2012) Comparative gallium-68 labeling of TRAP-, NOTA-, and DOTA-peptides: Practical consequences for the future of gallium-68-PET. *EJNMMI Res.* 2, 2–6.
- (42) Velikyan, I. (2015) ^{68}Ga -based radiopharmaceuticals: Production and application relationship. *Molecules* 20, 12913–12943.
- (43) Sinnes, J., Nagel, J., and Rösch, F. (2019) AAZTA⁵/AAZTA⁵-TOC: synthesis and radiochemical evaluation with ^{68}Ga , ^{44}Sc and ^{177}Lu . *EJNMMI Radiopharm Chem.* 4.
- (44) Waldron, B. P., Parker, D., Burchardt, C., Yufit, D. S., Zimny, M., and Roesch, F. (2013) Structure and stability of hexadentate complexes of ligands based on AAZTA for efficient PET labelling with gallium-68. *Chem. Commun.* 49, 579–581.
- (45) Farkas, E., Nagel, J., Waldron, B. P., Parker, D., Tóth, I., Brücher, E., Rösch, F., and Baranyai, Z. (2017) Equilibrium, Kinetic and Structural Properties of Gallium(III) and Some Divalent Metal Complexes Formed with the New DATAm and DATA5m Ligands. *Chem. - A Eur. J.* 23, 10358–10371.
- (46) Moon, E. S., Elvas, F., Vliegen, G., De Lombaerde, S., Vangstel, C., De Bruycker, S., Bracke, A., Eppard, E., Greifenstein, L., Klasen, B., et al. (2020) Targeting fibroblast activation protein (FAP): Next generation PET radiotracers using squaramide coupled bifunctional DOTA and DATA5m chelators. *EJNMMI Radiopharm Chem.* 5, 1–35.
- (47) Klasen, B., Moon, E. S., and Rösch, F. (2021) AAZTA⁵-squaramide ester competing with DOTA-, DTPA- and CHX-A-DTPA-analogues: Promising tool for ^{177}Lu -labeling of monoclonal antibodies under mild conditions. *Nucl. Med. Biol.* 96–97, 80–93.
- (48) Mucci, L. A., Wilson, K. M., and Giovannucci, E. L. (2016) Epidemiology of prostate cancer. *Pathol. Epidemiol. Cancer* 10, 107–125.

- (49) Donin, N. M., and Reiter, R. E. (2018) Why targeting PSMA is a game changer in the management of prostate cancer. *J. Nucl. Med.* 59, 177–182.
- (50) Silver, D. A., Pellicer, I., Fair, W. R., Heston, W. D. W., and Cordon-Cardo, C. (1997) Prostate-specific Membrane Antigen Expression in Normal and Malignant Human Tissues. *Clin. Cancer Research* 3, 81–85.
- (51) Benesová, M., Schäfer, M., Bauder-Wüst, U., Afshar-Oromieh, A., Kratochwil, C., Mier, W., Haberkorn, U., Kopka, K., and Eder, M. (2015) Preclinical evaluation of a tailor-made DOTA-conjugated PSMA inhibitor with optimized linker moiety for imaging and endoradiotherapy of prostate cancer. *J. Nucl. Med.* 56, 914–920.
- (52) Weineisen, M., Schottelius, M., Simecek, J., Baum, R. P., Yildiz, A., Beykan, S., Kulkarni, H. R., Lassmann, M., Klette, I., Eiber, et al. (2015) ⁶⁸Ga-and ¹⁷⁷Lu-labeled PSMA i and T: Optimization of a PSMA-targeted theranostic concept and first proof-of-concept human studies. *J. Nucl. Med.* 56, 1169–1176.
- (53) Eder, M., Eisenhut, M., Babich, J., and Haberkorn, U. (2013) PSMA as a target for radiolabelled small molecules. *Eur. J. Nucl. Med. Mol. Imaging* 40, 819–823.
- (54) Rahbar, K., Afshar-Oromieh, A., Jadvar, H., and Ahmadzadehfar, H. (2018) PSMA Theranostics: Current Status and Future Directions. *Mol. Imaging* 17, 1–9.
- (55) Kopka, K., Benešová, M., Bařinka, C., Haberkorn, U., and Babich, J. (2017) Glu-ureido-based inhibitors of prostate-specific membrane antigen: Lessons learned during the development of a novel class of low-molecular-weight theranostic radiotracers. *J. Nucl. Med.* 58, 17S-26S.
- (56) Edeani, A., and Cohen, E. P. (2016) Chapter 10: Radiation Nephropathy. *Onco-Nephrology Curric.* 1–6.
- (57) Vegt, E., Jong, M. De, Wetzels, J. F. M., Masereeuw, R., Melis, M., Oyen, W. J. G., Gotthardt, M., and Boerman, O. C. (2010, July) Renal toxicity of radiolabeled peptides and antibody fragments: Mechanisms, impact on radionuclide therapy, and strategies for prevention. *J. Nucl. Med. Society of Nuclear Medicine.*
- (58) Brennen, W. N., Isaacs, J. T., and Denmeade, S. R. (2012) Rationale behind targeting fibroblast activation protein-expressing carcinoma-associated fibroblasts as a novel chemotherapeutic strategy. *Mol. Cancer Ther.* 11, 257–266.
- (59) Hamson, E. J., Keane, F. M., Tholen, S., Schilling, O., and Gorrell, M. D. (2014) Understanding fibroblast activation protein (FAP): Substrates, activities, expression and targeting for cancer therapy. *Proteomics - Clin. Appl.* 8, 454–463.
- (60) Liu, R., Li, H., Liu, L., Yu, J., and Ren, X. (2012) Fibroblast activation protein: A potential therapeutic target in cancer. *Cancer Biol. Ther.* 13, 123–129.
- (61) Chen, X., and Song, E. (2019) Turning foes to friends: targeting cancer-associated fibroblasts. *Nat. Rev. Drug Discov.* 18, 99–115.
- (62) De Vlieghere, E., Verset, L., Demetter, P., Bracke, M., and De Wever, O. (2015) Cancer-associated fibroblasts as target and tool in cancer therapeutics and diagnostics. *Virchows Arch.* 467, 367–382.
- (63) Busek, P., Mateu, R., Zubal, M., Kotackova, L., and Sedo, A. (2018) Targeting Fibroblast activation protein in cancer - Prospects and caveats. *Front. Biosci. - Landmark* 23, 1933–1968.
- (64) Loktev, A., Lindner, T., Burger, E. M., Altmann, A., Giesel, F., Kratochwil, C., Debus, J., Marmé, F., Jäger, D., Mier, W., et al. (2019) Development of fibroblast activation protein-targeted radiotracers with improved tumor retention. *J. Nucl. Med.* 60, 1421–1429.
- (65) Lindner, T., Loktev, A., Altmann, A., Giesel, F., Kratochwil, C., Debus, J., Jäger, D., Mier, W., and Haberkorn, U. (2018) Development of quinoline-based theranostic ligands for the targeting of fibroblast activation protein. *J. Nucl. Med.* 59, 1415–1422.

- (66) Jansen, K., Heirbaut, L., Verkerk, R., Cheng, J. D., Joossens, J., Cos, P., Maes, L., Lambeir, A. M., De Meester, I., Augustyns, K., et al. (2014) Extended structure-activity relationship and pharmacokinetic investigation of (4-quinolinoyl)glycyl-2-cyanopyrrolidine inhibitors of fibroblast activation protein (FAP). *J. Med. Chem.* 57, 3053–3074.
- (67) Kreppel, B., Gaertner, F. C., Marinova, M., Attenberger, U., Meisenheimer, M., Toma, M., Kristiansen, G., Feldmann, G., Moon, E. S., Roesch, F., et al. (2020) [⁶⁸Ga]Ga-DATA^{5m}.SA.FAPi PET/CT : Specific Tracer-uptake in Focal Nodular Hyperplasia and potential Role in Liver Tumor Imaging [⁶⁸Ga]Ga-DATA^{5m}.SA.FAPi PET/CT : Uptake in fokal nodulärer Hyperplasie und potentielle Anwendung zur Tumor. *Nuklearmedizin* 8–10.
- (68) Ballal, S., Yadav, M. P., Moon, E. S., Kramer, V., Roesch, F., Kumari, S., Tripathi, M., AnrunRaj, S. T., Sarswat, S., and Bal, C. (2020) Biodistribution, pharmacokinetics, dosimetry of [⁶⁸Ga]Ga-DOTA.SA.FAPi, and the head-to-head comparison with [¹⁸F]F-FDGPET/CT in patients with various cancers. *Eur. J. Nucl. Med. Mol. Imaging*.
- (69) Ballal, S., Yadav, M. P., Kramer, V., Moon, E. S., Roesch, F., and Tripathi, M. (2020) A theranostic approach of [⁶⁸Ga]Ga-DOTA.SA.FAPi PET/CT-guided [¹⁷⁷Lu]Lu-DOTA.SA.FAPi radionuclide therapy in an end-stage breast cancer patient : new frontier in targeted radionuclide therapy. *Eur. J. Nucl. Med. Mol. Imaging*.
- (70) Adler, M. J., and Dimitrov, D. S. (2012) Therapeutic Antibodies Against Cancer. *Hematol. Oncol. Clin. North Am.* 26, 447–481.
- (71) Kimiz-Gebologlu, I., Gulce-Iz, S., and Biray-Avci, C. (2018) Monoclonal antibodies in cancer immunotherapy. *Mol. Biol. Rep.* 45, 2935–2940.
- (72) Toporivska, Y., and Gumienna-Kontecka, E. (2019) The solution thermodynamic stability of desferrioxamine B (DFO) with Zr(IV). *J. Inorg. Biochem.* 198, 110753.
- (73) Holland, J. P., Divilov, V., Bander, N. H., Smith-Jones, P. M., Larson, S. M., and Lewis, J. S. (2010) ⁸⁹Zr-DFO-J591 for immunoPET of prostate-specific membrane antigen expression in vivo. *J. Nucl. Med.* 51, 1293–1300.
- (74) Guerard, F., Yong-sok, L., Raphael, T., Szajed, L. P., Deschamps, J. R., and Brechbiel, Martin, W. (2013) Investigation of Zr(IV) and ⁸⁹Zr(IV) complexation with hydroxamates: Progress towards designing a better chelator than desferrioxamine B for immuno-PET imaging. *Chem Commun* 49, 1002–1004.
- (75) Abou, D. S., Ku, T., and Smith-Jones, P. M. (2011) In vivo biodistribution and accumulation of ⁸⁹Zr in mice. *Nucl. Med. Biol.* 38, 675–681.
- (76) Heskamp, S., Van Laarhoven, H. W. M., Molkenboer-Kuennen, J. D. M., Franssen, G. M., Versleijen-Jonkers, Y. M. H., Oyen, W. J. G., Van Der Graaf, W. T. A., and Boerman, O. C. (2010) ImmunoSPECT and immunoPET of IGF-1R expression with the radiolabeled antibody R1507 in a triple-negative breast cancer model. *J. Nucl. Med.* 51, 1565–1572.
- (77) Perk, L. R., Visser, G. W. M., Vosjan, M. J. W. D., Stigter-Van Walsum, M., Tjink, B. M., Leemans, C. R., and Van Dongen, G. A. M. S. (2005) ⁸⁹Zr as a PET surrogate radioisotope for scouting biodistribution of the therapeutic radiometals ⁹⁰Y and ¹⁷⁷Lu in tumor-bearing nude mice after coupling to the internalizing antibody cetuximab. *J. Nucl. Med.* 46, 1898–1906.
- (78) Laverman, P., Van Der Geest, T., Terry, S. Y. A., Gerrits, D., Walgreen, B., Helsen, M. M., Nayak, T. K., Freimoser-Grundschober, A., Waldhauer, I., Hosse, R. J., et al. (2015) Immuno-PET and immuno-SPECT of rheumatoid arthritis with radiolabeled anti-fibroblast activation protein antibody correlates with severity of arthritis. *J. Nucl. Med.* 56, 778–783.
- (79) Bhatt, N. B., Pandya, D. N., and Wadas, T. J. (2018) Recent advances in zirconium-89 chelator development. *Molecules* 23.

Hybrid chelator-based PSMA-radiopharmaceuticals: translational approach

Hanane Lahnif^{1, #}, [REDACTED],[#], [REDACTED], [REDACTED],³,
[REDACTED] and [REDACTED]

Both authors contributed equally

¹ Department of Chemistry – TRIGA site, Johannes Gutenberg University Mainz, 55128 Mainz, Germany;

² [REDACTED]
[REDACTED]

³ [REDACTED]

ABSTRACT

(1) Background: Prostate-specific membrane antigen PSMA has been extensively studied in the last decade. It became a promising biological target in diagnosis and therapy of PSMA-expressing cancer diseases. Although there are several radiolabeled PSMA inhibitors available, the search of new compounds with improved pharmacokinetic properties and simplified synthesis is still ongoing. In this study we developed PSMA ligands with two different hybrid chelators and a modified linker. Besides a simplified synthesis and labeling procedure, the compounds have displayed a promising pharmacokinetic profile.

(2) Methods: DATA^{5m}.SA.KuE and AAZTA⁵.SA.KuE were synthesized. DATA^{5m}.SA.KuE was labeled with ⁶⁸Ga and radiochemical yields of various amounts of precursor at different temperatures were determined. The complex stability in phosphate-buffered saline (PBS) and human serum (HS) was examined at 37 °C. Binding affinity and internalization rate were determined in *in vitro* assays using PSMA-positive LNCaP cells. Tumor accumulation and biodistribution were evaluated *in vivo* and *ex vivo* using an LNCaP Balb/c nude mouse model. All experiments were conducted with PSMA-11 as reference.

(3) Results: DATA^{5m}.SA.KuE was synthesized successfully in 14 steps. AAZTA⁵.SA.KuE was synthesized and labeled according to literature. Radiolabeling of DATA^{5m}.SA.KuE with ⁶⁸Ga was performed in ammonium acetate buffer (1 M, pH 5.5). High radiochemical yields (> 98 %) were obtained with 5 nmol at 70 °C, 15 nmol at 50 °C and 60 nmol (50 µg) at room temperature. [⁶⁸Ga]Ga-DATA^{5m}.SA.KuE was stable in human serum as well as in PBS after 120 min. PSMA binding affinities of AAZTA⁵.SA.KuE and DATA^{5m}.SA.KuE were in nanomolar range. PSMA-specific internalization rate was comparable to PSMA-11. *In vivo* and *ex vivo* studies of [¹⁷⁷Lu]Lu-AAZTA⁵.SA.KuE, [⁴⁴Sc]Sc-AAZTA⁵.SA.KuE and [⁶⁸Ga]Ga-DATA^{5m}.SA.KuE displayed specific accumulation in the tumor along with a fast clearance and reduced off-target uptake.

(4) Conclusions: Both KuE-conjugates showed promising properties especially *in vivo* allowing a translational theranostic use.

Keywords: prostate specific membrane antigen PSMA; hybrid chelator; radionuclide diagnosis and therapy

1. Introduction

Prostate-specific membrane antigen PSMA has become a very popular target in the diagnosis and therapy of prostate cancer in the last decade. PSMA is a glycoprotein with several functions originating from its glutamate-carboxypeptidase activity. In the central nervous system, PSMA acts as NAALADase, which cleaves the glutamate moiety from the neurotransmitter N-acetyl aspartyl glutamate. However, in the proximal small intestine this enzyme, called folate hydrolase FOLH1, releases glutamate residues from poly-glutamated folate ^{1,2}. Besides these physiological functions, PSMA seems to play an important role in prostate carcinogenesis since it is highly expressed in prostate tumor cells. These expression correlates with the aggressiveness and invasiveness of the tumor ³⁻⁵ and is a major reason for choosing PSMA as a molecular target in the management of prostate cancer (PC).

Prostate cancer is the second common cancer among men and the fifth leading cause of death worldwide ^{6,7}. However, an early detection of PC in a localized stage can significantly reduce its mortality leading to a 5-year survival rate of more than 90% ⁸. In contrast, a late-stage tumor is aggressive and almost resistant to the available therapies. The metastatic castration-resistant prostate cancer (mCRPC) is one of the most aggressive forms of prostate cancer with a poor outcome and restricted therapy options ⁹. One of the most promising approaches herein is the PSMA-targeted radioligand diagnosis and therapy. The unique characteristics of PSMA as molecular target in combination with the small-molecule PSMA inhibitors as target vectors paved the way for the development of highly sensitive radiopharmaceuticals like the PET-radioligand [⁶⁸Ga]Ga-PSMA-11 and its therapeutic counterpart [¹⁷⁷Lu]Lu-PSMA-617 ^{10,11}.

One of the challenges in designing appropriate PSMA inhibitors for a theranostic use is on the one hand the reduction of the off-target accumulation in order to minimize the exposure and irradiation of metabolizing organs like the kidney and in particular of the salivary glands ¹²⁻¹⁵, on the other hand the development of PSMA-ligands which can be easily synthesized and effectively labeled. To address some of these concerns, we developed AAZTA⁵.SA.KuE and DATA^{5m}.SA.KuE.

Like all PSMA ligands, the herein described PSMA radiopharmaceuticals consists of three parts: chelator, linker moiety and KuE-based PSMA-targeting vector.

The chelator is responsible for the introduction of the radionuclide. In this study, the bifunctional hybrid chelators DATA^{5m} (6-pentanoic acid-6-amino-1,4-diazapine-triacetate) and AAZTA⁵ (6-pentanoic acid-6-amino-1,4-diazepine tetra-acetic acid) are used as chelators (Figure 1). With regard to radiometals, hybrid chelators combine the positive complexation properties of acyclic chelators, such as fast complexation kinetics at mild temperatures, with the advantages of cyclic chelators, such as prolonged complex stability ^{16,17}. In these structures, the two tertiary diazepine amines provide the cyclic component for

complexation. Another amine outside the diazepine backbone provides another complexation unit (acyclic component). The remaining complexation sites are provided by carboxy groups alkylated to the amines ^{16,18-20}.

AAZTA⁵ shows ideal labeling properties for transition metals, such as scandium as well as for lanthanides, e.g., gadolinium and lutetium. Thus, AAZTA⁵ is suitable as a chelator for diagnostic use (e.g., scandium-44) as well as for therapeutic applications (e.g., lutetium-177) ^{17,21,22}.

The DATA^{5m} chelator has optimal labeling properties at mild conditions for the generator-based PET nuclide gallium-68. Furthermore, the AAZTA and DATA chelators are also suitable for instant kit-labeling applications with e.g. Lutetium-177 and gallium-68 ^{17,23}.

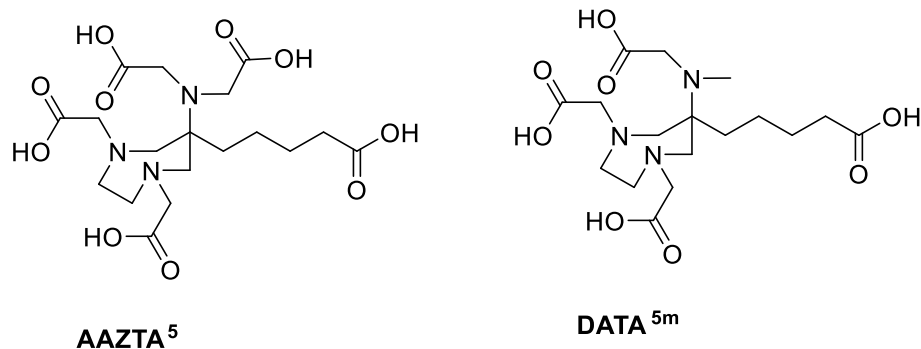


Figure 1 Bifunctional derivatives of the hybrid chelators AAZTA⁵ and DATA^{5m}

Lysine-urea-glutamate (KuE) has been established as PSMA inhibitor. KuE consists of lysine and glutamate which are both linked to each other via a urea unit. KuE is based on the natural PSMA-substrate NAAG, but cannot be cleaved by the enzyme ¹⁰. Both PSMA-617 and PSMA-11 carry this structural unit as the PSMA-binding entity ²⁴.

The third structural element found in PSMA radiopharmaceuticals is the linker moiety connecting the chelator to the urea-based target vector. In addition to the function of coupling, these linkers are usually designed to improve the pharmacokinetics of the compounds ¹⁰. These moieties can interact with the aromatic-binding region of the PSMA binding pocket leading to an increase in the affinity of the PSMA ligand ²⁵. The coupling of KuE is achieved via the side-chain amine of the lysine. Usually, amide coupling reactions are used for this purpose. Alternatively, conjugation can be achieved by using squaric acid diethyl esters (SADE). This group allows two amines to be selectively coupled via asymmetric amidation, forming a squaramide. This simplifies the synthesis in so far as, for example, no protective group chemistry is required, as is the case with standard amide couplings. The coupling reaction is selective with amines only and by controlling the amidation of both squaric acid esters via pH ^{17,26-29}.

The control of the asymmetric amidation via the pH value can be explained by the different aromaticity and thus the different mesomeric stabilities of the individual intermediates at the different pH values (Figure 2) ³⁰⁻³².

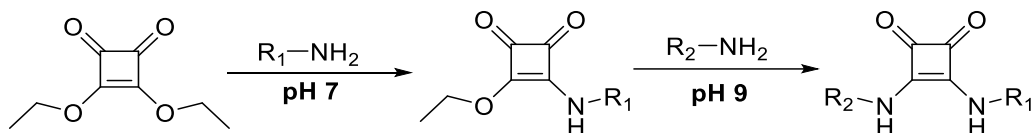


Figure 2 Asymmetric amidation of SADE with different amines. The reactions are driven by change in aromaticity of the different intermediates.

With regard to PSMA radiopharmaceuticals, the use of squaric acid shows another advantage. Squaric acid has an aromatic character and can therefore interact with the aromatic binding region in the PSMA binding pocket resulting in an increased affinity. Sophisticated linker units, as in PSMA-617, are no longer necessary. Greifenstein et al. recently showed that a square amide containing DOTAGA-KuE derivative is comparable to the standard compounds PSMA-617 and PSMA-11 in terms of *in vitro* binding affinity, tumor accumulation and *in vivo* kinetics ²⁸.

2. Results

2.1. Organic synthesis

Synthesis of AAZTA⁵.SA.KuE was according to literature ¹⁷.

The synthesis of the DATA chelator is based on the synthesis described by Farkas et al ¹⁶ and Greifenstein et al ¹⁷. It was synthesized according to figure 3.

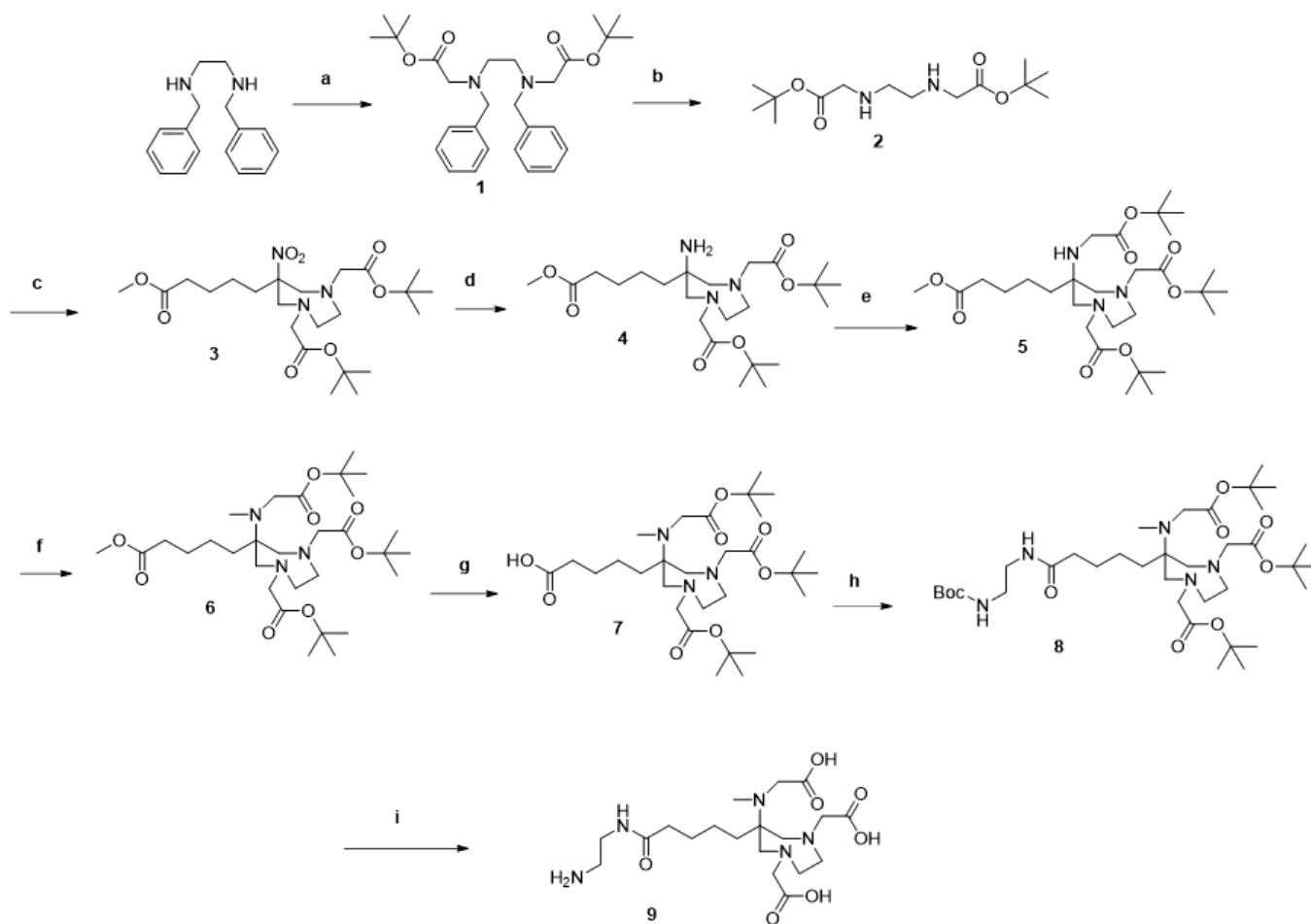


Figure 3 Synthesis of DATA^{5m}: (a) *tert*-butyl bromoacetate, Na₂CO₃, MeCN, 96 %; (b) Pd/C, EtOH, formic acid, H₂, 98 %; (c) paraformaldehyde, 2-nitrocyclohexanone, MeOH, 77 %; (d) Raney[®]-Nickel, EtOH, H₂, 72 %; (e) *tert*-butyl bromoacetate, DIPEA, MeCN, 62 %; (f) Formalin (37 %), AcOH, NaBH₄, ACN, 74 %; (g) LiOH, dioxane/H₂O, 84 %; (h) *tert*butyl(2-aminoethyl)carbamate, HATU, DIPEA, ACN, 94 %; (i) TFA/DCM, 1:1.

N,N'-dibenzylethyldiamines were first reacted with *tert*-butyl bromoacetate to give the di-alkylated compound **1**. The benzyl protecting groups were then removed by reduction. The diazepane **3** was formed by a double Mannich reaction. For this purpose, 2-nitrocyclohexanone was used, the ring of which was opened using the anion exchanger Amberlyst[®] A21. In the following Mannich reaction, this ring-opened intermediate reacted with **2** to form the desired diazepane **3**.

After reduction of the nitro group (**4**), *tert*-butyl bromoacetate was added in an undercurrent to give the mono-alkylated compound **5**. The secondary amine of **5** was then methylated in a reductive amination. This led to the protected chelator DATA^{5m} **6**. In order to functionalise **6** with the target vector, however, it was necessary to introduce an ethylenediamine bridge. For this purpose, the methyl ester of **6** was saponified using lithium hydroxide (compound **7**) and the mono Boc-protected ethylenediamine was linked via an amide coupling to get **8**. After an acidic deprotection compound **9** can be conjugated to the targetvector using squaric acid.

The PSMA inhibitor lysine-urea-glutamate (KuE) was synthesized and coupled to 3,4-dibutoxycyclobut-3-en-1,2-dione (SADE) according to figure 4.

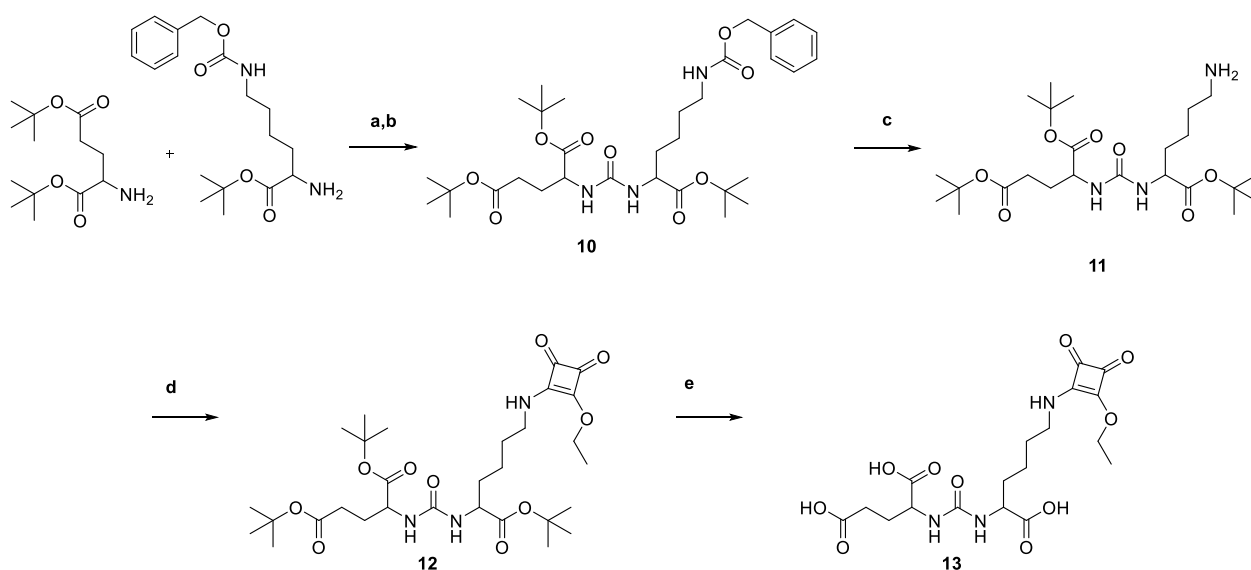


Figure 4 Synthesis of the PSMA-inhibitor lysine-urea-glutamate-squaric acid monoester: (a) *N*(*ε*)-benzyloxycarbonyl-L-lysine, triphosgene, triethylamine DCM, 0°C; (b) *L*-glutamic acid di-*tert*-butyl ester hydrochloride, triethylamine, DCM, 41 %; (c) Pd/C, MeOH, H₂, 96 %; (d) 3,4-dibutoxycyclobut-3-en-1,2-dione, 0.5 M phosphate buffer pH 7, ethyl acetate, 77 %; (e) TFA/DCM, 1:1, 83 %.

For the introduction of the urea unit the amino group of protected lysine was transformed into an isocyanate using triphosgene. The isocyanate was then reacted with *tert*-butyl protected glutamate and the protected PSMA-inhibitor lysine-urea-glutamate **10** was obtained and followed by reductive deprotection of the lysine side chain yielding **11**. This compound was then coupled to SADE in phosphate buffer at pH 7. Acidic deprotection of the protected compound **12** led to the couplable PSMA-inhibitor lysine-urea-glutamate-squaric acid monoester **13** (KuE.SAME).

The free primary amine of DATA^{5m} (**9**) was then coupled to the free coupling side of KuE.SAME (**13**) in 0.5 M phosphate buffer at pH 9 to obtain the final compound DATA^{5m}.SA.KuE (**14**) (Figure 5).

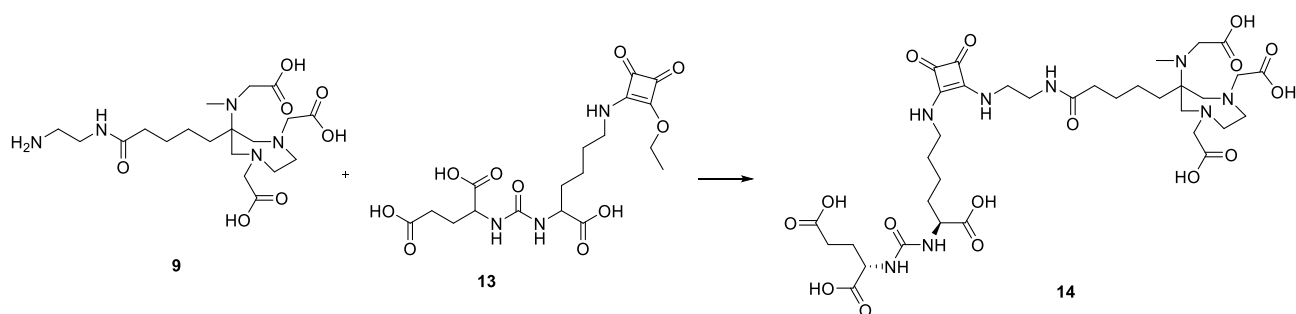


Figure 5 Synthesis of DATA^{5m}.SA.KuE (**14**) 0.5 M phosphate buffer pH 9, 10 %.

2.2. Radiolabeling

Radiolabeling of AAZTA⁵.SA.KuE with ⁶⁸Sc and ¹⁷⁷Lu was performed according to literature ¹⁷.

DATA^{5m}.SA.KuE was radiolabeled with gallium-68 in ammonium acetate buffer (1 M, pH 5.5), varying amounts of precursor (5 nmol to 60 nmol) and different temperatures (room temperature to 70 °C). Labeling was carried out in triplicate with 30 – 50 MBq of gallium-68. Figure 6A shows the kinetic studies of the ⁶⁸Ga-radiolabeling of DATA^{5m}.SA.KuE. The lower the quantity of precursor used, the higher the temperature required to obtain quantitative radiochemical yields (RCY). Labeling of 10 nmol at 50 °C only achieve a RCY of 56 % after 15 minutes. The increase to 15 nmol at 50 °C results in quantitative RCY (> 99 %). The increase of temperature even allows the quantitative labeling (> 99 % RCY) of 5 nmol. 50 µg (60 nmol) can be radiolabeled in yields of over 99 % with gallium-68 even at room temperature. The high radiochemical yield and high purity of [⁶⁸Ga]Ga-DATA^{5m}.SA.KuE was confirmed by radio-HPLC (Figure 6B).

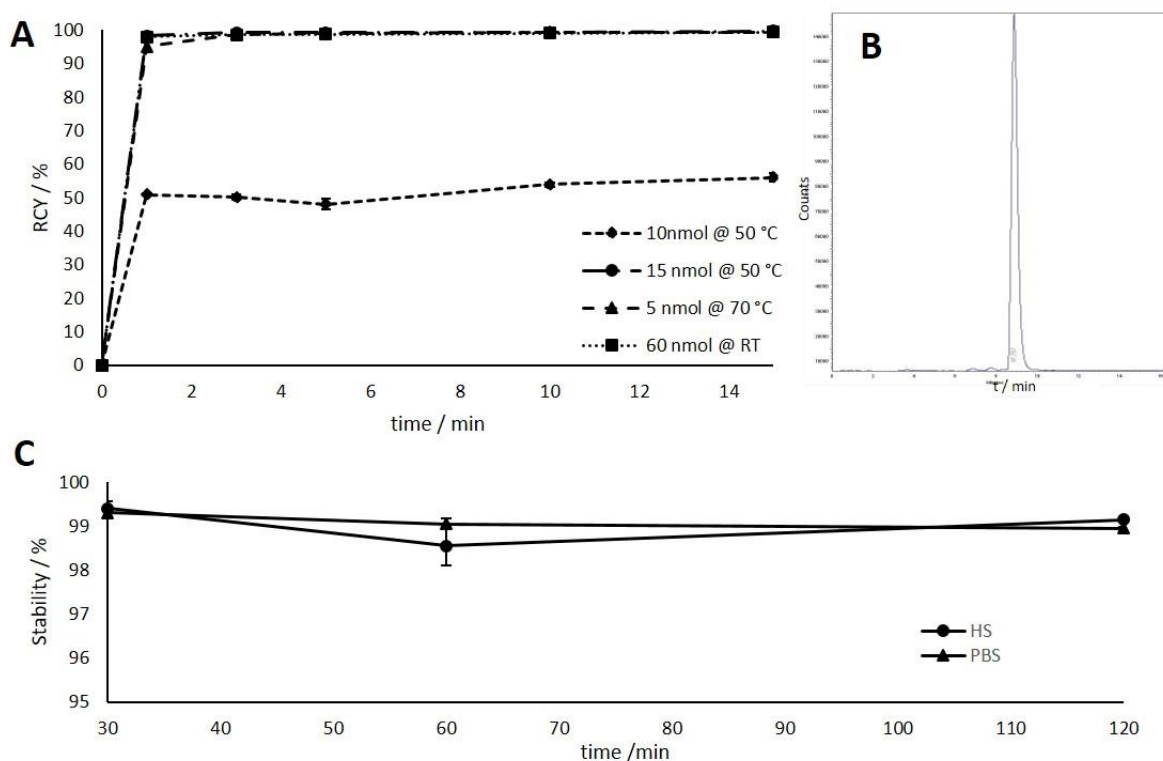


Figure 6 A: Kinetic studies of ⁶⁸Ga-radiolabeling of DATA^{5m}.SA.KuE for various amounts of precursor and different temperatures. Labeling of 15 nmol at 50 °C, 5 nmol at 70 °C and 60 nmol at RT resulting in quantitative RCYs after one minute. Radiolabeling of 10 nmol at 50 °C results in a RCY of 56 % after 15 minutes. B: radio-HPLC of [⁶⁸Ga]Ga-DATA^{5m}.SA.KuE. t_R (free ⁶⁸Ga) = 2.0 min; t_R ([⁶⁸Ga]Ga-DATA^{5m}.SA.KuE) = 8.8 min. radio-HPLC confirmed purity and high RCY of [⁶⁸Ga]Ga-DATA^{5m}.SA.KuE. C: Stability studies for [⁶⁸Ga] Ga-DATA^{5m}.SA.KuE complex in human serum (HS) and phosphate buffered saline (PBS) of intact conjugate at different time points.

Studies of the complex stability were performed in human serum (HS) and phosphate buffered saline (PBS). In both media, [^{68}Ga]Ga-DATA 5m .SA.KuE showed a stability of > 98 % over a period of 120 minutes (Figure 6C)

2.2. *In vitro* studies

2.2.1. PSMA-binding affinity

The potency of PSMA-binding of DATA 5m .SA.KuE and AAZTA 5 .SA.KuE has been determined in a competitive radioligand assay and compared with the binding affinity of PSMA-11 measured in the same assay. Results are plotted as inhibition curves (Figure 7) and IC $_{50}$ values are determined using GraphPad Prism (Table 1). AAZTA 5 .SA.KuE and DATA 5m .SA.KuE showed similar binding affinities while PSMA-11 seems to have two-fold higher potency *in vitro*.

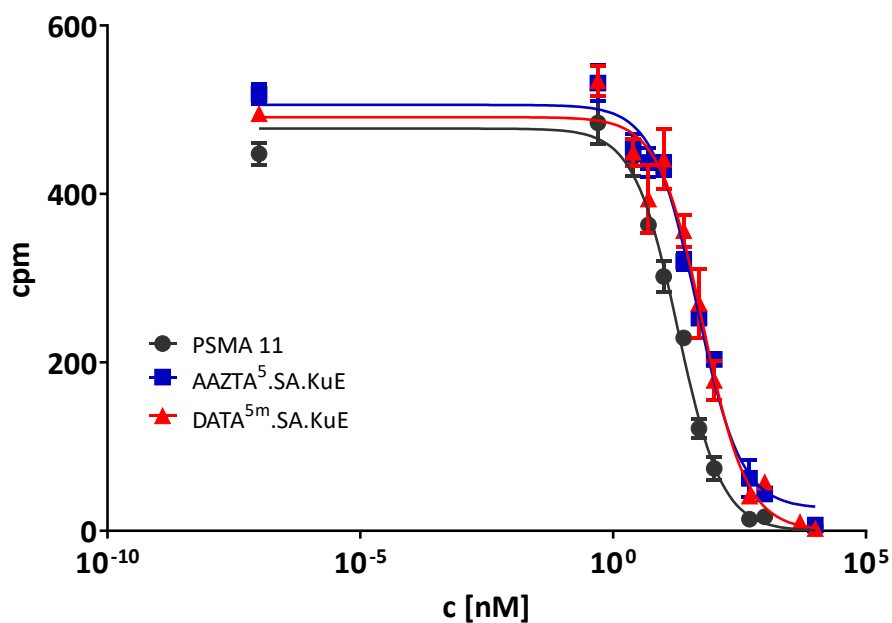


Figure 7 Inhibition curve of AAZTA 5 .SA.KuE, DATA 5m .SA.KuE and PSMA-11. cpm: counts per minute.

Table 1 IC₅₀ values of the investigated compounds. Data represented as Mean ± SD (n=3)

Compound	IC ₅₀ [nM]
DATA ^{5m} .SA.KuE	51.1 ± 5.5
AAZTA ⁵ .SA.KuE	52.1 ± 4.0
PSMA-11	26.2 ± 2.4

2.2.2. Internalization rate

PSMA ligands are internalized upon binding to PSMA probably via clathrin-mediated endocytosis^{33,34}. To determine the PSMA-specific cellular uptake of the developed PSMA ligands, we measured both the surface-bound and the internalized radioactivity in PSMA-positive LNCaP cells at four different conditions; at 37°C with and without blocking with the potent PSMA inhibitor PMPA (2-Phosphonomethyl pentanedioic acid) and at 4°C with and without blocking with PMPA. Results are plotted in Figure 8. [⁶⁸Ga]Ga-DATA^{5m}.SA.KuE displayed the highest internalization ratio 6.6 ± 0.6 %, whereas the uptake fractions of [⁴⁴Sc]Sc-AAZTA⁵.SA.KuE and [⁶⁸Ga]Ga-PSMA-11 were slightly lower (4.8 % and 5.2 % respectively). This PSMA-specific uptake was mainly reduced at 4°C.

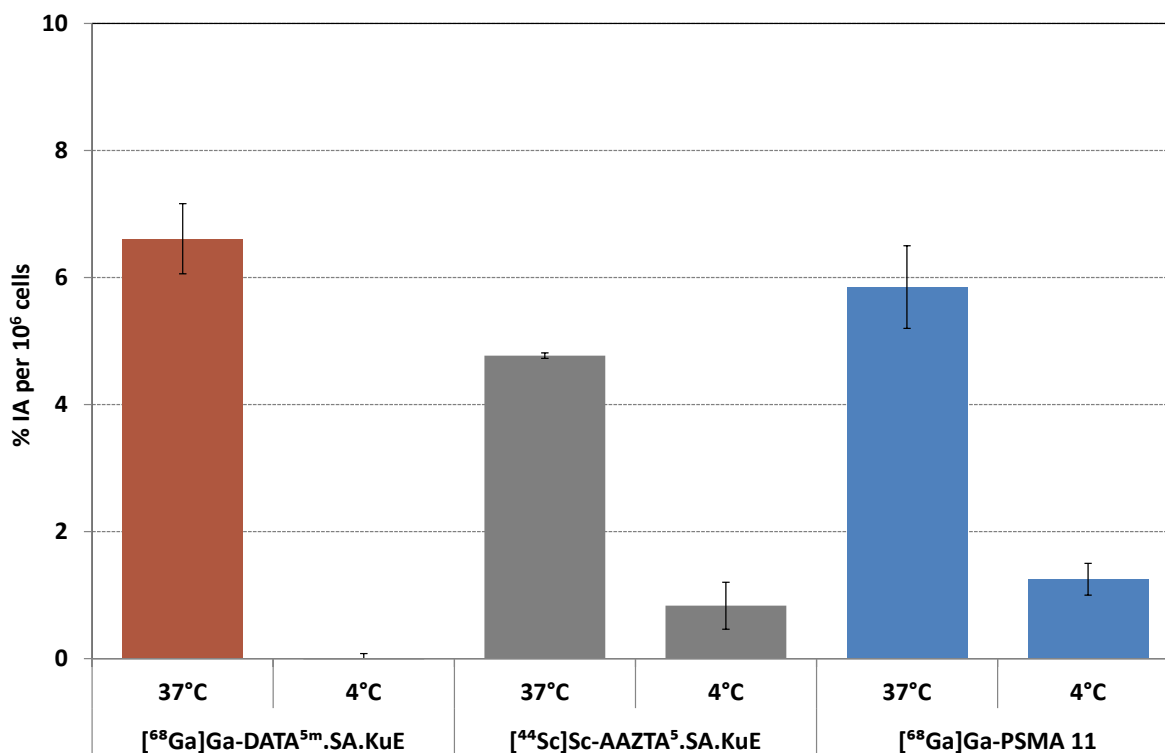


Figure 8 Internalization rate of [⁶⁸Ga]Ga-DATA^{5m}.SA.KuE and [⁴⁴Sc]Sc-AAZTA⁵.SA.KuE with [⁶⁸Ga]Ga-PSMA-11 as reference. % injected dose per 10⁶ LNCaP cells.

2.3. Animal studies

In order to evaluate the *in vivo* behavior of the SA.KuE-conjugates, an LNCaP-xenograft model was used. Labeling of AAZTA⁵.SA.KuE with the different nuclides scandium-44 and lutetium-177 seems to have no impact on the pharmacokinetic properties of the conjugates since there were no significant differences observed in the biodistribution data (Figure 9). Tumor accumulation values of all four compounds were similar, 3.92 ± 0.50 %ID/g; 5.41 ± 0.83 %ID/g; 4.43 ± 0.56 %ID/g and 5.52 ± 0.75 %ID/g for [⁴⁴Sc]Sc-AAZTA⁵.SA.KuE, [¹⁷⁷Lu]Lu-AAZTA⁵.SA.KuE, [⁶⁸Ga]Ga-DATA^{5m}.SA.KuE and [⁶⁸Ga]Ga-PSMA-11 respectively. Noteworthy is the higher Kidney-uptake of [⁶⁸Ga]Ga-PSMA-11 (73.39 ± 18.77 %ID/g) compared to the uptake of the SA.KuE-conjugates (20.69 ± 7.24 %ID/g, 22.70 ± 0.90 %ID/g, 13.63 ± 6.81 %ID/g for [⁴⁴Sc]Sc-AAZTA^{5m}.SA.KuE, [¹⁷⁷Lu]Lu-AAZTA^{5m}.SA.KuE and [⁶⁸Ga]Ga-DATA⁵.SA.KuE respectively. Both, tumor and kidney uptake of [⁶⁸Ga]Ga-DATA⁵.SA.KuE were found to be PSMA-specific since they could be blocked by co-injection of PMPA as seen in figure 10.

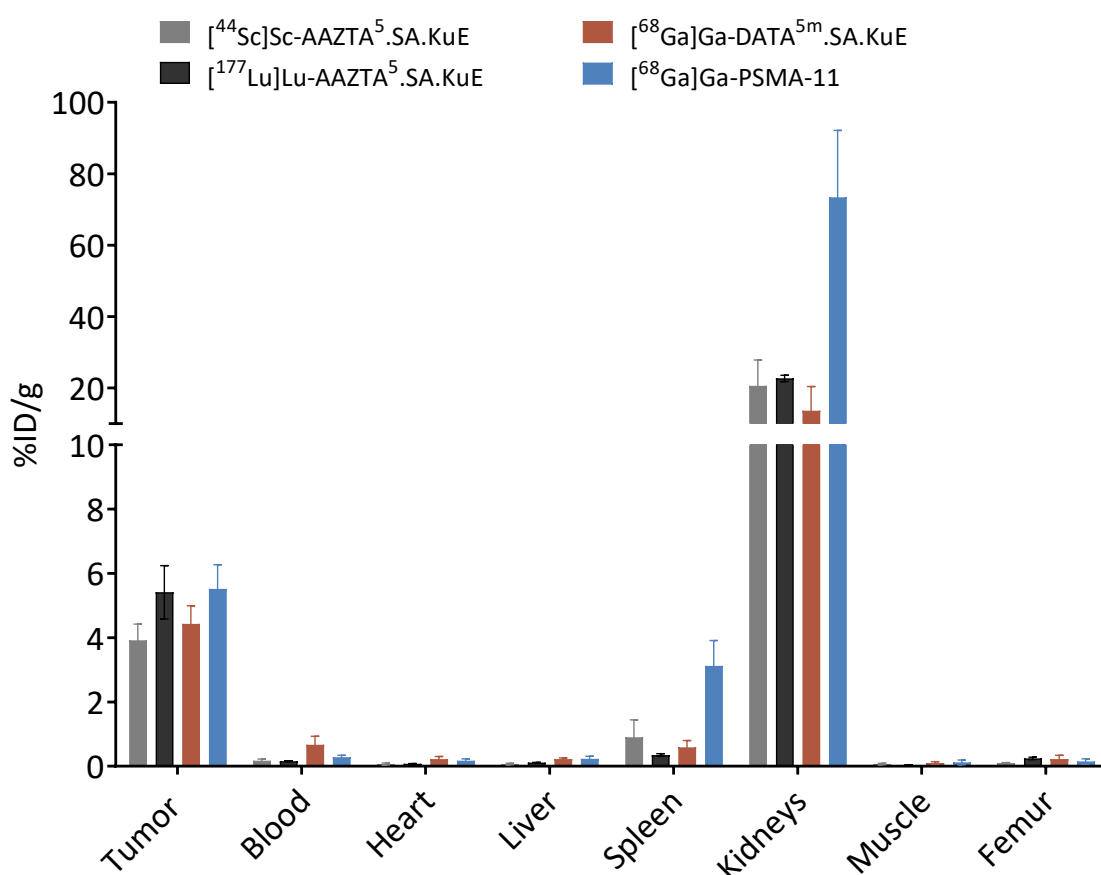


Figure 9 Ex vivo biodistribution data of [⁴⁴Sc]Sc-AAZTA⁵.SA.KuE, [¹⁷⁷Lu]Lu-AAZTA⁵.SA.KuE, [⁶⁸Ga]Ga-DATA^{5m}.SA.KuE and [⁶⁸Ga]Ga-PSMA-11 in LNCaP tumor-bearing Balb/c nude mice 1h p.i. %ID/g: % injected dose per gram. Values are mean ± SD.

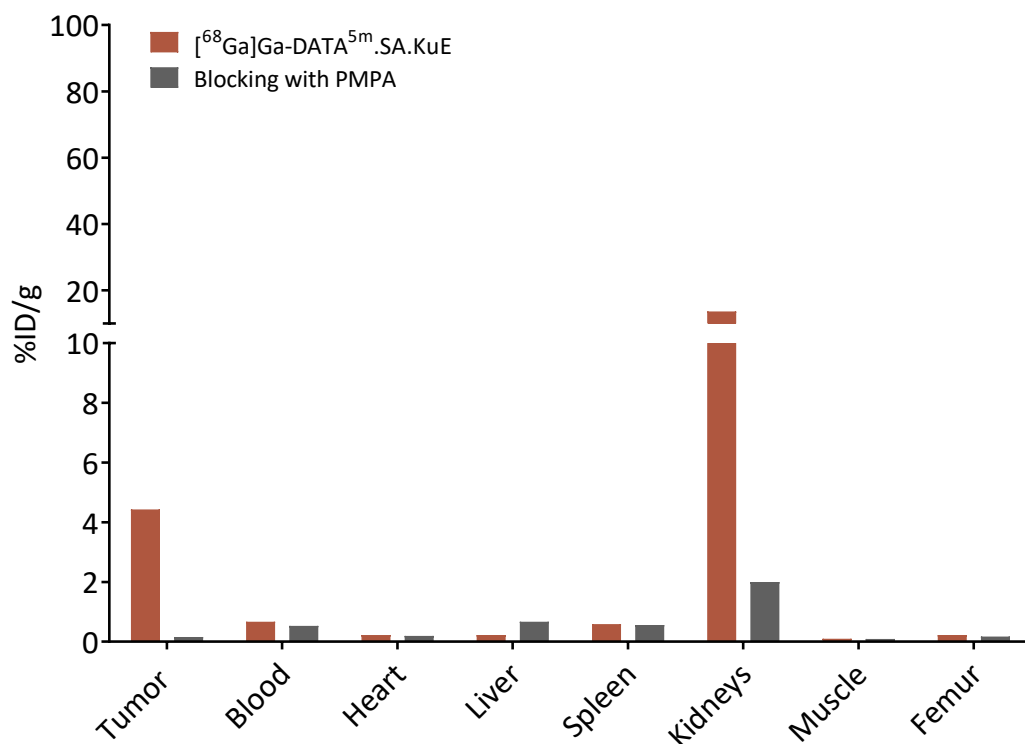
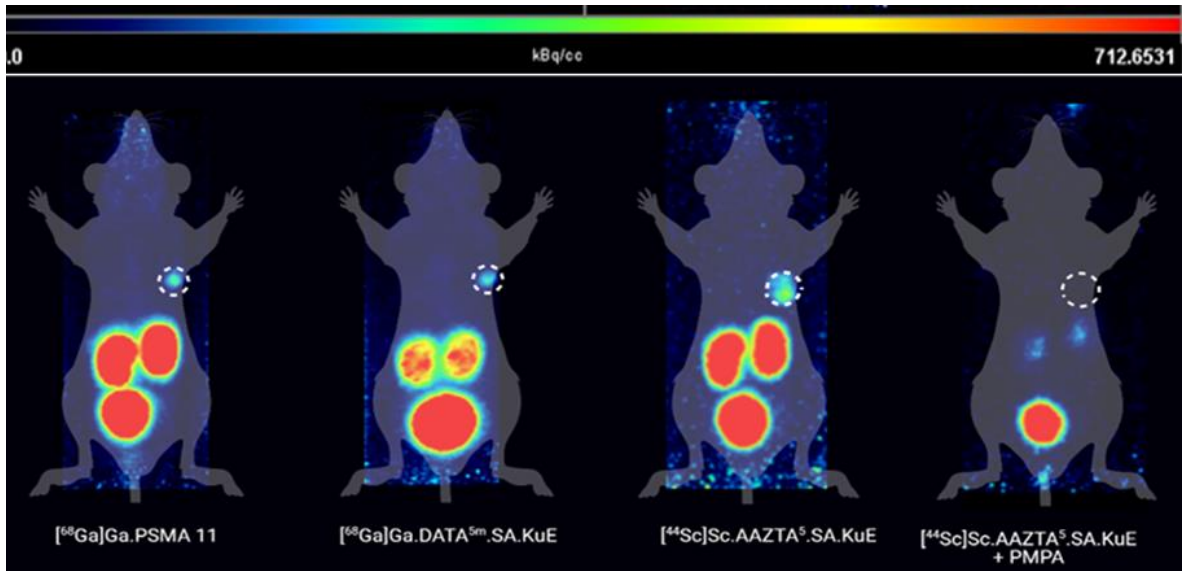


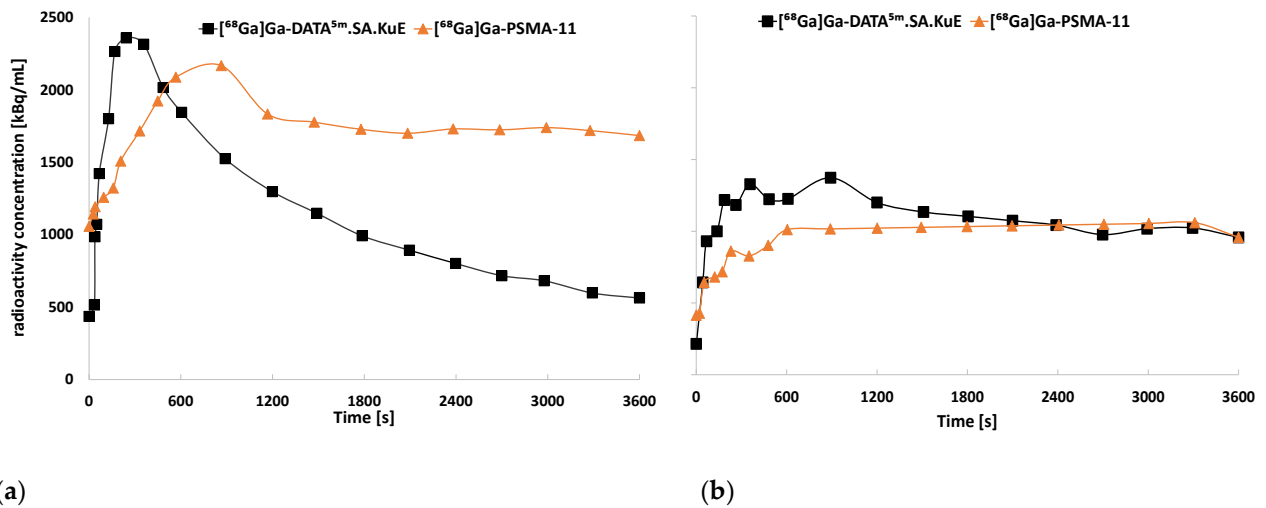
Figure 10 Ex vivo biodistribution of [⁶⁸Ga]Ga-DATA^{5m}.SA.KuE compared to organ accumulation after co-injection with an access PMPA.

To further understand the pharmacokinetics of the developed PSMA ligands, we performed μ PET-scans with the same xenograft model (Figure 11). Tumor accumulation of all three compounds was very similar. The kidney uptake of [⁶⁸Ga]Ga-DATA⁵.SA.KuE was remarkably lower than the reference compound [⁶⁸Ga]Ga-PSMA-11. This finding correlates with the results obtained from the time-activity curves of both compounds (Figure 12). Herein the radioactivity concentration of [⁶⁸Ga]Ga-DATA^{5m}.SA.KuE decreased continuously 10 min p.i. while the concentration in the tumor remained constant. However, the radioactivity concentration of [⁶⁸Ga]Ga-PSMA-11 remained at a higher level during the period of the scan. As demonstrated in the μ PET scans, uptake in the tumor as well as in the kidney was PSMA-specific. After co-injection of PMPA almost no radioactivity could be detected (Figure 11).



(a) (b) (c) (d)

Figure 11 Maximum intensity projections of μ PET scans 1h p.i. of (a) $[^{68}\text{Ga}]\text{Ga-PSMA-11}$, (b) $[^{68}\text{Ga}]\text{Ga-DATA}^{5m}.\text{SA.KuE}$, (c) $[^{44}\text{Sc}]\text{Sc-AAZTA}^5.\text{SA.KuE}$ and (d) co-injection of $[^{44}\text{Sc}]\text{Sc-AAZTA}^5.\text{SA.KuE}$ and PMPA. (tumor circled).



(a) (b)

Figure 12 Time-activity curves of the uptake of $[^{68}\text{Ga}]\text{Ga-DATA}^{5m}.\text{SA.KuE}$ and $[^{68}\text{Ga}]\text{Ga-PSMA-11}$ in the kidneys (a) and the tumor (b) over the total period of the μ PET scan.

3. Discussion

The discovery of PSMA as molecular target in diagnosis and therapy of prostate cancer as well as the application of radiolabeled PSMA inhibitors have revolutionized the management of this disease resulting in a significant improvement especially in staging and assessment of prostate cancer³⁵. Although several PSMA ligands have been developed over the last decades, the search for novel tracer with optimized pharmacokinetic properties particularly for therapeutic purposes is still present, since some of the clinically used PSMA radioligand therapeutics e.g. [²²⁵Ac]Ac-PSMA-617 showed some severe side effects like xerostomia^{12,13,36}.

To determine the effect of the chelator on the PSMA-binding affinity and the internalization rate of PSMA ligands, we synthesized two PSMA inhibitors with different hybrid chelators. In the cell-based assays, both DATA^{5m}.SA.KuE and AAZTA⁵.SA.KuE showed similar binding potency and internalization ratios indicating that an exchange of DATA^{5m} against AAZTA⁵ have no impact neither on the binding affinity nor on the internalization ratio in PSMA-positive LNCaP cells. These findings correlate with the results published elsewhere³⁷. PSMA-11 displayed higher potency *in vitro* which could be due to the better interaction with the PSMA binding pocket. However, the internalization ratio of PSMA-11 was similar to these of the SA.KuE-conjugates. The PSMA-specificity of binding and uptake in LNCaP cells and LNCaP-tumor could be demonstrated by blocking PSMA-receptors with the potent inhibitor PMPA.

In order to evaluate the pharmacokinetic behavior of our compounds and to compare them with PSMA-11, we performed animal studies using an LNCaP-xenograft model.

AAZTA⁵.SA.KuE was labeled with the positron emitter ⁴⁴Sc and the β -emitter ¹⁷⁷Lu. Both radiotracers displayed similar biodistribution data indicating that both isotopes do not impact the pharmacokinetic properties of the PSMA radioligand. This result makes this pair ideal for a theranostic use. In addition, [⁶⁸Ga]Ga-DATA^{5m}.SA.KuE equally showed a promising biodistribution profile and a good imaging contrast. Surprisingly, although PSMA-11 showed a two-fold higher binding potency *in vitro*, tumor accumulation was similar to the SA.KuE-conjugates. Furthermore the kidney uptake of [⁶⁸Ga]Ga-PSMA-11 was significantly higher than the SA.KuE-conjugated compounds. [⁶⁸Ga]Ga-DATA^{5m}.SA.KuE, [⁴⁴Sc]Sc-AAZTA⁵.SA.KuE and [¹⁷⁷Lu]Lu-AAZTA⁵.SA.KuE. Thus, these compounds seem to display a rapid renal clearance along with a good tumor accumulation.

Accordingly, the *in vivo* properties of both SA.KuE-conjugates were more favorable than PSMA-11 since the kidney uptake was remarkably reduced, whilst showing a similar tumor accumulation. The reduced kidney uptake may lower the nephrotoxicity of [¹⁷⁷Lu]Lu-PSMA inhibitors resulting in a minimization of side effects and an improvement of tolerability.

4. Materials and Methods

4.1. General

All chemicals were purchased from Sigma-Aldrich, Merck, Fluka, AlfaAesar, VWR, AcrosOrganics, TCI, Iris Biotech and Fisher Scientific and used without purification. Dry solvents were obtained from Merck and VWR, deuterated solvents for NMR spectra from Deutero. Thin layer chromatography was performed with silica gel 60 F254 coated aluminum plates from Merck. Evaluation was carried out by fluorescence extinction at $\lambda=254$ nm and staining with potassium permanganate. The radio TLCs were evaluated using a CR-35 Bio test imager and the AIDA software (Elysia-Raytest, Belgium). The ^1H and ^{13}C NMR measurements were performed on an Avance III HD 300 spectrometer (Bruker Corporation, Billerica, MA, USA) (300 MHz, 5mm BBFO sample head with z-gradient and ATM and BACS 60 sample changer), an Avance II 400 spectrometer (Bruker Corporation, Billerica, MA, USA) (400 MHz, 5 mm BBFO sample head with z-Gradient and ATM and SampleXPress 60 sample changer) and an Avance III 600 spectrometer (600 MHz, 5mm TCI CryoProbe sample head with z-Gradient and ATM and SampleXPress Lite 16 sample changer) from Bruker. The LC/MS measurements were performed on an Agilent Technologies 1220 Infinity LC system coupled to an Agilent Technologies 6130B Single Quadrupole LC/MS system. Semi-preparative HPLC purification was performed on a 7000 series Hitachi LaChrom (Hitachi, Chiyoda, Japan).

4.2. Organic Synthesis

DATA^{5m} was synthesized according to the procedure described by Farkas et al. and Greifenstein et al.¹⁷

N,N'-Dibenzyl-N,N'-di-(tert-butylacetate)-ethylenediamine (1)

N,N'-dibenzylethylenediamine (2.90 mL, 3.00 g, 12.50 mmol) and sodium carbonate (5.10 g, 48.70 mmol) were dissolved in acetonitrile (50 mL) and stirred for 30 min at room temperature. Tert butyl bromoacetate (3.60 mL, 4.60 g, 23.70 mmol) in acetonitrile (10 mL) was added dropwise at room temperature. The reaction mixture was stirred overnight at 90 °C and filtered. The solvent was evaporated under reduced pressure. The product was purified by column chromatography (hexane/ethyl acetate; 6:1, R_f = 0.37) and obtained as colourless solid (5.73 g, 12.2 mmol, 96 %).

$^1\text{H-NMR}$ (400 MHz, CDCl_3): δ [ppm] = 7.34-7.21 (m, 10H), 3.78 (s, 4H), 3.26 (s, 4H), 2.82 (s, 4H), 1.44 (s, 18H).

¹³C-NMR (400 MHz, CDCl₃): δ [ppm] = 171.03, 139.18, 129.05, 128.30, 127.10, 80.86, 58.39, 55.27, 51.73, 28.24.

MS (ESI⁺): 469.4 [M+H]⁺, calculated for C₂₈H₄₀N₂O₄: 468.30 [M]⁺.

N,N'-di-(tert-butylacetate)-ethylenediamine (2)

Product 1 (2.3 g; 5.60 mmol) was dissolved in abs ethanol (15 mL) and formic acid (0.43 mL, 0.52 g, 11.0 mmol). To this solution palladium on activated carbon (416 mg, 16 %wt) was added and the solution was saturated, kept and stirred overnight with hydrogen. Pd/C was filtered over celite and the solvent was evaporated under reduced pressure. The product (1.58 mg, 5.5 mmol, 98 %) was used without further purification.

MS (ESI⁺): 289.3 [M+H]⁺, calculated for C₁₄H₂₈N₂O₄: 288.36 [M]⁺.

1,4-Di(tert-butylacetate)-6-methyl-6-nitroperhydro-1,4-diazepane (3)

2-Nitrocyclohexanone (1.70 g, 12 mmol) and Amberlyst[®] A21 (2 mass equivalents) were dissolved in methanol (30 ml) and stirred at 90 °C for 1 h. Paraformaldehyde (1.30 g, 42.3 mmol) and Product (2) (3.50 g, 12 mmol) were added. The solution was heated overnight under reflux. The solvent was evaporated under reduced pressure. The product was purified by column chromatography (hexane/ethyl acetate; 2:1, R_f = 0.33) and obtained as yellowish oil (4.52 g, 9.28 mmol, 77 %).

¹H-NMR (400 MHz, CDCl₃): δ [ppm] = 3.65 (s, 3H), 3.60 (d, J = 14,6 Hz, 2H), 3.45 (d, J = 17,3 Hz, 2H), 3.30 (d, J = 17,3 Hz, 2H), 3.12 (d, J = 14,6 Hz, 2H), 2.84 (m, 4 H), 2.27 (t, 2H), 1.83 (m, 2H), 1.57 (m, 2H), 1.46 (s, 18H), 1.18 (m, 2H).

¹³C-NMR (400 MHz, CDCl₃): δ [ppm] = 173.73, 170.92, 95.12, 81.31, 61.57, 61.18, 56.87, 51.68, 37.27, 33.71, 28.35, 24.82, 22.99.

MS (ESI⁺): 488.3 [M+H]⁺, calculated for C₂₃H₄₁N₃O₈: 487.29 [M]⁺.

1,4-Di(tert-butylacetate)-6-methylpentanoate-6-amino-perhydro-1,4-diazepane (4)

Compound 3 (4.50 g, 9.30 mmol) was dissolved in abs. ethanol (40 mL). Raney[®] nickel was added and the solution was saturated, kept and stirred for four days with hydrogen at 40 °C. The nickel was filtered over celite and the solvent was evaporated under reduced pressure. Compound (4) (3.92 g, 8.60 mmol, 72 %), was obtained as greenish oil and used without further purification.

MS (ESI⁺): 458.3 [M+H]⁺, calculated for C₂₃H₄₃N₃O₆: 457.32 [M]⁺.

1,4-Di(tert-butylacetate)-6-methylpentonate-6-amino-tert-butylacetate-perhydro-1,4-diazepane (5)

Compound 4 (1.30 g, 2.84 mmol) and N,N-diisopropylethylamine (483 μL, 367 mg, 2.84 mmol) were dissolved in dry acetonitrile (20 mL) and stirred for 20 min at room temperature. Tert-butyl bromoacetate (538 μL, 720 mg, 3.69 mmol) was added dropwise and stirred overnight at room temperature. The solvent was evaporated under reduced pressure. The product was purified by column chromatography (cyclohexane/ethyl acetate; 3:1 + 3 % trimethylamine, R_f = 0.34) and obtained as yellowish oil (1.01 g, 1.77 mmol, 62 %)

¹H-NMR (400 MHz, CDCl₃): δ [ppm] = 3.65 (s, 3H), 3.29 (s, 4H), 3.21 (s, 2H), 2.83–2.60 (m, 8H), 2.30 (dd, J = 8.9, 6.3 Hz, 2H), 1.90 (s br, 1H), 1.62–1.54 (m, 2H), 1.46 (s, 9H), 1.44 (s, 18H), 1.32–1.23 (m, 4H).

MS (ESI⁺): 572.4 [M+H]⁺, calculated for C₂₉H₅₃N₃O₈: 571.38 [M]⁺.

1,4-Di(tert-butylacetate)-6-methylpentonate-6-(amino(methyl)-tert-butylacetate)-perhydro-1,4 diazepane (6)

Compound 5 (1.00 g, 1.75 mmol), formalin solution (482 μL, 526 mg, 6.47 mmol) and acetic acid (300 μL, 315 mg, 5.25 mmol) were dissolved in dry acetonitrile (20 mL) and stirred at room temperature for 30 min. Sodium borohydride (200 mg, 5.29 mmol) was added portionwise over 30 min. The reaction solution was stirred for 2 hours at room temperature. Water (25 mL) was added and extracted with chloroform (4 x 50 mL). The organic phase was separated and dried over sodium sulfate and evaporated under reduced pressure. The product was purified by column chromatography (cyclohexane/ethyl acetate; 5:1 + 2 % trimethylamine, R_f = 0.28) and obtained as colourless oil (0.76 g, 1.39 mmol, 74 %).

¹H-NMR (400 MHz, CDCl₃): δ [ppm] = 3.65 (s, 3H), 3.42 (s, 2H), 3.32–3.18 (m, 4H), 2.93 (d, J = 14.0 Hz, 2H), 2.83–2.73 (m, 2H), 2.70–2.58 (m, 4H), 2.35–2.24 (m, 5H), 1.63–1.48 (m, 4H), 1.45 (s, 9H), 1.44 (s, 18H), 1.41–1.22 (m, 2H).

MS (ESI⁺): 586.4 [M+H]⁺, calculated for C₃₀H₅₅N₃O₈: 585.40 [M]⁺.

1,4-Di(tert-butylacetate)-6-pentanoicacid-6-(amino(methyl)-tert-butylacetate)-perhydro-1,4-diazepane (7)

Compound 6 (0.75 g, 1.28 mmol) was dissolved in a 1,4-dioxane/water (2:1) mixture. 1 M lithium hydroxide solution (1.92 mL, 1.92 mmol) was added and stirred for 7 days. After 2, 4 and 6 days 1 M lithium hydroxide solution (0.32 mL, 0.32 mmol) was added. 1,4-dioxane was evaporated under reduced pressure. The remaining water phase was extracted with chloroform (5 x 50 mL). The organic phase was washed with 1 M sodium hydrogencarbonate solution (25 mL) and brine (2 x 25 mL) and dried over sodium sulfate and evaporated under reduced pressure. The product (615 mg, 1.07 mmol, 84 %) was obtained as yellowish oil.

¹H-NMR (400 MHz, CDCl₃): δ [ppm] = 3.44 (s, 2H), 3.25 (d, J = 2.2 Hz, 4H), 2.93 (d, J = 14.0 Hz, 2H), 2.82–2.73 (m, 2H), 2.71–2.61 (m, 4H), 2.34 (t, J = 7.7 Hz, 2H), 2.27 (s, 3H), 1.65–1.51 (m, 4H), 1.45 (s, 18H), 1.44 (s, 9H), 1.43–1.21 (m, 2H).

¹³C-NMR (400 MHz, CDCl₃): δ [ppm] = 178.46, 172.53, 170.98, 81.02, 80.44, 77.36, 62.86, 62.59, 62.48, 59.02, 54.21, 37.49, 36.92, 34.17, 28.37, 28.27, 25.71, 21.97.

MS (ESI⁺): 572.4 [M+H]⁺, calculated for C₂₉H₅₃N₃O₈: 571.38 [M]⁺.

1,4-Di(tert-butylacetate)-6-((5-(2-((2-ethoxy-3,4-dioxocyclobut-1-en-1yl)amino-ethyl)amino)-5-oxopentyl)-6-(amino(methyl)-tert-butylacetate)-perhydro-1,4-diazepane (8)

Compound 7 (100 mg, 0.175 mmol), HATU (66.5 mg, 0.175 mmol) and DIPEA (90 μL, 69 mg, 0.525 mmol) were dissolved in dry acetonitrile (2 mL) and stirred for 15 min at room temperature. Tert-butyl(2-aminoethyl) carbamate (45 μL, 46 mg, 0.280 mmol) was added to the solution and stirred over night at room temperature. The solvent was evaporated under reduced pressure. The product was purified by column chromatography (dichloromethane/methanol; 20:1, R_f = 0.22) and obtained as colourless oil (118.4 mg, 0.166 mmol, 94 %).

¹H-NMR (400 MHz, CDCl₃): δ [ppm] = 6.34 (br, 1H), 5.26 (br, 1H), 3.60 (s, 4H), 3.38-3.34 (m, 2H), 3.26-3.24 (m, 2H), 3.21 (s, 4H), 2.96 (d, J = 14.1 Hz, 2H), 2.75-2.63 (m, 2H), 2.66-2.63 (m, 2H), 2.59 (d, J = 14.1 Hz, 2H), 2.19 (t, 2H), 1.62-1.53 (m, 4H), 1.43 (s, 18H), 1.42 (s, 27H), 1.28-1.20 (m, 2H).

¹³C-NMR (400 MHz, CDCl₃): δ [ppm] = 174.38, 173.31, 172.80, 165.88, 82.85, 82.77, 63.44, 62.48, 62.05, 55.48, 54.47, 47.11, 40.81, 39.87, 35.55, 29.82, 28.53, 28.32, 28.14, 27.91, 26.17, 23.41.

MS (ESI⁺): 714.5 [M+H]⁺, calculated for C₃₆H₆₇N₅O₉: 713.49 [M]⁺.

1,4-Di(acetate)-6-((5-(2-(aminoethyl)amino)-5-oxopentyl)-6-(amino(methyl)-acetate)-perhydro-1,4-diazepane (9)

Compound 8 (20 mg, 0.028 mmol) was dissolved in a solution of dichloromethane and trifluoroacetic acid (2 mL, 1:1) and stirred over night at room temperature. The solvent was evaporated under reduced pressure and used without further purification.

MS (ESI⁺): 446.2 [M+H]⁺, calculated for C₁₉H₃₅N₅O₇: 445.25 [M]⁺.

2-[3-(5-benzyloxycarbonylamino-1-tert-butoxycarbonyl-pentyl)-ureido]-pentanedioic acid di-tert-butyl ester (10)

Triphosgene (420 mg, 1.40 mmol) was dissolved in dichloromethane (5 mL) and cooled to 0 °C. A solution of N(ε)-benzyloxycarbonyl-L-lysine (1.42 g, 3.80 mmol) and triethylamine (1.05 mL, 765 mg, 7.60 mmol) in dichloromethane (25 mL) was added dropwise over a period of 3 hours at 0 °C. The reaction mixture was stirred for 40 minutes and L-glutamic acid di-tert-butyl ester hydrochloride (1.13 g, 3.80 mmol) and triethylamine (1.05 mL, 765 mg, 7.60 mmol) in dichloromethane (20 mL) was added. The solution was stirred over night at room temperature. The solution was evaporated under reduced pressure. Ethyl acetate (25 mL) was added. The organic layer was washed with saturated NaHCO₃-solution (2x 10 mL) and brine (2x 10 mL), dried over sodium sulfate and evaporated under reduced pressure. The residue was purified by column chromatography (hexane/ethyl acetate; 20:1, R_f = 0.26) and the product was obtained as colourless oil (357.6 mg, 0.58 mmol, 41 %).

¹H-NMR (300 MHz, CDCl₃): δ [ppm] = 7.38 – 7.22 (m, 5H), 5.16 (d, J = 13.5 Hz, 1H), 5.09 (d, J = 3.2 Hz, 2H), 4.32 (dt, J = 7.5, 5.2 Hz, 2H), 3.16 (s, 2H), 2.40 – 2.15 (m, 2H), 1.93 – 1.68 (m, 2H), 1.43 (m, 29H).

¹³C-NMR (300 MHz, CDCl₃): δ [ppm] = 172.54, 172.25, 172.15, 157.09, 156.61, 136.67, 128.47, 128.04, 128.01, 82.29, 81.84, 80.65, 77.24, 66.56, 53.38, 53.03, 40.63, 32.53, 31.52, 29.36, 28.28, 28.07, 28.00, 22.26.

MS (ESI⁺): 622.4 [M+H]⁺, 644.4 [M+Na]⁺, calculated for C₃₂H₅₁N₃O₉: 621.36 [M]⁺.

2-[3-(amino-1-tert-butoxycarbonyl-pentyl)-ureido]-pentanedioic acid di-tert-butyl ester (11)

Compound 10 (337.6 mg, 0.55 mmol) was dissolved in methanol (3 mL). To this solution palladium on activated carbon (22 mg) was added and the solution was saturated, kept and stirred overnight with hydrogen. Pd/C was filtered over celite and the solvent was evaporated under reduced pressure. The product (260 mg, 0.53 mmol, 96 %) was used without further purification.

¹H-NMR (300 MHz, CDCl₃): δ [ppm] = 5.48 (dd, J = 10.3, 8.1 Hz, 2H), 4.31 (dd, J = 5.7, 2.4 Hz, 2H), 2.77 (t, J = 6.6 Hz, 2H), 2.36 – 2.25 (m, 2H), 2.05 (ddd, J = 7.1, 5.9, 2.1 Hz, 1H), 1.92 – 1.68 (m, 2H), 1.44 (d, J = 7.1 Hz, 33H).

¹³C-NMR (300 MHz, CDCl₃): δ [ppm] = 172.61, 172.47, 157.05, 82.07, 81.67, 80.55, 53.39, 52.99, 41.12, 32.40, 31.66, 31.43, 28.28, 28.08, 28.02, 22.20.

MS (ESI⁺): 488.3 [M+H]⁺, calculated for C₂₄H₄₅N₃O₇: 487.33 [M]⁺.

2-[3-(2-(2-ethoxy-3,4-dioxo-cyclobut-1-en-1-yl)amino-1-tert-butoxycarbonyl-pentyl)-ureido]-pentanedioic acid di-tert-butyl ester (12)

Compound 11 (260 mg, 0.53 mmol) was dissolved in 0.5 M phosphate buffer (pH 7, 2 mL), 3,4-dibutoxycyclobut-3-en-1,2-dione (82 μL, 95 mg, 0.53 mmol) was added and the pH was adjusted to 7. Ethyl acetate (1 mL) was added and stirred overnight. The solvent was then removed via lyophilisation and ethyl acetate (2 mL) was added. The solution was then filtered and the solvent was removed under reduced pressure. The product (248 mg, 0.41 mmol, 77 %) was obtained as colourless oil and used without further purification.

¹H-NMR (300 MHz, CDCl₃): δ [ppm] = 4.78 – 4.73 (m, 2H), 4.13 (q, J = 7,1 Hz, 2H), 3.45 (d, J = 5,7 Hz, 2H), 2.36 – 2.32 (m, 2H), 2.06 (s, 4H), 1.74 – 1.55 (m, 2H), 1.52-1.43 (m, 27H), 1.27 (t, J = 7,1 Hz, 2H).

¹³C-NMR (300 MHz, CDCl₃): δ [ppm] = 189.09, 172.22, 157.27, 124.41, 125.10, 77.35, 77.03, 76.71, 70.07, 53.20, 44.39, 31.59, 28.00, 21.93, 21.07, 14.20.

MS (ESI⁺): 612,4 [M+H]⁺, calculated for C₃₀H₄₉N₃O₁₀: 611,34 [M]⁺.

2-[3-(2-(2-ethoxy-3,4-dioxo-cyclobut-1-en-1-yl)amino-1-carboxy-pentyl)-ureido]-pentanedioic acid (13)

Compound 12 (50 mg, 0.082 mmol) was stirred with a mixture of dichloromethane and trifluoroacetic acid (2 mL, 1:1) at room temperature for 2 hours. The solvent was evaporated under reduced pressure. The product was obtained as colourless oil (30.2 mg, 0.068 mmol, 83 %) and used without further purification.

$^1\text{H-NMR}$ (300 MHz, D_2O): δ [ppm] = 4.75 – 4.65 (m, 2H), 4.30 – 4.12 (m, 2H), 3.59 (dt, $J = 23,5$ Hz, 6,6 Hz, 1H), 3.48 (t, $J = 6,6$ Hz, 1H) 2.49 (t, $J = 7,3$ Hz, 2H), 2.16 (dtd, $J = 15,3$ Hz, 7,4 Hz, 5,2 Hz, 1H), 2.04 – 1.90 (m, 1H) 1.86 – 1.75 (m, 2H), 1.73 – 1.46 (m, 3H), 1.41 (dt, $J = 7,1$ Hz, 3,6 Hz, 5H).

$^{13}\text{C-NMR}$ (300 MHz, D_2O): δ [ppm] = 188.86, 182.94, 177.13, 176.95, 176.05, 173.15, 159.08, 70.41, 52.91, 52.48, 30.26, 29.91, 28.86, 26.15, 21.59, 14.95.

MS (ESI⁺): 444,2 [M+H]⁺, calculated for $\text{C}_{18}\text{H}_{25}\text{N}_3\text{O}_{10}$: 443,15 [M]⁺.

DATA^{5m}.SA.KuE (14)

Compound 9 (30 mg, 0.067 mmol) and compound 13 (42 mg, 0.095 mmol) were dissolved in 0.5 M phosphate buffer (pH 9, 1 mL). The pH was adjusted to 9 and stirred for two days at room temperature. The crude product was purified by HPLC (column: LiChrospher 100 RP18 EC (250 x 10 mm) 5 μ , flow rate: 5 mL/min, $\text{H}_2\text{O}/\text{MeCN} + 0.1$ % TFA, 9 to 15 % MeCN in 20 min, $R_t = 10.1$ min) to obtain DATA^{5m}.SA.KuE as white powder (5.26 mg, 0.0062 mmol, 10 %).

MS (ESI⁺): 843.3 [M+H]⁺, 422.2 [M+2H]²⁺, 441.2 [M+K+H]²⁺, calculated for $\text{C}_{35}\text{H}_{54}\text{N}_8\text{O}_{16}$: 842.37 [M]⁺.

4.3. Radiolabeling

For radiochemical evaluation, gallium-68 was eluted from a $^{68}\text{Ge}/^{68}\text{Ga}$ -generator (ITG Graching, Munich, Germany) and purified manually with an ethanol based post-processing to separate iron, zinc and germanium impurities ³⁸.

Radiolabeling was performed in 0.4 mL 1 M ammonium acetate buffer at pH 5.5. Reactions were carried out with different amounts of precursor (5, 10, 15, 60 nmol) and at different temperatures (RT, 50 °C and 70 °C) with 30 – 50 MBq Ga-68. The pH was controlled at the start and after the labeling. For reaction control, radio-TLC (TLC Silica gel 60 F254 Merck) and citrate buffer pH 4 as mobile phase and radio-HPLC using an analytical HPLC 7000 series Hitachi LaChrom (Column: Merck Chromolith® RP-18e, linear gradient of 5-95 % MeCN (+0.1 % TFA)/ 95-5 % Water (+0.1 % TFA) in 10 min) was used. TLC's were measured in TLC imager CR-35 Bio Test-Imager from Elysia-Raytest (Straubenhardt, Germany) with the analysis software AIDA (Elysia-Raytest, Belgium).

Radiolabeling of AAZTA⁵.SA.KuE with scandium-44 and lutetium-177 was performed according to literature ¹⁷.

4.4. In vitro stability studies

Complex stability studies were performed in human serum (HS, human male AB plasma, USA origin, Sigma Aldrich) and phosphate buffered saline (Sigma Aldrich). 8-10 MBq of the labeled compound were added to 0.5 mL of the media. After 30-, 60- and 120-min aliquots were taken to evaluate the radiochemical stability. The studies were carried out as triplicate.

4.5. in vitro binding affinity

PSMA binding affinity was determined according to literature ³⁹. LNCaP-cells (purchased from Sigma-Aldrich) were cultured in RPMI 1640 (Thermo Fisher Scientific) supplemented with 10% fetal bovine serum (Thermo Fisher Scientific), 100 µg/ml streptomycin, and 100 units/ml penicillin at 37°C in 5% CO₂.

10⁵ LNCaP cells per well were applied in MultiScreen_{HTS} DV Filter Plates (Merck Millipore) and incubated with 0.75 nM [^{68}Ga]Ga-PSMA-10 in the presence of 12 increasing concentrations of the non-labeled SA-conjugated compounds. After incubation at room temperature for 45 min, cells were washed several times with ice-cold PBS to remove free radioactivity. Cell-bound activity was measured in a γ -counter (2480 WIZARD2 Automatic Gamma Counter, PerkinElmer). Data were analyzed in GraphPad Prism 9 using nonlinear regression. For each concentration. Experiments were replicated 4-times.

4.6. internalization ratio

Internalization ratio was determined according to literature^{39,40}. Prior to seeding cells, 24-well plates were coated with 0.1% poly-L-lysine (Sigma-Aldrich) in PBS for 20 min at room temperature. Subsequently 10^5 LNCaP cells in 1 mL RPMI 1640 Medium were added in each well and incubated for 24 h at 37 °C. 250 μ L of the ^{68}Ga -labeled compounds in Opti-MEM™ I Reduced Serum (ThermoFisher) were added to each well to a final concentration of 30 nM. The plates were then incubated for 45 min at 4°C and 37°C respectively either with or without adding PMPA (Sigma-Aldrich) to a final concentration of 500 μ M. The supernatant was removed and the cells were washed several times with ice-cold PBS. Afterwards cells were incubated twice with 50 mM glycine buffer pH 2.8 for 5 min to remove the surface-bound radioactivity. In order to determine the internalized fraction of the compounds, cells were lysed by incubating with 0.3 M NaOH for 10 min.

4.7. animal studies

6- to 8-week-old male BALB/cAnNRj (Janvier Labs) were inoculated subcutaneously with 5×10^6 LNCaP cells in 200 μ L 1:1 (v/v) Matrigel/PBS (Corning®). *In vivo* and *ex vivo* experiments are conducted after the tumor has reached a volume of approximately 100 mm³.

LNCaP-xenografts were anesthetized with 2% isoflurane prior to i.v. injection of 0.5 nmol of the radio-labeled compounds. The specific activities of the tracers were approximately 10 MBq/nmol, 6 MBq/nmol and 15 MBq/nmol of ^{68}Ga -labeled compounds, [^{44}Sc]Sc-AAZTA⁵.SA.KuE and [^{177}Lu]Lu-AAZTA⁵.SA.KuE respectively. For blocking experiments mice were co-injected with 1.5 μ mol PMPA/mouse.

Biodistribution studies. Animals were sacrificed 1 h p.i. Organs of interest were collected and weighed. The radioactivity was measured and calculated as decay-corrected percentage of the injected dose per gram of tissue mass %ID/g.

MicroPET-imaging. After i.v. injection of the labeled compounds, anesthetized mice (one mouse for each group) were placed in the prone position in a nanoScan® PET/MR (Mediso). MRI measurements were performed followed by a static PET scan with the nanoScan PET/MRI (Mediso, Budapest, Hungary). PET data were reconstructed with Teratomo 3D (four iterations, six subsets, voxel size 0.4 mm), co-registered to the MR, and analyzed with Pmod software (version 3.6) (PMOD Technologies LLC, Zürich, Switzerland). Material Map for co-registration of the PET scan; 3D Gradient Echo External Averaging (GRE-EXT), Multi Field of View (FOV); slice thickness, 0.6 mm; TE, 2 ms; TR, 15 ms; flip angle, 25 deg.

5. Conclusion

In summary, the synthesized hybrid chelator-based PSMA radiopharmaceuticals DATA^{5m}.SA.KuE and AAZTA⁵.SA.KuE could be labeled at mild conditions with high radiochemical yields. The stability of the labeled compounds in PBS and human serum was demonstrated. Both SA.KuE conjugates displayed good PSMA binding affinities in LNCaP cells along with good internalization ratios. Additionally, [⁶⁸Ga]Ga-DATA^{5m}.SA.KuE, [⁴⁴Sc]Sc-AAZTA⁵.SA.KuE, and [¹⁷⁷Lu]Lu-AAZTA⁵.SA.KuE showed similar *in vivo* behavior, suggesting that the exchange of either the chelator or the nuclide does not impact the pharmacokinetic of the investigated compounds. This finding renders [⁴⁴Sc]Sc-AAZTA⁵.SA.KuE and [¹⁷⁷Lu]Lu-AAZTA⁵.SA.KuE an interesting pair for theranostic application. Tumor accumulation of the tested PSMA radioligands was similar to that of [⁶⁸Ga]Ga-PSMA-11, although lower than the value reported in literature for PSMA-617. The decreased kidney uptake of the SA.KuE conjugates is noteworthy, which could be a major benefit in reducing irradiation of the kidneys, resulting in lower nephrotoxicity and improved tolerability.

Author Contributions:

All authors have read and agreed to the published version of the manuscript.

Funding: This research received no external funding

Institutional Review Board Statement: The study was conducted according to the guidelines of the Declaration of Helsinki, and approved by the Ethics Committee of the state of Rhineland Palatinate according to §8 Abs. 1 Tierschutzgesetz, Landesuntersuchungsamt (23 177-07 G 15-1-033).

Informed Consent Statement: Not applicable

Data Availability Statement: The data presented in this study are available on request from the corresponding author.

Acknowledgments: The authors thank the Max Planck Graduate Center Mainz (MPGC) for supporting [REDACTED] and [REDACTED]. The authors gratefully acknowledge Avicenna-Studienwerk and Mainz Research School of Translational Biomedicine (TransMed) for supporting Hanane Lahnif.

Conflicts of Interest: The authors declare no conflict of interest

Sample Availability: Not available

References

1. Chang, S.S.; Heston, W.D.W. The clinical role of prostate-specific membrane antigen (PSMA). *Urol. Oncol.* 2002, 7, 7–12.
2. Chang, S.S.; Bander, N.H.; Heston, W.D.W. Biology of PSMA As a Diagnostic and Therapeutic Target. In *Management of Prostate Cancer*; Humana Press, 2004; pp. 609–630.
3. Gourni, E.; Henriksen, G.; Gamez, P.; Caballero, A.B. Metal-based PSMA radioligands. *Molecules* 2017, 22.
4. Silver, D.A.; Pellicer, I.; Fair, W.R.; Heston, W.D.; Cordon-Cardo, C. Prostate-specific membrane antigen expression in normal and malignant human tissues. *Clin. Cancer Res.* 1997, 3.
5. Perner, S.; Hofer, M.D.; Kim, R.; Shah, R.B.; Li, H.; Möller, P.; Hautmann, R.E.; Gschwend, J.E.; Kuefer, R.; Rubin, M.A. Prostate-specific membrane antigen expression as a predictor of prostate cancer progression. *Hum. Pathol.* 2007, 38, 696–701.
6. Prostate cancer statistics | World Cancer Research Fund International Available online: <https://www.wcrf.org/dietandcancer/prostate-cancer-statistics/> (accessed on May 19, 2021).
7. Ferlay, J.; Colombet, M.; Soerjomataram, I.; Mathers, C.; Parkin, D.M.; Piñeros, M.; Znaor, A.; Bray, F. Estimating the global cancer incidence and mortality in 2018: GLOBOCAN sources and methods. *Int. J. Cancer* 2019, 144, 1941–1953.
8. Rawla, P. Epidemiology of Prostate Cancer. *World J. Oncol.* 2019, 10, 63–89.
9. Kirby, M.; Hirst, C.; Crawford, E.D. Characterising the castration-resistant prostate cancer population: A systematic review. *Int. J. Clin. Pract.* 2011, 65, 1180–1192.
10. Kopka, K.; Benešová, M.; Bařinka, C.; Haberkorn, U.; Babich, J. Glu-ureido-based inhibitors of prostate-specific membrane antigen: Lessons learned during the development of a novel class of low-molecular-weight theranostic radiotracers; Society of Nuclear Medicine Inc., 2017; Vol. 58, pp. 17S-26S.
11. Benesová, M.; Schäfer, M.; Bauder-Wüst, U.; Afshar-Oromieh, A.; Kratochwil, C.; Mier, W.; Haberkorn, U.; Kopka, K.; Eder, M. Preclinical evaluation of a tailor-made DOTA-conjugated PSMA inhibitor with optimized linker moiety for imaging and endoradiotherapy of prostate cancer. *J. Nucl. Med.* 2015, 56, 914–920.
12. Valstar, M.H.; de Bakker, B.S.; Steenbakkers, R.J.H.M.; de Jong, K.H.; Smit, L.A.; Klein Nulent, T.J.W.; van Es, R.J.J.; Hofland, I.; de Keizer, B.; Jasperse, B.; et al. The tubarial salivary glands: A potential new organ at risk for radiotherapy. *Radiother. Oncol.* 2021, 154, 292–298.

13. Rupp, N.J.; Umbricht, C.A.; Pizzuto, D.A.; Lenggenhager, D.; Töpfer, A.; Müller, J.; Muehlematter, U.J.; Ferraro, D.A.; Messerli, M.; Morand, G.B.; et al. First clinicopathologic evidence of a non-PSMA-related uptake mechanism for ^{68}Ga -PSMA-11 in salivary glands. *J. Nucl. Med.* 2019, 60, 1270–1276.
14. Afshar-Oromieh, A.; Malcher, A.; Eder, M.; Eisenhut, M.; Linhart, H.G.; Hadaschik, B.A.; Holland-Letz, T.; Giesel, F.L.; Kratochwil, C.; Haufe, S.; et al. Pet imaging with a ^{68}Ga -labelled psma ligand for the diagnosis of prostate cancer: Biodistribution in humans and first evaluation of tumour lesions. *Eur. J. Nucl. Med. Mol. Imaging* 2013, 40, 486–495.
15. Hofman, M.S.; Hicks, R.J.; Maurer, T.; Eiber, M. Prostate-specific membrane antigen PET: Clinical utility in prostate cancer, normal patterns, pearls, and pitfalls. *Radiographics* 2018, 38, 200–217.
16. Farkas, E.; Nagel, J.; Waldron, B.P.; Parker, D.; Tóth, I.; Brücher, E.; Rösch, F.; Baranyai, Z. Equilibrium, Kinetic and Structural Properties of Gallium(III) and Some Divalent Metal Complexes Formed with the New DATA^m and DATA^{5m} Ligands. *Chem. - A Eur. J.* 2017, 23, 10358–10371.
17. Greifenstein, L.; Grus, T.; Nagel, J.; Sinnes, J.P.; Rösch, F. Synthesis and labeling of a squaric acid containing PSMA-inhibitor coupled to AAZTA5 for versatile labeling with ^{44}Sc , ^{64}Cu , ^{68}Ga and ^{177}Lu . *Appl. Radiat. Isot.* 2020, 156.
18. Baranyai, Z.; Uggeri, F.; Giovenzana, G.B.; Bényei, A.; Brücher, E.; Aime, S. Equilibrium and kinetic properties of the lanthanoids(III) and various divalent metal complexes of the heptadentate ligand AAZTA. *Chem. - A Eur. J.* 2009, 15, 1696–1705.
19. Seemann, J.; Waldron, B.P.; Roesch, F.; Parker, D. Approaching “kit-type” labelling with ^{68}Ga : The DATA chelators. *ChemMedChem* 2015, 10, 1019–1026.
20. Waldron, B.P.; Parker, D.; Burchardt, C.; Yufit, D.S.; Zimny, M.; Roesch, F. Structure and stability of hexadentate complexes of ligands based on AAZTA for efficient PET labelling with Ga-68. *Chem. Commun.* 2013, 49, 579–581.
21. Nagy, G.; Szikra, D.D.; Trencsényi, G.; Fekete, A.; Garai, I.; Giani, A.M.; Negri, R.; Masciocchi, N.; Maiocchi, A.; Uggeri, F.; et al. AAZTA: An Ideal Chelating Agent for the Development of ^{44}Sc PET Imaging Agents. *Angew. Chemie - Int. Ed.* 2017, 56, 2118–2122.
22. Aime, S.; Calabi, L.; Cavallotti, C.; Gianolio, E.; Giovenzana, G.B.; Losi, P.; Maiocchi, A.; Palmisano, G.; Sisti, M.; Giuria, V.P.; et al. [Gd-AAZTA]-: A new structural entry for an improved generation of MRI contrast agents. *Inorg. Chem.* 2004, 43, 7588–7590.
23. Tsionou, M.I.; Knapp, C.E.; Foley, C.A.; Munteanu, C.R.; Cakebread, A.; Imberti, C.; Eykyn, T.R.; Young, J.D.; Paterson, B.M.; Blower, P.J.; et al. Comparison of macrocyclic and acyclic chelators for Ga-68 radiolabelling. *RSC Adv.* 2017, 7, 49586–49599.
24. Benešová, M.; Bauder-Wüst, U.; Schäfer, M.; Klika, K.D.; Mier, W.; Haberkorn, U.; Kopka, K.; Eder, M. Linker Modification Strategies to Control the Prostate-Specific Membrane Antigen (PSMA)-Targeting and Pharmacokinetic Properties of DOTA-Conjugated PSMA Inhibitors. *J. Med. Chem.* 2016, 59, 1761–1775.
25. Zhang, A.X.; Murelli, R.P.; Barinka, C.; Michel, J.; Cocleaza, A.; Jorgensen, W.L.; Lubkowski, J.; Spiegel, D.A. A Remote arene-binding site on prostate specific membrane antigen revealed by antibody-recruiting small molecules. *J. Am. Chem. Soc.* 2010, 132, 12711–12716.
26. Tietze, L.F.; Arlt, M.; Beller, M.; Gliisenkamp, K.; Jahdeb, E.; Rajewsky, M.F.; Glüsenkamp, K.; Jähde, E.; Rajewsky, M.F. Anticancer Agents, Squaric Acid Diethyl Ester: A New Coupling Reagent for the Formation of Drug Biopolymer Conjugates. Synthesis of Squaric Acid Ester Amides and Diamides. *Chem. Ber.* 1991, 124, 1215–1221.
27. Wurm, F.R.; Klok, H.A. Be squared: Expanding the horizon of squaric acid-mediated conjugations. *Chem. Soc. Rev.* 2013, 42, 8220–8236.

28. Greifenstein, L.; Engelbogen, N.; Lahnif, H.; Sinnes, J.P.J.-P.; Bergmann, R.; Bachmann, M.; Rösch, F. Synthesis, Labeling and Preclinical Evaluation of a Squaric Acid Containing PSMA Inhibitor Labeled with ^{68}Ga : A Comparison with PSMA-11 and PSMA-617. *ChemMedChem* 2020, 15, 695–704.
29. Grus, T.; Lahnif, H.; Klasen, B.; Moon, E.-S.; Greifenstein, L.; Roesch, F. Squaric Acid-Based Radiopharmaceuticals for Tumor Imaging and Therapy. *Bioconjug. Chem.* 2021, 32, 1223–1231.
30. Prohens, R.; Portell, A.; Font-Bardia, M.; Bauzá, A.; Frontera, A. Experimental and theoretical study of aromaticity effects in the solid state architecture on squaric acid derivatives. *Cryst. Growth Des.* 2014, 14, 2578–2587.
31. Quiñonero, D.; Frontera, A.; Ballester, P.; Deyà, P.M. A theoretical study of aromaticity in squaramide and oxocarbons. *Tetrahedron Lett.* 2000, 41, 2001–2005.
32. Dingels, C.; Wurm, F.; Wagner, M.; Klok, H.A.; Frey, H. Squaric acid mediated chemoselective PEGylation of proteins: Reactivity of single-step-activated α -amino poly(ethylene glycol)s. *Chem. - A Eur. J.* 2012, 18, 16828–16835.
33. Liu, H.; Rajasekaran, A.K.; Moy, P.; Xia, Y.; Kim, S.; Navarro, V.; Rahmati, R.; Bander, N.H. Constitutive and Antibody-induced Internalization of Prostate-specific Membrane Antigen. *Cancer Res.* 1998, 58.
34. Winter, G.; Vogt, A.; Jiménez-Franco, L.D.; Rinscheid, A.; Yousefzadeh-Nowshahr, E.; Solbach, C.; Beer, A.J.; Glatting, G.; Kletting, P. Modelling the internalisation process of prostate cancer cells for PSMA-specific ligands. *Nucl. Med. Biol.* 2019, 72–73, 20–25.
35. Killock, D. PSMA PET–CT improves staging. *Nat. Rev. Clin. Oncol.* 2020, 17, 337.
36. Langbein, T.; Chaussé, G.; Baum, R.P. Salivary gland toxicity of PSMA radioligand therapy: Relevance and preventive strategies. *J. Nucl. Med.* 2018, 59, 1172–1173.
37. Sinnes, J.-P.; Bauder-Wüst, U.; Schäfer, M.; Moon, E.S.; Kopka, K.; Rösch, F. ^{68}Ga , ^{44}Sc and ^{177}Lu -labeled AAZTA⁵-PSMA-617: synthesis, radiolabeling, stability and cell binding compared to DOTA-PSMA-617 analogues. *EJNMMI Radiopharm. Chem.* 2020, 5, 1–11.
38. Eppard, E.; Wuttke, M.; Nicodemus, P.L.; Rösch, F. Ethanol-based post-processing of generator-derived ^{68}Ga Toward kit-type preparation of ^{68}Ga -radiopharmaceuticals. *J. Nucl. Med.* 2014, 55, 1023–1028.
39. Eder, M.; Schäfer, M.; Bauder-Wüst, U.; Hull, W.E.; Wängler, C.; Mier, W.; Haberkorn, U.; Eisenhut, M. ^{68}Ga -complex lipophilicity and the targeting property of a urea-based PSMA inhibitor for PET imaging. *Bioconjug. Chem.* 2012, 23, 688–697.
40. Askoxylakis, V.; Mier, W.; Zitzmann, S.; Ehemann, V.; Zhang, J.; Krämer, S.; Beck, C.; Schwab, M.; Eisenhut, M.; Haberkorn, U. Characterization and development of a peptide (p160) with affinity for neuroblastoma cells. *J. Nucl. Med.* 2006, 47, 981–988.

**Old drug, new delivery strategy:
MMAE repackaged**

Hanane Lahnif¹, [REDACTED], [REDACTED], [REDACTED]

¹Department of Chemistry – TRIGA site, Johannes Gutenberg University Mainz, 55128 Mainz, Germany

[REDACTED]

ABSTRACT

(1) Background: Targeted therapy is a concept that has gained significant importance in the last years, especially in oncology. The severe dose-limiting side effects of chemotherapy necessitate the development of novel, efficient and tolerable therapy approaches. In this regard, PSMA has been well established as a molecular target for diagnosis as well as therapy of prostate cancer. Although most PSMA-targeting ligands are radiopharmaceuticals used in imaging or radioligand therapy, this article describes an evaluation of MMAE.VC.SA.617, a PSMA inhibitor small molecule-drug conjugate, thus addressing a hitherto little-explored field.

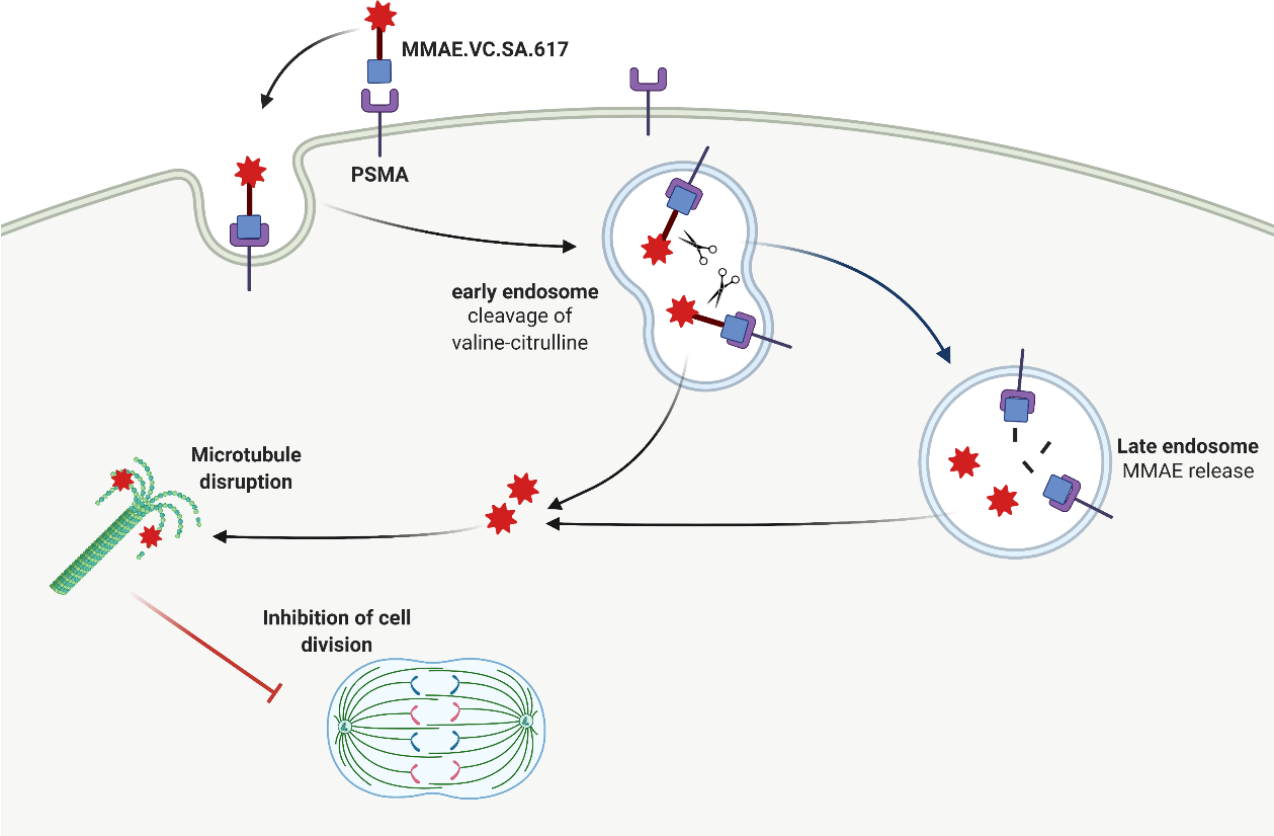
(2) Methods: The PSMA small-molecule drug conjugate, MMAE.VC.SA.617, consisting of the PSMA-binding unit KuE, valine-citrulline linker and the antimetabolic drug MMAE, was synthesized starting from the commercially available compounds MMAE.VC and NH₂-PSMA-617. The *in vitro* PSMA binding affinity and cytotoxicity were determined in cell-based assays. Enzyme-specific cleavage of the active drug was quantified via a cathepsin B-based assay. Efficacy and tolerability *in vivo* were assessed using an LNCaP xenograft model.

(3) Results: The binding affinity of the MMAE-conjugate was moderate compared to the drug-free PSMA inhibitor. Cytotoxicity *in vitro* was in the nanomolar range. Both binding and cytotoxicity were found to be PSMA-specific. Additionally, complete MMAE release could be reached after incubation with cathepsin B. *In vivo*, the MMAE-conjugate displayed good tolerability and dose-dependent inhibition of tumor growth.

(4) Conclusion: The developed MMAE-conjugate showed good properties *in vitro* as well as *in vivo*. Nevertheless, further optimization is required to better exploit the translational potential of this compound.

Keywords: MMAE; PSMA; drug targeting; Small-molecule drug conjugates; prostate cancer

Abstract figure



Introduction

Chemotherapy is one of the most important pillars in the treatment of cancer diseases. However, the toxicity of this approach, resulting from the unspecific interaction of cytotoxic drugs with healthy tissue, presents one of the major drawbacks of this cancer treatment ^{1,2}.

Targeted drug delivery was one of the strategies developed in the last decades to face this challenge. Antibody Drug-Conjugates (ADCs) thereby represented a breakthrough ^{3,4}. ADCs consist of a cytotoxic drug and an antibody with high affinity to its target. Both components are connected via a linker, mostly a cleavable linker. Since ADCs are supposed to be stable constructs, the cytotoxic payload is only released after binding to the target. Nevertheless, this approach seems to have some limitations and disadvantages such as long circulation time and therefore high exposure of healthy tissues, the reduced EPR effect due to low penetration of the large antibodies into tumor tissue and the expensive and sophisticated synthesis of these drug conjugates ⁴⁻⁷. Small-molecule drug conjugates (SMDCs) have been developed to tackle all these challenges. The low molecular weight of targeting vectors in SMDCs allows a circumventing of practically all the disadvantages mentioned above.

Prostate cancer is the most common cancer in men and the second-leading cause of cancer death worldwide ^{8,9}. In the management of prostate cancer, the prostate-specific membrane antigen (PSMA) has been validated as a reliable tumor-associated biomarker and target for diagnosis as well as for therapy of this disease ^{10,11}. PSMA is a membrane glycoprotein expressed on prostate tumor cells at significantly higher concentrations than on healthy tissue. Additionally, PSMA-expression correlates with the grade of metastasis and progression of the tumor, allowing a concise staging and therapy ¹²⁻¹⁴.

In the last decade, several PSMA-targeting pharmaceuticals have been developed. Radionuclide-based PSMA inhibitors like [⁶⁸Ga]Ga-PSMA-11 and [¹⁷⁷Lu]Lu-PSMA-617 have played a significant role in the tremendous progress made in the diagnosis and therapy of prostate cancer ¹⁵⁻¹⁸. Beyond the radionuclide therapy approach, PSMA-targeted drug conjugates have been also thoroughly investigated. Two PSMA-targeting ADCs, MLN2704 and PSMA-ADC have even entered clinical studies but failed due to side effects and lack of tolerability. These disappointing outcomes are probably resulting from the instability of the ADCs and the subsequent deconjugation as well as the long circulation time of these immunoconjugates ¹⁹⁻²¹.

Another promising approach to target PSMA was the use of small-molecule high affinity PSMA inhibitors as homing ligands. Several groups have reported positive results in preclinical studies, thus demonstrating the potential of SMDCs to circumvent the restrictions on tolerability, safety and efficacy of ADCs ²²⁻²⁵. Developing a small molecule drug conjugate requires a thorough design and the right choice of building components. The SMDC described in this study consists of three main modules. The targeting unit KuE-617 refers to the combination of the PSMA- inhibitor KuE (lysine-urea-glutamate) and the naphthyl-cyclohexyl linker of PSMA-617. This moiety is crucial in the design of targeted drug delivery systems, since it is responsible for delivering the cytotoxic payload to the desired “address”. Obviously, this cytotoxic payload needs to be a highly potent drug mostly with a narrow therapeutic window and therefore not applicable as single drug. Herein the potent antimetabolic drug Monomethyl auristatin E (MMAE) was selected which is part of several ADCs, such as the FDA-approved brentuximab vedotin (ADCETRIS™) ²⁶. Besides these essential components, the linker plays a decisive role in the efficacy, stability and resulting tolerability of the whole SMDC. In the developed SMDC, a valine-citrulline linker is used to conjugate MMAE to KuE-617. This dipeptide belongs to the class of enzyme-cleavable linkers. It is cleaved by cathepsin B, which is a lysosomal protease overexpressed in various forms of cancer, including prostate cancer ^{27,28}.

Results

Synthesis

The synthesis of MMAE.VC.SA.617 was carried out in a fast and straightforward two-step synthesis. The commercially available compounds MMAE.VC and NH₂-KuE-617 were used as starting components and were coupled using squaric acid diester as linking unit. The synthesis route is shown in Figure 1.

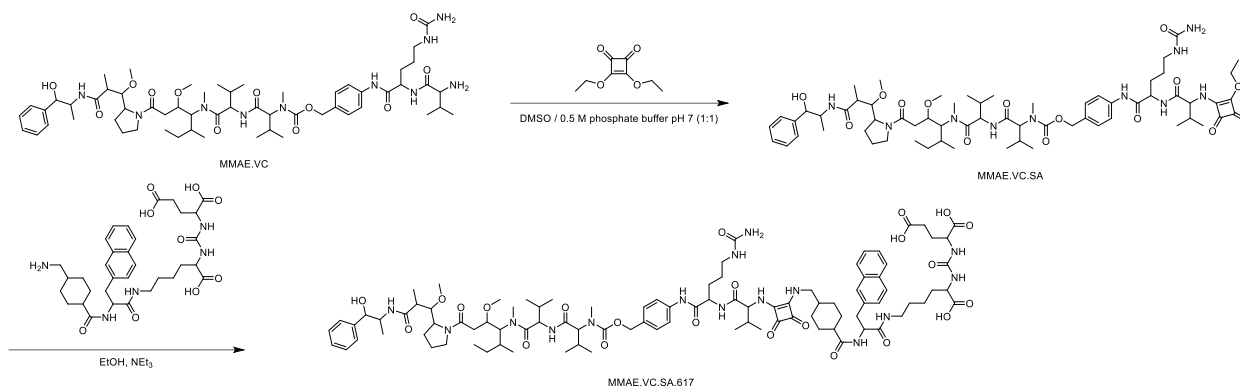


Figure 1 Synthesis of MMAE.VC.SA.617

The use of the squaric acid diester as a coupling reagent is particularly suitable because of its ability to conjugate two amines quickly, selectively and under mild conditions. This asymmetric amidation can be performed in both aqueous and organic media, which makes it very versatile. It is highly selective towards amines, making the use of protecting groups on other nucleophilic groups unnecessary. This coupling method is receiving more and more attention, ranging from the conjugation of bioconjugates and nanoparticles to use in radiopharmaceuticals²⁹⁻³¹.

In the first step the primary amine of the terminal valine of MMAE.VC was conjugated to squaric acid diethyl ester through an asymmetric amidation in an aqueous phosphate buffer at pH 7. To improve the solubility of MMAE.VC, DMSO was added. The reaction resulted in a quantitative conversion of MMAE.VC to MMAE.VC.SA. monitored by LC-MS. In the second step, MMAE.VC.SA as well as NH₂-KuE-617 were dissolved in Ethanol and in the presence of triethylamine, the second asymmetric amidation took place. MMAE.VC.SA.617 was isolated in a yield of 43 % by semi-preparative HPLC purification.

Binding affinity

One of the most important characteristics of drug conjugates is the specific and strong interaction with the addressed target. In order to evaluate the binding potency of the MMAE-conjugate, we performed a competitive radioligand binding assay using PSMA-positive LNCaP cells. Furthermore, we determined the affinity of the drug-free KuE-617 in the same assay to get a better understanding of the effect of conjugation regarding the interaction within the PSMA binding pocket. The binding affinity of KuE-617 expressed as the IC_{50} value was in the same range as the clinically-used PSMA radiopharmaceutical PSMA-11 and PSMA-617. However, the insertion of MMAE resulted in a significant decrease in binding potency (Table 1). It should be noted that the binding of MMAE.VC.SA.617 was demonstrated to be PSMA-specific since no binding occurs after co-incubation with the potent PSMA inhibitor PMPA, thus blocking of the PSMA receptors (Figure 2).

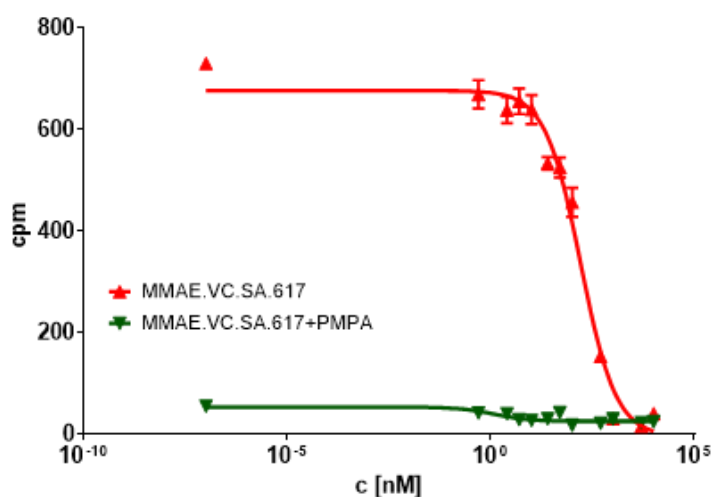


Figure 2 Concentration-inhibition curve of MMAE.VC.SA.617 compared to MMAE.VC.SA.617 + PMPA (n=3). cpm: counts per minute.

Table 1 binding potency of the PSMA-targeted compounds. Values are expressed as Mean \pm SD

compound	IC_{50} [nM]
PSMA-11	17.4 \pm 1.6
PSMA 617	15.1 \pm 3.8
KuE-617	21.5 \pm 1.9
MMAE.VC.SA.617	188.6 \pm 24.7

In vitro cytotoxicity

CellTiter-Blue® Viability Assay

The cytotoxicity of MMAE.VC.SA.617 was evaluated *in vitro* using Celltiter-Blue®. The conjugation of MMAE to KuE-617 resulting in the dimeric compound seems to affect *in vitro* cytotoxicity, since the IC₅₀ value of the MMAE conjugate is approx. 100-times higher than the non-conjugated MMAE. Nevertheless, following the blockade of PSMA receptors by excess addition of PMPA, the cytotoxic effect of MMAE.VC.SA.617 decreased. Furthermore, co-incubation of the LNCaP cells with the cathepsin inhibitor E-64 led to a similar decrease in cytotoxicity. This is probably due to the inhibition of cathepsin B, which is responsible for cleavage of the valine-citrulline linker and thus the subsequent release of MMAE. Table 2 shows the results of the Celltiter-Blue® cytotoxic assay.

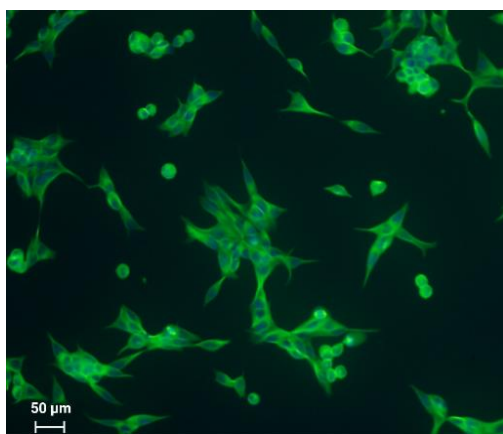
Table 2 IC₅₀ values of the compounds tested in the Celltiter-Blue® cytotoxic assay. Values are mean ± SD

compound	IC₅₀ [nM]
MMAE	0.23 ± 0.06
MMAE.VC.SA.617	33.0 ± 4.9
MMAE.VC.SA.617 + PMPA	92.8 ± 8.3
MMAE.VC.SA.617 + E-64	84.4 ± 0.1

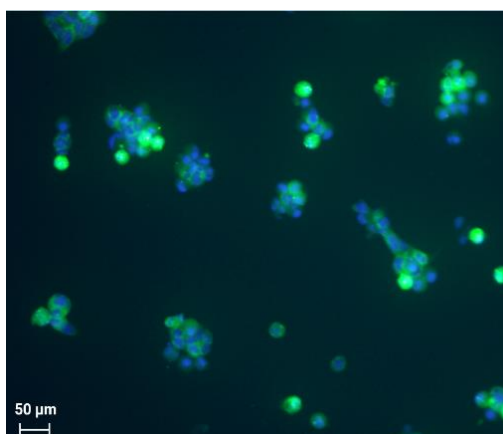
Immunofluorescence studies

To further evaluate the cytotoxic effect of MMAE compared to MMAE.VC.SA.617 we treated LNCaP cells for 24 h with either MMAE (Figure 4b), MMAE.VC.SA.617 (Figure 3c) or MMAE.VC.SA.617 plus PMPA (Figure 3d) prior to co-staining with DAPI and α -tubulin antibody. Cells incubated with both MMAE and MMAE.VC.SA.617 showed a distinctive tubulin disruption resulting in a significant damage of the microtubule cytoskeleton. However, co-incubation with PMPA reduced the cytotoxic effect of MMAE.VC.SA.617 and therefore demonstrated the PSMA-selectivity of this SMDC.

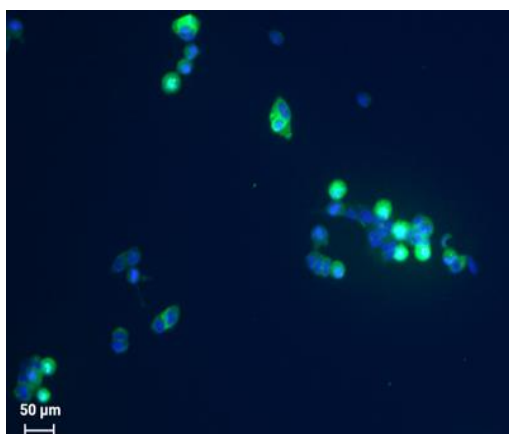
a) Control



b) LNCaP + MMAE



c) LNCaP + MMAE.VC.SA.617



d) LNCaP + MMAE.VC.SA.617 + PMPA

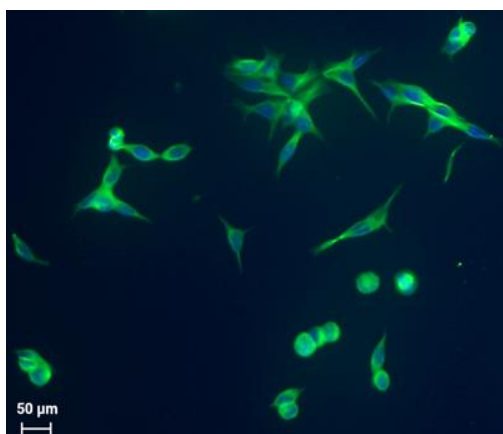


Figure 3 Immunofluorescent staining of α -tubulin (green) with Alexa fluor 488 α -tubulin antibody. Cell nuclei are counterstained with DAPI (blue). Images were taken at 20X magnification. LNCaP cells were used as control (a), incubated with either 1 nM MMAE (b), or 100 nM MMAE.VC.SA.617 (c). PSMA-specific effect was determined by co-incubation of 100 μ M PMPA (d).

Cathepsin B cleavage assay

The cathepsin-specific cleavage of MMAE.VC.SA.617 was evaluated by incubating LNCaP cells at 37 °C with cathepsin B (Figure 4a). A control experiment was conducted by determining the stability of MMA.VC.SA.617 in PBS (in the absence of cathepsin) (Figure 4b). Aliquots were taken at different time points and analysed via liquid chromatography mass spectrometry LC/MS. The concentration of MMAE increased continuously after incubation with cathepsin B. Complete release from the drug conjugate was reached after approx. 20 min. In contrast, in the absence of cathepsin B, MMAE.VC.SA.617 remained almost stable.

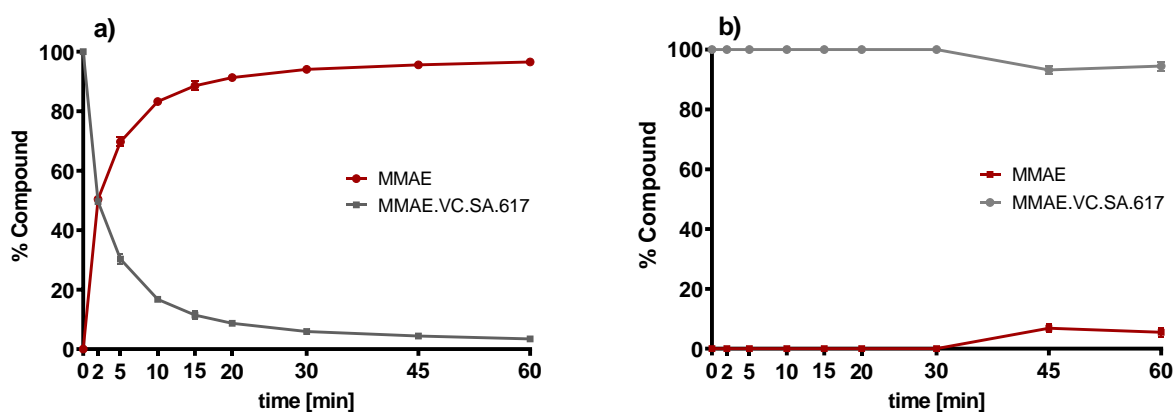


Figure 4 a) Quantification of MMAE release after incubation with cathepsin B; b) control experiment: stability of MMAE.VC.SA.617 in PBS without incubation with cathepsin B.

Animal studies

In order to specify the pharmacological properties of MMAE.VC.SA.617 we inoculated LNCaP cells into NOD-SCID mice to generate a xenograft model. Prior to *in vivo* studies in tumor-bearing mice, we conducted a toxicological study in healthy NOD-SCID mice to determine the maximal tolerable dose of MMAE. Mice injected with 1 mg/kg MMAE had to be euthanized 5 days post-injection due to massive body-weight loss (Figure 5).

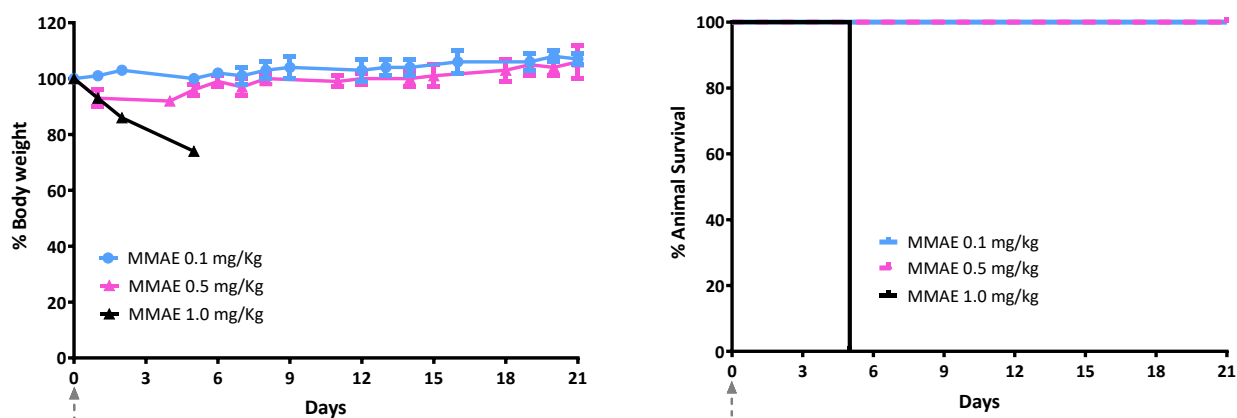


Figure 5 Body-weight change (left) and survival curve (right) of NOD-SCID mice after one i.v. injection of MMAE (n=3 mice per group).

Based on these findings, *in vivo* therapeutic efficacy studies were conducted with 3 different active drug concentrations of MMAE.VC.SA.617, namely 0.1 mg/kg, 0.5 mg/kg and 1.0 mg/kg. In the reference group, mice were injected with either 0.1 mg/kg or 0.5 mg/kg MMAE.

In the MMAE.VC.SA.617 group, mice injected with either 0.5 mg/kg or 1.0 mg/kg seemed to well tolerate the treatment since body weight remained almost constant and all mice survived until the end of the experiment. Surprisingly, in the 0.1 mg/kg MMAE.VC.SA.617 group only one mouse survived the treatment. In this group tumor volume increased continuously over time while in the group with the higher concentrations, treatment seemed to inhibit tumor growth resulting in a constant tumor volume. On the other hand, 4 mice injected with 0.5 mg/kg MMAE were sacrificed after the 5th injection due to massive weight loss. Although one mouse survived and was cured after the 4th injection, the treatment led to a weight loss of about 40 % indicating the toxicity of therapy with this MMAE concentration. In contrast, all animals survived in the 0.1 mg/kg MMAE group. However, tumor volume remained constant so that tumor regression could not be observed.

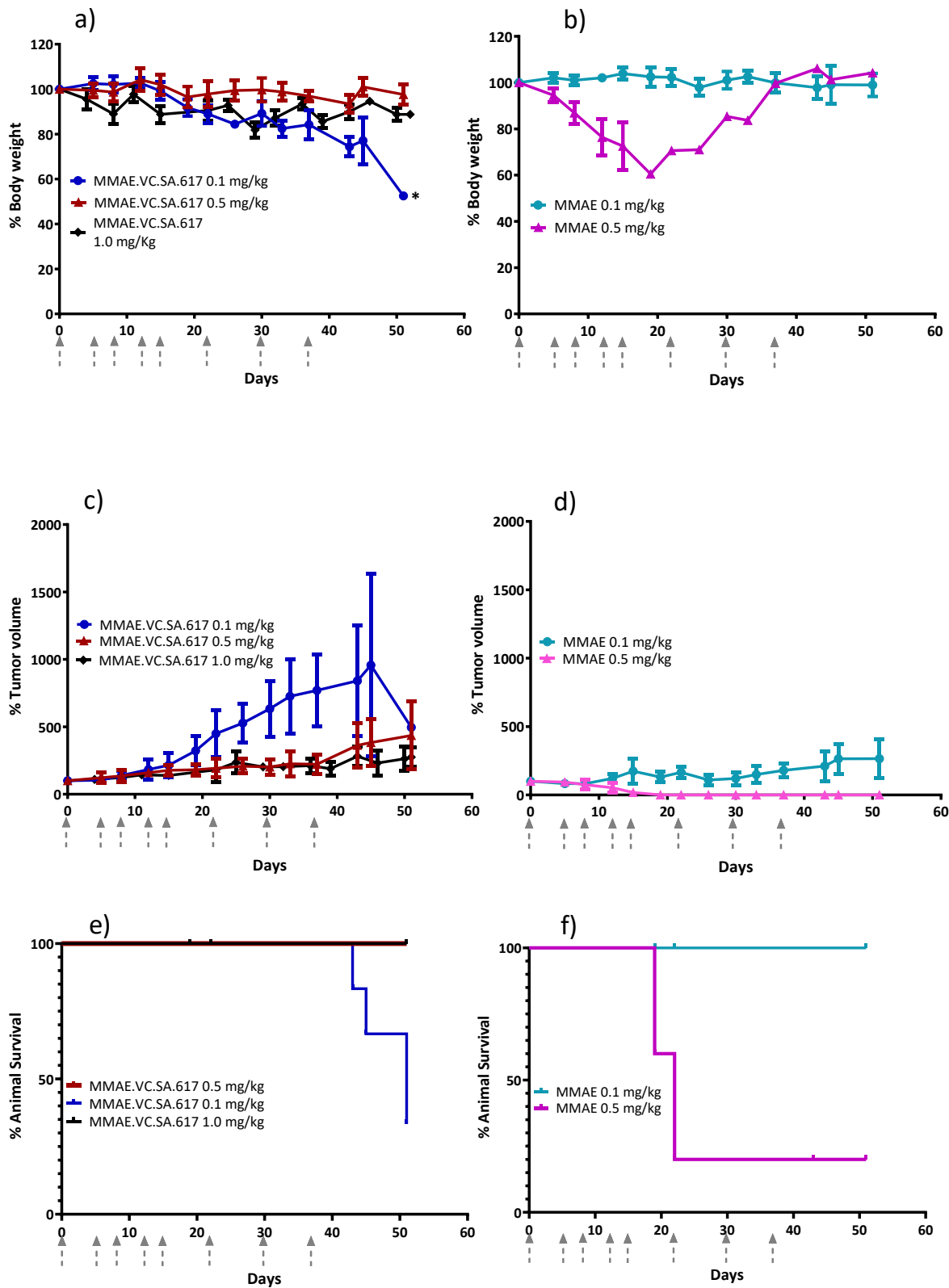


Figure 6 Antitumor effect and tolerability of MMAE and MMAE.VC.SA.617. a) body weight change of animals injected vial tail vein with different doses of MMAE.SA.617 and b) MMAE. Grey arrows indicate time of injection. b) + c) monitoring of tumor volume development of mice during and post treatment. Values are mean \pm SD (n=5). e) + f) Kaplan-Meier survival curves.

Discussion

The development of strategies for selective drug delivery is one of the most important research fields in the fight against cancer. Herein we described a small-molecule drug conjugate consisting of the potent antimitotic drug MMAE and the high affinity PSMA inhibitor derivative KuE-617. Both entities are linked via a valine-citrulline linker. The design, synthesis and subsequent *in vitro* and *in vivo* evaluation were performed in several steps.

The compound MMAE.VC.SA.617 was synthesized in a fast and straightforward 2-step synthesis. The two units of the compound, the drug-linker conjugate MMAE.VC and the PSMA-binding unit KuE-617, were conjugated via asymmetric amidation using a squaric acid linking unit. In the first step, squaric acid had to be added every second day, as it was observed via LC-MS to be consumed during the reaction. After 8 days, MMAE had been quantitatively converted. In this case, the amidation was carried out in an aqueous buffer solution, as the progress of the reaction is controlled by the pH value. However, since the MMAE conjugate did not dissolve completely in water, DMSO was added. The second stage of the reaction was carried out in ethanol. In the organic medium, triethylamine was added as a base to enable the second asymmetric amidation of the squaric acid linker unit. The final compound MMAE.VC.SA.617 was obtained after semi-preparative HPLC purification.

The PSMA-binding affinities of MMAE.VC.SA.617 as well as of the drug-free conjugate KuE-617 were determined in a cell-based radioligand competitive assay. The IC_{50} value of KuE-617 was in the low nanomolar range, similar to the chelator-based PSMA radioligands PSMA-617 and PSMA-11 (21.5 ± 1.9 nM, 15.1 ± 3.8 nM and 17.4 ± 1.6 nM respectively). However, the insertion of MMAE led to a significant decrease in PSMA-binding affinity resulting in nearly 10-fold higher IC_{50} value than KuE-617 (188.6 ± 24.7 nM vs. 21.5 ± 1.9 nM) indicating that the conjugation of KuE-617 to MMAE had a negative impact on binding affinity of the PSMA inhibitor, probably due to changes in the conformation of the drug conjugate and its orientation within the PSMA binding pocket.

In the field of drug targeting, selecting a potent drug is as important as designing a high affinity targeting unit. The cytotoxic drug used herein is the tubulin inhibitor MMAE, which is already used in several ADCs^{26,32,33}. To characterize the pharmacological properties of the MMAE-conjugate we determined its cytotoxicity using CellTiter-Blue®. This assay is based on the ability of viable cells to transform resazurin into the fluorescence-emitter resorufin. Thus, the fluorescence signal correlates with cell viability. The IC₅₀ value of the single drug MMAE was as expected in the picomolar range whereas the cytotoxicity of MMAE.VC.SA.617 was about 100-fold lower (0.23 ± 0.06 nM vs. 33.0 ± 4.9 nM). This could be related to a potential decrease in lipophilicity of MMAE.VC.SA.617 due to the added carboxylic groups of the KuE unit and the ureido group of citrulline resulting in a reduction in passive diffusion through the cell membrane. Another possible reason could be an incomplete release of MMAE within tumor cells as a result of a low cathepsin B level in LNCaP cells or even an impaired internalization ratio. Nevertheless, the PSMA-specific uptake of MMAE.VC.SA.617 could be demonstrated by blocking PSMA receptors using PMPA which leads to a 3-times lower cytotoxicity (92.8 ± 8.3 nM). Additionally, the inhibition of cathepsin B via co-incubation with E-64 and the resulting decrease in cytotoxicity proved the essential role that this enzyme plays in the cleavage of the valine-citrulline linker and the subsequent release of MMAE. This enzyme-dependent cleavage of the dipeptide linker is a crucial feature in targeted therapeutics, since the active drug should be released only after uptake in tumor cells.

In a further step, we tried to better characterize the cytotoxicity of MMAE.VC.SA.617 using immunofluorescence imaging. It is known that the antimetabolic drug MMAE acts by inhibiting the α -tubulin polymerization. This could be proved with the conducted Immunofluorescence studies which showed a distinctive disturbance in tubulin formation of LNCaP cells incubated with either MMAE or MMAE.VC.SA.617 (Figure 3b-c). The cytotoxic effect of MMAE.VC.SA.617 could be reduced by co-incubation with PMPA and thus blocking of PSMA receptors (Figure 3d). These results were in accordance with the findings described above.

The targeted delivery of cytotoxic drugs to tumor cells requires not only binding to tumor-associated structures but also a specific release of the conjugated drug in tumor tissue. The SMDC described herein includes a valine-citrulline linker, which is one of the commonly used linkers in ADCs³⁴⁻³⁶. Valine-citrulline is cleaved by enzymes of the cathepsin-family, especially cathepsin B, which is highly expressed in tumor cells^{27,37,106,107}. In order to verify the cathepsin-specific cleavage of MMAE.VC.SA.617, the ratio of MMAE over time in the presence or absence of cathepsin B was quantified (Figure 4a-b). As expected, MMAE could be released completely after about 20 min of incubation with cathepsin B whereas MMAE.VC.SA.617 remained almost stable in PBS.

Based on the positive results obtained from the *in vitro* assays, animal studies were performed in order to characterize the *in vivo* profile of MMAE.VC.SA.617 in terms of antitumor effect and tolerability. Thereby, the single drug MMAE is used as reference. According to the results from the toxicity study, two different concentrations of MMAE.VC.SA.617 were selected: 0.1 mg/kg and 0.5 mg/kg MMAE respectively. Additionally, we decided to treat one group with 1 mg/kg MMAE.VC.SA.617. This MMAE concentration was found to be toxic in non-tumor-bearing NOD-SCID mice, since all animals died after only one injection (Figure 5).

Animals treated with 0.1 mg/kg MMAE survived until the end of the experiment. Although the treatment was well tolerated, the tumor volume remained constant so that no tumor regression could be observed.

Surprisingly, four mice treated with 0.1 mg/kg MMAE.VC.SA.617 died before the end of the experiment due to grave body weight loss and large tumor volume. These unexpected results could be attributed to insufficient drug delivery into the tumor tissue. As concluded from *in vitro* studies the cytotoxicity of the MMAE conjugate was ten-fold of magnitude lower than the single drug MMAE, which could have different reasons as explained above. This loss in cytotoxicity could not be compensated by the active PSMA-targeting since MMAE.VC.SA.617 displayed a moderate binding affinity. Despite these unexpected results in the 0.1 mg/kg MMAE.VC.SA.617 group, the tolerability of MMAE.VC.SA.617 in the two other concentrations 0.5 mg/kg and 1.0 mg/kg could be demonstrated (100 % animal survival). Consequently, MMAE.VC.SA.617 seems to be stable in mouse blood, since no toxic side effects occurred in these groups even after 8 i.v. injections. Moreover, tumor growth could be effectively inhibited. On the other hand, only one mouse survived in the 0.5 mg/kg MMAE group, indicating a severe toxicity of the single drug.

In summary, the synthesized MMAE.VC.SA.617 was proved to be selective in terms of PSMA binding and cytotoxicity toward PSMA-positive LNCaP cells. The *in vitro* cleavage of the valine-citrulline linker by cathepsin B has also been demonstrated. Animal studies have shown a good tolerability of MMAE.VC.SA.617 even at high concentrations. In addition, tumor growth could be effectively inhibited in both the 0.5 mg/kg and 1.0 mg/kg groups.

However, further optimization of the chemical structure of the MMAE SMDC is required to improve the PSMA binding affinity and the cytotoxicity of the compound. Possible approaches would be on the one hand, the use of a target vector with a higher PSMA binding affinity than KuE-617, on the other hand the use of a different linker/ spacer either to enhance the lipophilicity of the molecule and thus the passive diffusion through the cell membrane or to avoid a possible interaction of MMAE with the targeting unit, which could lead to a change in the conformation of the SMDC and therefore to a disadvantageous orientation within the PSMA binding pocket.

Materials and Methods

4.1. General

Chemicals were purchased from Sigma-Aldrich, Merck, VWR, AcrosOrganics and TCI. MMAE.VC was purchased from Hycultec GmbH and PSMA-617-NH₂ from Huayi Isotopes Co. Deuterated solvents for NMR spectra from Deutero. Silica gel 60 F254 coated aluminum plates from Merck were used for thin layer chromatography. NMR measurements were performed on an Avance III 600 spectrometer (600 MHz, 5mm TCI CryoProbe sample head with z-Gradient and ATM and SampleXPress Lite 16 sample changer) from Bruker. The LC/MS measurements were performed on an Agilent Technologies 1220 Infinity LC system coupled to an Agilent Technologies 6130B Single Quadrupole LC/MS system. Semi-preparative HPLC purification was performed on a 7000 series Hitachi LaChrom using a semi-preparative LiChrospher 100 RP18 EC (250 x 10 mm) 5 μ column.

4.2. Organic Synthesis

MMAE.VC.SA

MMAE.VC (20 mg, 0.018 mmol) was dissolved in 0.5 M phosphate buffer pH 7 (500 μL) and DMSO (500 μL). 3,4-Diethoxycyclobut-3-ene-1,2-dione (5 mg, 4 μL, 0.027 mmol) was added and stirred for 8 days. Every second day 0.5 eq of 3,4-Diethoxycyclobut-3-ene-1,2-dione were added. The solvent was removed via lyophilisation and the product was used in the next step without purification.

MS (ESI⁺): 236.0 ([M+H]⁺/2), calculated for C₆₄H₉₈N₁₀O₁₅: 1246.72 [M]⁺.

MMAE.VC.SA.617

MMAE.VC.SA (20 mg, 0.016 mmol) and PSMA-617-NH₂ (10 mg, 0.016 mmol) were dissolved in ethanol (3 mL). Triethylamine (50 μ L) was added and the reaction mixture was stirred for 6 days. The solvent was removed under reduced pressure. MMAE.VC.SA.617 was obtained as white powder (14.2 mg, 43 %) after HPLC purification (LiChrospher 100 RP18 EC (250 x 10 mm) 5 μ , flow rate: 5 mL/min, H₂O/MeCN + 0.1 % TFA, 45 % to 55 % MeCN in 20 min, t_R = 9.0 min).

MS (ESI⁺): 929.0 ([M+H]⁺/2), calculated for C₉₅H₁₃₇N₁₅O₂₃: 1857.22 [M]⁺.

¹H NMR (600 MHz, EtOD-*d*₆) δ [ppm] = 7.77 (dd, J = 19.3, 9.2 Hz, 2H), 7.69 (d, J = 31.8 Hz, 3H), 7.41 (t, J = 7.9 Hz, 5H), 7.30 (dt, J = 15.4, 7.4 Hz, 3H), 7.24 – 7.15 (m, 1H), 5.18 (dt, J = 28.3, 15.2 Hz, 1H), 5.07 (d, J = 11.7 Hz, 1H), 4.93 (d, J = 31.6 Hz, 1H), 4.32 – 4.04 (m, 4H), 3.93 – 3.87 (m, 1H), 3.84 (s, 1H), 3.70 (s, 3H), 3.45 (d, J = 14.1 Hz, 2H), 3.41 – 3.26 (m, 9H), 3.23 (s, 1H), 3.11 (d, J = 15.3 Hz, 3H), 2.96 (td, J = 18.7, 7.0 Hz, 3H), 2.52 (s, 1H), 2.34 – 2.15 (m, 3H), 2.06 (s, 1H), 2.01 – 1.77 (m, 2H), 1.75 – 1.27 (m, 12H), 1.27 – 1.16 (m, 6H), 1.08 – 0.69 (m, 28H).

4.3. *In vitro* binding affinity

LNCaP prostate cancer cells (purchased from Sigma-Aldrich) were cultured in RPMI 1640 (Thermo Fisher Scientific) supplemented with 10% fetal bovine serum (Thermo Fisher Scientific), 100 μ g/ml streptomycin, and 100 units/ml penicillin at 37°C in 5% CO₂.

LNCaP cells were incubated for 45 min with different concentrations of the MMAE-conjugates in the presence of 0.75 nM [⁶⁸Ga]Ga-PSMA-10. Free radioactivity was removed by several washing steps with ice-cold PBS. Probes were measured in a γ -counter (2480 WIZARD² Automatic Gamma Counter, PerkinElmer). Obtained data were analyzed in GraphPad Prism 9 using nonlinear regression.

4.4. CellTiter-Blue® Viability Assay

10⁴ cells per well were seeded in a 96-well plate for 24 h prior to incubation with increasing concentrations of either MMAE (0.1 nM to 0.5 μ M) or MMAE.VC.SA.617 (2.5 nM to 10 μ M). Subsequently 20 μ L of CellTiter-Blue® Reagent were added in each well and incubated for 2 h at 37°C. For blocking studies, 2.5 nmol of PMPA was added to each well prior to incubation with SMDC. Fluorescence (560_{Ex}/590_{Em}) was recorded using a Tecan Spark multimode reader.

4.5. Immunofluorescence studies

2000 cells/well were seeded in Nunc® Lab-Tek® II - CC2™ Chamber Slide™ (Sigma Aldrich) and incubated with the test compounds at 37 °C for 24 h. After fixation with 4 % PFA, cells were permeabilized with 0.5 % Triton X-100 for 15 min at room temperature. Cells were then washed several times with PBS and blocked with 3 % BSA in PBS for 1 h at room temperature. α -tubulin staining was performed by incubating the cells with alpha-Tubulin Antibody, Alexa Fluor® 488 conjugate (B-5-1-2) (ThermoFisher Scientific) at a final concentration of 2 μ g/mL for 3h at room temperature. Counterstaining with DAPI was carried out with ProLong™ Gold Antifade Mountant with DAPI (ThermoFisher Scientific) according to the manufacturer's protocol. Cells were visualized using a fluorescence microscope (Keyence BZ-8000) at 20x.

4.6. Cathepsin B cleavage assay

Cathepsin B from human liver (Sigma Aldrich) was activated by incubation at room temperature with 30 mM dithiothreitol DTT and 15 mM EDTA at pH 5.5. Subsequently, 2.5 μ M of the activated cathepsin B was added to 25 μ M of MMAE.VC.SA.617 and incubated at 37 °C. Aliquots were taken at different time points. The enzymatic activity of cathepsin B was blocked by adding 1 μ L of E-64 (1 mM) in each vial. Samples were analyzed using an Agilent Technologies 1220 Infinity LC system coupled to an Agilent Technologies 6130B Single Quadrupole LC/MS system.

4.7. Animal studies

Animals used for the biodistribution studies were obtained from the breeding facilities of the Institute of Biosciences and Applications, NCSR "Demokritos". Our experimental animal facility is registered according to the Greek Presidential Decree 56/2013 (Reg. Number: EL 25 BIO 022), in accordance to the European Directive 2010/63 which is harmonized with national legislation, on the protection of animals used for scientific purposes. All applicable national guidelines for the care and use of animals were followed. The study protocol was approved by the Department of Agriculture and Veterinary Service of the Prefecture of Athens.

4.7.1. Toxicology study in healthy NOD-SCID mice

Prior to the therapeutic efficacy study in LNCaP tumor-bearing mice, a toxicology study is carried on healthy NOD-SCID mice to determine the tolerable dose of the single drug MMAE. Nine NOD-SCID mice were divided into 3 groups and received a single dose of MMAE. Group A received 0.1 mg (54 nmol)/kg body weight, Group B received 0.5 mg (270 nmol)/kg body weight while Group C received 1 mg (540 nmol)/kg body weight. Mice injected with 1 mg/kg MMAE had to be euthanized 5 days post-injection due to massive body-weight loss.

4.7.2. Therapeutic efficacy study in LNCaP tumor-bearing NOD-SCID mice

A therapeutic efficacy study of the MMAE.VC.SA.617 vs MMAE was performed in six groups of LNCaP tumor-bearing NOD/SCID mice, two of which acted as reference groups while an additional group acted as the control group. LNCaP cells were cultured in RPMI-1640 medium of pH 7.4, supplemented with 10% FBS, 100 U/mL of penicillin, 100 µg/mL of streptomycin, 2 mM glutamine, 10

mM HEPES and 1 mM sodium pyruvate. Cell cultures were maintained in 75 cm² flasks, grown at 37°C in 5% CO₂ in a humidified atmosphere and the medium was changed approximately every 72 hours (doubling time is about 40 hrs). Cells in exponential phase of growth were harvested by a 10 min treatment with a 0.05% trypsin–0.02% EDTA solution and neutralized with medium containing serum immediately. Cultures at passages 8–10 were used for the experiments. For the LNCaP xenograft development, cells were suspended in 100 µL in RPMI-1640 medium (supplemented as described above) and 100 µL Matrigel (ratio 1:1) (1×10⁶ cells/200 µL) and maintained on ice until the inoculation. All equipment (syringes and needles) was chilled on ice prior to use in tumor cell inoculation. The mice were subcutaneously inoculated on the left shoulder with the LNCaP cells. The tumor-bearing animals were ready for experimentation approximately 14 days after cell inoculation.

The six groups of experimentation were as follows:

Group A: MMAE 0.1 mg/kg mouse body weight (reference group A)

Group B: MMAE 0.5 mg/kg mouse body weight (reference group B)

Group C: MMAE.VC.SA.617, 0.1 mg/kg mouse body weight

Group D: MMAE.VC.SA.617, 0.5 mg/kg mouse body weight

Group E: MMAE.VC.SA.617, 1 mg/kg mouse body weight

All groups of mice were intravenously injected twice a week, for the first 5 doses of MMAE, MMAE.VC.SA.617 or saline, and then an additional 3 doses once a week, resulting in a total of 8 doses over a period of 7 weeks. Body weight and tumor volume were assessed on each day of i.v. injection, and every 3-4 days after the end of treatment administration, to 52 days after the initiation of the therapeutic efficacy study.

Acknowledgment

[Redacted Acknowledgment Content]

References

1. Krementz, E.T, Kokame, G.M. Iglesias, F. Current status of chemotherapy of cancer. *Postgrad. Med.* 35, 384–394 (1964).
2. Brockman, R. W. Mechanisms of Resistance to Anticancer Agents. *Adv. Cancer Res.* 7, 129–234 (1963).
3. Nissim, A. & Chernajovsky, Y. Historical development of monoclonal antibody therapeutics. *Handb. Exp. Pharmacol.* 181, 3–18 (2008).
4. Firer, M. A. & Gellerman, G. Targeted drug delivery for cancer therapy: the other side of antibodies. *J. Hematol. Oncol.* 5, 70 (2012).
5. SV, G. & DM, G. Designing immunoconjugates for cancer therapy. *Expert Opin. Biol. Ther.* 12, 873–890 (2012).
6. M, V.-R. & DA, L. Aggregates in monoclonal antibody manufacturing processes. *Biotechnol. Bioeng.* 108, 1494–1508 (2011).
7. Hedrich, W. D., Fandy, T. E., Ashour, H. M., Wang, H., Hassan, H. E. Antibody–Drug Conjugates: Pharmacokinetic/Pharmacodynamic Modeling, Preclinical Characterization, Clinical Studies, and Lessons Learned. *Clin. Pharmacokinet.* 57, 687 (2018).
8. Prostate cancer statistics | World Cancer Research Fund International. <https://www.wcrf.org/dietandcancer/prostate-cancer-statistics/>.
9. Barsouk, A. et al. Epidemiology, Staging and Management of Prostate Cancer. *Med. Sci.* 8, 28 (2020).
10. Chang, S. S. & Heston, W. D. W. The clinical role of prostate-specific membrane antigen (PSMA). *Urol. Oncol.* 7, 7–12 (2002).
11. Ghosh, A. & Heston, W. D. W. Tumor target prostate specific membrane antigen (PSMA) and its regulation in prostate cancer. *Journal of Cellular Biochemistry* vol. 91 528–539 (2004).
12. Perner, S. et al. Prostate-specific membrane antigen expression as a predictor of prostate cancer progression. *Hum. Pathol.* 38, 696–701 (2007).
13. Donin, N. M. & Reiter, R. E. Why targeting PSMA is a game changer in the management of prostate cancer. *J. Nucl. Med.* 59, 177–182 (2018).

14. Silver, D. A., Pellicer, I., Fair, W. R., Heston, W. D. W. & Cordon-Cardo, C. Prostate-specific Membrane Antigen Expression in Normal and Malignant Human Tissues. *Clin. Cancer Research* 3, 81–85 (1997).
15. Bräuer, A. et al. ¹⁷⁷Lu-PSMA-617 radioligand therapy and outcome in patients with metastasized castration-resistant prostate cancer. *Eur. J. Nucl. Med. Mol. Imaging* 44, 1663–1670 (2017).
16. Kularatne, S. A., Wang, K., Santhapuram, H. K. R. & Low, P. S. Prostate-specific membrane antigen targeted imaging and therapy of prostate cancer using a PSMA inhibitor as a homing ligand. *Mol. Pharm.* 6, 780–789 (2009).
17. von Eyben, F. E., Picchio, M., von Eyben, R., Rhee, H. & Bauman, G. ⁶⁸Ga-Labeled Prostate-specific Membrane Antigen Ligand Positron Emission Tomography/Computed Tomography for Prostate Cancer: A Systematic Review and Meta-analysis. *Eur. Urol. Focus* 4, 686–693 (2018).
18. A, E. et al. The role of ⁶⁸Ga-PSMA PET/CT scan in biochemical recurrence after primary treatment for prostate cancer: a systematic review of the literature. *Minerva Urol. Nefrol.* 70, 462–478 (2018).
19. Petrylak, D. P. et al. A phase 2 study of prostate specific membrane antigen antibody drug conjugate (PSMA ADC) in patients (pts) with progressive metastatic castration-resistant prostate cancer (mCRPC) following abiraterone and/or enzalutamide (abi/enz) (2015).
20. Milowsky, M. I. et al. Phase 1/2 Multiple Ascending Dose Trial of the Prostate-Specific Membrane Antigen (PSMA)-Targeted Antibody Drug Conjugate MLN2704 in Metastatic Castration-Resistant Prostate Cancer. *Urol. Oncol.* 34, 530.e15 (2016).
21. Niaz, M. O., Sun, M., Ramirez-Fort, M. K. & Niaz, M. J. Prostate-specific Membrane Antigen Based Antibody-drug Conjugates for Metastatic Castration-resistance Prostate Cancer. *Cureus* 12, (2020).
22. Boinapally, S. et al. A prostate-specific membrane antigen (PSMA)-targeted prodrug with a favorable in vivo toxicity profile. *Sci. Reports* | 11, 7114 (123AD).
23. Q, L. et al. Prostate-Specific Membrane Antigen Targeted Therapy of Prostate Cancer Using a DUPA-Paclitaxel Conjugate. *Mol. Pharm.* 15, 1842–1852 (2018).
24. CP, L. et al. Prostate-Specific Membrane Antigen-Specific Antitumor Activity of a Self-Immolative Tubulysin Conjugate. *Bioconjug. Chem.* 30, 1805–1813 (2019).
25. Wang, X. et al. Small Molecule-Based Prodrug Targeting Prostate Specific Membrane Antigen for the Treatment of Prostate Cancer. *Cancers (Basel)*. 13, 1–21 (2021).
26. Li, C. et al. Clinical pharmacology of vc-MMAE antibody–drug conjugates in cancer patients: learning from eight first-in-human Phase 1 studies. *MAbs* 12, (2020).
27. SINHA, A. A. et al. Cathepsin B Expression is Similar in African-American and Caucasian Prostate Cancer Patients. *Anticancer Res.* 27, (2007).
28. Gondi, C. S. & Rao, J. S. Cathepsin B as a Cancer Target. *Expert Opin. Ther. Targets* 17, 281 (2013).
29. Wurm, F. R. & Klok, H.-A. Be squared: expanding the horizon of squaric acid-mediated conjugations. *Chem. Soc. Rev.* 42, 8220–8236 (2013).
30. Huppertsberg, A. et al. Squaric Ester-Based, pH-Degradable Nanogels: Modular Nanocarriers for Safe, Systemic Administration of Toll-like Receptor 7/8 Agonistic Immune Modulators. *J. Am. Chem. Soc.* 143, 9872–9883 (2021).
31. Grus, T. et al. Squaric Acid-Based Radiopharmaceuticals for Tumor Imaging and Therapy. *Bioconjug. Chem.* 32, 1223–1231 (2021).
32. A. Akaiwa, et al. Antibody-Drug Conjugate Payloads; Study of Auristatin Derivatives. *Chem. Pharm. Bull. (Tokyo)*. 68, 201–211 (2020).

33. C. Connors et al. Brentuximab vedotin for relapsed or refractory Hodgkin's lymphoma. *Drug Des. Devel. Ther.* 9, 1729–1733 (2015).
34. Dragovich, P. S. et al. Antibody-Mediated Delivery of Chimeric BRD4 Degraders. Part 1: Exploration of Antibody Linker, Payload Loading, and Payload Molecular Properties. *J. Med. Chem.* 64, 2534–2575 (2021).
35. Su. Zheng et al. Antibody–drug conjugates: Recent advances in linker chemistry. *Acta Pharm. Sin. B* (2021) doi:10.1016/J.APSB.2021.03.042.
36. Bargh, J. D., Isidro-Llobet, A., Parker, J. S. & Spring, D. R. Cleavable linkers in antibody-drug conjugates. *Chem. Soc. Rev.* 48, 4361–4374 (2019).
37. Fernández, P. L. et al. Expression of Cathepsins B and S in the progression of prostate carcinoma. *Int. J. Cancer* 95, 51–55 (2001).

**DOTA conjugate of Bisphosphonate and PSMA-inhibitor:
A promising combination for therapy of prostate cancer
related bone metastases**

[REDACTED], Hanane Lahnif¹, [REDACTED], [REDACTED]
and [REDACTED]

¹ Department of Chemistry – TRIGA site, Johannes Gutenberg University, 55128 Mainz, Germany

[REDACTED]

Abstract

Background: Prostate cancer (PCa) is one of the most common cancer types worldwide. 90 % of men with late stage PCa will develop bone metastases. [¹⁷⁷Lu]Lu-PSMA-617 therapy is often not as successful in patients with bone metastases as in patients without bone metastases. Since the expression level of PSMA (prostate-specific membrane antigen) in bone metastases can also vary significantly, a compound is being searched for which accumulates in bone metastases independently of tumour stage and PSMA level. With DOTA-L-Lys(SA.Pam)-PSMA-617, we present in this paper a compound that, in addition to a PSMA inhibitor as a target vector, also contains a bisphosphonate that is established as a bone tracer and thus combines the advantages of PSMA targeting and bone targeting. The molecule can be labelled with ¹⁷⁷Lu via the DOTA chelator and used for the therapy of PCa-related bone metastases.

Results: [¹⁷⁷Lu]Lu-labelling of DOTA-L-Lys(SA.Pam)-PSMA-617 showed quantitative RCY within 10 minutes and a high complex stability over a period of 14 days. The lipophilicity of the labelled compound was similar to the lipophilicity of the reference compound [¹⁷⁷Lu]Lu-PSMA-617 (-2.29 ± 0.12 % vs. -2.23 ± 0.20) and showed an excellent and selective HAP binding of 98.2 ± 0.11 %. With a K_i of 42.3 ± 7.7 nM the PSMA binding affinity is lower in comparison to [¹⁷⁷Lu]Lu-PSMA-617. First *ex vivo* biodistribution studies with LNCaP tumor-bearing Balb/c mice showed a PSMA dependent tumor accumulation of 4.2 ± 0.7 %ID/g and a femur accumulation of 3.4 ± 0.4 %ID/g. High tumor-to-blood and bone-to-blood-ratios (210 and 170) were also achieved.

Conclusions: [¹⁷⁷Lu]Lu-DOTA-L-Lys(SA.Pam)-PSMA-617 is a promising compound for therapy of PCa related bone metastases. Accumulation on the bone metastases via two mechanisms also enables the treatment of bone metastases that show little or no PSMA expression. The DOTA chelator also enables a theranostic approach of the compound.

Keywords: PSMA, Bisphosphonate, Pamidronate, Bone metastases, prostate cancer, Lutetium-177

Introduction

Prostate cancer (PCa) is one of the most commonly diagnosed cancer diseases in the world and one of the leading causes of cancer-related deaths worldwide ¹. The 5-year survival rate for early diagnosed and localised PCa is 98 %. However, if metastases have already formed, the rate drops to 30 % ².

The introduction of prostate-specific membrane antigen (PSMA) as a molecular target has revolutionised the diagnosis and treatment of PCa. In recent years, there has been a rapid increase in new radiopharmaceuticals for diagnosis and targeted radionuclide therapy of PCa ^{3,4}. Particularly small molecule-based PSMA ligands have received a lot of attention ^{5,6}. The type II transmembrane glycoprotein PSMA or glutamate carboxypeptidase II (GCPII) consists of 750 amino acids and is located in the cell membrane of prostate epithelial cells. Usually, PSMA expression is upregulated in PCa and correlates with the severity of the disease. Apart from PCa, PSMA is physiologically expressed only in few normal tissues, such as the kidney and the salivary glands ⁷. Upon binding of a substrate to PSMA, internalisation occurs. With regard to therapy, a targeted and irreversible uptake of the therapeutic nuclide into the PCa cell is thus possible ⁸.

The most commonly used PSMA inhibitors are based on urea derivatives. The currently most promising PET-PSMA radiopharmaceutical is PSMA-11, which can be labelled with ⁶⁸Ga ^{9,10}. PSMA-617, labelled with ¹⁷⁷Lu ([¹⁷⁷Lu]Lu-PSMA-617, Lu-PSMA) is the most important therapeutic compound until now ^{7,11,12}. The results of the clinical phase III study have just been published. The so-called VISION study demonstrated a good tolerability of the [¹⁷⁷Lu]Lu-PSMA-617 therapy along with an increase in the overall survival rate. Hence, introduction of [¹⁷⁷Lu]Lu-PSMA-617 as standard treatment is recommended ¹³.

Most men with advanced PCa develop bone metastases ¹⁴. This affects about 90 % of men with late stage PCa ¹⁵. The presence of bone metastases is a negative indicator for the survival of the patient. The WARMTH study has shown that the overall survival rate of patients with bone metastases treated with [¹⁷⁷Lu]Lu-PSMA-617 is lower than when there is no metastasis ¹⁶. Independently of this, bone metastases cause a significant reduction in quality of life due to, e.g., pain or compression of the spinal cord and nerve roots or the displacement of red bone marrow, which appears especially in advanced PCa ¹⁷.

While metastasis in bone tissue can be osteoblastic, osteolytic or mixed forms, PCa-related metastases are usually osteoblastic ^{18,19}. In both cases, the hydroxyapatite (HAP), the mineral material of the bone, is uncovered. The release takes place either by degradation of the bone by osteoclasts (osteolytic lesion) or by rebuilding and remodelling of the bone (osteoblastic lesion) ²⁰.

Over the last 40 years, bisphosphonates have become established as drugs for various bone diseases ²¹. The efficacy of these pyrophosphate derivatives is based on a high affinity to HAP, which is due to the chelation of the calcium ions of HAP ²². Bisphosphonates, such as MDP (methylene diphosphonate) or EDTMP (ethylenediamine tetra(methylene phosphonic acid)), are acyclic phosphonic acids that can both complex a radionuclide and adsorb to HAP, enabling diagnosis or therapy via the radioactivity of the nuclide ²³. [¹⁵³Sm]Sm-EDTMP is used, for example, for reduction of bone metastases-induced pain ²⁴. In addition, there are bisphosphonates that are functionalised with a chelator that enables the radiolabelling. These include compounds such as BPAMP ²⁵ or the most promising [¹⁷⁷Lu]Lu-DOTA^{ZOL} ^{26,27}. One of the first clinically investigated nitrogen-containing bisphosphonate is pamidronate (Pam). The conjugation of Pam to squaric acid (SA) not only allows an easy and rapid conjugation with other moieties, such as chelators ²⁸, but also supports the antiresorptive effect of the bisphosphonate due to the presence of an amine component at this position ^{29,30}. This is also the case, for example, with the highly potent bisphosphonate zoledronate ^{26,27,29}. Unpublished data indicate that SA.Pam has a higher bone uptake than, for example, DOTA^{ZOL}.

Prostate cancer can vary widely in the expression of PSMA. It is known that primary tumors and especially metastases can be PSMA-negative³¹⁻³⁴. This can also be the case for bone metastases ^{33,34}. Here it was shown that there is a high correlation between bone metabolic activity and cancer-related PSMA expression in bone lesions at early stages of the disease, implying that bone metastases have significantly high PSMA expression at early stages. In later stages, this correlation is increasingly absent or there is a greater deviation, which implies a lower PSMA expression in bone metastases ³⁵. The reasons for this heterogeneous expression are manifold and many effects can play a role. These can be the complex biochemical and pathobiological processes due to genetically and non-genetically induced differentiation types of the tumor and the metastases in the progress of the disease ^{15,34,36,37}. Another influence can be, for example, the type of therapy ³⁸.

It was found, that low average PSMA expression in metastases is associated with a shorter overall survival rate. At the moment, it is not yet clear whether patients with low PSMA-levels benefit from a therapy with lutetium-177 labelled PSMA-617 ³⁷. Therefore, there is a need for a compound that can accumulate at PCa-related bone metastases independently of tumor-stage and PSMA-level. In terms of imaging, different pairs of PSMA PET-tracers and bone scan agents have been studied in the past with varying results in their performance ^{35,38-43}.

The combination of the advantages of PSMA targeting and bone targeting in one compound would reduce the complexity of the treatment, enables expression-independent therapy of bone metastases and thus would be favourable. In this way, bone metastases can be treated via two mechanisms, the possible PSMA expression and the imbalanced metabolic mechanism of the bone cells. In this study, we developed a chimeric compound containing the highly affine PSMA inhibitor KuE on the one side and a bisphosphonate drug (pamidronate, Pam) on the other side. Both targeting moieties are coupled to the DOTA chelator and can therefore be used for endoradiotherapy with e.g., lutetium-177. Furthermore, we used the PSMA-617 linker for coupling the KuE unit to DOTA, since it has been proven that this linker plays an important role in enhancing the PSMA binding affinity ⁷. Moreover, pamidronate was coupled to DOTA via squaric acid amide, which has also shown a positive impact in terms of simplified synthesis and improved pharmacokinetics ⁴⁴.

Results

Organic synthesis of DOTA-L-Lys(SA.Pam)-PSMA-617

The synthesis of DOTA-L-Lys(SA.Pam)-PSMA-617 was divided into three parts. First the solid-phase based synthesis route of the PSMA-617 motif (**6**) based on the synthetic route developed by Benesova et al.⁷ (Figure 1). The bisphosphonate-based target vector (**8**) unit was synthesized in a two-step synthesis (Figure 2). Both target vectors were then combined in a third synthesis step using lysine as a linking bridge and functionalised with a DOTA chelator for radiolabelling (Figure 3).

The eight-step solid-phase synthesis of the PSMA-617-backbone (Figure 1) started from L-lysine which is bound to a Wang-resin. In the first step, an isocyanate was generated by adding triphosgene to bis(*tert*-butyl)-L-glutamate, which was then added to the Fmoc-protected lysine-resin to generate the KuE unit of the PSMA inhibitor. To add the PSMA-617-linker unit, the alloc protecting group of the side chain amine of **1** was removed by reduction. This was followed by addition of the amino acids 3-(2-naphthyl)-L-alanine and 4-aminomethylcyclohexane-OH (4-Amc-OH) to the side chain amine of lysine, using a standardised solid-phase based peptide synthesis protocol with HATU (1-[Bis(dimethylamino)methylene]-1H-1,2,3-triazolo[4,5-b]pyridinium 3-oxide hexafluorophosphate) as coupling reagent. The final solid-phase bound and protected PSMA-617-target vector motif (**5**) was obtained. The Fmoc protecting group of the aminomethylcyclohexane group was removed for further functionalisation.

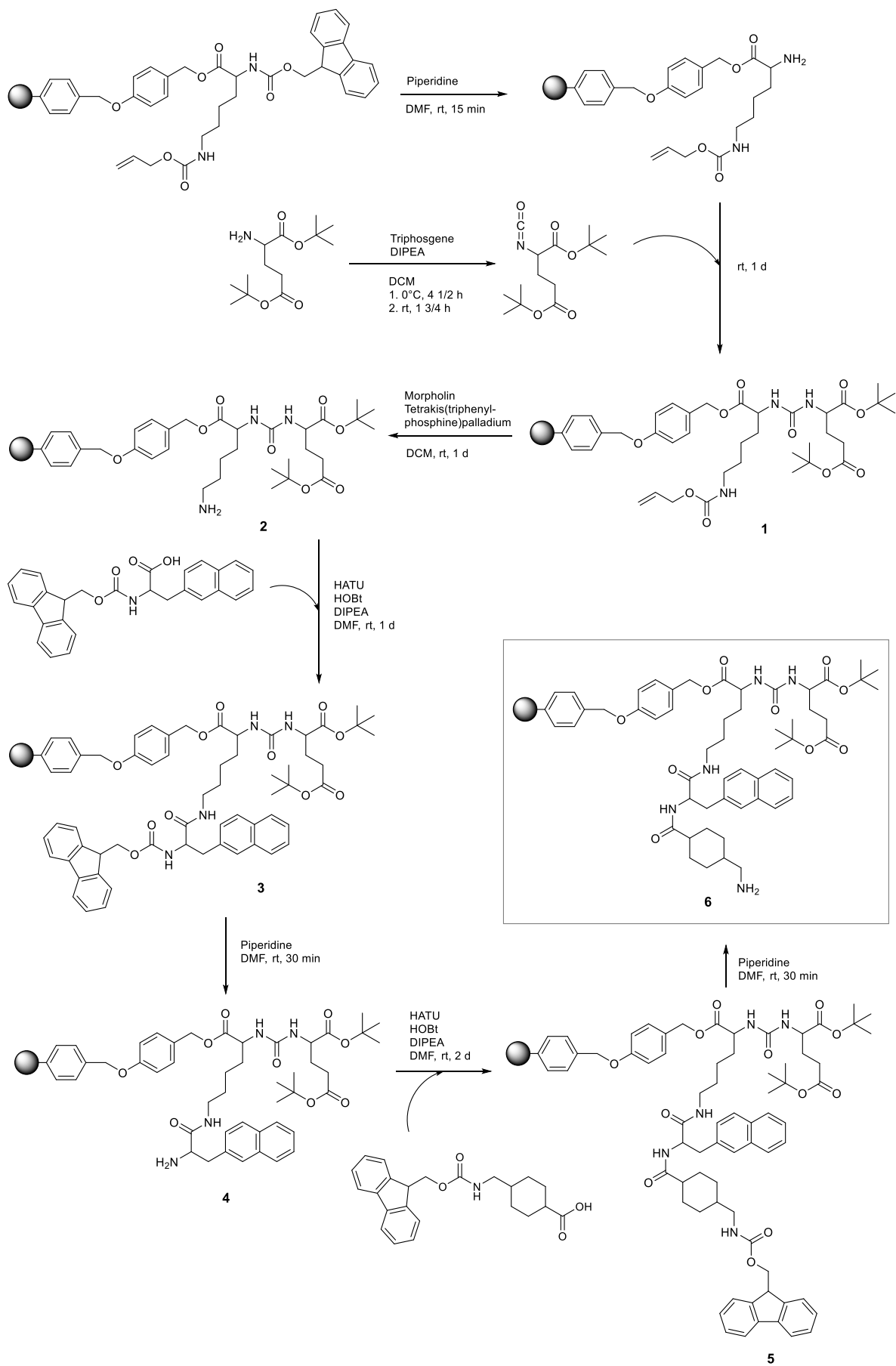


Figure 1 Synthesis scheme of the resin bound PSMA-617 backbone.

The second target vector, the squaric acid conjugated bisphosphonate pamidronate (**8**) was synthesized in a two-step synthesis with an overall yield of 28 % (Figure 2). According to literature, β -Alanine was transformed into pamidronate (**7**) using phosphorus acid and phosphorus trichloride⁴⁵. This was followed by an asymmetric amidation to conjugate the amine of the bisphosphonate to the squaric acid ester.

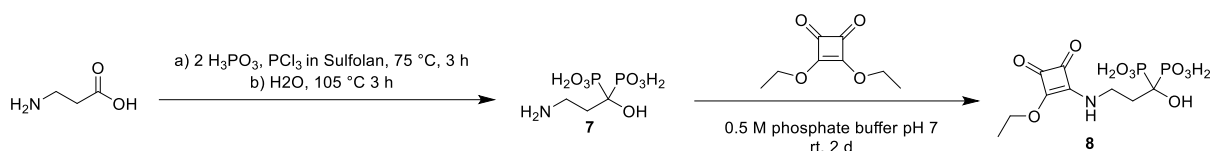


Figure 2 Synthesis scheme of the pamidronate target vector (**8**)

The final part of the synthesis was the conjugation of the two target vectors **6** and **8** and the DOTA-chelator using lysine as bridging unit (Figure 3). First, protected lysine was conjugated to the free amine of the resin bound compound **6**. After Fmoc deprotection, DOTA-Tris(*tert*-butyl ester) was conjugated. Both steps were carried out with HATU as reagent for amide formation. This reaction led to the completely protected and resin bound compound **11**. This compound was completely deprotected under acidic conditions and removed from the solid phase. In the further process of the reaction, protective groups are no longer necessary, as the following asymmetric amidation is highly selective for amines. Compound **12** was purified via semi preparative HPLC resulting in a yield of 4 % after the amide formation steps. Finally, the second target vector Pam.SA (**8**) was added - this was done via the asymmetric amidation of the squaric acid monoester and the free amine of compound **12**. Due to poor solubility of the bisphosphonate **8** in organic solvents, this reaction was carried out in aqueous phosphate buffer at a pH value of 9. The final compound **13** was purified via semi-preparative HPLC with a yield of 84 %. The entire compound DOTA-L-Lys(SA.Pam)-PSMA-617 was prepared in 15 steps with a total yield of 1 %.

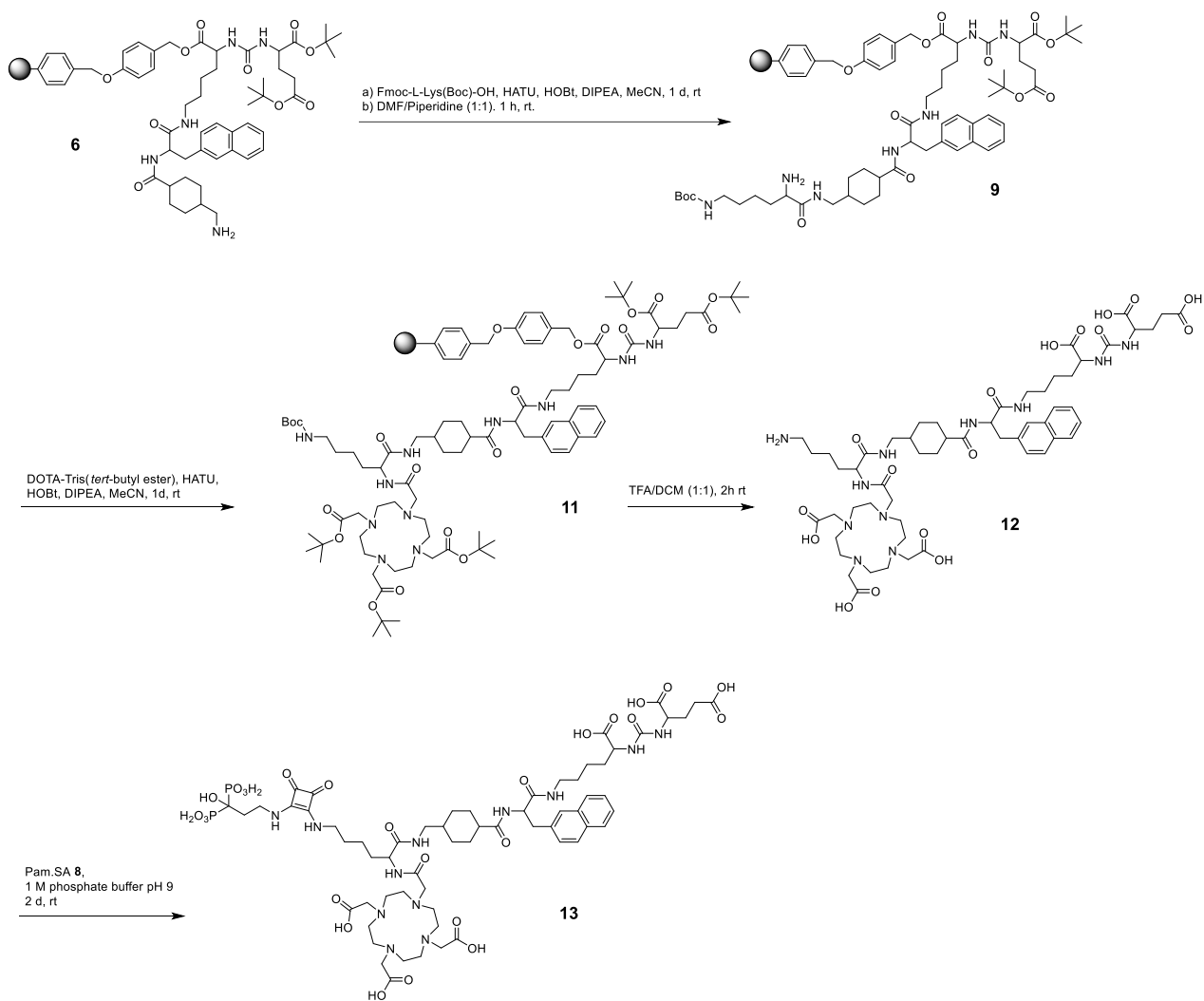


Figure 3 Synthesis scheme of DOTA-L-Lys(SA.Pam)-PSMA-617 (13)

Radiochemical evaluation with lutetium-177

Radiolabelling of compound **13** with lutetium-177 was carried out at 95°C in 1 mL of ammonium acetate buffer (1 M, pH 5.5). The radiochemical yield (RCY) as a function of precursor amount (5 to 30 nmol) was evaluated and illustrated in figure 4.

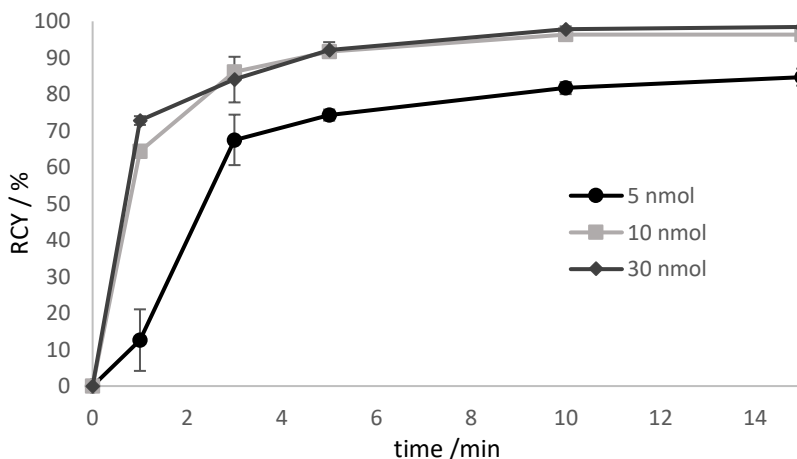


Figure 4 Labelling kinetics of [¹⁷⁷Lu]Lu-13 for various amounts of precursor at 95 °C in 1 M ammonium acetate buffer pH 5.5 at 95 °C. Precursor amounts of > 10 nmol resulting in RCYs of > 96 % after 10 min.

For substance amounts higher than 10 nmol, radiochemical yields of over 90 % were already achieved after 5 min. The RCY was almost quantitative after 10 min. In contrast, with a substance quantity of 5 nmol, the RCY obtained after 5 min was of only 75 %. In the further progress of the reaction, the yield increased to 85 %, but then stagnated there indicating that the labelling kinetics are depending on the amount of the precursor. RCY and radiochemical purity were analysed by radio-TLC and radio-HPLC. On radio-TLC the labelled compound [¹⁷⁷Lu]Lu-**13** showed a R_f of 0.0, while free unlabelled [¹⁷⁷Lu]Lu³⁺ showed a R_f of 0.8 – 1 in citrate buffer as mobile phase. On analytical radio-HPLC, the compound had a retention time (t_R) of 9.8 min.

Since the stability of the ligand-chelator conjugate is crucial for a translational use, complex stability studies were carried out in different media (phosphate buffered saline (PBS), isotonic saline (NaCl) and human serum (HS)). Results are shown in figure 5.

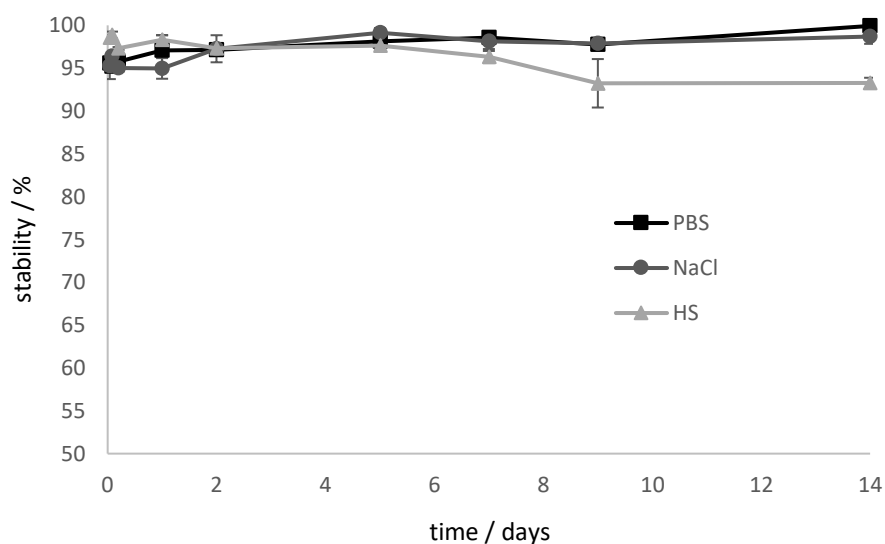


Figure 5 Stability studies of $[^{177}\text{Lu}]\text{Lu-13}$ in different media for 14 d. $[^{177}\text{Lu}]\text{Lu-13}$ is stable in PBS and NaCl. The stability in HS decreases to 93 % after 9 days.

In PBS and saline, $[^{177}\text{Lu}]\text{Lu-13}$ showed > 98 % intact conjugate even after 14 days. Stability in human serum decreases slightly. However, after 9 d, 93 % are still intact. Stability is preserved and even after 14 days the stability in HS is still at 93 %.

The lipophilicity of the compound was determined via the equilibrium distribution in a mixture of n-octanol and PBS using the shake flask method. $\log D_{7.4}$ values of $[^{177}\text{Lu}]\text{Lu-13}$ and the reference compound $[^{177}\text{Lu}]\text{Lu-PSMA-617}$ are shown in table 1. The lipophilicity of the lutetium-labelled compound **13** was similar to the lipophilicity of $[^{177}\text{Lu}]\text{Lu-PSMA-617}$.

Table 1 Experimentally determined $\log D_{7.4}$ values of $[^{177}\text{Lu}]\text{Lu-13}$ and the reference $[^{177}\text{Lu}]\text{Lu-PSMA-617}$

Compound	$\log D_{7.4}$ (n-octanol/PBS)
$[^{177}\text{Lu}]\text{Lu-13}$	-2.29 ± 0.12
$[^{177}\text{Lu}]\text{Lu-PSMA-617}$	-2.23 ± 0.20

Binding studies on hydroxyapatite (HAP)

The Ca-containing hydroxyapatite is found in mammal bones⁴⁶. Crystalline HAP is therefore suitable as a model compound to investigate the accumulation potential of bisphosphonates to the bone structure or bone metastases *in vitro*. Figure 6 shows the enrichment of [¹⁷⁷Lu]Lu-**13**, [¹⁷⁷Lu]Lu-PSMA-617 and free [¹⁷⁷Lu]Lu to HAP in comparison to the enrichment of [¹⁷⁷Lu]Lu-**13** and free [¹⁷⁷Lu]Lu³⁺ to HAP previously blocked with pamidronate.

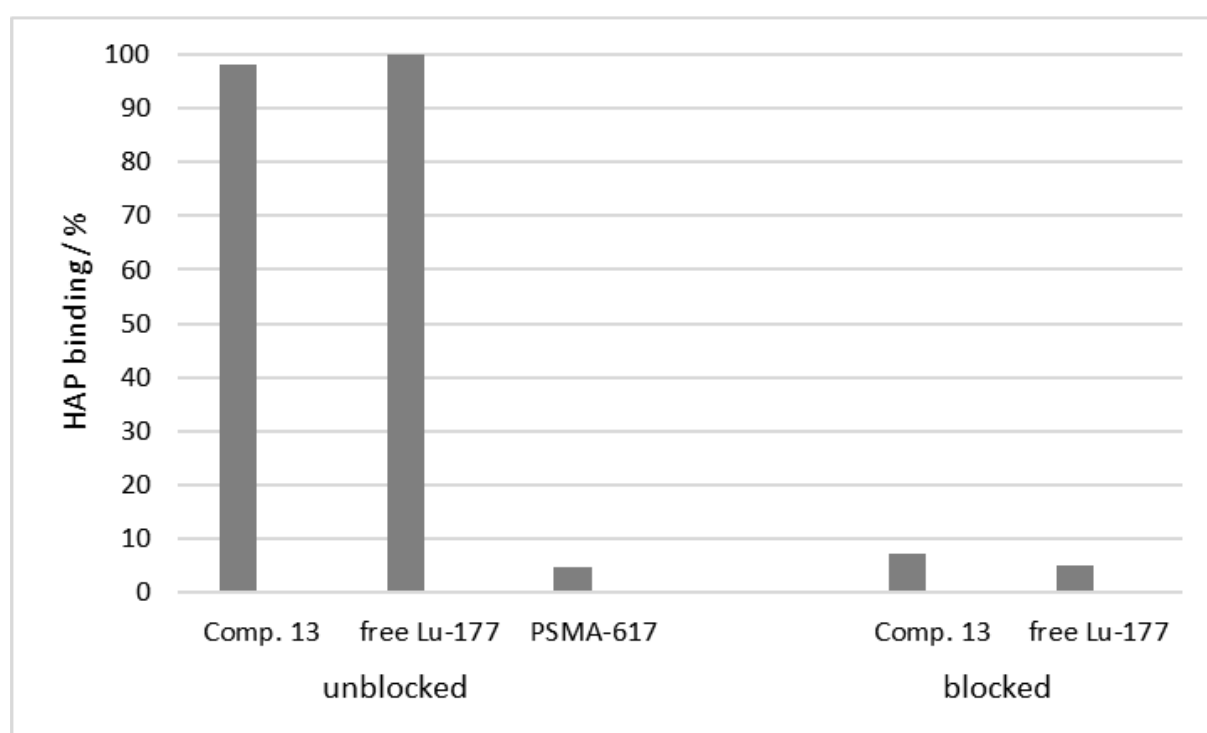


Figure 6 Percent enrichment of [¹⁷⁷Lu]Lu-**13** (98.2 ± 0.11 %), [¹⁷⁷Lu]Lu-PSMA-617 (4.77 ± 1.35 %) and free [¹⁷⁷Lu]Lu³⁺ (99.89 ± 0.02 %) to HAP in comparison to the percent enrichment of [¹⁷⁷Lu]Lu-**13** (7.31 ± 1.08 %) and free [¹⁷⁷Lu]Lu³⁺ (4.89 ± 0.51 %) to HAP previously blocked with pamidronate.

Uncomplexed lutetium cation [¹⁷⁷Lu]Lu³⁺ is known for its high affinity towards HAP⁴⁶. Therefore, it was used as positive sample. In this study, it showed a HAP-binding of 99.89 ± 0.02 %. [¹⁷⁷Lu]Lu-**13** also showed also a nearly complete enrichment at the HAP surface (98.2 ± 0.11 %), comparable to the free lutetium cation. In contrast, [¹⁷⁷Lu]Lu-PSMA-617 displayed no notable binding (4.77 ± 1.35 %). To evaluate the selectivity of binding, HAP was blocked with an excess of pamidronate prior to incubation with the test compounds. The binding of [¹⁷⁷Lu]Lu-**13** (7.31 ± 1.08 %) as well as [¹⁷⁷Lu]Lu³⁺ (4.89 ± 0.51 %) decreased significantly, indicating a specific binding to the calcium ions of the apatite structure.

***In vitro* affinity assay**

In a further step, we evaluated the PSMA binding affinity of compound **13** in a competitive radioligand assay and compared the calculated K_i value to the inhibition constant values of compound **12** to evaluate the influence of the SA.Pam unit and to PSMA-617 as seen in table 2. Compound **13** showed good binding affinity similar to that of [^{nat}Lu]Lu-**13**, thus indicating that radionuclide complexation does not have any impact on PSMA-binding. However, the bisphosphonate-free PSMA tracer DOTA-L-Lys-PSMA-617 (compound **12**) displayed 2-fold higher binding potency than the pamidronate-PSMA conjugates, indicating an influence of the SA.Pam unit. In addition, the binding affinity of the reference compound PSMA-617 in this assay is also higher than in comparison to compound **13**. Compound **12** shows a comparable affinity to PSMA-617.

Table 2 Inhibition constant values of PSMA ligands. Values are mean \pm SD.

Compound	K_i [nM]
compound 13	52.6 \pm 3.5
[^{nat} Lu]Lu- 13	42.3 \pm 7.7
compound 12 (DOTA-L-Lys-PSMA-617)	19.7 \pm 3.3
PSMA-617	6.9 \pm 1.3

ex vivo studies

Biodistribution studies of [¹⁷⁷Lu]Lu-**13** were performed using LNCaP tumor-bearing Balb/c mice. The accumulation of the ¹⁷⁷Lu-labelled tracer in several organs was determined and illustrated in figure 7. Although the accumulation of the tracer in both tumor and femur were similar (4.2 ± 0.7 %ID/g and 3.4 ± 0.4 %ID/g respectively), the bone-uptake was, in contrast to tumor-uptake, not PSMA-specific since it could not be blocked by the PSMA inhibitor PMPA (2-(Phosphonomethyl)pentanedioic acid). Additionally, [¹⁷⁷Lu]Lu-**13** showed the highest accumulation in the kidneys 16.5 ± 2.1 %ID/g, which seems to be PSMA-specific since it could be reduced by co-injection of PMPA. In contrast, the uptake in the liver as well as in the spleen was PSMA-unspecific. Noteworthy is the high tumor-to-blood and bone-to-blood ratios (210 and 170 respectively) resulting from a minimal accumulation in the blood.

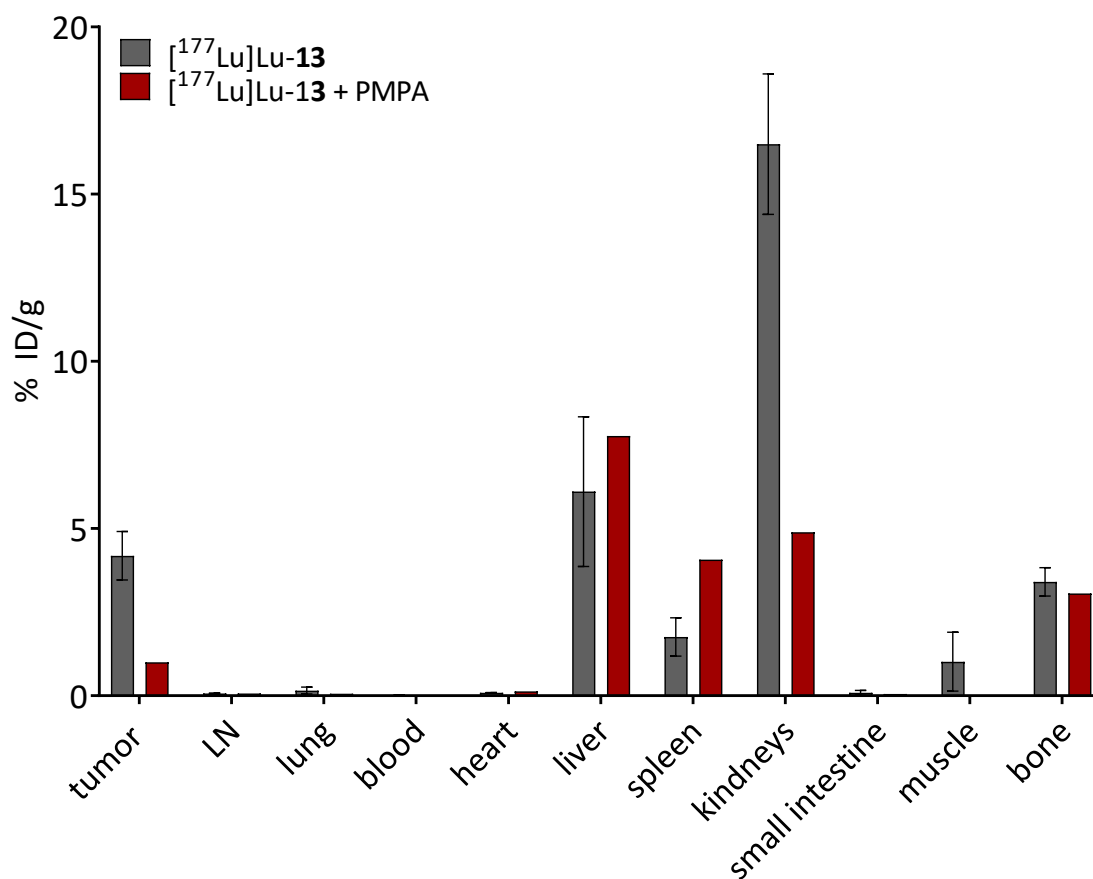


Figure 7 Biodistribution of 0.5 nmol [¹⁷⁷Lu]Lu-**13** at 24 h p.i. (n=3). PSMA-selectivity was assessed by co-injection of 1,5 mol PMPA. Data are % injected dose per gram tissue.

Discussion

Due to the heterogeneity in PSMA-expression of many bone metastases, the dual-targeting strategy could be an advantageous approach in the treatment of prostate cancer-related bone metastases. A new heterodimeric compound containing a PSMA inhibitor target vector, a bisphosphonate drug and a DOTA chelator was developed and evaluated regarding radiolabelling, lipophilicity, HAP binding, *in vitro* affinity towards PSMA and *ex vivo* kinetic properties.

The compound DOTA-L-Lys(SA.Pam)-PSMA-617 (**13**) was prepared in 15 steps with a total yield of 1 %.

Radiolabelling of **13** with ^{177}Lu showed a fast and quantitative RCY after 10 min with quantities over 10 nmol. The ^{177}Lu -labelled compound is stable (< 98 %) in PBS and saline for 14 days and in HS for 5 days, releasing 7 % of the ^{177}Lu until day 9 and remaining stable even after 14 days (93 %). Thus, the complexation of the therapeutic nuclide seems to be stable even after two weeks. Due to the long half-life of ^{177}Lu (7 days), it is also possible to store the labelled compound for a short time before injection, for example, for the treatment of several patients with one batch of tracer. The most suitable medium here is isotonic saline, which could also serve as injection medium. Moreover, the high stability of [^{177}Lu]Lu-**13** in HS makes it unlikely that ^{177}Lu will be released during the circulation time in the blood. The experimentally determined $\log D_{7,4}$ value as a measure of lipophilicity is almost identical to the value of [^{177}Lu]Lu-PSMA-617, which serves as reference, indicating the hydrophilic character of both compounds.

An aqueous suspension of crystalline HAP was used as a bone tissue model to test the HAP binding potency of the novel compound. The adsorption of [^{177}Lu]Lu-**13** to HAP was almost quantitative. It is nearly identical to the adsorption shown by free $^{177}\text{Lu}^{3+}$. Uncomplexed $^{177}\text{Lu}^{3+}$ is known for its high HAP affinity and correspondingly strong accumulation in bone tissue.¹⁰⁸ Compared to other literature-known DOTA conjugated bisphosphonates, e.g. DOTAM^{PAM} (92.2 ± 2.7 %), DOTAM^{ZOL} (92.7 ± 1.3 %) or BPAPD (83.0 ± 0.8 %), [^{177}Lu]Lu-**13** showed an even better adsorption⁴⁸.

By blocking of HAP with an excess of pamidronate prior to addition of [^{177}Lu]Lu-**13** or [^{177}Lu]Lu³⁺, no significant adsorption was observed. This proves that the selective binding of [^{177}Lu]Lu-**13** to HAP is due to the adsorption of the SA.Pam unit at the calcified HAP surface. As expected, [^{177}Lu]Lu-PSMA-617 showed no notable binding to HAP. This shows that, in contrast to [^{177}Lu]Lu-**13**, [^{177}Lu]Lu-PSMA-617 can only accumulate in bone metastases via one mechanism, namely PSMA-binding.

In addition to HAP adsorption, [^{nat}Lu]Lu-**13** displayed a PSMA binding affinity in the nanomolar range. the complexation of the radiometal had no impact on the binding potency, since the K_i values of both complexed and uncomplexed conjugates were similar (42.3 ± 7.7 nM and 52.6 ± 3.5 nM for [^{nat}Lu]Lu-**13** and comp **13** respectively). However, the bisphosphonate-free compound **13** showed 2-fold higher binding potency revealing that the coupling of pamidronate affects the interaction of the tracer with the PSMA binding pocket, possibly through changes in the conformation of the molecule.

Biodistribution studies were conducted in LNCaP tumor-bearing mice in order to better characterize the translational potential of the dual-targeting properties of [¹⁷⁷Lu]Lu-**13**. In terms of PSMA-specific accumulation, [¹⁷⁷Lu]Lu-**13** showed good PSMA-specific tumor accumulation 4.2 ± %ID/g which could be reduced by blocking the PSMA receptors with the potent PSMA inhibitor PMPA. According to literature the tumor-uptake of [¹⁷⁷Lu]Lu-PSMA-617 seems to be significantly higher 11.2 ± 4.17 %ID/g.¹⁰⁹ However, this could be due to the higher binding affinity of this tracer K_i= 6.9 ± 1.3 nM vs. 42.3 ± 7.7 nM for [^{nat}Lu]Lu-**13**. Nevertheless, [¹⁷⁷Lu]Lu-PSMA-617 did not display any binding to HAP as discussed above, thus accumulation in bone metastases is supposed to be minimal since bone-uptake is depending on PSMA-expression. In contrast, [¹⁷⁷Lu]Lu-**13** showed bone accumulation in the same range as tumor accumulation. As this could not be blocked by PMPA suggesting that bone uptake is solely resulting from HAP binding. As already discussed, compound **13** can therefore be used in contrast to PSMA-617 for the therapy of PSMA negative bone metastases, since it can also accumulate at the metastases via the increased bone metabolism. Compared to the results published by Meckel et al, [¹⁷⁷Lu]Lu-**13** showed similar bone uptake as [¹⁷⁷Lu]Lu-DOTA^{ZOL} (3.4 ± 0.4 %ID/g and 3.2 ± 0.4 %ID/g respectively)⁴⁸. However, kidney accumulation of [¹⁷⁷Lu]Lu-**13** was higher than [¹⁷⁷Lu]Lu-DOTA^{ZOL} (16.5 ± 2.1 %ID/g vs. 1,3 ± 0.1 %ID/g respectively). This could be due to the existence of PSMA receptors in the kidneys as known from literature⁴⁹. Furthermore, the uptake in the liver and the spleen seems to be PSMA-independent, since no blocking effects were observed. The reason has yet to be found, as increased liver uptake is not known here for either bisphosphonates or PSMA-617. Nevertheless, target-to-background ratio of [¹⁷⁷Lu]Lu-**13**, 24h after injection, was remarkably high (tumor-to-blood-ratio, 210; bone-to-blood ratio, 170) revealing the promising potential of this compound. Especially with regard to the conjugated DOTA-chelator, which is a versatile chelator not only used in complexing the therapeutic β⁻nuclide Lu-177, which is evaluated in this study, but is also applicable with other clinically relevant nuclides used in diagnosis by PET (e.g. ⁶⁸Ga or ⁴⁴Sc) or SPECT (e.g. ¹¹¹In or ⁶⁷Ga). Furthermore, the use of compound **13** in combination with α-emitters (e.g. ²²⁵Ac or ²¹³Bi) would be interesting for the treatment of bone metastases in close distance to the bone marrow due to the short range of these nuclides.

Conclusion

In this work, a novel chimeric compound for therapy of prostate cancer related bone metastases was designed and successfully synthesized. Key structure elements of the novel compound are the following. The well-known and established PSMA inhibitor KuE in combination with the PSMA-617 linker unit enables high affinity towards PSMA. The bisphosphonate pamidronate as HAP target vector shows high bone accumulation. It is conjugated via SA unit, which allows easy conjugation chemistry as well as increase of the antiresorptive effect of the bisphosphonate. Finally, the DOTA chelator allows the labelling with a wide range of diagnostic and therapeutic radiometals.

DOTA-L-Lys(SA.Pam)-PSMA-617 shows both excellent labelling properties and very good and selective HAP binding, which is superior to other DOTA-conjugated bisphosphonate compounds. The *in vitro* PSMA affinity is lower than that of PSMA-617, which can be ascribed to an influence of the Pam.SA group. Nevertheless, the compound shows both PSMA-dependent tumor uptake and PSMA-independent uptake into bone tissue and a remarkably high tumor-to-blood as well as bone-to-blood-ratio after 24 h.

The available results show that the new compound is well suited for the therapy of PCa-related bone metastases. Despite the low affinity and *in vivo* uptake compared to [¹⁷⁷Lu]Lu-PSMA-617, the new compound could contribute significantly to the therapy of bone metastases by exploiting the heterodimeric dual-targeting mechanism and thereby increasing avidity as discussed above. This is particularly the case when PSMA expression in metastases is low or absent and therapy with [¹⁷⁷Lu]Lu-PSMA-617 or other PSMA-based therapeutics is not possible. In addition, it enables a simpler therapeutic approach. Likewise, PSMA-negative metastases cannot be "overlooked". The possibility to target via both target vectors with a single theranostic radiotracer could improve patient management. Although the compound in the first studies is a promising compound for theranostics of PCa related bone metastases, further investigation and optimisation is needed to improve the radiotracer. For example, with regard to PSMA affinity or liver uptake.

Materials and Methods

General

All chemicals were purchased from Sigma-Aldrich, Merck, Fluka, AlfaAesar, VWR, AcrosOrganics, TCI, Iris Biotech and Fisher Scientific and used without purification. Dry solvents were obtained from Merck and VWR, deuterated solvents for NMR spectra from Deutero. PSMA-617 was purchased from Hycultec. Thin layer chromatography was performed with silica gel 60 F254 coated aluminum plates from Merck. Evaluation was carried out by fluorescence extinction at $\lambda=254$ nm and staining with potassium permanganate. The radio TLCs were evaluated using a CR-35 Bio test imager from Raytest and the AIDA (Raytest) software. The ^1H and ^{13}C NMR measurements were performed on an Avance III HD 300 spectrometer (300 MHz, 5mm BBFO sample head with z-gradient and ATM and BACS 60 sample changer), an Avance II 400 spectrometer (400 MHz, 5mm BBFO sample head with z-Gradient and ATM and SampleXPress 60 sample changer) and an Avance III 600 spectrometer (600 MHz, 5mm TCI CryoProbe sample head with z-Gradient and ATM and SampleXPress Lite 16 sample changer) from Bruker. The LC/MS measurements were performed on an Agilent Technologies 1220 Infinity LC system coupled to an Agilent Technologies 6130B Single Quadrupole LC/MS system. Semi-preparative HPLC purification was performed on a 7000 series Hitachi LaChrom and the respectively mentioned conditions and column. For radiolabelling experiments n.c.a. [^{177}Lu]LuCl₃ in 0.04 M HCl (ITM, Garching, Germany) was used.

Organic synthesis

Solid phase synthesis of the PSMA ligand (PSMA-167-resin)

The synthesis of the glutamate-urea-lysine binding motif and the linker of the PSMA-617 backbone was carried out following the established solid phase peptide chemistry as described by Benesova et al. with slight adjustments to the reaction procedures ¹¹.

Bis(*tert*-butyl)-L-glutamate-hydrochloride (4.5 g, 15.21 mmol) and DIPEA (7.98 g, 10.5 mL, 61.74 mmol) were dissolved in dry dichloromethane (200 mL) and cooled to 0 °C. Triphosgene (1.56 g, 5.26 mmol) in dichloromethane (30 mL) were added dropwise over a period of 4.5 h. After the complete addition, the solution was stirred for an additional hour.

The Fmoc protecting group of Fmoc-L-Lysine(Alloc)-Wang resin (1.65 g, 1.5 mmol, 0.9 mmol/g) was removed by stirring it in a piperidine/DMF (1:1) solution for 15 minutes followed by a washing step with dichloromethane.

The deprotected L-lysine(Alloc)-Wang resin was added to the previous prepared solution and stirred overnight at room temperature. The resin (compound **1**) was washed with dichloromethane (15 mL) and used without further purification.

Tetrakis(triphenylphosphin)palladium (516.0 mg, 0.45 mmol) und morpholine (3.92 g, 3.92 mL, 45.00 mmol) were dissolved in dichloromethane (12 mL) and added to compound **1**. The solution was stirred for 1 d under exclusion of light. Afterwards it was washed with dichloromethane (15 mL), a 1 % DIPEA solution in DMF (3 x 10 mL) and a sodium diethyldithiocarbamate trihydrate solution (15 mg/mL) in DMF (9 x 10 mL x 5 minutes), resulting in compound **2**, the resin-immobilized and Alloc-deprotected glutamate-urea-lysine conjugate.

Fmoc-3-(2-naphthyl)-L-alanine (1.75 g, 4.00 mmol), HATU (1.52 g, 4.00 mmol), HOBt (540 mg, 4.00 mmol) and DIPEA (780 mg, 1.02 mL, 6.03 mmol) were dissolved in dry DMF (10 mL) and added to the resin. The solution was stirred overnight and then washed with DMF (10 mL) and dichloromethane (10 mL). To remove the Fmoc-group, the resin (compound **3**) was stirred in a piperidine/DMF (1:1, 8 mL) solution for 20 minutes and washed with DMF (10 mL) and dichloromethane (10 mL), resulting in compound **4**.

Fmoc-4-Amc-OH (1.52 g, 4 mmol), HATU (1.52 g, 4.00 mmol), HOBt (540 mg, 4.00 mmol) and DIPEA (780 mg, 1.02 mL, 6.03 mmol) were dissolved in dry DMF (10 mL) and added to the resin (compound **4**). The solution was stirred for two days and then washed with DMF (10 mL) and dichloromethane (10 mL). To remove the Fmoc-group from compound **5**, it was stirred in a piperidine/DMF (1:1, 8 mL) solution for 20 minutes and washed with DMF (10 mL) and dichloromethane (10 mL), leading to the final resin bound PSMA-617 backbone (**6**).

Pamidronate (7, Pam)

β -Alanine (1.5 g, 0.017 mol) and phosphorus acid (2.76 g, 0.034 mol) were dissolved in Sulfolane (5.5 mL) and cooled to 0 °C. Phosphorus trichloride (4.62 g, 2.95 mL, 0.034 mmol) was added dropwise. The solution was stirred for 3 h at 75 °C. Water (15 mL) was added and stirred for 12 h at 100°C. Ethanol (15 mL) was added and the product (**7**, 1.48 g, 0.006 mol, 37 %) was obtained as yellow solid after crystallisation at 0°C for 3 days.

^1H NMR (300 MHz, D_2O) δ [ppm] = 3.34 (t, J = 7.1 Hz, 2H), 2.31 (tt, J = 13.7, 7.1 Hz, 2H).

^{13}C -NMR (400 MHz, D_2O): δ [ppm] = 72.58, 36,14, 30.54.

^{31}P NMR (121.5 MHz, D_2O) δ [ppm] = 17,58 (s, 2P).

MS (ESI⁺): 236.0 [M+H]⁺, calculated for $\text{C}_3\text{H}_{11}\text{NO}_7\text{P}_2$: 235.07 [M]⁺.

Pamidronate-squaric acid ethylester (8, SA.Pam)

Pamidronate (**7**, 500 mg, 2.13 mmol) was dissolved in phosphate buffer (0.5 M, pH 7, 5 mL). 3,4-Diethoxycyclobut-3-ene-1,2-dione (squaric acid diethylester, SADE, 542 mg, 468 μ L, 3.2 mmol) was added and the mixture was stirred for 2 days at room temperature. Ethanol (3 mL) was added for crystallisation. The mixture was allowed to stand for 3 days in the freezer to complete crystallisation. The white precipitation was washed with cold ethanol and compound **8** (0.58 g, 1.62 mol, 76 %) was obtained as white solid.

^1H NMR (400 MHz, D_2O) δ [ppm] = 4.79-4.62 (m, 2H), 3.31 (t, J = 6.6 Hz, 2H), 2.32-2.15 (m, 2H) 1.42 (dt, J = 11.7, 7.2 Hz, 3H).

^{31}P NMR (162 MHz, D_2O) δ [ppm] = 17,92 (s), 2.26 (s).

MS (ESI $^+$): 360.0 [M+H] $^+$, 720.0 2[M+H] $^+$, 763.0 2[M+Na] $^+$, calculated for $\text{C}_9\text{H}_{15}\text{NO}_{10}\text{P}_2$: 359.16 [M] $^+$.

Fmoc-L-Lys(Boc)-PSMA-617-resin (9)

Fmoc-L-Lys(Boc)-OH (506 mg, 0.0011 mmol), HATU (415 mg, 0.0011 mmol), HOBt (146 mg, 0.0011 mmol) and DIPEA (277 μ L, 211 mg, 0.00162 mmol) were dissolved in acetonitrile (4 mL) and stirred for 30 min. The PSMA-617-resin (300 mg, 0.0027 mmol, 0.09 mmol/g) was added and the mixture was stirred for one day at room temperature. The resin was washed with acetonitrile (10 mL) and dichloromethane (10 mL) and used in the next step.

L-Lys(Boc)-PSMA-617-resin (10)

The Fmoc-L-Lys(Boc)-PSMA-617-resin (**9**) was stirred for one hour in a mixture of DMF and Piperidine (1:1, 6 mL). The Fmoc deprotected resin was washed with DMF (10 mL) and dichloromethane (10 mL) and used in the next step without further purification.

*DOTA(*t*Bu) $_3$ -L-Lys(Boc)-PSMA-617-resin (11)*

DOTA-Tris(*tert*-butyl ester) (310 mg, 0.54 μ mol), HATU 308 mg, 0.00081 mmol), HOBt (110 mg, 0.00081 mmol) and DIPEA (184 μ L, 140 mg, 0.0011 mmol) were dissolved in acetonitrile (4 mL) and stirred for 30 min. L-Lys(Boc)-PSMA-617-resin (**10**, 461 mg, 0.00027 mmol, 0.9 mmol/g) was added and the mixture was stirred for one day at room temperature. The resin was washed with acetonitrile (10 mL) and dichloromethane (10 mL) and used in the next step without further purification.

DOTA-L-Lys-PSMA-617 (12)

DOTA(tBu)₃-L-Lys(Boc)-PSMA-617-resin (**11**, 536 mg, 0.00027 mmol, 0.9 mmol/g) was stirred in a solution of TFA and dichloromethane (1:1, 4 mL) for 2 hours. The TFA/dichloromethane solution was evaporated under reduced pressure and the product (**12**, 10.6 mg, 0.0091 mmol, 4 %) was obtained as a colourless powder after semi-preparative HPLC purification (column: LiChrospher 100 RP18 EC (250 x 10 mm) 5 μ, flow rate: 5 mL/min, H₂O/MeCN + 0.1 % TFA, 25 % MeCN isocratic, t_R = 10.3 min).

MS (ESI⁺): 1172.5 [M+2H]⁺, 585.9 1/2[M+2H]⁺, 391.0 1/3[M+2H]⁺, calculated for C₅₅H₈₃N₁₁O₁₇: 1170.33 [M]⁺

DOTA-L-Lys(SA.Pam)-PSMA-617 (13)

Compound **12** (10 mg, 0.0085 mmol) and compound **8** (16 mg, 0.043 mmol) were dissolved in phosphate buffer (0.5 M, pH 9, 1 mL) and stirred for 2 days. The product (**13**, 10.56 mg, 0.0071 mmol, 84 %) was obtained as a colourless powder after semi-preparative HPLC purification (column: LiChrospher 100 RP18 EC (250 x 10 mm) 5 μ, flow rate: 5 mL/min, H₂O/MeCN + 0.1 % TFA, 23 % to 28 % MeCN in 20 min, t_R = 8.2 min).

MS (ESI⁺): 511.3 1/3[M+H+2Na]⁺, 520.0 [1/3M+2K]⁺, 781.0 1/2[M+2K]⁺, calculated for C₆₂H₉₂N₁₂O₂₆P₂: 1483.42 [M]⁺

Radiolabelling of DOTA-L-Lys(SA.Pam)-PSMA-617 with Lutetium-177 ([¹⁷⁷Lu]Lu-13)

For radiolabelling experiments n.c.a. [¹⁷⁷Lu]LuCl₃ in 0.04 M HCl (ITG, Garching, Germany) was used.

Radiolabelling was performed in 0.4 μL and 1 mL 1 M ammonium acetate buffer at pH 5.5. Reactions were carried out with different amounts of precursor (5, 10, 30 nmol) and at 95 °C with 40 – 50 MBq n.c.a. lutetium-177. Radio-TLC (TLC Silica gel 60 F254 Merck) and citrate buffer (pH 4) as mobile phase and radio-HPLC using an analytical HPLC 7000 series Hitachi LaChrom (Column: Merck Chromolith® RP-18e, 5-95 % MeCN (+0,1 % TFA)/ 95-5 % Water (+0,1 % TFA) in 10 min) was used for reaction control. TLC's were measured in TLC imager CR-35 Bio Test-Imager from Elysia-Raytest (Straubenhardt, Germany) with AIDA software.

***In vitro* stability studies**

Complex stability studies were carried out in human serum (HS, human male AB plasma, USA origin, Sigma Aldrich) and phosphate buffered saline (Sigma Aldrich). 5 MBq of the radioactive compound were incubated in 0.5 mL of the media for 14 d. After several time points (1h, 2h, 5h, 1d, 2d, 5d, 7d, 9d and 14d), aliquots were taken out to evaluate the radiochemical stability. Experiments were carried out as triplicate.

Lipophilicity determination

Using the shake flask method, the $\log D_{7.4}$ value of the compound was determined. The labelling solution was adjusted to pH 7.4 and 5 MBq were diluted in 700 μ l n-octanol and 700 μ l PBS. It was shaken for 2 min at 1500 U/min and then centrifuged. 400 μ l of the n-octanol phase and 400 μ l of the PBS phase were each transferred to a new Eppendorf tube. 3-6 μ l were then pipetted on a TLC plate and analysed via phosphor imager. $\log D_{7.4}$ value was calculated by determining the ratio of the activities of the two phases. This procedure was repeated twice more with the respective phase with higher activity, so that three coefficients were obtained and the mean value was calculated.

Binding studies of ^{177}Lu -labelled compound on hydroxyapatite (HAP)

Hydroxyapatite (20 mg) was incubated in saline (1 mL) for 24 h. 50 μ l of the labelled [^{177}Lu]Lu-**13** (5 MBq) and respectively [^{177}Lu]Lu-PSMA-617 (5 MBq) was added. The suspension was vortexed for 20 s and incubated for 1 h at room temperature. The samples were passed through a filter (CHROMAFIL® Xtra PTFE-45/13) and the supernatant was washed with water (500 μ l). The radioactivity of the liquids and the HAP-containing supernatant were measured with a curiemeter (Aktivimeter Isomed 2010 MED Nuklear-Medizintechnik Dresden GmbH). The binding of [^{177}Lu]Lu-**13** and [^{177}Lu]Lu-PSMA-617 was determined as percent of activity absorbed to HAP. Free Lu-177 was examined as a positive probe analogously.

For blocking experiments, Hydroxyapatite (20 mg) was incubated in saline (1 mL) with pamidronate (100 mg) and evaluated with [^{177}Lu]Lu-**13** and free Lu-177 as described above.

***In vitro* binding affinity**

Cold [^{nat}Lu]Lu complexes were synthesized by shaking a mixture of **13** (371 µL of a 1 mg/ml solution, 250 nmol) and LuCl₃ (129 µL of a 1 mg /mL solution, 375 nmol; metal to ligand ratio 1.5 to 1) in 1 M ammonium acetate buffer at 95 °C for 2 hours. Complexation was monitored by ESI-LC/MS.

Based on the protocol published by Benešová et al. the PSMA binding affinity was determined in a competitive radioligand assay ⁷. PSMA-positive LNCaP-cells (purchased from Sigma-Aldrich) were cultured in RPMI 1640 (Thermo Fisher Scientific) supplemented with 10 % fetal bovine serum (Thermo Fisher Scientific), 100 µg/ml streptomycin, and 100 units/ml penicillin at 37°C in 5 % CO₂. These cells were incubated for 45 min with rising concentrations of the test compounds in the presence of 0.75 nM [⁶⁸Ga]Ga-PSMA-10. Free radioactivity was removed by several washing steps with ice-cold PBS. Probes were measured in a γ-counter (2480 WIZARD² Automatic Gamma Counter, PerkinElmer). Obtained data were analyzed in GraphPad Prism 9 using nonlinear regression.

Animal studies

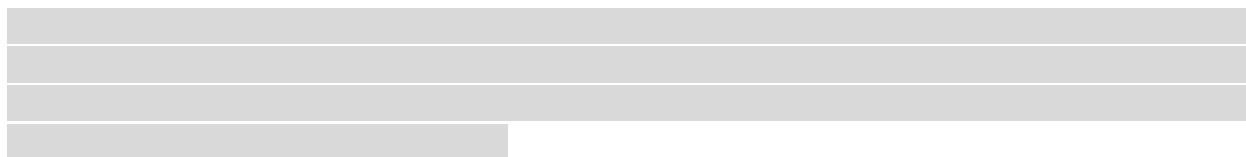
All animal experiments were approved by the ethical committee of the state of Rhineland Palatinate (according to §8 Abs. 1 Tierschutzgesetz, Landesuntersuchungsamt) and performed in accordance with relevant federal laws and institutional guide-lines approval Nr. 23 177-07/G 21-1-022.

6- to 8-week-old male BALB/cAnNRj (Janvier Labs) were inoculated subcutaneously with 5x10⁶ LNCaP cells in 200 µL 1:1 (v/v) Matrigel/PBS (Corning®). *ex vivo* experiments are conducted after the tumor has reached a volume of approximately 100 cm³.

LNCaP xenografts were anesthetized with 2% isoflurane prior to i.v. injection of 0.5 nmol of [¹⁷⁷Lu]Lu-**13**. The specific activity was approximately 3 MBq/nmol. PSMA-selectivity was investigated by co-injection of 1.5 µmol PMPA/mouse.

Animals were euthanized 24 h p.i. Organs were collected and weighed. The radioactivity was measured and calculated as decay-corrected percentage of the injected dose per gram of tissue mass %ID/g.

Acknowledgment



References

- (1) Ferlay, J., Colombet, M., Soerjomataram, I., Parkin, D. M., Piñeros, M., Znaor, A., and Bray, F. (2021) Cancer statistics for the year 2020: An overview. *Int. J. Cancer* 149, 778–789.
- (2) American Cancer Society. (2021) American Cancer Society. *Cancer Facts & Figures 2021*. Atlanta: American Cancer Society; 2021.
- (3) Donin, N. M., and Reiter, R. E. (2018) Why targeting PSMA is a game changer in the management of prostate cancer. *J. Nucl. Med.* 59, 177–182.
- (4) Rahbar, K., Afshar-Oromieh, A., Jadvar, H., and Ahmadzadehfar, H. (2018) PSMA Theranostics: Current Status and Future Directions. *Mol. Imaging* 17, 1–9.
- (5) Rowe, S. P., Gorin, M. A., and Pomper, M. G. (2019) Imaging of Prostate-Specific Membrane Antigen with Small-Molecule PET Radiotracers: From the Bench to Advanced Clinical Applications. *Annu. Rev. Med.* 70, 461–477.
- (6) Kopka, K., Benešová, M., Bařinka, C., Haberkorn, U., and Babich, J. (2017) Glu-ureido-based inhibitors of prostate-specific membrane antigen: Lessons learned during the development of a novel class of low-molecular-weight theranostic radiotracers. *J. Nucl. Med.*, pp 17S-26S. Society of Nuclear Medicine Inc.
- (7) Benesová, M., Schäfer, M., Bauder-Wüst, U., Afshar-Oromieh, A., Kratochwil, C., Mier, W., Haberkorn, U., Kopka, K., and Eder, M. (2015) Preclinical evaluation of a tailor-made DOTA-conjugated PSMA inhibitor with optimized linker moiety for imaging and endoradiotherapy of prostate cancer. *J. Nucl. Med.* 56, 914–920.
- (8) Haberkorn, U., Eder, M., Kopka, K., Babich, J. W., and Eisenhut, M. (2016) New strategies in prostate cancer: Prostate-specific membrane antigen (PSMA) ligands for diagnosis and therapy. *Clin. Cancer Res.* 22, 9–15.
- (9) Khawar, A., Eppard, E., Roesch, F., Ahmadzadehfar, H., Kürpig, S., Meisenheimer, M., Gaertner, F. C., Essler, M., and Bundschuh, R. A. (2019) Preliminary results of biodistribution and dosimetric analysis of [⁶⁸Ga]Ga-DOTA ZOL : a new zoledronate-based bisphosphonate for PET/CT diagnosis of bone diseases. *Ann. Nucl. Med.* 404–413.
- (10) Eder, M., Eisenhut, M., Babich, J., and Haberkorn, U. (2013) PSMA as a target for radiolabelled small molecules. *Eur. J. Nucl. Med. Mol. Imaging* 40, 819–823.
- (11) Benešová, M., Bauder-Wüst, U., Schäfer, M., Klika, K. D., Mier, W., Haberkorn, U., Kopka, K., and Eder, M. (2016) Linker Modification Strategies to Control the Prostate-Specific Membrane Antigen (PSMA)-Targeting and Pharmacokinetic Properties of DOTA-Conjugated PSMA Inhibitors. *J. Med. Chem.* 59, 1761–1775.
- (12) Rahbar, K., Ahmadzadehfar, H., Kratochwil, C., Haberkorn, U., Schafers, M., Essler, M., Baum, R. P., Kulkarni, H. R., Schmidt, M., Drzezga, A., Bartenstein, P., Pfestroff, A., Luster, M., Lutzen, U., Marx, M., Prasad, V., Brenner, W., Heinzel, A., Mottaghy, F. M., Ruf, J., Meyer, P. T., Heuschkel, M., Eveslage, M.,

- Bögemann, M., Fendler, W. P., and Krause, B. J. (2017) German multicenter study investigating ^{177}Lu -PSMA-617 Radioligand therapy in advanced prostate cancer patients. *J. Nucl. Med.* 58, 85–90.
- (13) Sartor, O., de Bono, J., Chi, K. N., Fizazi, K., Herrmann, K., Rahbar, K., Tagawa, S. T., Nordquist, L. T., Vaishampayan, N., El-Haddad, G., Park, C. H., Beer, T. M., Armour, A., Pérez-Contreras, W. J., DeSilvio, M., Kpamegan, E., Gericke, G., Messmann, R. A., Morris, M. J., and Krause, B. J. (2021) Lutetium-177–PSMA-617 for Metastatic Castration-Resistant Prostate Cancer. *N. Engl. J. Med.* 1–13.
- (14) Theodore, Thomas S., Pachynski, R. K. (2018) Treatment of Advanced Prostate Cancer. *Mo. Med.* 115, 156–161.
- (15) Larson, S. R., Zhang, X., Dumpit, R., Coleman, I., Lakely, B., Roudier, M., Higano, C. S., True, L. D., Lange, P. H., Montgomery, B., Corey, E., Nelson, P. S., Vessella, R. L., and Morrissey, C. (2013) Characterization of osteoblastic and osteolytic proteins in prostate cancer bone metastases. *Prostate* 73, 932–940.
- (16) Ahmadzadehfar, H., Matern, R., Baum, R. P., Seifert, R., Kessel, K., Bögemann, M., Kratochwil, C., Rathke, H., Ilhan, H., Sviridenka, H., Sathekge, M., Kabasakal, L., Yordanova, A., Garcia-Perez, F. O., Kair-emo, K., Maharaj, M., Paez, D., Virgolini, I., and Rahbar, K. (2021) The impact of the extent of the bone involvement on overall survival and toxicity in mCRPC patients receiving [^{177}Lu]Lu-PSMA-617: a WARMTH multicentre study. *Eur. J. Nucl. Med. Mol. Imaging.*
- (17) Sartor, O., Hoskin, P., and Bruland, S. (2013) Targeted radio-nuclide therapy of skeletal metastases. *Cancer Treat. Rev.* 39, 18–26.
- (18) Fang, J., and Xu, Q. (2015) Differences of osteoblastic bone metastases and osteolytic bone metastases in clinical features and molecular characteristics. *Clin. Transl. Oncol.* 17, 173–179.
- (19) Saad, Fred; Gleason, Donald M.; Murray, Robin; Tchekmedyan, Simon; Venner, Peter; Lacombe, Louis; Chin, Joseph L.; Vinholes, Jeferson J.; Goas, J. Allen; Chen, B. (2002) A randomized, placebo-controlled trial of zoledronic acid in patients with hormone-refractory metastatic prostate carcinoma. *J. Natl. Cancer Inst.* 94, 1458–1468.
- (20) Wong, S. K., Mohamad, N. V., Giaze, T. R., Chin, K. Y., Mohamed, N., and Ima-Nirwana, S. (2019) Prostate cancer and bone metastases: The underlying mechanisms. *Int. J. Mol. Sci.* 20.
- (21) Fleisch, H. (2002) Development of bisphosphonates. *Breast Cancer Res.* 4, 30–34.
- (22) Palma, E., Correia, J. D. G., Campello, M. P. C., and Santos, I. (2011) Bisphosphonates as radionuclide carriers for imaging or systemic therapy. *Mol. Biosyst.* 7, 2950–2966.
- (23) Ogawa, K., and Ishizaki, A. (2015) Well-designed bone-seeking radiolabeled compounds for diagnosis and therapy of bone metastases. *Biomed Res. Int.* 2015.
- (24) Eary, Janet, F.; Collins, Carolyn; Stabin, Michael; Vernon, Cheryl; Petersdorf, Steve; Baker, Melissa; Hartnett, S., Ferency, S., Addison, S. J., Appelbaum, F., and Gordon, E. E. (1993) Samarium-153-EDTMP Biodistribution and Estimation. *J. Nucl. Med.* 34, 1031–1036.
- (25) Meckel, M., Nauth, A., Timpe, J., Zhernosekov, K., Puranik, A. D., Baum, R. P., and Roesch, F. (2015) Development of a [^{177}Lu]Lu-BPAMD labeling kit and an automated synthesis module for routine bone targeted endoradiotherapy. *Cancer Biother. Radiopharm.* 30, 94–99.
- (26) Khawar, A., Eppard, E., Roesch, F., Ahmadzadehfar, H., Kürpig, S., Meisenheimer, M., Gaertner, F. C., Essler, M., and Bundschuh, R. A. (2019) Biodistribution and post-therapy dosimetric analysis of [^{177}Lu]Lu-DOTAZOL in patients with osteoblastic metastases: first results. *EJNMMI Res.* 9.
- (27) Kreppel, B., Gaertner, F. C., Ahmadzadehfar, H., Khawar, A., Roesch, F., Kuerpig, S., Meisenheimer, M., Essler, M., and Bundschuh, R. A. (2020) [^{177}Lu]Lu-DOTA-zoledronate therapy – first application in a patient with primary osseous metastatic bronchial carcinoma Background. *Nuklearmedizin ahead of p.*

- (28) Grus, T., Lahnif, H., Klasen, B., Moon, E.-S., Greifenstein, L., and Roesch, F. (2021) Squaric Acid-Based Radiopharmaceuticals for Tumor Imaging and Therapy. *Bioconjug. Chem.* 32, 1223–1231.
- (29) Meisenheimer, M., Kürpig, S., Essler, M., and Eppard, E. (2020) DOTA-ZOL: A promising tool in diagnosis and palliative therapy of bone metastasis—challenges and critical points in implementation into clinical routine. *Molecules* 25.
- (30) Van Beek, E., Löwik, C., Que, I., and Papapoulos, S. (1996) Dissociation of binding and antiresorptive properties of hydroxybisphosphonates by substitution of the hydroxyl with an amino group. *J. Bone Miner. Res.* 11, 1492–1497.
- (31) Hyvääkä, A., Virtanen, V., Kemppainen, J., Grönroos, T. J., Minn, H., and Sundvall, M. (2021) More than meets the eye: Scientific rationale behind molecular imaging and therapeutic targeting of prostate-specific membrane antigen (psma) in metastatic prostate cancer and beyond. *Cancers (Basel)*. 13.
- (32) Mannweiler, S., Amersdorfer, P., Trajanoski, S., Terrett, J. A., King, D., and Mehes, G. (2009) Heterogeneity of prostate-specific membrane antigen (PSMA) expression in prostate carcinoma with distant metastasis. *Pathol. Oncol. Res.* 15, 167–172.
- (33) Acar, E., Bekis, R., and Polack, B. (2019) Comparison of Bone Uptake in Bone Scan and Ga-68 PSMA PET/CT Images in Patients with Prostate Cancer. *Curr. Med. Imaging* 15, 589–594.
- (34) Silver, D. A., Pellicer, I., Fair, W. R., Heston, W. D. W., and Cordon-Cardo, C. (1997) Prostate-specific Membrane Antigen Expression in Normal and Malignant Human Tissues. *Clin. Cancer Research* 3, 81–85.
- (35) Harmon, S. A., Mena, E., Shih, J. H., Adler, S., McKinney, Y., Bergvall, E., Mehralivand, S., Sowalsky, A. G., Couvillon, A., Madan, R. A., Gulley, J. L., Eary, J., Mease, R. C., Pomper, M. G., Dahut, W. L., Turkbey, B., Lindenberg, L., and Choyke, P. L. (2018) A comparison of prostate cancer bone metastases on ¹⁸F-sodium fluoride and prostate specific membrane antigen (¹⁸F-PSMA) PET/CT: Discordant uptake in the same lesion. *Oncotarget* 9, 37676–37688.
- (36) Roudier, M. P., True, L. D., Higano, C. S., Vesselle, H., Ellis, W., Lange, P., and Vessella, R. L. (2003) Phenotypic heterogeneity of end-stage prostate carcinoma metastatic to bone. *Hum. Pathol.* 34, 646–653.
- (37) Seifert, R., Seitzer, K., Herrmann, K., Kessel, K., Schäfers, M., Kleesiek, J., Weckesser, M., Boegemann, M., and Rahbar, K. (2020) Analysis of PSMA expression and outcome in patients with advanced Prostate Cancer receiving ¹⁷⁷Lu-PSMA-617 Radioligand Therapy. *Theranostics* 10, 7812–7820.
- (38) Harmon, S. A., Bergvall, E., Mena, E., Shih, J. H., Adler, S., McKinney, Y., Mehralivand, S., Citrin, D. E., Couvillon, A., Madan, R. A., Gulley, J. L., Mease, R. C., Jacobs, P. M., Pomper, M. G., Turkbey, B., Choyke, P. L., and Lindenberg, M. L. (2018) A Prospective Comparison of 18F-Sodium Fluoride PET/CT and PSMA-Targeted 18F-DCFBC PET/CT in Metastatic Prostate Cancer. *J. Nucl. Med.* 59, 1665–1671.
- (39) Pyka, T., Okamoto, S., Dahlbender, M., Tauber, R., Retz, M., Heck, M., Tamaki, N., Schwaiger, M., Maurer, T., and Eiber, M. (2016) Comparison of bone scintigraphy and ⁶⁸Ga-PSMA PET for skeletal staging in prostate cancer. *Eur. J. Nucl. Med. Mol. Imaging* 43, 2114–2121.
- (40) Rowe, S. P., Mana-Ay, M., Javadi, M. S., Szabo, Z., Leal, J. P., Pomper, M. G., Pienta, K. J., Ross, A. E., and Gorin, M. A. (2016) PSMA-Based Detection of Prostate Cancer Bone Lesions with ¹⁸F-DCFPyL PET/CT: A Sensitive Alternative to ^{99m}Tc-MDP Bone Scan and Na¹⁸F PET/CT? *Clin. Genitourin. Cancer* 14, e115–e118.
- (41) Rowe, S. P., Macura, K. J., Mena, E., Blackford, A. L., Nadal, R., Antonarakis, E. S., Eisenberger, M., Carducci, M., Fan, H., Dannals, R. F., Chen, Y., Mease, R. C., Szabo, Z., Pomper, M. G., and Cho, S. Y. (2016) PSMA-Based [¹⁸F]F-DCFPyL PET/CT Is Superior to Conventional Imaging for Lesion Detection in Patients with Metastatic Prostate Cancer. *Mol. Imaging Biol.* 18, 411–419.

- (42) Uprimny, C., Sviriydenka, A., Fritz, J., Kroiss, A. S., Nilica, B., Decristoforo, C., Haubner, R., von Guggenberg, E., Buxbaum, S., Horninger, W., and Virgolini, I. J. (2018) Comparison of [⁶⁸Ga]Ga-PSMA-11 PET/CT with [¹⁸F]NaF PET/CT in the evaluation of bone metastases in metastatic prostate cancer patients prior to radionuclide therapy. *Eur. J. Nucl. Med. Mol. Imaging* 45, 1873–1883.
- (43) Janssen, J. C., Meißner, S., Woythal, N., Prasad, V., Brenner, W., Diederichs, G., Hamm, B., and Makowski, M. R. (2018) Comparison of hybrid ⁶⁸Ga-PSMA-PET/CT and ^{99m}Tc-DPD-SPECT/CT for the detection of bone metastases in prostate cancer patients: Additional value of morphologic information from low dose CT. *Eur. Radiol.* 28, 610–619.
- (44) Greifenstein, L., Engelbogen, N., Lahnif, H., Sinnes, J. P. J.-P., Bergmann, R., Bachmann, M., and Rösch, F. (2020) Synthesis, Labeling and Preclinical Evaluation of a Squaric Acid Containing PSMA Inhibitor Labeled with ⁶⁸Ga: A Comparison with PSMA-11 and PSMA-617. *ChemMedChem* 15, 695–704.
- (45) Kovacs, R., Grün, A., Nemeth, O., Garadnay, S., Greiner, I., and Keglevich, G. (2014) The Synthesis of Pamidronic Derivatives in Different Solvents: An Optimization and a Mechanistic Study. *Heteroat. Chem.* 25, 186–193234.
- (46) Cawthray, J. F., Creagh, A. L., Haynes, C. A., and Orvig, C. (2015) Ion exchange in hydroxyapatite with lanthanides. *Inorg. Chem.* 54, 1440–1445.
- (47) Breeman, W. A. P., Van der Wansem, K., Bernard, B. F., Van Gameren, A., Erion, J. L., Visser, T. J., Krenning, E. P., and De Jong, M. (2003) The addition of DTPA to [¹⁷⁷Lu]Lu-DOTA octreotate prior to administration reduces rat skeleton uptake of radioactivity. *Eur. J. Nucl. Med. Mol. Imaging* 30, 312–315.
- (48) Meckel, M., Bergmann, R., Miederer, M., and Roesch, F. (2017) Bone targeting compounds for radiotherapy and imaging: *Me(III)-DOTA conjugates of bisphosphonic acid, pamidronic acid and zoledronic acid. *EJNMMI Radiopharm. Chem.* 1, 1–14.
- (49) Silver, D. A., Pellicer, I., Fair, W. R., Heston, W. D., and Cordon-Cardo, C. (1997) Prostate-specific membrane antigen expression in normal and malignant human tissues. *Clin. Cancer Res.* 3.

4 Summary and outlook

The high incidence of PCa, as well as the high mortality rate of the advanced and metastatic forms, highlight the need for the development of accurate and sensitive diagnostic approaches as well as effective treatment strategies.

The discovery of prostate-specific membrane antigen PSMA as a reliable tumor-associated biomarker for prostate cancer led to a breakthrough in targeted imaging and endoradiotherapy of this disease. Several PSMA-targeted radioligands have been developed and evaluated in preclinical and clinical trials. The recent FDA-approval of [⁶⁸Ga]Ga-PSMA-11 and [¹⁷⁷Lu]Lu-PSMA-617 demonstrates the tremendous promise of the PSMA targeting approach and encourages researchers to develop further PSMA inhibitors with better properties especially in terms of easier synthesis and labeling but also lower off-target accumulation. Furthermore, Efforts are also being made to identify theranostic compounds for use in personalized medicine that are suitable for both diagnosis and therapy.

Beyond the use of PSMA as molecular target for nuclear medicine and radiopharmacy, it has also been demonstrated that this molecular target is equally appropriate for application in targeted drug delivery, although this approach is still in its early stages.

i) PSMA radiopharmaceuticals for diagnosis and therapy

the development of PSMA inhibitors for use in PET-imaging and endoradiotherapy was based on the hitherto known information about the PSMA binding pocket. Several studies on structure-activity-relationships were conducted to evaluate the impact of the different components of the PSMA radioligands on the *in vitro* binding affinity and to identify the most suitable compounds for further testing. An overview of the molecular design of the PSMA radiopharmaceuticals is shown in Figure 24.

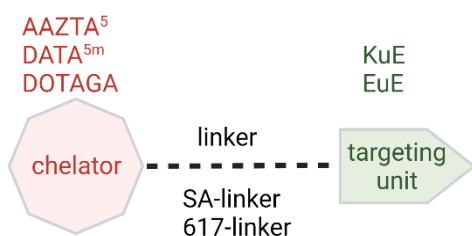
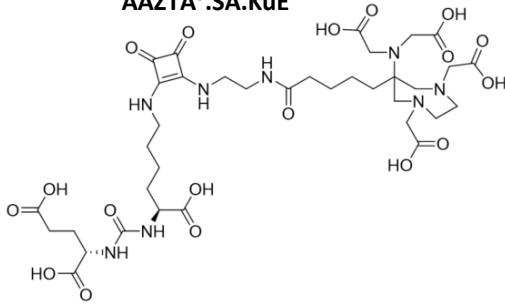
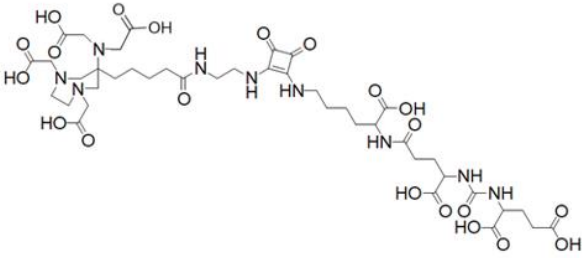
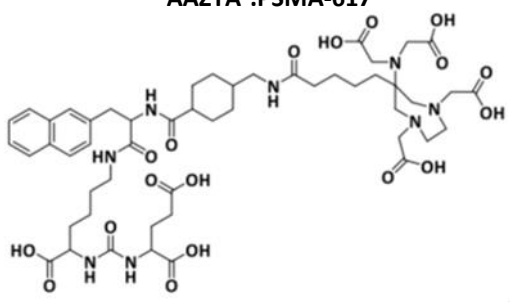
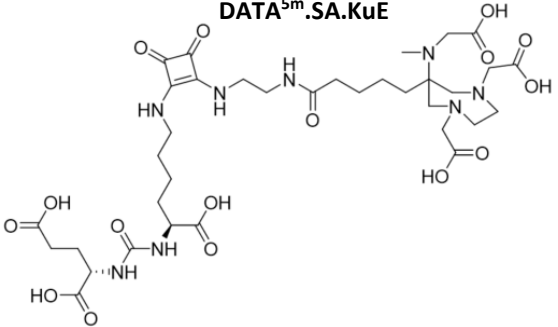
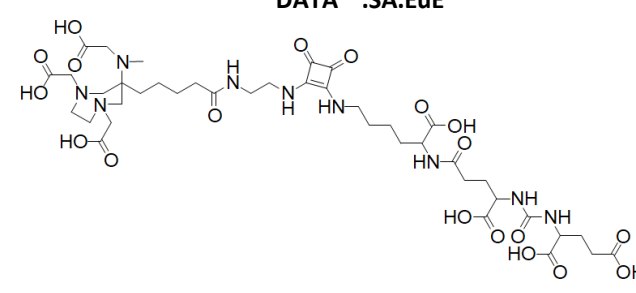
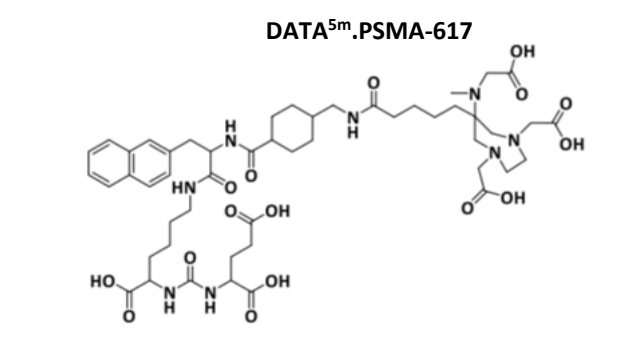
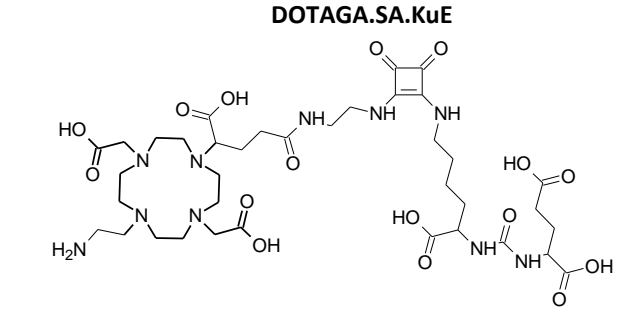
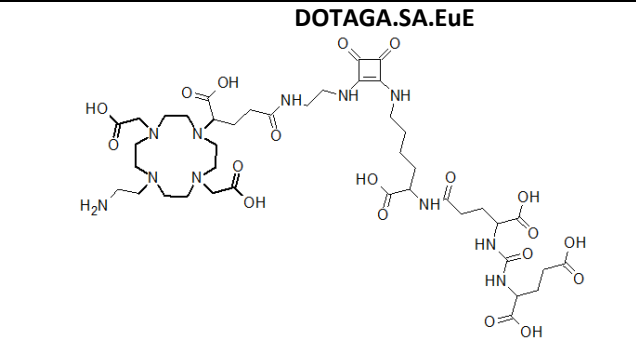
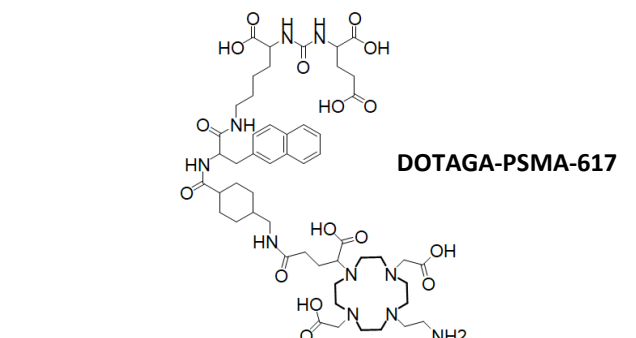


Figure 23 Molecular design of the evaluated PSMA radiopharmaceuticals. To address the pharmacophore pocket of PSMA, glutamate-urea-glutamate (EuE), was tested in addition to the established lysine-urea-glutamate (KuE). Furthermore, two different linker structures have been evaluated the SA-based linker and the naphthyl-cyclohexyl linker of PSMA-617. The impact of the chelator on the PSMA binding affinity has also been determined through the use of the hybrid-based chelators AAZTA⁵, DATA^{5m} and the DOTA-derivative DOTAGA.

In vitro binding affinities of the evaluated PSMA radiopharmaceuticals, expressed as IC₅₀ values, are summarized in table 4.

Table 4 IC₅₀ values of the investigated compounds. Data represented as Mean ± SD (n=3)

Chelator	Linker	Targeting unit	Chemical structure	IC ₅₀ [nM]
AAZTA ⁵	SA	KuE	<p>AAZTA⁵.SA.KuE</p> 	52.1 ± 4.0
		EuE	<p>AAZTA⁵.SA.EuE</p> 	178.2 ± 42.7
	617-linker	KuE	<p>AAZTA⁵.PSMA-617</p> 	12.7 ± 1.7
DATA ^{5m}	SA	KuE	<p>DATA^{5m}.SA.KuE</p> 	51.1 ± 5.5

DATA ^{5m}	SA	EuE	<p>DATA^{5m}.SA.EuE</p> 	386.2 ± 81.0
	617-linker	KuE	<p>DATA^{5m}.PSMA-617</p> 	92.1 ± 11.7
DOTAGA	SA	KuE	<p>DOTAGA.SA.KuE</p> 	20.2 ± 3.5
		EuE	<p>DOTAGA.SA.EuE</p> 	407.1 ± 19.2
	617-linker	KuE	<p>DOTAGA-PSMA-617</p> 	20.6 ± 3.4

The KuE targeting moiety seems to interact better with the binding pocket than EuE since all KuE- derivatives showed higher affinities than the EuE-based analogs. Such a clear statement could not be made in the case of the two implied linkers. While DOTAGA.SA.KuE and DOTAGA-PSMA-617 showed similar IC_{50} values, the use of the 617-linker in AAZTA⁵-PSMA-617 showed a significant improvement in binding affinity compared to AAZTA.SA.KuE. However, this effect could not be shown in the case of DATA^{5m}-PSMA-617, since the binding affinity was almost 2-fold lower than DATA^{5m}.SA.KuE. A clear effect of the chelator on the affinity could also not be stated. Rather, it is the totality of the components that is important since these building blocks define the orientation of the whole molecule in the binding pocket and its interaction with the amino acids located there.

Based on the results discussed above, DATA^{5m}.SA.KuE and AAZTA⁵.SA.KuE were selected for further evaluation. The hybrid chelators DATA^{5m} and AAZTA⁵ displayed promising properties in several studies, in terms of fast complexation kinetics at mild temperatures along a prolonged complex stability. The selection of squaric acid as linker moiety was based on the aforementioned *in vitro* results but also on the work of Engelbogen et al. who first described favorable characteristics of squaric acid in terms of a straightforward synthesis and coupling. Further investigations of Greifenstein et al. revealed a positive impact of this chemical functionality on the pharmacokinetic properties *in vivo*.

[⁶⁸Ga]Ga.DATA^{5m}.SA.KuE, [⁴⁴Sc]Sc.AAZTA⁵.SA.KuE and [¹⁷⁷Lu]Lu.AAZTA⁵.SA.KuE showed good binding affinity and internalization ratio *in vitro*. Moreover, tumor accumulation in xenograft models was similar to the clinically used [⁶⁸Ga]Ga.PSMA-11. It should be mentioned that the kidney uptake of the squaric acid-based PSMA ligands was significantly lower than that of [⁶⁸Ga]Ga.PSMA-11, which is regarding kidney irradiation and the resulting nephrotoxicity of great benefit. Interestingly, both [⁴⁴Sc]Sc.AAZTA⁵.SA.KuE and [¹⁷⁷Lu]Lu.AAZTA⁵.SA.KuE displayed similar favorable properties *in vivo* which makes them a promising pair for a theranostic use.

ii) PSMA-targeted small-molecule drug conjugates

The tremendous progress made in the field of nuclear medicine with PSMA radiopharmaceuticals made this molecular structure a promising target for a targeted drug delivery, a field that has gained significant importance in recent years. Although the development of ADCs represented a breakthrough in targeted therapy, PSMA-targeted antibody drug conjugates did not achieve the anticipated results. The insufficient stability of the conjugate and the associated systemic toxicity are the main challenges to be overcome. One of the most promising strategies being pursued for this purpose is the development of SMDCs.

The design of MMAE.VC.SA.617 was based on preliminary studies revealing the potency of the KuE binding unit and the positive effect of the PSMA-617 linker on the binding affinity. Additionally, squaric acid was used not only to facilitate the subsequent coupling to the drug but also to benefit from the favourable properties investigated in previous studies. The SA.617 unit showed high PSMA binding affinity *in vitro*. However, coupling to the MMAE.VC. unit led to a loss in binding potency suggesting that the interaction within the PSMA pocket has been significantly impaired. A closer look at the structural formula of MMAE.VC.SA.617 suggests that an intramolecular reaction may have taken place, probably facilitated by the proximity of the ureido group of citrulline to the carboxyl group of glutamate (Figure 23).

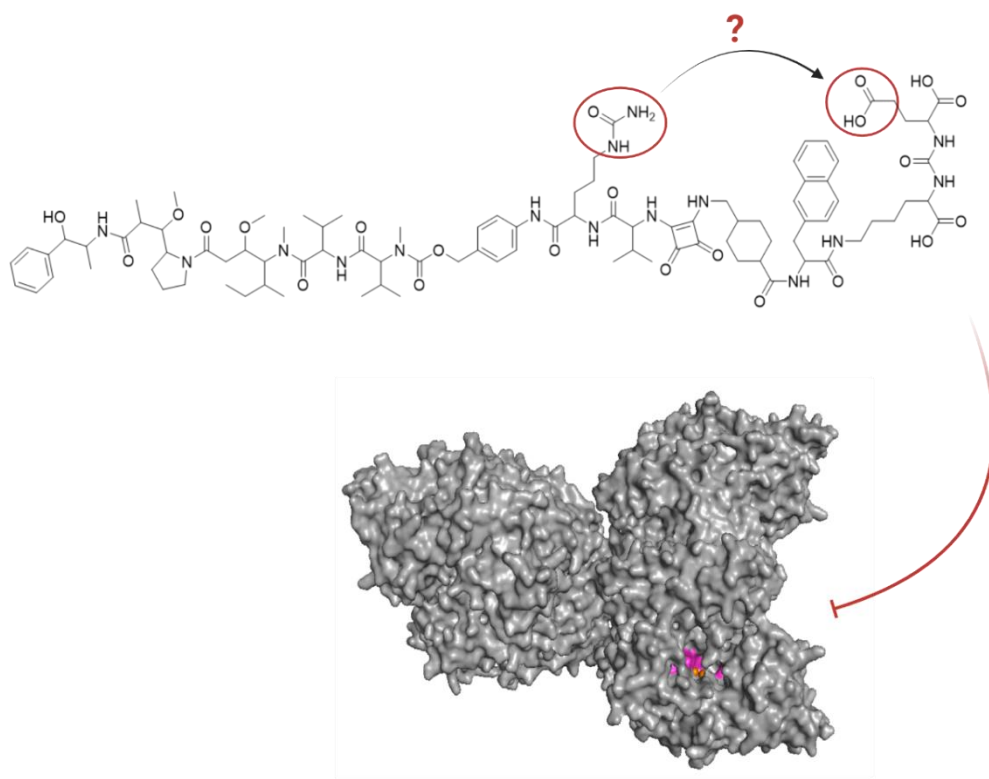


Figure 24 Suggested intramolecular reaction of the ureido group of citrulline with the carboxyl group of glutamate which can lead to impairment of the binding capability since the pharmacophore site of PSMA (pink region) only recognize unmodified glutamate.

By looking at the structural formula of PSMA-1-VcMMAE published by Wang et.al and SBPD-1 published by the Pomper group, it is noticeable that these SMDCs have almost the same components as MMAE.VC.SA.617 except the linker localized between the KuE unit and the enzyme cleavable linker (Figure 24). Since PSMA-1-VcMMAE as well as SBPD-1 displayed outstanding results *in vitro* as well as *in vivo*, it can be assumed that this linker structure plays a decisive role thereby.

While PSMA-1-VcMMAE consists of a long highly negative peptide linker that ensures a sufficient distance between the binding unit and the rest of the molecule, SBPD-1 includes only an aliphatic spacer that was probably flexible enough to allow the entire molecule to adopt a favorable conformation for optimal interaction with the PSMA binding pocket.

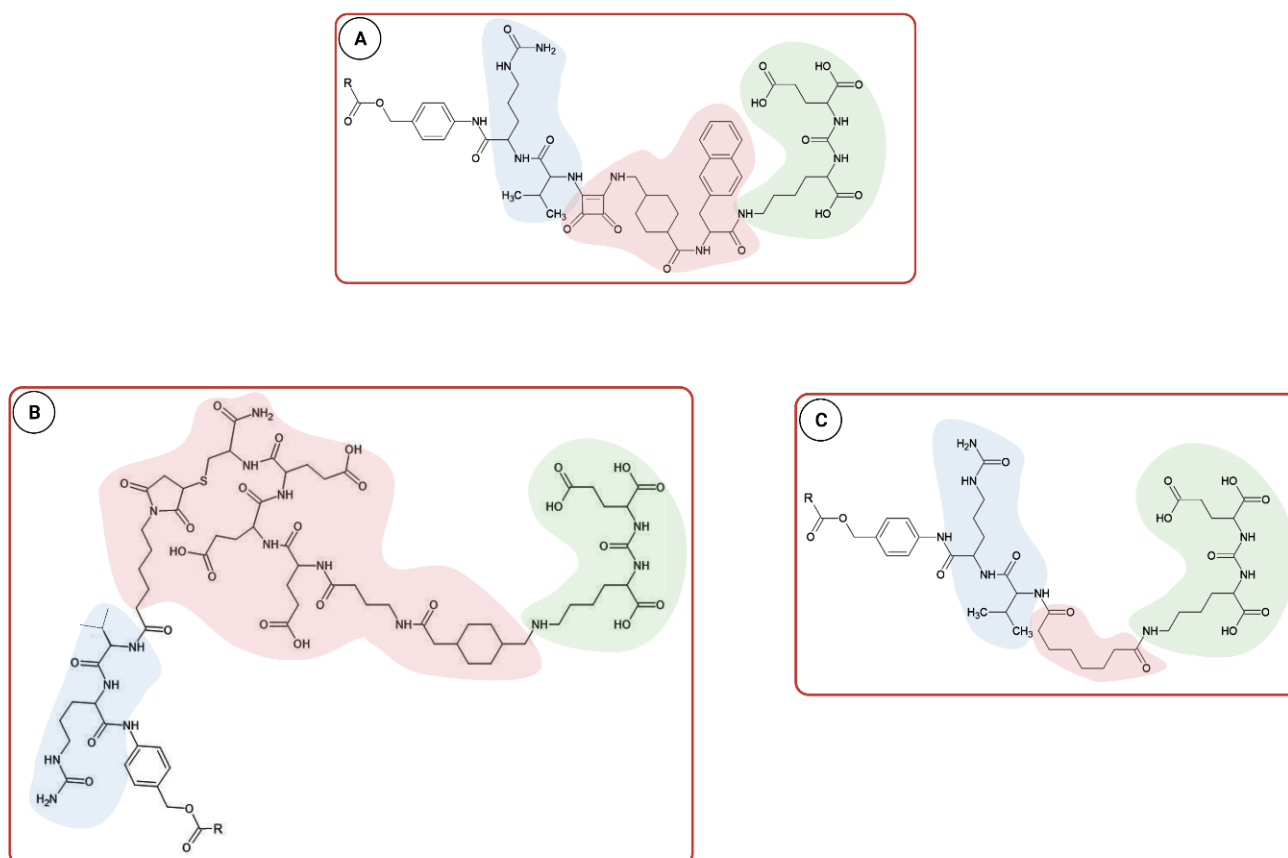


Figure 25 Comparison of the different linker structures of (A) MMAE.VC.SA.617, (B) PSMA-1-VcMMAE and (C) SBPD-1 highlighted in pink. All three PSMA drug conjugates have the same KuE PSMA binding unit (green) and valine-citrulline linker (blue). R= MMAE

As reported by Zhang et al., an interaction of PSMA-ligands with the arene-binding region e.g., through π -stacking, plays a crucial role in the orientation and positioning of these ligands within the PSMA pocket and therefore their binding affinity⁵³. By comparing the two structural formulas of MMAE.VC.SA.617 and DNP-ARM-P2, it is noticeable that citrulline is located almost exactly at the position of the DNP ring thus probably in the arene-binding site. The protonated ureido group could impede the interaction within this region and could even have a negative effect due to electrostatic repulsion (Figure 25). The insertion of a spacer moiety between the binding unit of the SMDC and the valine-citrulline linker could help circumventing the above discussed issues. Otherwise, a more flexible linker should be used in order to enable a better orientation in the binding pocket.

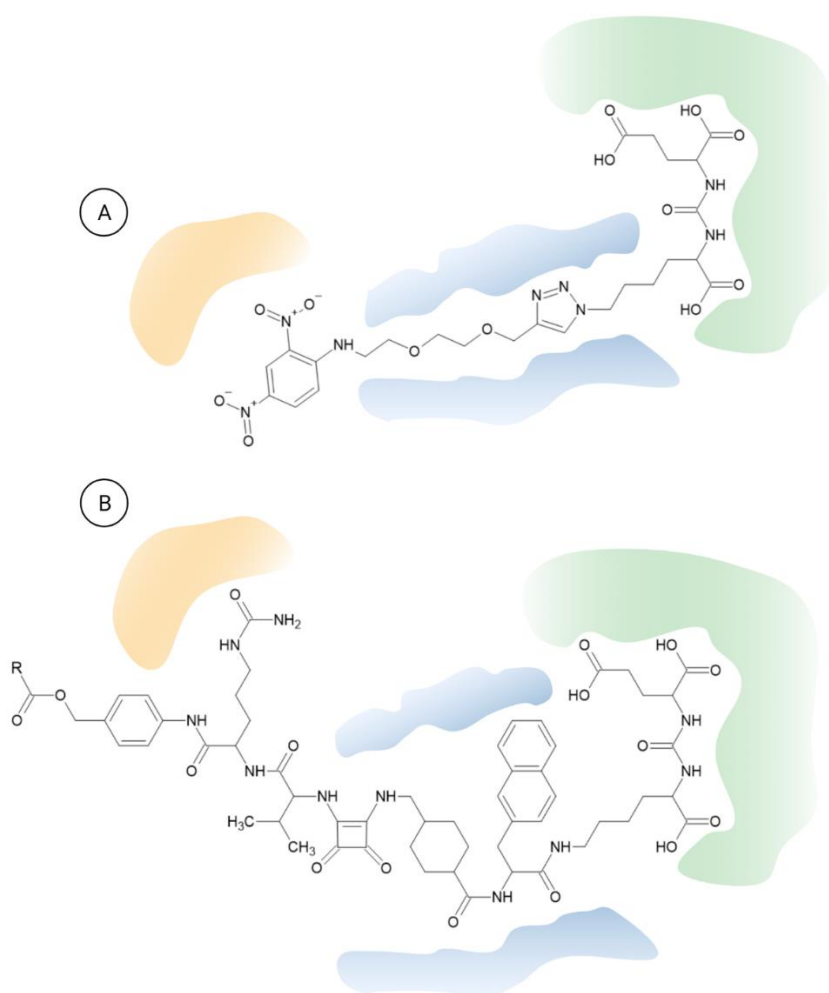


Figure 26 Hypothetical positioning of DNP-ARM-P2 (A) and MMAE.VC.SA.617 (B) in the PSMA-binding pocket. The arene-binding site is highlighted in orange whereas the pharmacophore pocket is green. The hydrophobic entrance funnel of PSMA is marked in blue.

Besides a good binding affinity, the success of the targeted therapy approach depends also on the selective delivery of the cytotoxic payload to the tumor and more importantly on a controlled drug release. MMAE.VC.SA.617 consists of MMAE, one of the most potent antimitotic drugs linked to valine-citrulline to ensure the selective proteolytic cleavage by cathepsin B, an enzyme high expressed in tumor cells.

According to the performed studies, MMAE.VC.SA.617 showed a cytotoxicity in the nanomolar range. This toxic effect could be considerably reduced by blocking PSMA receptors with PMPA thus, indicating a PSMA-selective uptake. Nevertheless, the cytotoxicity of MMAE.VC.SA.617 was significantly lower than that of MMAE indicating that the conjugation has, here as well, a negative impact on the effectiveness of the drug conjugate. In addition, the reduced lipophilicity of MMAE.VC.SA.617 due to the carboxyl groups of the KuE binding unit may have led to this loss in cytotoxicity. Since MMAE penetrates the cell membrane via passive diffusion, the intracellular uptake of the charged drug conjugate will be strongly limited.

By increasing the binding affinity of MMAE.VC.SA.617 e.g., through the use of an appropriate lipophilic linker, the impaired passive diffusion could be compensated by the PSMA-dependent uptake. Nevertheless, the enzyme-specific cleavage of MMAE.VC.SA.617 and the subsequent release of MMAE within few minutes could be demonstrated, thus fulfilling one of the most crucial criteria of targeted therapy. These findings were in accordance to the results obtained from the conducted *in vivo* studies. The tolerability of MMAE.VC.SA.617 and thus its stability *in vivo* could be demonstrated. Additionally, MMAE.VC.SA.617 has shown an effective tumor-growth inhibition even several weeks post treatment.

Finally, it is important to mention that the setup and design of *in vitro* and *in vivo* experiments play a decisive role in preclinical research. The results reported herein seem to be inferior to those published elsewhere, however, direct comparability cannot be made. The *in vitro* and *in vivo* studies conducted with both PSMA-1-VcMMAE and SBPD-1 were based on the use of PC3 PIP cells. This cell line was transduced to overexpress PSMA to a significantly higher extent than the patient-derived LNCaP cells used for testing of MMAE.VC.SA.617^{110,111}. It will be interesting to determine the *in vitro* and *in vivo* properties of MMAE.VC.SA.617 using PC3 PIP cells and to compare them with the results obtained with LNCaP cell-based studies.

iii) PSMA-targeted radiolabeled small-molecule drug conjugates

One of the serious consequences of the progression of PCa is metastasis. 90% of patients with late-stage PCa develop mainly bone metastases, which cannot always be successfully treated with [¹⁷⁷Lu]Lu-PSMA-617 due to differential mostly insufficient PSMA expression. To meet this challenge, DOTA-L-Lys(SA.Pam)-PSMA-617 was developed, which contains pamidronate in addition to the PSMA binding unit KuE. Like all bisphosphonates, pamidronate binds with high affinity to HAP structures of the bone.

The dual-targeted DOTA-L-Lys(SA.Pam)-PSMA-617 demonstrated its potential as theranostic agent for imaging and therapy of PC-related bone metastases independent of PSMA expression. Beside high stability in human serum, an excellent, selective HAP binding and a binding affinity in the nanomolar range could be shown. Additionally, DOTA-L-Lys(SA.Pam)-PSMA-617 displayed good PSMA-dependent tumor uptake along with a PSMA-independent femur accumulation.

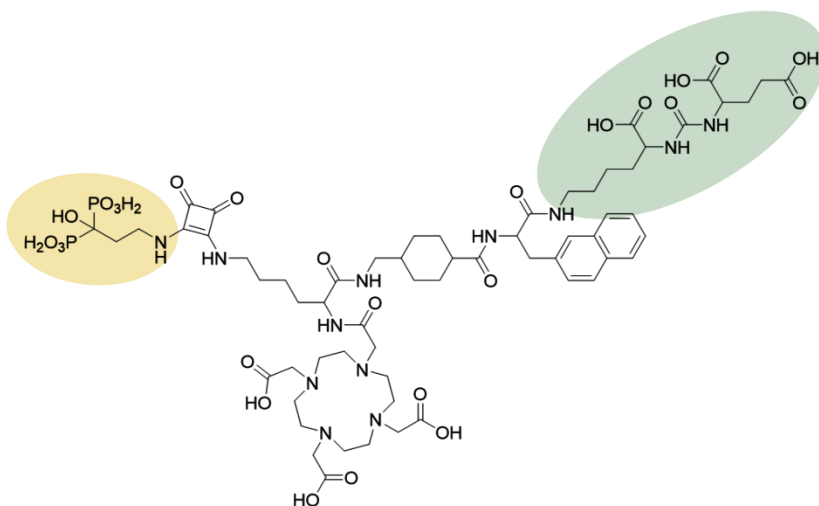


Figure 27 Chemical structure of DOTA-L-Lys(SA.Pam)-PSMA-617. Pamidronate (orange) binds to HAP while KuE (green) targets PSMA.

Finally, the dual targeting approach was implemented in the development of radiolabeled SMDC that consists of the cytotoxic drug MMAE, the PSMA-targeting unit KuE and the DOTAGA chelator. Combining chemotherapy and endoradiotherapy in one molecule is a novel strategy to improve patient quality of life by both determining patient-specific suitability for therapy with the gallium-68-labeled SMDC and enhancing antitumor efficacy while minimizing resistance development. Based on the positive results obtained from the preclinical evaluation of MMAE.VC.SA.617, a trimeric SMDC was developed by inserting the bifunctional DOTAGA chelator to the dimeric MMAE.VC.SA.617 as seen in figure 29.

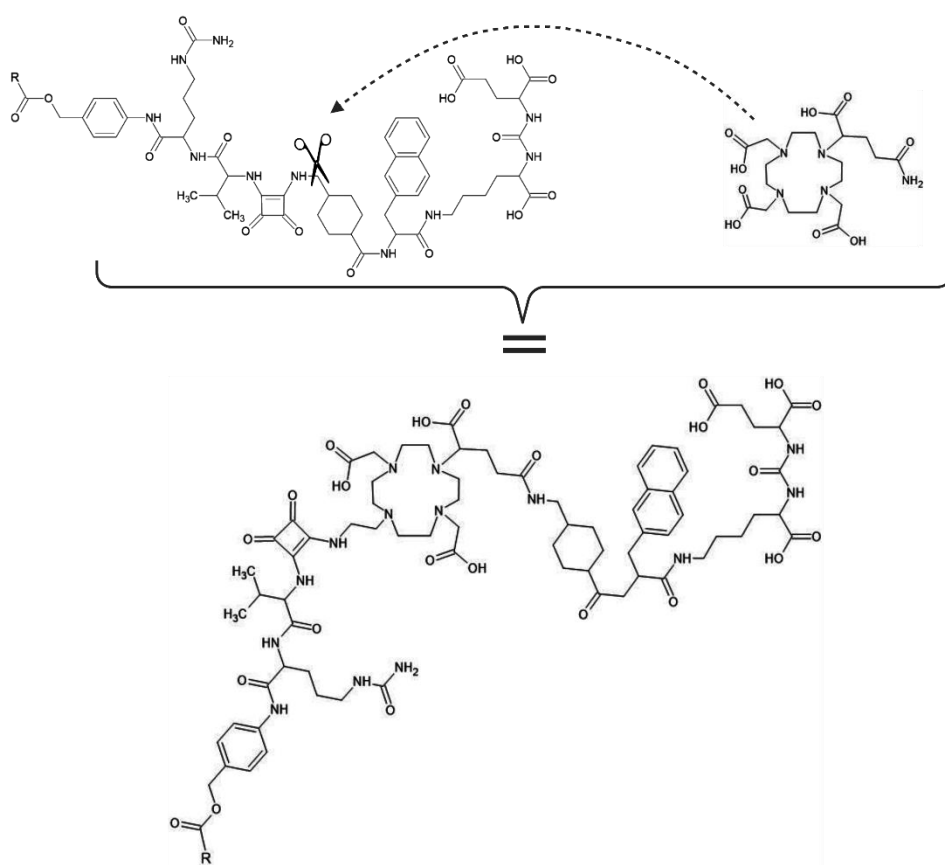


Figure 28 Insertion of the bifunctional DOTAGA chelator led to the trimeric PSMA SMDC. R= MMAE.VC

Although the synthesis of DOTAGA.MMAE.VC.SA.617 was carried out successfully, this trimeric SMDC could not be labeled with gallium-68. One possible explanation would be the deficient formation of an octahedral complex, which is necessary for the stable complexation of gallium-68 due to an intramolecular reaction between the ureido group of citrulline and one carboxyl group of DOTAGA. An alternative chemical arrangement of the macrocyclic chelator within the conjugate could overcome this problem.

Regarding the *in vitro* properties of DOTAGA.MMAE.VC.SA.617, the binding affinity as well as the cytotoxicity were determined analogously to the dimeric counterpart MMAE.VC.SA.617. The IC₅₀ value of DOTAGA.MMAE.VC.SA.617 was almost 20-fold higher than that of MMAE.VC.SA.617 ($3.9 \pm 0.5 \mu\text{M}$ vs. $188.6 \pm 24.7 \text{ nM}$) indicating a decrease in PSMA binding affinity. The negative effect of the DOTAGA insertion were even more pronounced in terms of cytotoxic potency which decreased drastically. The half maximal inhibitory concentration of DOTAGA.MMAE.VC.SA.617, determined in *in vitro* cytotoxic assays, was $13.9 \pm 1.3 \mu\text{M}$, more than 400-fold higher than that of MMAE.VC.SA.617 ($33.0 \pm 4.9 \text{ nM}$).

These results necessitate optimization of the drug design to counteract the deterioration in binding affinity and cytotoxicity. Possible strategies would be, on the one hand, to replace the valine-citrulline linker with another linker such as disulfide groups to inhibit potential intramolecular reactions, and on the other hand, to introduce a lipophilic spacer such as an alkyl chain, which would increase the required distance between the pharmacophore binding unit KuE and the rest of the conjugate, but also increase its lipophilicity leading to improved passive diffusion across the cell membrane.

In summary, the dual targeting and drug delivery approach could be successfully implemented with both PSMA-targeted conjugates, i.e. DOTA-L-Lys(SA.Pam)-PSMA-617 and MMAE.VC.SA.617. Nevertheless, further studies are required in order to optimize the *in vitro* and *in vivo* behavior of these drug conjugates. Especially in the case of MMAE.VC.SA.617 and DOTAGA.MMAE.VC.SA.617, optimizations are to be made with regard to the molecular structure in order to ensure better orientation in the PSMA binding pocket, thus better binding affinity and cell-uptake. At this point, it is worth mentioning again that other cleavable linkers should be tested, as well as the introduction of a spacer that should preferably have lipophilic properties to also improve passive diffusion across the cell membrane.

Furthermore, the *in vitro* assays should be performed with other cell lines such as PC3-PIP to allow a better comparison with the drug conjugates already described in the literature.

5 Appendix

5.1 References

1. H. SUNG et al., "Global Cancer Statistics 2020: GLOBOCAN Estimates of Incidence and Mortality Worldwide for 36 Cancers in 185 Countries," *CA. Cancer J. Clin.* 71 3, 209, American Cancer Society (2021)
2. "Cancer Statistics Review, 1975-2015 -SEER Statistics
3. "SEER*Explorer Application;" seer.cancer.gov
4. C. PARKER et al., "Prostate cancer: ESMO Clinical Practice Guidelines for diagnosis, treatment and follow-up" (2020)
5. G. GANDAGLIA et al., "Distribution of metastatic sites in patients with prostate cancer: A population-based analysis," *Prostate* 74 2, 210 (2014)
6. C. PARKER et al., "Prostate cancer: ESMO Clinical Practice Guidelines for diagnosis, treatment and follow-up" *Ann. Oncol.* 31, 1119 (2020)
7. P. W. KANTOFF et al., "Sipuleucel-T Immunotherapy for Castration-Resistant Prostate Cancer," 3635, 411 (2010)
8. P. KAWALEC et al., "Systematic review/Meta-analysis Sipuleucel-T immunotherapy for castration-resistant prostate cancer. A systematic review and meta-analysis," *Arch. Med. Sci.* 8 5, 767 (2012)
9. "FDA Approves First PSMA-Targeted PET Imaging Drug for Men with Prostate Cancer | FDA;" <https://www.fda.gov/news-events/press-announcements/fda-approves-first-psma-targeted-pet-imaging-drug-men-prostate-cancer>; (current as of Sep. 29, 2021).
10. "Novartis receives FDA Breakthrough Therapy designation for investigational ¹⁷⁷Lu-PSMA-617 in patients with metastatic castration-resistant prostate cancer (mCRPC) | Novartis;" <https://www.novartis.com/news/novartis-receives-fda-breakthrough-therapy-designation-investigational-177lu-psma-617-patients-metastatic-castration-resistant-prostate-cancer-mcrpc>; (current as of Sep. 29, 2021).
11. M. Gottardi et al., "Gemtuzumab ozogamicin in acute myeloid leukemia: past, present and future," *Minerva Med.* 111 5, 395 (2020)
12. C. SELBY et al. "Gemtuzumab Ozogamicin: Back Again," *J. Adv. Pract. Oncol.* 10 1, 68 (2019).
13. G. Govindan et al. "Designing immunoconjugates for cancer therapy," *Expert Opin. Biol. Ther.* 12 7, 873 (2012)
14. M. A. FIRER et al. "Targeted drug delivery for cancer therapy: the other side of antibodies," *J. Hematol. Oncol.* 5, 70 (2012)
15. J. D. BARGH et al., "Cleavable linkers in antibody-drug conjugates," *Chem. Soc. Rev.* 48 16, 4361 (2019)
16. J. LU et al., "Linkers having a crucial role in antibody–drug conjugates," in *International Journal of Molecular Sciences* 17 4, MDPI AG (2016)
17. N. C. RICHARDSON et al., "FDA Approval Summary: Brentuximab Vedotin in First-Line Treatment of Peripheral T-Cell Lymphoma," *Oncologist* 24 5, Wiley (2019)
18. S. García-Alonso et al. "Trastuzumab Emtansine: Mechanisms of Action and Resistance, Clinical Progress, and Beyond," *Trends in cancer* 6 2, 130 (2020)
19. W. D. HEDRICH et al., "Antibody–Drug Conjugates: Pharmacokinetic/Pharmacodynamic Modeling, Preclinical Characterization, Clinical Studies, and Lessons Learned," *Clin. Pharmacokinet.* 57 6, 687, NIH Public Access (2018)

20. Y. Choi et al. "Polatuzumab Vedotin: a New Target for B Cell Malignancies," *Curr. Hematol. Malig. Rep.* 15 2, 125 (2020)
21. A. Markham et al. "Belantamab Mafodotin: First Approval," *Drugs* 80 15, 1607 (2020)
22. A. LEE, "Loncastuximab Tesirine: First Approval," *Drugs* 2021 81:10 (2021)
23. I. Kimiz-Gebologlu et al. "Monoclonal antibodies in cancer immunotherapy," *Mol. Biol. Rep.* 45 6, 2935(2018)
24. A. Nissim et al., "Historical development of monoclonal antibody therapeutics," *Handb. Exp. Pharmacol.* 181, 3 (2008)
25. R. M. Vázquez-Rey et al. "Aggregates in monoclonal antibody manufacturing processes," *Biotechnol. Bioeng.* 108 7, 1494 (2011)
26. C. ZHUANG et al., "Small molecule-drug conjugates: A novel strategy for cancer-targeted treatment," *Eur. J. Med. Chem.* 163, 883 (2019)
27. T. K. PATEL et al., "Small molecule drug conjugates (SMDCs): an emerging strategy for anticancer drug design and discovery," *New J. Chem.* 45 12, 5291 (2021)
28. A. V. GAPONOVA et al., "A Novel HSP90 Inhibitor–Drug Conjugate to SN38 Is Highly Effective in Small Cell Lung Cancer," *Clin. Cancer Res.* 22 20, 5120 (2016)
29. J. A. REDDY et al., "Pre-clinical evaluation of EC1456, a folate-tubulysin anti-cancer therapeutic," *Sci. Reports* 2018 81 8 1, 1 (2018)
30. L. CP et al., "Prostate-Specific Membrane Antigen-Specific Antitumor Activity of a Self-Immolative Tubulysin Conjugate," *Bioconjug. Chem.* 30 6, 1805 (2019)
31. Y.-W. LIU et al., "Targeting Tumor Associated Phosphatidylserine with New Zinc Dipicolylamine-Based Drug Conjugates," *Bioconjug. Chem.* 28 7, 1878 (2017)
32. Q. LV et al., "Prostate-Specific Membrane Antigen Targeted Therapy of Prostate Cancer Using a DUPA-Paclitaxel Conjugate," *Mol. Pharm.* 15 5, 1842 (2018)
33. R. KURZROCK et al., "Safety, Pharmacokinetics, and Activity of GRN1005, a Novel Conjugate of Angiopep-2, a Peptide Facilitating Brain Penetration, and Paclitaxel, in Patients with Advanced Solid Tumors," *Mol. Cancer Ther.* 11 2, 308 (2012)
34. JS. Horoszewicz et al. "Monoclonal antibodies to a new antigenic marker in epithelial prostatic cells and serum of prostatic cancer patients.," *Anticancer Res.* 7 5B, 927 (1987).
35. R. S. ISRAELI et al., "Molecular Cloning of a Complementary DNA Encoding a Prostate-specific Membrane Antigen," *Cancer Res.* 53 2 (1993).
36. MI. Davis et al., "Crystal structure of prostate-specific membrane antigen, a tumor marker and peptidase," *Proc. Natl. Acad. Sci. U. S. A.* 102 17, 5981 (2005)
37. K. RAHBAR et al., "PSMA Theranostics: Current Status and Future Directions," *Mol. Imaging* 17, 1 (2018)
38. S. S. CHANG et al. "Biology of PSMA as a Diagnostic and Therapeutic Target," in *Management of Prostate Cancer*, pp. 609–630 (2004).
39. G. ANILKUMAR et al., "Prostate-specific Membrane Antigen Association with Filamin A Modulates Its Internalization and NAALADase Activity 1," *CANCER Res.* 63, 2645 (2003).

- 40 F. P. Mhaweche-Fauceglia et al., "Prostate-specific membrane antigen (PSMA) protein expression in normal and neoplastic tissues and its sensitivity and specificity in prostate adenocarcinoma: an immunohistochemical study using multiple tumour tissue microarray technique," *Histopathology* 50 4, 472 (2007)
41. T. D. SCHMITTGEN et al., "Expression of prostate specific membrane antigen and three alternatively spliced variants of PSMA in prostate cancer patients," *Int. J. Cancer* 107 2, 323 (2003)
42. A. GHOSH et al. "Tumor target prostate specific membrane antigen (PSMA) and its regulation in prostate cancer," *J. Cell. Biochem.* 91 3, 528 (2004)
43. V. YAO et al., "Expression of prostate-specific membrane antigen (PSMA), increases cell folate uptake and proliferation and suggests a novel role for PSMA in the uptake of the non-polyglutamated folate, folic acid," *Prostate* 70 3, 305 (2010)
44. P. BACKHAUS et al., "Targeting PSMA by radioligands in non-prostate disease—current status and future perspectives," *Eur. J. Nucl. Med. Mol. Imaging* 2018 455 45 5, 860 (2018)
45. A. Baccala et al., "Expression of prostate-specific membrane antigen in tumor-associated neovasculature of renal neoplasms," *Urology* 70 2, 385 (2007)
46. W. C. Van de Wiele et al., "PSMA expression on neovasculature of solid tumors," *Histol. Histopathol.* 35 9, 919 (2020)
47. M. MATSUDA et al., "Potential use of prostate specific membrane antigen (PSMA) for detecting the tumor neovasculature of brain tumors by PET imaging with ⁸⁹Zr-Df-IAB2M anti-PSMA minibody," *J. Neurooncol.* 138 3, 581 (2018)
48. D. S. O'KEEFE et al., "A Perspective on the Evolving story of PSMA Biology and PSMA Based Imaging and Endoradiotherapeutic Strategies. Short running title: PSMA biology," *J. Nucl. Med.* (2018)
49. M. I. DAVIS et al., "Crystal structure of prostate-specific membrane antigen, a tumor marker and peptidase," *Proc. Natl. Acad. Sci. U. S. A.* 102 17, 5981 (2005)
50. C. Barinka et al., "Structural insight into the pharmacophore pocket of human glutamate carboxypeptidase II," *J. Med. Chem.* 50 14, 3267, *J Med Chem* (2007)
51. J. PAVLICEK et al. "Glutamate Carboxypeptidase II: An Overview of Structural Studies and Their Importance for Structure-Based Drug Design and Deciphering the Reaction Mechanism of the Enzyme," *Curr. Med. Chem.* 19 9, 1300 (2012)
52. A. L. SHELDON et al. "The Role of Glutamate Transporters in Neurodegenerative Diseases and Potential Opportunities for Intervention," *Neurochem. Int.* 51 6–7, 333 (2007)
53. A. X. ZHANG et al., "A Remote arene-binding site on prostate specific membrane antigen revealed by antibody-recruiting small molecules," *J. Am. Chem. Soc.* 132 36, 12711 (2010)
54. P. F. Jackson et al., "Design, synthesis, and biological activity of a potent inhibitor of the neuropeptidase N-acetylated alpha-linked acidic dipeptidase," *J. Med. Chem.* 39 2, 619, *J Med Chem* (1996)
55. Z. NOVAKOVA et al., "Design of composite inhibitors targeting glutamate carboxypeptidase II: the importance of effector functionalities," *FEBS J.* 283 1, 130 (2016)
56. S. C. Behr et al., "Phase I Study of CTT1057, an 18 F-Labeled Imaging Agent with Phosphoramidate Core Targeting Prostate-Specific Membrane Antigen in Prostate Cancer," *J. Nucl. Med.* 60 7, 910 (2019)
57. R. J. Barren et al., "Monoclonal Antibody 7E11.C5 Staining of Viable LNCaP Cells" *Prostate*; 30(1):65-68. (1997)
58. R. J. ELLIS et al. "Role of ProstaScint® for brachytherapy in localized prostate adenocarcinoma," *Expert Rev Mol Diagn.*;4(4):435-441 (2004)

59. H. LIU et al., "Monoclonal Antibodies to the Extracellular Domain of Prostate-specific Membrane Antigen Also React with Tumor Vascular Endothelium," *Cancer Res.* 57 17 (1997).
60. S. HAMMER et al., "Preclinical Efficacy of a PSMA-Targeted Thorium-227 Conjugate (PSMA-TTC), a Targeted Alpha Therapy for Prostate Cancer," *Clin. Cancer Res.* 26 8, 1985 (2020)
61. MG. Pomper et al., "¹¹C-MCG: synthesis, uptake selectivity, and primate PET of a probe for glutamate carboxypeptidase II (NAALADase)," *Mol. Imaging* 1 2, 96 (2002)
62. B. Turkbey et al., "¹⁸F-DCFBC Prostate-Specific Membrane Antigen-Targeted PET/CT Imaging in Localized Prostate Cancer: Correlation With Multiparametric MRI and Histopathology," *Clin. Nucl. Med.* 42 10, 735 (2017)
63. S. P. ROWE et al. "¹⁸F-DCFBC PET/CT for PSMA-Based Detection and Characterization of Primary Prostate Cancer," *J. Nucl. Med.* 56 7, 1003 (2015)
64. S. P. ROWE, et al., "Imaging of Prostate-Specific Membrane Antigen Using [¹⁸F]DCFPyL," *PET Clin.* 12 3, 289 (2017)
65. R. A. WERNER et al., "Semiquantitative Parameters in PSMA-Targeted PET Imaging with [¹⁸F]DCFPyL: Impact of Tumor Burden on Normal Organ Uptake," *Mol. Imaging Biol.* 22 1, 190 (2020)
66. Z. Szabo et al., "Initial Evaluation of [(¹⁸F)]DCFPyL for Prostate-Specific Membrane Antigen (PSMA)-Targeted PET Imaging of Prostate Cancer," *Mol. imaging Biol.* 17 4, 565 (2015)
67. C. Y et al., "2-(3-{1-Carboxy-5-[(6-[¹⁸F]fluoro-pyridine-3-carbonyl)-amino]-pentyl}-ureido)-pentanedioic acid, [¹⁸F]DCFPyL, a PSMA-based PET imaging agent for prostate cancer," *Clin. Cancer Res.* 17 24, 7645 (2011)
68. JA. Barrett et al., "First-in-man evaluation of 2 high-affinity PSMA-avid small molecules for imaging prostate cancer," *J. Nucl. Med.* 54 3, 380 (2013)
69. SM. Hillier et al., "¹²³I-MIP-1072, a small-molecule inhibitor of prostate-specific membrane antigen, is effective at monitoring tumor response to taxane therapy," *J. Nucl. Med.* 52 7, 1087 (2011)
70. SM. Hillier et al., "^{99m}Tc-labeled small-molecule inhibitors of prostate-specific membrane antigen for molecular imaging of prostate cancer," *J. Nucl. Med.* 54 8, 1369 (2013)
71. KE. Goffin et al., "Phase 2 Study of ^{99m}Tc-Trofolostat SPECT/CT to Identify and Localize Prostate Cancer in Intermediate- and High-Risk Patients Undergoing Radical Prostatectomy and Extended Pelvic LN Dissection," *J. Nucl. Med.* 58 9, 1408 (2017)
72. SR. Banerjee et al., "⁶⁸Ga-labeled inhibitors of prostate-specific membrane antigen (PSMA) for imaging prostate cancer," *J. Med. Chem.* 53 14, 5333 (2010)
73. G. CARLUCCI et al., "⁶⁸Ga-PSMA-11 NDA Approval: A Novel and Successful Academic Partnership," *J. Nucl. Med.* 62 2, 149 (2021)
74. M. SCHÄFER, U. BAUDER-WUST, and K. LEOTTA, "A dimerized urea-based inhibitor of the prostate-specific membrane antigen for ⁶⁸Ga-PET imaging of prostate cancer.," *EJNMMI Res* 2 1, 23 (2012)
75. "Novartis receives FDA Breakthrough Therapy designation for investigational ¹⁷⁷Lu-PSMA-617 in patients with metastatic castration-resistant prostate cancer (mCRPC) | Novartis," <https://www.novartis.com/news/novartis-receives-fda-breakthrough-therapy-designation-investigational-177lu-psma-617-patients-metastatic-castration-resistant-prostate-cancer-mcrpc>; (current as of Oct. 5, 2021).
76. M. Weineisen et al., "Synthesis and preclinical evaluation of DOTAGA-conjugated PSMA ligands for functional imaging and endoradiotherapy of prostate cancer," *EJNMMI Res.* 4 1 (2014)

77. M. Weineisen et al., “⁶⁸Ga- and ¹⁷⁷Lu-Labeled PSMA I&T: Optimization of a PSMA-Targeted Theranostic Concept and First Proof-of-Concept Human Studies,” *J. Nucl. Med.* 56 8, 1169 (2015)
78. M. McCarthy et al., “Comparison of PSMA-HBED and PSMA-I&T as diagnostic agents in prostate carcinoma,” *Eur. J. Nucl. Med. Mol. Imaging* 44 9, 1455 (2017)
79. M. S. SADAGHIANI et al., “A Systematic Review and Meta-analysis of the Effectiveness and Toxicities of Lutetium-177-labeled Prostate-specific Membrane Antigen-targeted Radioligand Therapy in Metastatic Castration-Resistant Prostate Cancer,” *Eur. Urol.* 80 1 (2021)
80. “FDA Authorization of IND for ²²⁵Ac-PSMA I&T Targeted Alpha Therapy for – RadioMedix;” <https://radiomedix.com/blogs/news/excel-diagnostics-and-nuclear-oncology-center-announces-fda-authorization-of-ind-for-225ac-psma-i-t-targeted-alpha-therapy-for-castration-resistant-prostate-cancer>; (current as of Oct. 5, 2021).
81. M. D. HENRY et al., “A Prostate-Specific Membrane Antigen-Targeted Monoclonal Antibody-Chemotherapeutic Conjugate Designed for the Treatment of Prostate Cancer,” *Cancer Res.* 64 21, 7995 (2004)
82. M. I. MILOWSKY et al., “Phase 1/2 multiple ascending dose trial of the prostate-specific membrane antigen-targeted antibody drug conjugate MLN2704 in metastatic castration-resistant prostate cancer,” *Urol. Oncol. Semin. Orig. Investig.* 34 12, 530.e15 (2016)
83. V. A. DIPIPO et al., “Efficacy studies of an antibody-drug conjugate PSMA-ADC in patient-derived prostate cancer xenografts,” *Prostate* 75 3, 303 (2015)
84. DP. Petrylak et al., “Phase 1 study of PSMA ADC, an antibody-drug conjugate targeting prostate-specific membrane antigen, in chemotherapy-refractory prostate cancer,” *Prostate* 79 6, 604 (2019)
85. J. S. de BONO et al., “Phase I Study of MEDI3726: A Prostate-Specific Membrane Antigen-Targeted Antibody-Drug Conjugate, in Patients with mCRPC after Failure of Abiraterone or Enzalutamide,” *Clin. Cancer Res.* 27 13, 3602 (2021)
86. J. ROY et al., “DUPA Conjugation of a Cytotoxic Indenoisoquinoline Topoisomerase I Inhibitor for Selective Prostate Cancer Cell Targeting,” *J. Med. Chem.* 58 7, 3094 (2015)
87. Q. Yang et al., “Prostate-Specific Membrane Antigen Targeted Therapy of Prostate Cancer Using a DUPA-Paclitaxel Conjugate,” *Mol. Pharm.* 15 5, 1842 (2018)
88. C. P. LEAMON et al., “Prostate-Specific Membrane Antigen-Specific Antitumor Activity of a Self-Immortal Tubulysin Conjugate” (2019)
89. S. EJADI et al., “Phase 1 study of the PSMA-tubulysin small-molecule drug conjugate EC1169 in pts with metastatic castrate-resistant prostate cancer (mCRPC).,” *J. Clin. Oncol.* 33 15_suppl, e13527 (2015)
90. X. WANG et al., “Small Molecule-Based Prodrug Targeting Prostate Specific Membrane Antigen for the Treatment of Prostate Cancer,” *Cancers (Basel)*. 13 3, 1 (2021)
91. S. BOINAPALLY et al., “A prostate-specific membrane antigen (PSMA)-targeted prodrug with a favorable in vivo toxicity profile,” *Sci. Reports |* 11, 7114 (123AD)
92. R. TÖNNESMANN et al., “[¹⁷⁷Lu]Lu-PSMA-617 Salivary Gland Uptake Characterized by Quantitative In Vitro Autoradiography,” *Pharmaceuticals* 12 1 (2019)
93. J. C. JEWETT, E. M. SLETTEN, and C. R. BERTOZZI, “Rapid Cu-free click chemistry with readily synthesized biarylazacyclooctynones,” *J. Am. Chem. Soc.* 132 11, 3688 (2010)
94. E. M. SLETTEN and C. R. BERTOZZI, “Bioorthogonal Reactions,” *Acc. Chem. Res.* 44 9, 666 (2011).
95. C. GRÖST and T. BERG, “PYRROC: The first functionalized cycloalkyne that facilitates isomer-free generation of organic molecules by SPAAC,” *Org. Biomol. Chem.* 13 13, 3866 (2015)

96. C. DINGELS et al., "Squaric acid mediated chemoselective PEGylation of proteins: Reactivity of single-step-activated α -amino poly(ethylene glycol)s," *Chem. - A Eur. J.* 18 52, 16828 (2012)
97. L. GREIFENSTEIN et al., "Synthesis and labeling of a squaric acid containing PSMA-inhibitor coupled to AAZTA5 for versatile labeling with ^{44}Sc , ^{64}Cu , ^{68}Ga and ^{177}Lu ," *Appl. Radiat. Isot.* (2020)
98. F. R. WURM and H. A. KLOK, "Be squared: Expanding the horizon of squaric acid-mediated conjugations," *Chem. Soc. Rev.* 42 21, 8220 (2013)
99. L. GREIFENSTEIN et al., "Synthesis, labeling and preclinical evaluation of a squaric acid containing PSMA-inhibitor labeled with ^{68}Ga – a comparison with PSMA-11 and PSMA-617," *ChemMedChem*, 1 (2020)
100. E. S. MOON et al., "Targeting fibroblast activation protein (FAP): Next generation PET radiotracers using squaramide coupled bifunctional DOTA and DATA 5m chelators," *EJNMMI Radiopharm Chem.* 5 19, 1 (2020)
101. S. E. RUDD et al., "A desferrioxamine B squaramide ester for the incorporation of zirconium-89 into antibodies," *Chem. Commun.* 52 80, 11889 (2016)
102. S. YOGANATHAN et al. "Chemical synthesis and biological evaluation of gallidermin-siderophore conjugates," *Org. Biomol. Chem.* 9 7, 2133 (2011)
103. E. BERG et al., "Total-Body PET and Highly Stable Chelators Together Enable Meaningful ^{89}Zr -Antibody PET Studies up to 30 Days After Injection," *J. Nucl. Med.* 61 3, 453 (2020).
104. B. KLASSEN, et al. "AAZTA 5 -squaramide ester competing with DOTA-, DTPA- and CHX-A-DTPA-analogues: Promising tool for ^{177}Lu -labeling of monoclonal antibodies under mild conditions," *Nucl. Med. Biol.* 96–97, 80 (2021)
105. M. J. ADLER et al., "Therapeutic Antibodies Against Cancer," *Hematol. Oncol. Clin. North Am.* 26 3, 447 (2012)
106. P. L. FERNÁNDEZ et al., "Expression of Cathepsins B and S in the progression of prostate carcinoma," *Int. J. Cancer* 95 1, 51 (2001)
107. A. A. SINHA et al., "Cathepsin B Expression is Similar in African-American and Caucasian Prostate Cancer Patients," *Anticancer Res.* 27 5A (2007).
108. W. A. P. BREEMAN et al., "The addition of DTPA to [^{177}Lu -DOTA0, Tyr3]octreotate prior to administration reduces rat skeleton uptake of radioactivity," *Eur. J. Nucl. Med. Mol. Imaging* 30 2, 312 (2003)
109. M. BENESOVÁ et al., "Preclinical evaluation of a tailor-made DOTA-conjugated PSMA inhibitor with optimized linker moiety for imaging and endoradiotherapy of prostate cancer," *J. Nucl. Med.* 56 6, 914 (2015)
110. Z. WANG et al., "Single Low-Dose Injection of Evans Blue Modified PSMA-617 Radioligand Therapy Eliminates Prostate-Specific Membrane Antigen Positive Tumors," *Bioconjug. Chem.* 29 9, 3213 (2018)
111. H.-T. KUO et al., "Enhancing Treatment Efficacy of ^{177}Lu -PSMA-617 with the Conjugation of an Albumin-Binding Motif: Preclinical Dosimetry and Endoradiotherapy Studies" (2018)

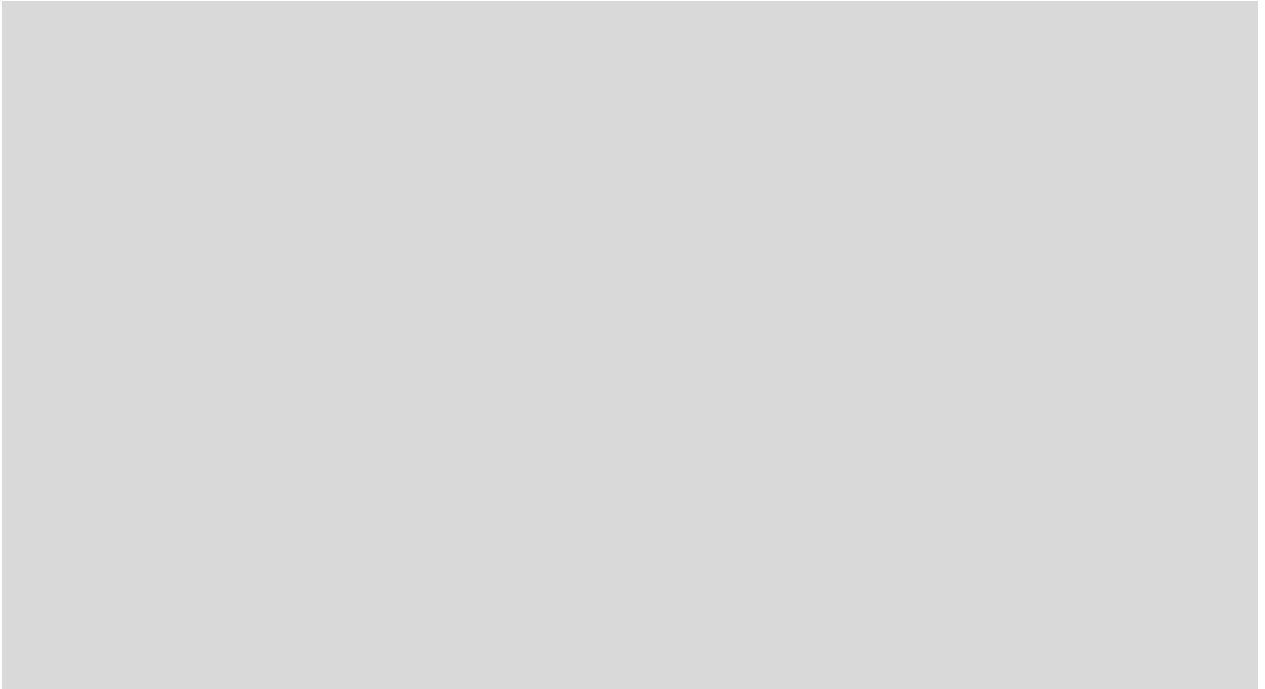
5.2 List of abbreviations

Å	angstroem
AAZTA ⁵	(6-pentanoic acid-6-amino-1,4-diazepine tetra-acetic acid)
ADC	antibody-drug conjugate
approx.	approximately
Arg	arginine
ARM	antibody-recruiting molecules
BCR-ABL	breakpoint cluster region gene- Abelson proto-oncogene
CAFs	cancer associated fibroblasts
CD	cluster of differentiation
cpm	counts per minute
CT	computed tomography
DAPI	4',6-diamidino-2-phenylindole
DATA ^{5m}	6-pentanoic acid-6-amino-1,4-diazapine-triacetate
DFO	desferrioxamine
DMSO	dimethylsulfoxide
DNP	dinitrophenol
DOTA	1,4,7,10-tetraazacyclododecane-1,4,7,10-tetraacetic acid)
DOTAGA	1,4,7,10-tetraaza-cyclododecane-1-pentandiacid-4,7,10-tri-acetic acid),
DPP	dipeptidyl peptidases
DSB	double-strand breaks
DTT	dithiothreitol
EDTMP	(ethylenediamine tetra(methylene phosphonic acid
EGFR	epidermal growth factor receptor
ESB	single strand breaks
FAP	fibroblast activation protein
FDA	U.S. Food and Drug Administration
FOLH1	folate hydrolase
HAP	hydroxyapatite
HATU	(1-[Bis(dimethylamino)methylene]-1H-1,2,3-triazolo[4,5-b]pyridinium 3-oxide hexafluorophosphate)
HBED	N,N-bis(2-hydroxybenzyl)ethylenediamine-N,N-diacetic acid
Her2	human epidermal growth factor receptor 2
HOPO	hydroxypyridine-1-oxide
HPLC	high performance liquid chromatography
HR	homologous recombination
HS	human serum
IC ₅₀	half maximal inhibitory concentration
kDa	kilodalton
K _i	inhibitory constant
KuE	(4-amino-1-carboxybutyl)carbamoyl)glutamine
LC/MS	liquid chromatography mass spectrometry
LNCaP	Lymph Node Carcinoma of the Prostate
mAb	monoclonal antibody
MDP	methylene diphosphonate
MRI	magnetic resonance imaging
NAAG	N-acetyl-aspartyl-glutamate

NAALADase	N-Acetylated alpha-linked acidic dipeptidase
NHS	N-hydroxysuccinimide
NIH	National Institutes of Health
NODAGA	1,4,7-triazacyclononane,1-glutaric acid-4,7-acetic acid)
NOTA	1,4,7-triazacyclononane-1,4,7-triacetic acid)
PABC	p-aminocarbamate
Pam	pamidronate
PBS	phosphate buffered saline
PET	Positron Emission Tomography
PFA	paraformaldehyde
PMPA	2-phosphonomethyl pentanedioic acid
p.i.	post injection
PSA	prostate-specific antigen
PSMA	prostate-specific membrane antigen
RCY	radiochemical yield
SADE	square acid diethyl esters
SAR	structure-activity-relationship
SMDC	small-molecule drug conjugate
SPAAC	strain-promoted-azide-alkyne-cycloaddition
SPECT	single-photon emission computerized tomography
SUV	standardized uptake value
TAT	targeted alpha therapy
TRAM	(1,4,7-triazonane-1,4,7-triyl)tris(methylene))tris((1-amino-15-oxo-4,7,10-trioxa-14-azaheptadecan-17-yl)phosphinic acid)
TRAP	1,4,7-triazacyclononane-1,4,7-tris(methyl(2-carboxyethyl))-phosphinic acid)
Trp	tryptophane
VC	valine-citrulline
WARMTH	World Association of Radiopharmaceutical and Molecular Therapy
Zol	zoledronate

5.3 Danksagung





5.4 Curriculum Vitae

[Redacted]

[Redacted]

[Redacted]

[Redacted]

[Redacted]

[Redacted]

[Redacted]

[Redacted]

[Redacted]

[Redacted]

[Redacted]

[Redacted]

[Redacted]

[Redacted]

[Redacted]

[Redacted]

[Redacted]

[Redacted]

[Redacted]

[Redacted]

[Redacted]

[Redacted]

[Redacted]

[Redacted]

[Redacted]

[Redacted]

[Redacted]

[Redacted]

[Redacted]

[Redacted]

[Redacted]

[Redacted]

[Redacted]

[Redacted]

[Redacted]

[Redacted]	[Redacted]
------------	------------

[Redacted]	[Redacted]
------------	------------

[Redacted]

[Redacted]	[Redacted]
------------	------------

